DESIGN CRITERIA FOR ROLLING CONTACT FATIGUE RESISTANCE IN BACK-UP ROLLS

Michael Fraser Frolish

Thesis submitted for the degree of Doctor of Philosophy

Department of Mechanical Engineering

September 2002

SUMMARY

The demands placed on back-up rolls in hot strip mills have been investigated by a combination of literature and industrial studies. The tribological operating conditions have been established and the maximum local loads and pressure distributions at the work roll/back-up roll interface have been obtained by processing mill and roll schedule data using a computer program (commercial software developed by VAI Industries (UK) Ltd) and applying the theories of contact mechanics.

After a study of the responses of the rolls to these demands and possible failure mechanisms, research has centred on surface initiated damage whereby cracks can propagate into the roll substrate potentially reaching the internal residual stress fields and leading to catastrophic failure. A proposed qualitative contact and fracture mechanics model, for the rolling contact fatigue and spalling failure, has been quantified theoretically using published methods for determining the stress intensity factors at the tips of pressurised and water lubricated, inclined rolling contact fatigue cracks. The predictions of the quantitative model in terms of crack directions and lengths have been validated by microscopic observation of the morphologies cracks produced in test discs used in the "SUROS" Rolling-Sliding Testing Machine and also in a sample of material spalled from a back-up roll.

The quantitative failure model includes criteria for crack branching either upwards leading to micro spalling or downwards (potentially catastrophic) and the link between these two cases has been related quantitatively to the value of the mode I threshold for the roll material.

After linking mechanics to microstructure and quantifying the interactions between wear and rolling contact fatigue in this case, practical quantitative recommendations have been made for the design of bainitic back-up roll materials, back-up roll redressing procedures and the surface roughness of both the work rolls and back-up rolls presented to the mill.

CONTENTS

Preface

This thesis is based on research carried out in the Departments of Mechanical Engineering and Engineering Materials at the University of Sheffield between September 1997 and September 2001.

The author would like to thank his supervisors Professor John H. Beynon, Professor Mark Rainforth and Dr. Ajay Kapoor for their guidance and advice throughout the project.

The author would also like to thank the postgraduate students and staff of the Departments of Mechanical Engineering and Engineering Materials and the Institute for Microstructural and Mechanical Process Engineering: The University of Sheffield (IMMPETUS) for their support during the project. Particular thanks are due to the Dr. David Fletcher for his help and advice concerning the experimental simulations and facilitating the mathematical computations, Dr. Rebecca Higginson and Dr. John Whiteman for facilitating the EBSD analysis and Dr. Bradley Wynne and Dr. Reme Carmona for their valuable discussions, support and friendship.

Many thanks are due to the technical staff of both departments, especially Mr. David Butcher, Mr. John Goodliffe, Ms. Dawn Bussey, Mrs Barbara Horsfield and Mr. Philip Staton. The author also thanks Professors Tomlinson and Beynon, Heads of the Department of Mechanical Engineering and Professor West, Head of the Department of Engineering Materials, for the use of the laboratory facilities.

The author gratefully acknowledges the information provided by Corus Steel Strip Products and the computations facilitated by VAI Industries (UK) Ltd, which provided the work roll/back-up roll loading profiles used in the project.

The author would like to thank the members of the Materials Forum for general and financial support during the project and in particular Sheffield Forgemasters Rolls Ltd for supplying the test disc specimens and also for their help and support throughout the work.

Chapter 1

INTRODUCTION

There are demands in the steel industry for longer rolling campaigns, smaller roll inventories and lower maintenance costs. These demands, coupled with the desire to roll ever thinner gauges particularly in hot strip mills, have placed heavier duties on back-up rolls. This has increased the possibility of catastrophic failure due to rolling contact fatigue. The economic costs of such failures in both hot and cold strip mills can be severe, but so can the costs of re-dressing the rolls too frequently or removing too much material at each re-dressing. When compared with the considerable amount of work which is being carried out into improving work roll performance, research into the chemistry and design of back-up rolls has been limited. There is therefore a need for more work in this area.

Past approaches to improving back-up roll design have been based primarily on a combination of experience, the available empirical data and trial and error. Roll metallurgy changes, both compositional and microstructural are proposed and trials on the mill are used to assess them. This approach is both time consuming and expensive. This project aims for a different approach, that is, to develop an understanding of the requirements for the roll material, specify these to dictate the required mechanical properties and finally link the mechanics to the required microstructures for the roll materials.

The project objectives have been achieved by examining field evidence, determining the loading and tribological conditions at the work roll/back-up roll interface (Chapters 2 and 3), investigating both theoretically and experimentally the mechanisms involved in rolling contact fatigue (Chapters 4 and 5) and establishing qualitative and quantitative contact and fracture mechanics models for the rolling contact and spalling failure of back-up rolls (Chapter 5). The results obtained from these damage tolerance models, the experimental simulations and the microscopic examination of the back-up roll materials have been used to identify important links between mechanics and microstructure (Chapter 6).

During the work important insights have been gained concerning the possible influence of work roll surface roughness on the surface wear of back-up rolls, the initiation and early propagation of surface initiated rolling contact fatigue cracks and the interaction between wear and rolling contact fatigue (Chapter 6).

Finally, criteria which it is considered will improve back-up roll performance, particularly with regard to rolling contact fatigue, have been established for both the microstructural design of the roll materials and the maintenance of the rolls (Chapter 7).

The work in this study has been based on the loading and operating conditions at the work roll/back-up roll interface on hot strip mills. However, the results can be broadly applied to all back-up rolls used in any mill rolling hot or cold flat products, where work roll cooling or lubrication is used.

Chapter 2

INDUSTRIAL STUDIES

2.1. THE OPERATION OF THE HOT STRIP MILL

The production of hot steel strip in coil form can be carried out in a single stand reversing mill or a multi-stand tandem mill, but the higher production rate and better quality control have made the latter the preferred option for the hot strip mill (Eibe, 1990). The finishing train generally consists of up to seven stands, which are preceded by a five stand roughing tandem or a reversing rougher and coil box. The use of a coil box enables the production of breakdown bars from the roughing section with thinner gauges than could otherwise be accommodated. The use of a coil box also allows the head and tail of the coil to be reversed, this reduces the temperature gradient along the strip as it passes through the finishing train. These processing conditions produce strip with more consistent properties along the whole length of the coil. A flow process chart for a typical hot strip mill with a reversing rougher is shown in Figure 2.1

Each stand in the finishing train is four high, with two back-up rolls to prevent the relatively smaller work rolls deflecting due to the high rolling loads.

Strip thickness on a modern mill is controlled by an hydraulic gauge control system and strip profile by a combination of specified work roll and back-up roll cambers, roll bending and work roll shifting. Typically the mill would have hydraulic gauge control and work roll shifting on the last four stands and roll bending on all seven stands of the finishing tandem. On a four high mill the work roll bending is achieved by using hydraulic cylinders to apply separating forces between the work roll chocks ("crowned in" or " positive crown") or between the work roll and back-up roll chocks ("crowned out" or "negative crown") (Roberts, 1990). Schematic layouts of these two systems, Figure 2.2 (after Roberts, 1990), show how the positive crown system increases the total load between the work roll and back-up roll and raises the local loads near the ends of the back-up roll barrel. Back-up roll bending systems are

available and can be used to obtain a level of crown control not always achievable with work roll bending, but due to the high cost of the equipment and engineering problems the use of this method has declined (Eibe, 1990).

In hot strip mills the rolls experience cyclic temperature variations during the rolling process [Roberts 1990]. In order to limit the thermal fatigue damage to the rolls, water is used to cool the work rolls and in some cases both work rolls and back-up rolls. Work roll cooling is also used to provide more control of strip thickness and strip profile by limiting the effects of "thermal crown" (Ginsburg et al., 1997).

The effects of the presence of water as a roll coolant have been investigated in both the experimental simulations (Chapter 4) and mathematical modelling (Chapter 5).

The technical and production details of a typical hot strip mill and two cold reduction mills are given in the Appendix.

2.2. ROLL MANAGEMENT

2.2.1. *Back-up roll campaign*

As part of a comprehensive planned mill maintenance programme, all the back-up rolls in the finishing train of a hot strip mill are changed at the same time and the period in which the back-up rolls are in the mill is called the back-up roll campaign. The length of a campaign varies from mill to mill, but is generally one, two or three weeks. For the mill considered in this study the length of the campaign is currently three weeks and the tonnage rolled during a campaign is typically 170,000 tonnes.

An analysis of the mill traffic during a campaign has indicated that the number of loading cycles experienced by the back-up rolls varied from approximately 190000 at stand 1 to 3.5 million at stand 7.

After removal from the mill, the back-up rolls are inspected ultrasonically and also with a "Sarclad Rollscan" eddy current on-line inspection system. After inspection

the rolls are redressed in the roll shop by grinding. The amount of material removed per regrind is normally a minimum of 2 mm on diameter. However if, after checking the surface hardness along the roll barrel, any material is found to have a hardness in excess of 5 Shore C above the specified hardness, extra grinding is carried out to remove the work hardened material. In cases of severe bruising or cracking, the area in the vicinity of the damage is dished out to leave a maximum depth of damage of 0.3mm for a crack and 0.8mm for a bruise.

2.2.2. *Work roll round*

During a back-up roll campaign, the work rolls in the finishing train are changed periodically and the period that each full set of work rolls is in the mill is called a round. For the mill considered in this study, each round lasts for up to four hours and up to 2500 tonnes of material are rolled in each round.

During each round the surface quality of the strip is continuously monitored and if necessary intermediate work roll changes are carried out in the last two stands. Examination of the mill schedules, roll dimensions and other production data indicated that during a full campaign, all the back-up rolls would be in rolling contact with approximately 100 redressed (reground) work rolls. Also in the course of each round, each point on the back-up roll surface would experience between 2000 loading cycles (stand 1) and 35000 loading cycles (stand 7).

2.3. BACK-UP ROLL ECONOMICS

The full cost of an individual back-up roll during its working life is the sum of the costs arising from:

1. The initial purchase of the new roll.
2. The periodic removal from and refitting of the roll in the mill and the redressing and inspection of the roll carried out under the planned maintenance procedures.
3. Unplanned maintenance carried out on the roll.

4. The loss of production arising from unplanned maintenance or catastrophic failure of the roll.
5. Damage to the rest of the mill resulting from the failure of the back-up roll.

The cost of a back-up roll in terms of the cost per tonne of material produced is therefore given by equation (1).

$$C = \frac{C_{BR} + N\left(C_R + C_G\right) + C_{UM} + C_{LP}}{N \times T \times P} \tag{1}$$

where,

$$N = \frac{D_I - D_F}{\Delta_W + \Delta_D} \tag{2}$$

$$C_G = C_S + k\left(\Delta_W + \Delta_D\right) + C_I \tag{3}$$

and,

C = Back-up roll cost per tonne of strip produced in the life of the Roll (£/tonne)

C_{BR} = Initial cost of new back-up roll (£)

C_R = Total cost of removing from and refitting the back-up roll in the mill and transportation between mill and roll shop (£)

C_G = Cost of carrying out one redressing of the roll by grinding (£)

C_S = Cost of setting up the roll in the grinding machine (£)

C_I = Cost of inspection during redressing (£)

k = Cost of cleaning up worn areas and removing additional material affected by fatigue and other damage by grinding (£/diametral mm)

C_{UM} = Cost of unplanned maintenance attributed to the roll (£)

C_{LP} = Cost of loss of production attributed to the roll (£)

D_I = Initial barrel diameter of the new roll (mm)

D_F = Final barrel diameter when the roll is scrapped (mm)

Δ_W = Diametral amount of material affected by wear during a campaign (mm)

Δ_D = Additional diametral amount of material removed after clean-up for

wear (mm)

T = Length of a back-up roll campaign (weeks)

P = Average production rate during a campaign (tonnes/week)

If catastrophic failure of the roll does not occur, the normal working life of a back-up roll can be up to ten years. If this is the case and there are no other causes of unplanned maintenance, equation (1) reduces to equation (4).

$$C = \frac{1}{T \times P}\left[\left(\frac{C_{BR}}{D_I - D_F} + k\right)\left(\Delta_W + \Delta_F\right) + C_R + C_S + C_I\right] \qquad (4)$$

Inspection of equation (4) indicates that for any given mill, back-up roll and mill production rate, the cost of a back-up roll (in terms of the cost per tonne produced in the life of the roll) is determined by the length of the back-up roll campaign and the amount of material removed during redressing. Using nominal but realistic figures for the values of C_{BR}, k, C_R, C_S and C_I (confirmed by a private communication), a representative family of curves showing the trends as the above variables are changed is shown in Figure 2.3. Inspection of the appropriate curves for any particular mill will indicate which changes to the roll maintenance programme will give the most cost benefit when weighed against the risk of catastrophic failure.

It should be noted that any extension of the length of the back-up roll campaign would need to be a whole number multiple of the periodic planned mill maintenance programme during which the back-up rolls are changed.

Improvements in the design of back-up rolls should be aimed at preventing catastrophic failure and reducing the frequency of redressing and the amount of material removed during redressing by:

1. Reducing the degradation of the roll surface due to wear and rolling contact fatigue, in particular, minimising the penetration of surface initiated cracks into the deeper substrate.

2. Stopping the propagation of or reducing the propagation rate of both surface and subsurface initiated cracks.

2.4. WORK ROLL/BACK-UP ROLL INTERFACE LOADING PROFILES

2.4.1. *Introduction*

As part of the support for the programme of theoretical work, experimental simulations and assessment of field evidence it was necessary to establish representative and verifiable work roll/back-up roll loading profiles. After discussions with our industrial partners it was decided to concentrate the study on the loading and operating conditions arising in the early stands of a hot strip mill finishing train because the highest rolling loads are experienced in these stands.

The shape and magnitude of the normal load distribution profile at the work roll/back-up roll interface is determined by the applied rolling load, the roll bending forces, the original work roll and back-up roll contours, work roll and back-up roll wear, the changes in work roll shape due to uneven temperature distribution ("thermal crown"), the type of roll bending system employed and the relief profile applied to the ends of the back-up roll barrel.

2.4.2. *Methodology*

The accurate determination of loading profiles is difficult and very little verifiable quantitative information is available. With the co-operation and permission of our industrial partners detailed mill schedule and roll schedule information was obtained and with the other relevant operating information was processed using computer program "hspcb" which is an iterative hot strip profile coupled beam computer model. The model uses linear elastic theory, an empirical hot strength model for the strip properties and an Orowan-style rolling load model (Dieter, 1998) to calculate the work roll/strip contact forces and then iterates until all the contact forces and roll/strip deformations are compatible. This proprietary software which takes into account all the system variables except non-parallel back-up roll contours, has been

developed by VAI Industries (UK) Ltd and was used to produce the required representative work roll/back-up roll interface loading profiles.

2.4.3. *The effect of work roll wear*

The "start and end of round" roll profiles were obtained for several hot strip mill "high chrome" work rolls. These profiles demonstrated the effects of wear and thermal crown on the work roll contours. A typical example is shown in Figure 2.4. The representative wear trapezium shown in Figure 2.5 was used in the loading profile computations.

2.4.4. *The effect of thermal crown*

In general the effect of the work roll thermal crown is to counteract the effect of work roll wear and can therefore be considered to be protective. The size of the thermal crown is difficult to predict because it depends on the temperature variations in the rolls which in turn depends on the efficiency of the roll cooling system and such things as mill stoppages. The effect of the thermal crown was therefore been ignored in the estimation of the maximum contact loads.

2.4.5. *Relief profile at the ends of the back-up roll barrel*

On the mill studied, back-up roll relief profiles were applied to the ends of the back-up roll barrels. Back-up roll edge relief is used to reduce the high local contact loads, which can arise at the ends of the back-up roll barrel. Details of the edge relief profiles, which were used in the computations, are shown in Figure 2.6.

2.4.6. *Work roll and back-up roll dimensions*

The dimensions of the work rolls and back-up rolls were obtained from the manufacturers drawings (drawing numbers 4262 and 4832), which are shown in the Appendix.

2.4.7. *Loading profiles*

Mill and roll schedules were obtained for the rolling of 260 bars. These schedules indicated that the rolls in the first two stands experience the highest rolling loads in the finishing train. The scheduled rolling loads in the seven stands, for bar number 36, are shown in Figure 2.7.

Examples of the interface loading profiles obtained are shown in Figures 2.8-2.11. The loading profile shown in Figure 2.8 is for the second stand of the finishing train and shows the results for the loading conditions which resulted in the highest local interface loads (bar number 36) in the schedules supplied. This result represents the conditions arising with cold newly dressed work rolls and back-up rolls, a heavily loaded positive crown work roll bending system in operation and a relief profile applied to the edges of the back-up roll barrel.
The loading profile shown in Figure 2.9 (bar number 34) is for the same stand and similar strip width and shows the effect of rolling with much lower work roll bending forces.

In order to investigate the effect of work roll wear on the work roll/back-up roll loading profiles, the computer analyses were repeated with the wear trapezium shown in Figure 2.5 applied to the original work roll profiles. The effects of this work roll wear on the loading profiles already shown in Figures 2.8 and 2.9 are shown in Figures 2.10 and 2.11 respectively.

The maximum value of local interface load, shown in Figure 10 (12000 N/mm), was the highest obtained in the analyses and has been used as the basis for determining the value of the normal traction used in the experimental simulations (Chapter 4) and mathematical modelling (Chapter 5).

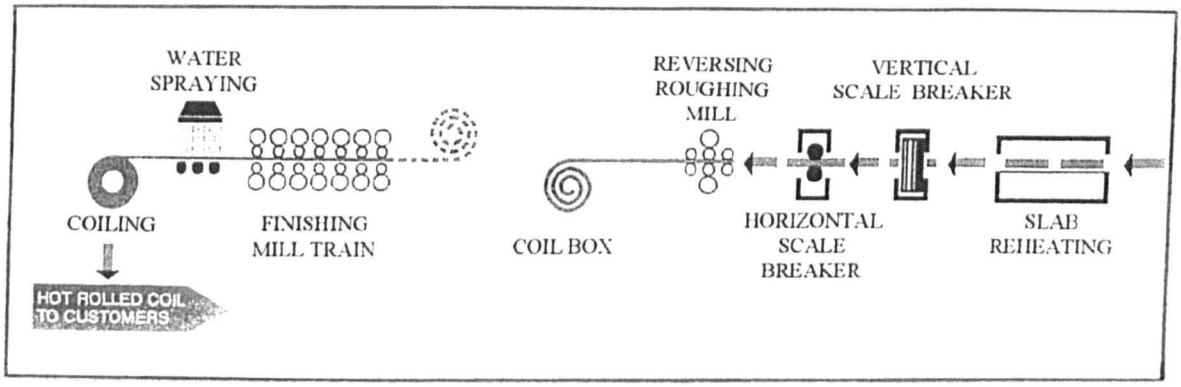

Figure 2.1 Schematic layout of a typical hot strip mill with a reversing rougher

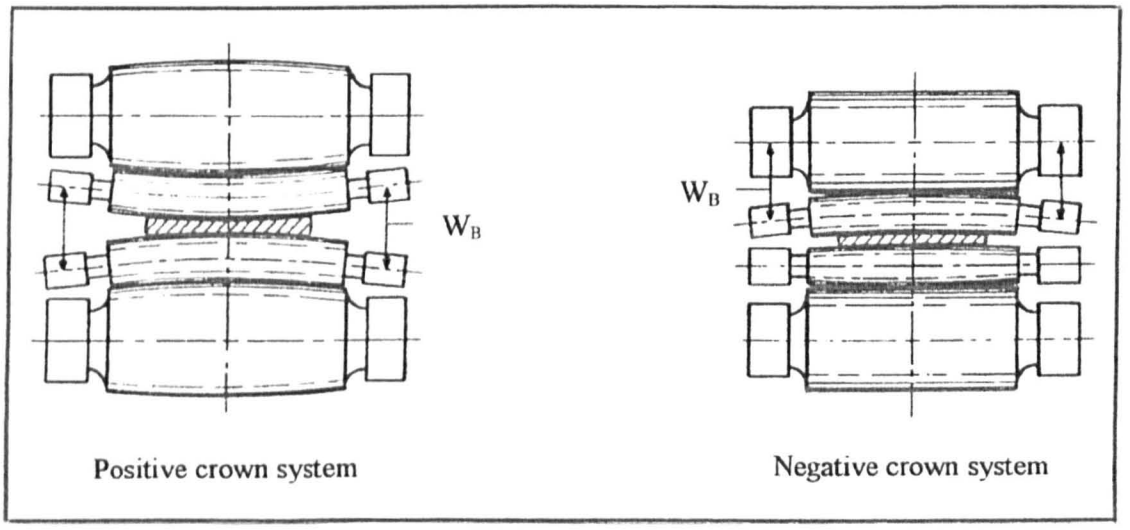

Figure 2.2. Work roll bending systems (after Roberts, 1990)

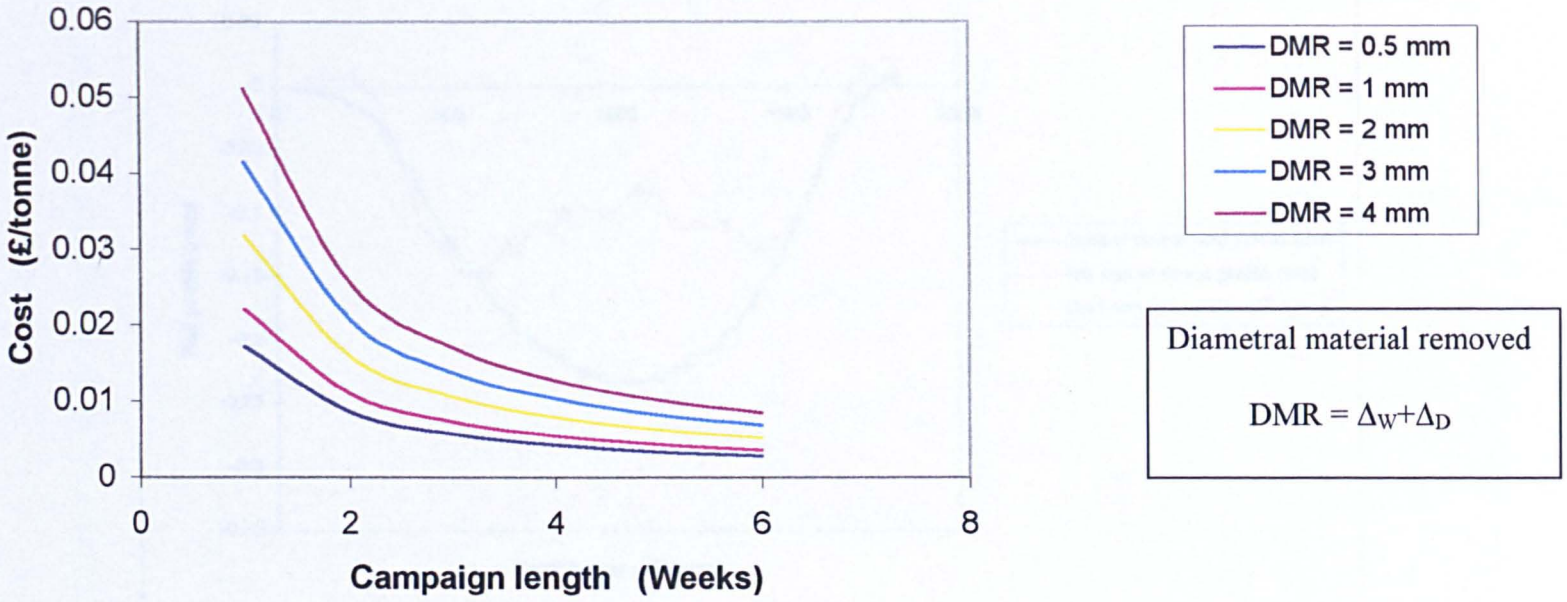

Figure 2.3. Back-up roll economic prediction model

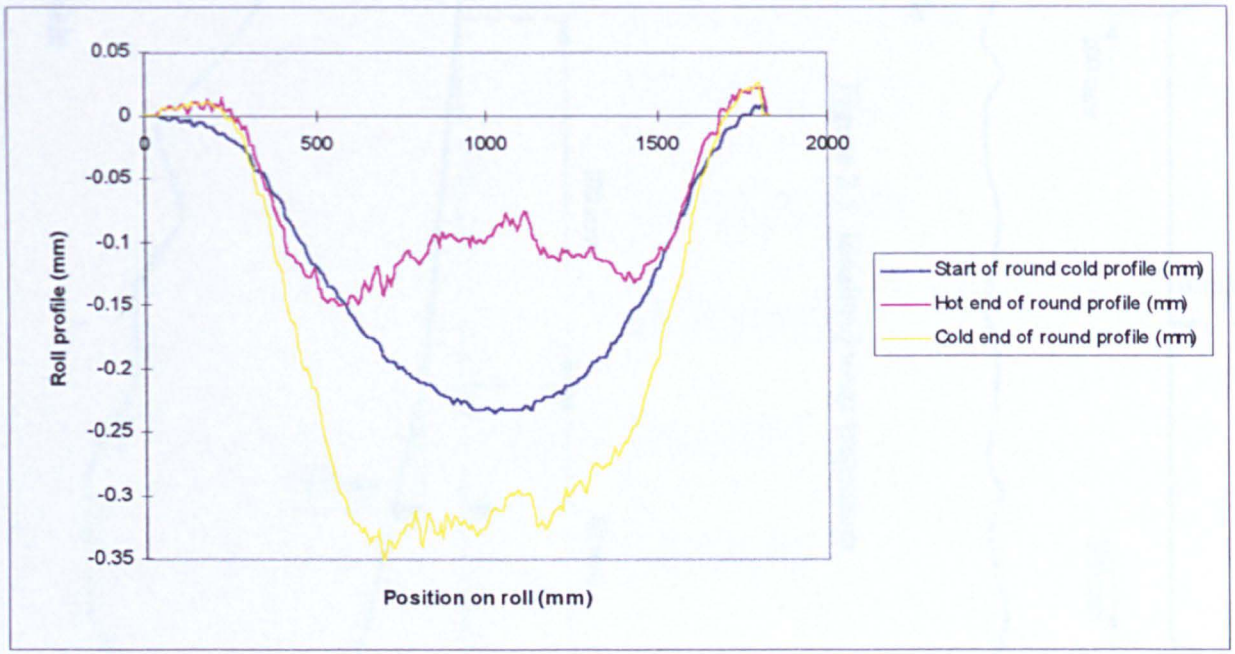

Figure 2.4. Work roll contours showing the effects of wear and thermal crown

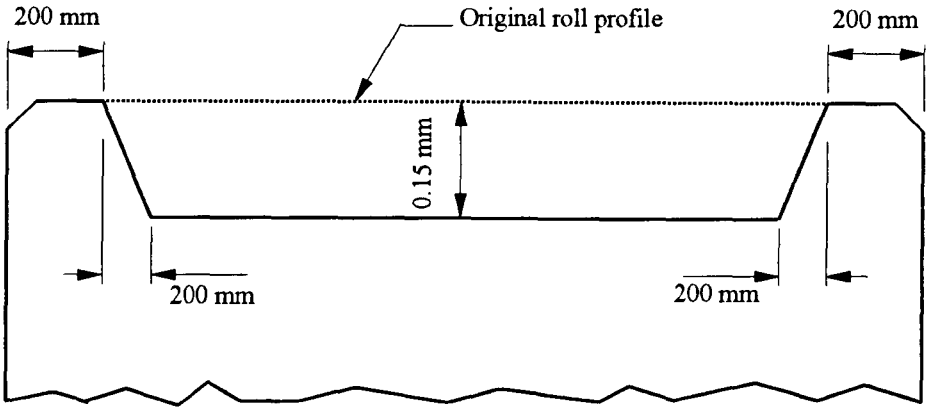

Not to scale

Figure 2.5. Idealised wear trapezium

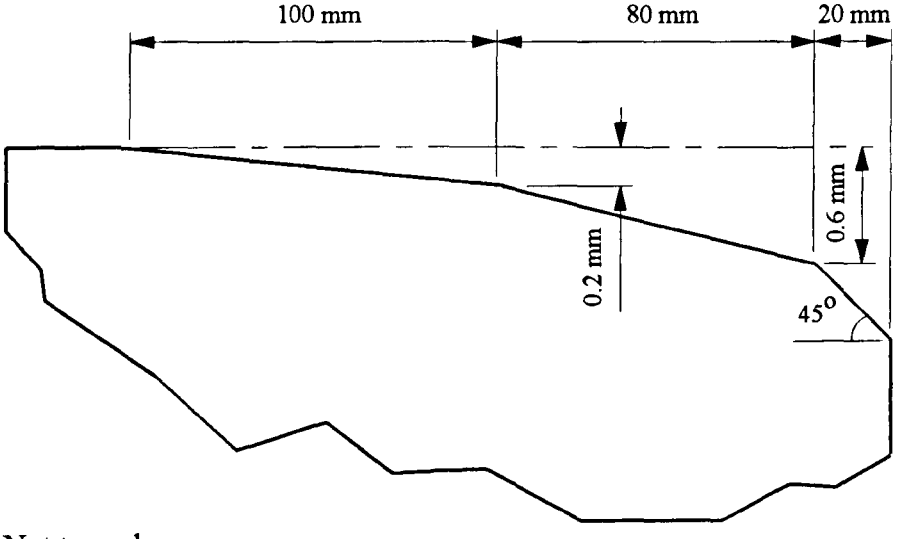

Not to scale

Figure 2.6. Relief profile applied to the edges of the back-up roll barrel

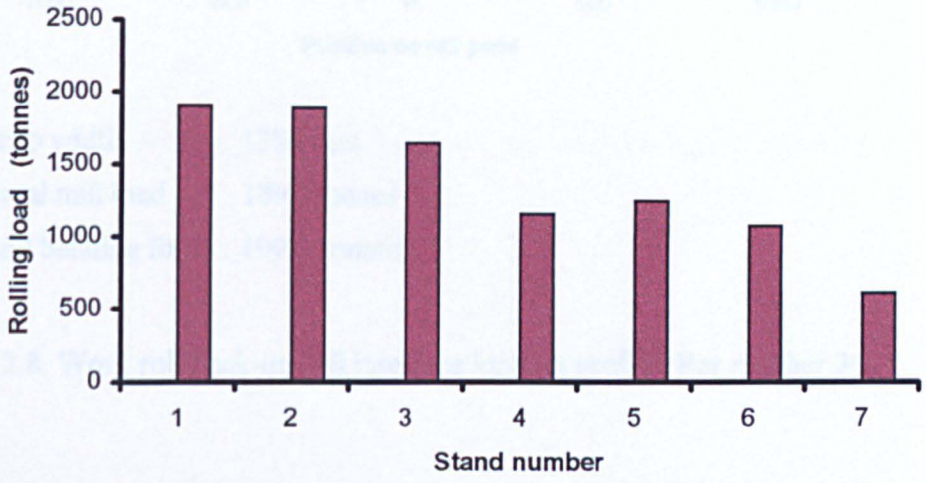

Figure 2.7. Scheduled finishing train stand rolling loads (bar 36)

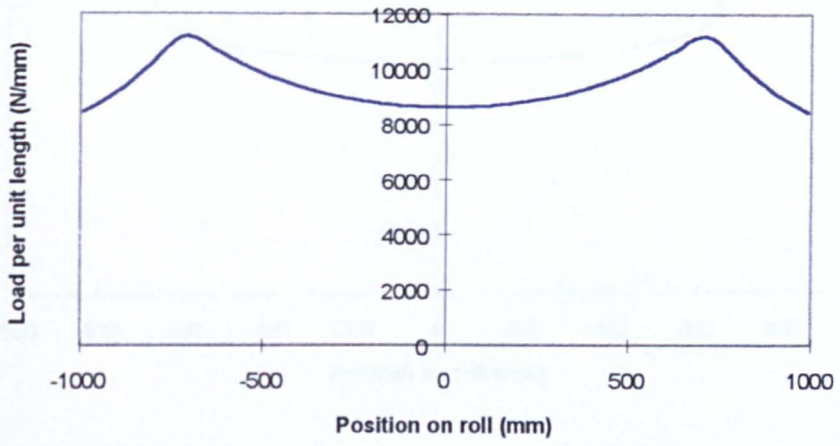

Strip width	1294 mm
Total mill load	1893 tonnes
Roll bending force	190.8 tonnes

Figure 2.8. Work roll/back-up roll interface loading profile (Bar number 36)

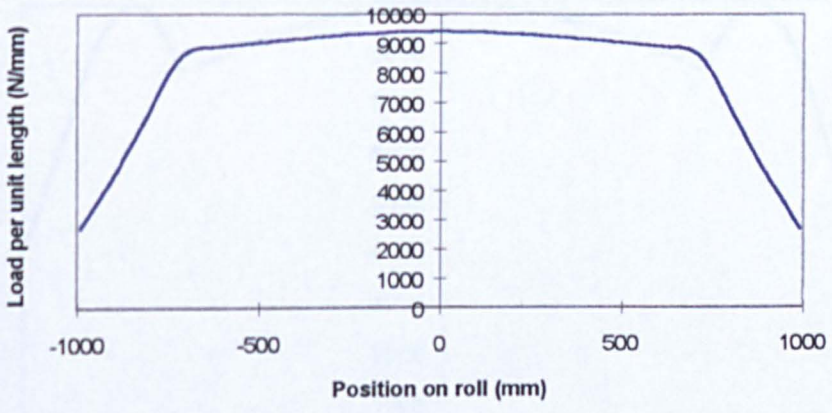

Strip width	1275 mm
Total mill load	1586 tonnes
Roll bending force	20.7 tonnes

Figure 2.9. Work roll/back-up roll interface loading profile (Bar number 34)

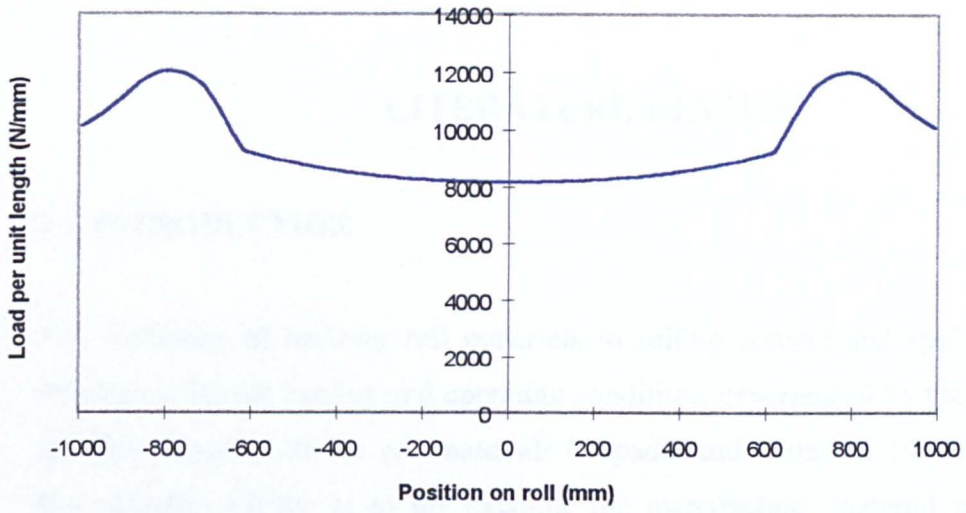

Figure 2.10. Work roll/back-up roll interface loading profile with wear trapezium applied to work roll

(bar number 36)

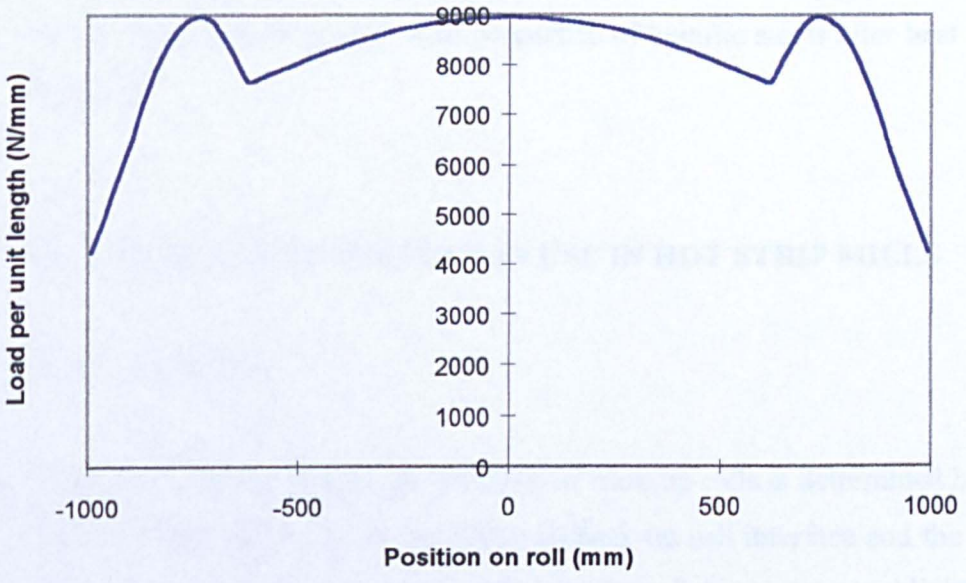

Figure 2.11 work roll/back-up roll interface loading profile with wear trapezium applied to work roll

(bar number 34)

Chapter 3

LITERATURE REVIEW

3.1. INTRODUCTION

The resistance of back-up roll materials to rolling contact and spalling failure is determined by the loading and operating conditions experienced by the back-up rolls and the properties of the roll materials (Kapadia and Marsden, 1997). The aim of this literature review is to the examine the manufacture, material properties and maintenance of current back-up rolls, the demands placed on the rolls, the responses of the rolls, the possible failure mechanisms which may be responsible for rolling contact fatigue failure and the experimental methods available for studying these failure mechanisms.

As the back-up roll steels considered in this project have essentially a bainitic microstructure in the working area of the roll barrel, the bainitic transformation, the main features of bainitic microstructures and the effect of micro alloying on the bainitic transformation and final properties of bainitic steels after heat treatment are described.

3.2. THE ROLLS CURRENTLY IN USE IN HOT STRIP MILLS

3.2.1. *Introduction*

The rolling contact fatigue performance of back-up rolls is determined by the loading and operating conditions at the work roll/back-up roll interface and the properties of the roll surfaces and materials. This section of the review highlights the factors affecting the properties of the rolls by considering the selection, specification and development of the roll materials and the manufacturing and maintenance of the rolls.

3.2.2. *Work rolls*

The three types of work roll used in hot strip mills are high chromium alloy iron (HI-Cr) and high speed steel (HSS) in the early stands and alloy indefinite chill iron (AIC) in the later stands. Ryu and Park (1999) describe the microstructures of both HI-Cr and HSS work rolls considered in their study as a tempered martensitic matrix and carbides, with the former having a lower volume fraction of finer carbides and smaller grain size. The carbides in the HSS were MC-type vanadium carbides (M = metal), M_7C_3-type chromium carbides and M_6C-type molybdenum carbides whereas the HI-Cr contained coarser M_7C_3-type chromium carbides.

The use of HSS rolls is now well established in the early stands of many hot strip mills throughout the world and in some mills trials are being carried out to introduce these rolls throughout the whole finishing train. In the first three stands, performance results show that rolls manufactured from the current HSS grades are capable of rolling more than three times the linear length with less than half the normal dressing when compared with HI-Cr rolls (Collins, 1996). The problems encountered with the introduction of HSS work rolls, the performance of the rolls and the benefits obtained from their introduction in the hot strip mills of the then British Steel and the hot mill at Dofasco are described by Beverley et al. (1999) and Kerr et al. (1999) respectively and Kudo (1999) describes the influence of composition, processing route and the resulting carbide morphology on the performance of HSS work rolls.

In spite of the potential benefits which can be obtained from the use of HSS work rolls, their introduction has raised mill concerns with regard to excessive wear on the back-up rolls and whether there is an increased risk of spalling due to rolling contact fatigue (Ohkomori and Kaku, 1997; Honeyman et al., 1996). In the light of these concerns and for relevance to modern industrial practice, it was considered desirable that the work roll test discs used in the experimental simulations reported here should be manufactured from HSS.

Cast work rolls used in strip mills can be manufactured from iron or steel using a single pour (a single material composition) or double pour (different materials for the

core and outer shell of the roll). The methods used to manufacture duplex or double poured rolls-core displacement, partition wall and centrifugal casting-are described by Scoular et al. (1990). Currently work rolls, where the outer shell of the barrel is manufactured from HSS, are manufactured by the Vertical Spin Casting (VSC) or by the Continuous Process Cladding method (CPC). In the former, the core of the roll is a cast nodular graphite iron and in the latter the shell material is cast onto a steel arbor (Collins, 1996).

The selection of the type of roll for a particular stand in the finishing train is dependent on the loading and operating conditions and the requirements for the quality of the surface finish on the strip. The rolls in the early stands are subjected to higher loads and temperature variations and must therefore be resistant to surface wear, thermal fatigue and oxide banding (Barbadillo and Trozzi, 1981). The rolls in the later stands are subjected to high abrasion and damage arising from mill incidents and must therefore be resistant to surface damage and have the ability to impart a good surface finish to the strip (Betts and Baxter, 1990).

In establishing the demands which are placed on back-up rolls, the most important work roll parameters have been considered to be the high roll hardness, surface roughness, the initial roll contours, the roll wear profiles, the "thermal crown" on the rolls and the effect of the roll materials on the tribological conditions and traction coefficients at the work roll/back-up roll interface.

Ryu and Park (1999) give representative figures for the bulk hardness of HSS and HI-Cr work rolls as 702 Hv (82 SHC) and 513 Hv (66 SHC) respectively.

Caithness et al. (1999) found that HSS rolls entering service in the former BSSP hot strip mill at Llanwern had ground finishes of the order of Ra 0.1 μm to Ra 0.7 μm. They also found that during a round, a smooth oxide layer built up to a roughness of Ra 0.2 μm to Ra 1.2 μm, which could then roughen up to a level of Ra 3.5 μm, before it began to breaking down later in the round. Unfortunately no information is presented regarding the time scale of these processes within each round. However it is clear that in each round the back-up roll surfaces are subjected to a period of

contact with the ground surfaces of the work rolls followed by periods of contact with oxidised or part oxidised surfaces with varying roughnesses. Barbidillo and Trozzi (1981) describe oxide banding as the surface deterioration of early finishing stand work rolls brought about by the tearing out of small pieces of roll metal. The failure process is characterised by the formation of fine surface fire cracks, followed by the formation and peeling off of a shiny black oxide band leaving a roughened surface, which is unsuitable for rolling. This characterisation suggests that even when oxide banding occurs, wear and rolling contact fatigue on the back-up roll surface will still be affected by the initial ground finish on the work roll surface for a substantial part of the round.

The possible influence of work roll hardness and roughness on the rolling contact fatigue and wear performance of back-up rolls is of considerable industrial significance and hence has been investigated, with the results presented Chapter 6.

Information on roll contours, wear profiles and "thermal crown" is commercially sensitive and is not generally available in published literature. This information was obtained from mill operators and has been previously discussed in Chapter 2.

3.2.3. *Back-up rolls*

3.2.3.1. Introduction

The back-up rolls used in hot strip mills fall into three groups: cast steel, forged steel (Ott, 1990 and 1996) and composite rolls with forged steel sleeves (Yanata, 1990). The work in this study has centred on solid rolls, so the remainder of this review has been focussed on the composition and processing route for cast and forged rolls.

The performance of back-up rolls has been improved in recent years by the introduction of "spall prevention" roll maintenance procedures (Honeyman et al., 1996; Kapadia and Marsden, 1997; Ohkomori et al., 1985), optimising of hardness levels (Barbidillo and Trozzi, 1981) and adjusting the alloy content of the roll material. It is clear therefore that work on establishing design criteria should be

aimed at investigating how changes in each of these areas may influence rolling contact fatigue performance.

3.2.3.2. Back-up roll material properties

Kapadia and Marsden (1997) present the results of an extensive range of tests, which provide the mechanical properties and describe the microstructural features of several back-up roll steels. The data presented on the tensile and fatigue properties and fatigue crack growth have been used in the quantitative model for predicting the morphology of surface initiated rolling contact fatigue cracks in back-up roll steels, presented in Chapter 5.

3.2.3.3. Back-up roll composition

The chemical compositions of a representative sample of steels used in an evaluation exercise for differentially hardened forged steel rolls are shown in Table 3.1 (Honeyman et al., 1996) and typical specifications for differentially hardened cast steel rolls together with available hardness ranges are shown in Table 3.2 (Cox, 1996).

Honeyman et al. (1996) describe the effects of carbon and other alloying elements, particularly chromium, on the wear resistance, hardening properties, fracture toughness and fatigue strength of the shell material of the roll barrel. The main conclusions from this work were:

1. Increasing carbon reduces the hardenability of both 3CrMo and 5CrMo back-up roll steels due to the formation of carbides, which deplete the matrix of alloying elements
2. The presence of carbides improves the wear resistance but has an adverse effect on fatigue and fracture toughness properties of roll steels, which could lead to excessive spalling
3. Increasing chromium from Wt 3% to Wt 5% has a beneficial effect on both wear resistance and toughness for a given carbon content and leads to an improved performance for back-up rolls in operation

4. Wear resistance is not directly proportional to surface hardness and is more sensitive to composition and microstructure

The improvement of wear performance by increasing the carbon and chromium content of back-up roll steels was also shown by Ohkomori et al. (1987) and Ohkomori and Kaku (1997) have investigated the effects on wear resistance and toughness of increasing the matrix strength by the addition of molybdenum, vanadium and niobium.

Following the results obtained from earlier work, in recent years developments in the design of back-up roll steels have centred on increasing the chromium content of the material in order to improve wear resistance without compromising the other mechanical properties. The effect on in-service performance of increasing the chromium content from 3% to 5% in differentially hardened forged back-up rolls is discussed by Marston et al. (1999) and the development of a cast 5% chromium back-up roll is described by M^{c}Corry (1999). The improvements in in-service and laboratory performance exhibited by the 5% chromium material highlighted in these studies, are attributed to low level of primary alloy carbides (fatigue performance) (M^{c}Corry, 1999) and the high level of fine complex alloy lathe secondary carbides (wear performance) produced in the bainitic microstructure during the tempering phase of the heat treatment (Marston et al., 1999; M^{c}Corry, 1999). The 5% chromium rolls also offer the advantage that higher neck and journal strengths can be achieved (Marston et al., 1999).

Due to the availability of existing field evidence as a basis for establishing design criteria for the future design of back-up rolls, it was decided to manufacture the back-up roll test disc specimens from a standard 3% chromium back-up roll steel.

3.2.3.4. Back-up roll manufacture

The back-up rolls considered in this study, whether forged or cast, were produced by a single pour cast (Scoular and McPate, 1990; Cox, 1996; Kapadia and Marsden, 1997) followed by a preliminary heat treatment, pre-machining, differential hardening, tempering and final machining.

The preliminary heat treatment consists of a low temperature anneal to remove excess hydrogen by solid state diffusion and a normalising and temper treatment to homogenise the microstructure and achieve the bulk properties of the roll. The differential heat treatment is carried out in a gas fired "Selas" furnace and the subsequent tempering treatment is carried out immediately after the quench to optimise the microstructure to produce the required body hardness (up to 75 SHC with 5% chromium content) (Marston et al., 1999).

Inspection of the available literature concerning bainitic back-up roll steels indicated that carbides are produced in each part of the manufacturing process. For the sake of clarity in this study the carbides produced at different stages in the process route should be classified as:

1. Casting – primary carbides
2. Hardening – secondary carbides
3. Tempering – precipitation carbides

3.2.4. *Roll maintenance*

3.2.4.1. Introduction

In parallel with the significant technical advances which have been made in rolling technology in the last twenty years, very important improvements have taken place in roll grinding equipment and the operation of the roll shops which service hot strip mills. The main areas in which these improvements have taken place are:

1. The use of non destructive testing and automated inspection
2. The introduction of automated roll grinding
3. The monitoring of roll shop performance and computerisation of roll shop management (this is particularly relevant for producing data for use with the economic model (Section 2.3)
4. The reduction in staffing and the move towards unstaffed roll shops

3.2.4.2. Roll inspection

The detection of surface flaws in rolls can be carried out using magnetic particle, liquid penetrant, ultrasonic and eddy current inspection techniques. Near the surface linear discontinuities can also be detected using magnetic particle inspection but internal flaws are detected using ultrasonic techniques. Shelestowsky (1990) describes in detail the procedures carried out for all these techniques and identifies the types of flaw which can detected using each method and Corallo (1999) describes how roll surface inspection was automated using eddy current systems.

3.2.4.3. Automated roll grinding

To ensure the dimensional accuracy and surface integrity of each roll supplied to the mill the grinding must be carried out using fully automated roll grinders which can inspect the finished roll and produce a test certificate for each roll ground. Boyd and Maddalena (1990) describe the installation and operation of an automated roll shop and give details of the type of information recorded for each roll ground.

Corallo (1999) describes the moves towards fully automated and almost unmanned roll shops and Beverley et al. (1999) present details of the computerised roll shop management system used in the then British Steel hot strip mill at Port Talbot Works.

3.3. BAINITIC STEELS

3.3.1. *Introduction*

"During the late 1920s in the course of pioneering work into the isothermal transformation of austenite at temperatures above that at which martensite first forms and below that at which fine pearlite is produced, Davenport and Bain identified a microstructure which was different from either pearlite or martensite produced in the same steel. The process which produced this microstructure is known as the bainitic transformation and the resulting microstructure is called bainite" (Bhadeshia, 1992).

The difference between the microstructures of pearlite, the two forms of bainite and martensite are shown in Figure 3.1 (Bhadeshia, 1992)

The bainitic transformation, which can also occur in non-ferrous metals and other materials, has a great influence on the mechanical properties of ferrous alloys. For example, in low carbon steels, a useful combination of strength and toughness can be obtained after this transformation.

The aim of this part of the review is to produce a general overview of the nature of bainitic steels, which would examine the role of alloying elements in the processing of bainitic steels, identify the microstructural features which may influence the performance bainitic steels in this case and characterise the material in order to link mechanics to microstructure as discussed in Section 6.5

3.3.2. *The bainitic transformation*

3.3.2.1. The transformation mechanisms

The proposed models for the bainitic transformation fall into two broad categories:

(1) displacive transformation involving a martensite-like shear process of at least the substitutional atoms and often the interstitial atoms as well and (2) diffusional transformations.

Reynolds et al. (1991) present a summary of the present diffusionist views on bainite, discussing both the similarities and differences between the two mechanisms. They take particular care to define the shear mechanism in this case as the co-ordinated movement of atoms across an interface boundary consisting of glissile dislocations or thin, alternately twinned regions, martensite being the prototype for this mode of transformation. An examination of the requirements of the phenomenological theory of martensite crystallography led them to conclude that, although the diffusional growth mechanism does not explain all the complex phenomena associated with bainite, the shear growth mechanism fails to account for many of them.

Ochmori and Maki (1991) in an overview of the bainitic transformation in favour of the displacive mechanism took the opposite view and concluded that, although various aspects can be explained in terms of both mechanisms, many characteristic properties of bainite are better understood on the basis of the displacive model. The main characteristics cited were surface relief, the morphologies, the α/γ orientation relationships, the characteristics of the C-curves, the morphologies of cementite precipitation and the incomplete transformation.

Yamamoto et al. (1995) have studied the effect of austenitic grain size and deformation in the un-recrystallized austenitic region. In an interesting contribution to the argument, they concluded as a result of this study, that increasing the extent of austenite grain boundaries did not contribute to the growth of bainitic ferrite, thus indicating the intensive involvement of the displacive mechanism in the transformation. In contrast however, other researchers have found that the rate of transformation decreases with an increase in grain size (Bhadeshia, 1992).

It is evident from the literature that a rigorous and universally accepted model for the transformation has yet to be produced, but the two separable stages in the process of producing this non-equilibrium microstructure are well established and these are discussed in the next section.

3.3.2.2. Bainitic ferrite

It is well known that the bainitic transformation occurs in two separable stages, that of the formation of ferrite followed by the precipitation of carbides. Both the upper and lower forms of bainite consist of aggregates of laths or plates of ferrite in packets or sheaths, separated by residual phases of un-transformed austenite, cementite and martensite, the latter two forming subsequent to the formation of the bainitic ferrite. The rate of the bainite reaction needs to be considered in terms of a number of distinct events as shown in Figure 3.2 (Honeycombe and Bhadeshia, 1995). The sub-units or laths nucleate at the grain boundaries and lengthen at a decreasing rate until the growth is stopped by plastic deformation within the austenite (Bhadeshia, 1992).

New sub-units nucleate at the tips of the arrested sub-units and thus the packet or sheaf structure develops as the transformation continues.

3.3.2.3. The transition from upper to lower bainite

As the isothermal transformation temperature is reduced, lower bainite is obtained in which carbides precipitate within the ferrite. When this occurs there is a corresponding reduction in the precipitation from the austenite between the ferrite lathes. The transition from upper to lower bainite, which can be explained in terms of rapid tempering processes occurring after the growth of supersaturated plates of bainite, is shown schematically in Figure 3.3 (Honeycombe and Bhadeshia, 1995).

The change from upper bainite to lower bainite is best explained by reference to the TTT diagram, which consists of two separate C-shaped curves. An example of the TTT diagram for an alloy steel is shown in Figure 3.4 (Thelning, 1975). The characteristic bay can be seen in the region of the B_s temperature.

Details of typical ferrite packets in lower bainite are shown in Figures 3.5 and a schematic representation of a plate and a lath are shown in Figure 3.6 (Honeycombe and Bhadeshia, 1995).

3.3.2.4. Carbide precipitation

Alongside the morphology of the ferrite laths and packets, the carbide phases play an important role in the mechanical properties of bainitic steels.

In lower bainite two kinds of carbide are precipitated. As in upper bainite there is some precipitation of carbides from the enriched austenite between the ferrite platelets or laths. In addition there is usually a fine dispersion of plate-like carbides within the lenticular ferrite plates (Bhadeshia, 1992). The inter-plate carbides in lower bainite are finer than those in upper bainite, giving the more highly refined microstructure, which normally results in a material with higher strength and toughness (Honeycombe and Bhadeshia, 1995). This point has important implications for this project because it suggests that a lower bainitic microstructure

in the working area of the roll barrel should be the aim of the processing route when manufacturing back-up rolls.

3.3.3. *The role of alloying elements in steels*

Alloying elements have played an important part in the development of back-up roll steels, but before considering the specific effects of micro alloying on bainitic steels, it is useful to consider the alloying of steels in general. Cottrell (1995), in an overview of the ways in which the properties of steels can be modified by alloying, identifies the six main features which can be developed by alloying as: hardenability, formation of carbides, solubility, stabilisation of austenite or ferrite, corrosion resistance and precipitation hardening. In bainitic back-up roll steels chromium is the most important alloying element.

3.3.4. *The effects of micro alloying on the bainitic transformation*

Although carbon has the greatest effect on the range of temperature over which upper and lower bainite occur, other alloying elements have substantial effects.

Bhadeshia (1992) presents an empirical equation (derived by Steven and Haynes 1956) for expressing the bainite start temperature as a function of the steel chemistry for a range of wrought steels. The equation is shown below:

$$B_s\ ^{\circ}C = 830 - 270w_C - 90w_{Mn} - 37w_{Ni} - 70w_{Cr} - 83w_{Mo}$$

where w_i is the wt% of the element i which is in solid solution in the austenite.

Increases in the tensile strength of low carbon low alloy steels which may be obtained by reducing the "temperature of maximum rate of transformation" (Irvine et al., 1957) or the B_s temperature (Coldren et al., 1969) are highlighted by Bhadeshia (1992).

Bodnar et al. (1989) determined the partial continuous cooling transformation (CCT) diagrams for a range of low carbon (0.14-0.29 C) Fe-Ni-Cr-Mo-C high temperature

bainitic steels and found that the upper temperature at which bainite formed as a function of cooling rate was insensitive to the rate of cooling. This is in fact expected when no other transformation precedes bainite, since its C curves in TTT diagrams have a flat top (Bhadeshia, 1992). Inspection of the CCT diagrams for these steels also indicates that over the range of cooling curves presented the final microstructure may be bainitic or a mixture of ferrite and bainite. In the latter case the bainite would be expected to contain a higher level of carbon. This work highlights the influence of manganese, sulphur and a range of impurities on the final microstructure and mechanical properties.

It is well known that carbon is a very good austenite stabiliser but there are limits to the proportion of carbon in the steel because of the need to ensure the mechanical properties of the steel by controlling the fraction of carbides in the final microstructure. This raises one of the needs for the other alloying elements.

The addition of the other alloying elements also usually retards the ferrite and pearlite reactions and depresses the bainite transformation to lower temperatures. Although the TTT curves for many alloy steels show well separated C curves for the pearlite and bainite reactions, the proximity of the martensite reaction makes it difficult to obtain a fully bainitic microstructure (Honeycombe and Bhadeshia, 1992).

Two very effective alloying elements for promoting the bainite transformation without enhancing the martensite reaction are molybdenum (0.5 wt%) to promote the bainite transformation and boron (0.002 wt%) to retard the ferrite reaction.

The effect of the alloying elements on the bainite transformation can be seen by examination of the schematic diagrams shown in Figures 3.7, 3.8 and 3.9 (Honeycombe and Bhadeshia, 1995). Figure 3.7 shows how in plain carbon steels the bainitic reaction is kinetically shielded by the ferrite and pearlite reaction and demonstrates the need for the use of alloying elements. Figure 3.8 shows how in a low alloy steel, the ferrite and pearlite reactions are retarded and the bainite reaction depressed to lower temperatures. Finally Figure 3.9 shows the effect of boron on the bainite reaction in a low carbon, 0.5wt% manganese steel.

3.3.5. *The effects of micro alloying on the properties of heat treated bainitic steels*

3.3.5.1. The tempering of bainitic steels

The tempering of bainite depends to a large extent on the excess of carbon in solution. Most of the carbon in transformed bainite is in the form of cementite particles in low carbon steels or transition carbides in higher carbon steels. Also the extent of the changes during tempering depends on the amount of the recovery during the transformation process. For these reasons there are often only minor changes in the recovery, morphology or the carbide particles (Honeycombe and Bhadeshia, 1995).

In contrast with martensitic steels, small variations in carbon concentration have little effect on the tempering of bainite (Honeycombe and Bhadeshia, 1995). This is a direct effect of the small amount of carbon left in solid solution and thus the strengthening effect, after the bainitic transformation. This means that the tempering response will be more insensitive to the bulk carbon concentration.

In the early stages of the tempering process there is a drop in hardness and strength. In alloy steels if tempering is continued, alloy carbides eventually form at the expense of cementite and there is an increase in hardness. If the heat treatment is further continued, growth and coarsening reactions make these carbides less effective in hindering dislocation motion and minor changes in both hardness and strength occur monotonically with time. Major changes in strength only occur when the bainite plate microstructure coarsens or recrystallizes into one of equiaxed grains of ferrite (Honeycombe and Bhadeshia, 1995).

It would appear from this discussion, that apart from the fraction of carbon content in solid solution, the alloying element composition of bainitic steels does not have a significant effect on the early part of the tempering process. However the alloying elements do have a significant effect on the final material properties as a result of the secondary hardening processes, which arise due to the precipitation of alloy carbides.

3.3.5.2. Secondary hardening

Bainitic steels containing strong carbide forming elements such as chromium, vanadium, molybdenum and niobium undergo secondary hardening during annealing at high temperatures. Secondary hardening occurs when fine alloy carbides form at the expense of cementite (Bhadeshia, 1992).

Secondary hardening peaks are not always observed in the heat treatment of alloyed baintic steels but all experimental evidence indicates that the tempering resistance of bainite is improved by the addition of alloying elements (Bhadeshia, 1992).

3.3.6. *The characterisation of bainite*

The microstructure of bainite is complex and difficult to characterise, but Gladman and Pickering (1983) describe the main features as:

1. Packets of lath-like ferrite grains, with low misorientation of grains within a packet
2. High angle packet and prior austenite grain boundaries
3. A variable dislocation density, with dislocation arrays between ferrite laths
4. Large carbides at ferrite lath, packet and prior austenite grain boundaries and carbides within the ferrite laths in lower bainite
5. Alloy-enriched ferrite islands or high carbon bainite, martensite or retained austenite between ferrite laths
6. Solid solutions of interstitial carbon and nitrogen and substitutional solutes

Bhadeshia (1992) discusses the approaches used to characterise and measure the grain size of bainite, but suggests that the specific manner in which the grain size of an anisotropic structure is defined, is somewhat dependent on the application.

For the purposes of this work it was decided that the back-up roll material would be characterised by the ability of the microstructure to resist fatigue crack propagation. The assumptions made and the influence of particular microstructural features are discussed in detail in Chapters 5 and 6.

3.3.7. *Conclusions*

1. Apart from carbon, the micro alloying elements do not determine the mechanisms of the bainitic transformation, but they do have an effect on the initial strength and toughness of the steel after quenching.

2. The micro alloying elements have a substantial effect on both the kinetic and temperature characteristics of the bainitic transformation.

3. Apart from the fraction of the carbon content in solid solution the alloying element composition does not have a significant effect on the early part of the tempering process.

4. The micro alloying elements have a significant effect on the final material properties of baintic steels as a result of secondary hardening processes, which arise due to the precipitation of alloy carbides.

5. It is clear that the bainitic transformation in ferrous alloys can provide a range of microstructures with varying mechanical properties and that it may therefore be possible to design a back-up roll material to provide an optimum balance between resistance to surface wear and rolling contact fatigue.

6. If the "Selas" heat treatment process places constraints on the cooling rates that can be achieved during the heat treatment of back-up roll steels, micro alloying may be the means of obtaining the required strength for the material by altering the B_s start temperature.

7. In order to accurately predict the final microstructure of bainitic back-up roll steels the following are required:

   - The possible range of cooling curves in the quenching stage of the "Selas" heat treatment process.

- CCT curves for the appropriate steels over the range of cooling curves.

8. A material with a flat B_s start temperature, over the range of cooling curves obtainable in the "Selas" heat treatment process, would be desirable for controlling the microstructure of the material in the working area of the back-up roll barrel.

9. The high misorientation (angle) ferrite packet and prior austenite grain boundaries should provide the main barriers to fatigue crack growth in bainitic steels.

3.4. THE DEMANDS PLACED ON BACK-UP ROLLS

3.4.1 *Introduction*

The demands placed on back-up rolls arise from the loads experienced by the rolls during the normal rolling process, the effects of uncontrolled incidents during mill operations (Kapadia and Marsden, 1997; Ohkomori et al., 1987), the environmental operating conditions and the presence of residual stresses (Roberts, 1990 and Kapadia and Marsden, 1997), the tribological conditions at the work roll/back-up roll interface and the presence of non-metallic inclusions and microstructural inhomogeneities in the roll material (Kapadia and Marsden, 1997).

3.4.2. *Loads acting normally to the contact surface*

As discussed in Chapter 2, the total load acting normally to the surface at the work roll/back-up roll interface is determined by the rolling load, the total roll bending force and the type of roll bending system employed.

The shape of the load distribution profile is determined by the applied loads, the original roll contours, roll wear, the changes in roll shape due to uneven temperature distribution ("thermal crown"), the effect of applying roll bending and the relief profile at the ends of the back-up roll barrel.

The benefits of applying back-up roll edge relief profiles to reduce localised contact loads and stresses are discussed by Kneppe and Hormes (1996) and Easter (1996) and are shown schematically in Figure 3.10 (Kneppe and Hormes, 1996).

Kneppe and Hormes (1996) also discuss the shape of the load distribution profiles for a variety of work roll/back-up roll combinations including continuously variable contour (CVC) rolls, but give very little quantitative information. They claim that the use of CVC rolls changes the shape of the loading profile considerably, but the maximum value of the distributed load is only increased slightly. Schematic examples of the loading profiles for six roll combinations are shown in Figures 3.11a and 3.11b (Kneppe and Hormes, 1996). The loading profiles presented for the conventional roll combinations do not appear to include the effects of work roll bending.

Ohkomori et al. (1987) used the mean value of distributed load to estimate contact stresses and then applied stress increase ratios to determine the maximum value of contact stress near the roll edges whereas Kapadia and Marsden (1997) and Easter (1996) appear to have used the mean value of distributed load in their calculations of contact stresses. The magnitudes of the applied interface loads used by these authors were similar to those presented in Section 2.4.7, Chapter 2.

3.4.3. *Loads acting tangentially to the contact surface*

When considering the dynamics of the motor/drive/work roll/back-up roll system it is evident that the motion of the back-up roll is determined by its own inertia and the tangential friction forces which occur at the work roll/back-up roll interface. During mill operations the rolls will therefore experience conditions of rolling-sliding contact.

Kapadia and Marsden (1997) and Ohkomori et al. (1987) identify the thermal damage arising from excessive roll slip ("skidding") and excessive mill loads ("squeezing") during mill incidents, as the main cause of crack initiation at the roll surface, but do not consider the effects of the friction forces prior to or at very low levels of slip. In addition to the direct effects of the friction forces which arise due to

excessive roll slip, thermal shock leads to metallurgical damage (Ohkomori et al., 1987) and plastic deformation due to the high levels of tensile and compressive stresses produced by the rapid heating and cooling of the roll surface (Roberts, 1990 and Ohkomori et al., 1987) Nayak and Paul (1979) do not consider the tangential friction forces at all in their analysis of spalling failure.

Even if no slip occurs, it must be assumed that these friction forces can reach the limiting value and should therefore be considered when determining the stress fields on and below the contact area.

It can be shown theoretically that when a tangential traction acts on the contact area, shear stresses are produced on the contact surface and a tensile stress exists at the leading edge of the contact (Johnson, 1985)

3.4.4. *The presence of water as a roll coolant*

The water used for roll cooling provides a lubricating fluid for the work roll/back-up roll contact. Johnson, 1985 and Williams, 1994 present analyses and discussions concerning the lubrication conditions which can exist at the line contact of non-conforming bodies, but more research is needed to establish the lubrication conditions which exist in the particular case of the work roll/back-up roll contact.

For the purposes of this work it was concluded that the presence of water at the work roll/back-up roll interface would affect the value of the coefficient of traction and would have an important influence on the propagation of rolling contact fatigue cracks.

Values for the coefficients of traction at work roll/back-up roll interfaces are not available in literature. The values of the traction coefficients at a water lubricated twin disc line contacts have been determined experimentally as described in Chapter 4 and it has been assumed that these values would apply at the contact interface of work roll/back-up roll pair.

The effect of the presence of water on the propagation rolling contact fatigue cracks in back-up rolls has not been considered in any of the literature. Its possible influence is discussed further in the section on failure mechanisms (Chapter 3, Section 3.7.3) and is included and investigated in the qualitative and quantitative models presented in Chapter 5.

3.4.5. *Residual stresses*

As a result of the roll metallurgy and the manufacturing processes, residual stresses remain in the finished rolls (Roberts, 1990). The magnitude and distribution of these stresses can be complex, but in general the stresses in the outer shell of the roll barrel are compressive in the circumferential and longitudinal directions and tensile in the radial direction, with the radial tensile stress falling to zero at the back-up roll surface.

The determination of the magnitude of these stresses, particularly radial stresses, is difficult but Kapadia and Marsden (1997) and Roberts (1990) give some representative figures and discuss their effect on the spalling behaviour of back-up rolls. Kapadia and Marsden (1997) suggest that surface residual stresses in the longitudinal and tangential directions, determined by hole drilling and other methods, are generally compressive with typical values in the range 275 to 415 MPa. Residual stresses in the radial direction can only be determined by finite element modelling and Kapadia and Marsden (1997) indicate that they are tensile and lower in magnitude than the longitudinal and tangential stresses. Li (1997) used finite element thermo-elastic-plastic modelling of the heat treatment processing of large steel rolls to determine residual stresses remaining in the rolls after manufacture. The results demonstrate the complexity of the residual stress fields and predict some stresses of the same order as those suggested by Kapadia and Marsden (1997).

For the purposes of modelling the propagation of surface initiated rolling contact fatigue cracks, the compressive residual stresses at the roll surface have been assumed to be beneficial. Conservatively, residual stresses have therefore not been included in the early part of the failure models.

3.4.6. *The tribological conditions at the work roll/back-up roll interface*

Information on the tribological conditions at the work roll/back-up roll interface and values for traction coefficients are not available anywhere. The latter have been determined in the laboratory using test disc specimens under conditions of water lubrication and the values have been assumed to be applicable to the work roll/back-up roll interface.

3.4.7. *Non-metallic inclusions and microstructural inhomogeneities*

It is well known that subsurface cracks tend to initiate at angular non-metallic inclusions and microstructural inhomogeneities (Kapadia and Marsden, 1997; Johnson, 1989; Brooksbank and Andrews, 1970). The elimination of such defects is therefore considered to be a basic design and manufacturing criterion for improving the rolling contact fatigue resistance of roll materials.

Brooksbank and Andrews (1970) estimated the residual stress distributions surrounding inclusions in bearing steels and suggest that these stresses may be responsible for matrix yielding and crack initiation. The main result of this work was the identification of the types of inclusion which give rise to the highest stresses and the conclusion that manganese sulphide does not affect fatigue properties.

As the use of clean steel and high integrity manufacturing processes have reduced the incidence of such defects (Honeyman et al., 1996; Johnson, 1989), it has been assumed for the purpose of the project that rolling contact fatigue cracks initiate only at the surface of the rolls. This assumption is further supported by claims by many authors that the use of modern roll dressing techniques, in which between one and two millimetres of material are removed from the roll surface, has substantially reduced the incidences of spalling failure. This indicates that in many cases cracks must initiate at or very close to the surface. The presence of microstructural defects may however assist the propagation of surface initiated cracks, even in fairly quiescent zones.

3.4.8. *Mill incidents*

In view of the fact that excursions outside normal operating conditions occur during mill incidents, it was decided that a damage tolerance approach should be adopted when establishing criteria for the design of back-up roll materials.

3.5. CONTACT MECHANICS

3.5.1. *Introduction*

The study of contact mechanics centres on the non-conformal contact of two elastic half spaces. In this study, the contact between the work roll and back-up roll has been considered to be the particular case of the two dimensionally loaded line contact of two cylindrical elastic half spaces over a long strip of width *2b*, Figure 3.12a. The assumption has also been made that the deformations are under conditions of plane strain and the normal assumptions of Hertzian theory apply (Johnson, 1985; Timoshenko and Goodier, 1970). As a result of the literature studies in Section 3.4, it has been assumed that forces are transmitted across the contact area by a normal traction due to pressure and a tangential traction due to friction.

Hertzian theory was developed for clean, smooth, unlubricated contacts with normal tractions, but the results are also found to hold good for conditions of boundary lubrication. Developments of the theory also allow for tangential tractions due to friction (Johnson, 1985; ESDU International-London, 1995).

The loading conditions experienced by the back-up rolls during service can result in plastic deformation of the material at the contact surface and also of material in the substrate below the contact area. No adjustments can be made to the theory to take this plasticity into account, but the shakedown processes will reduce its effects (Johnson, 1989). Hertzian theory is the simplest and most appropriate theory available for determining the contact parameters required for the experimental simulations and theoretical analyses and has therefore been used in the project.

3.5.2. *Stresses arising from the normal Hertzian pressure distribution*

The normal elliptical pressure distribution on the contact surface given by Hertzian theory, Figure 3.12b, and the surface and subsurface stress fields which arise from it for the case of two parallel contacting cylinders are discussed in detail by Johnson (1985), Timoshenko and Goodier (1970) and ESDU International-London (1995). The elliptical pressure distribution $p_{(x)}$, the maximum value of the normal traction p_0 and the contact half width b for the line contact of two cylinders have been determined using equations 3.1, 3.2 and 3.3 respectively.

$$p_{(x)} = p_0\left(b^2 - x^2\right)^{\frac{1}{2}} \tag{3.1}$$

$$p_0 = \left(\frac{PE^*}{\pi R}\right)^{\frac{1}{2}} \tag{3.2}$$

$$b = \left(\frac{4PR}{\pi E^*}\right)^{\frac{1}{2}} \tag{3.3}$$

where

$$\frac{1}{R} = \frac{1}{R_1} + \frac{1}{R_2} \tag{3.4}$$

and

$$\frac{1}{E^*} = \frac{1-\nu_1^2}{E_1} + \frac{1-\nu_2^2}{E_2} \tag{3.5}$$

The direct stresses along the load axis and the principal shear stress τ_1 (τ_{45}) are shown in Figure 3.13 (after Kapadia and Marsden, 1997). The distributions of orthogonal shear stress τ_{xz} and principal shear stress τ_1 arising from a normal traction only are shown in Figures 3.14a and 3.14b respectively (after Bailey and Sayles, 1991). The limiting conditions for which shakedown is just possible occur at the point in the solid where the value of the orthogonal shear stress τ_{xz} is a maximum (Williams et al., 1999). Shakedown therefore ensures that direct stresses tend to become hydrostatic leaving the orthogonal shear stresses to do the damage.

3.5.3. *Stresses arising from a tangential traction due to sliding friction*

If two cylinders are in sliding contact a tangential traction due to friction $q_{(x)}$ is applied to the contact surface. If the two solids have similar elastic properties there is no interaction between the normal traction (pressure) and the tangential traction and the resultant stresses can be superposed (Johnson, 1985). The most important consequences of the application of a tangential traction in addition to a normal traction are that shear stresses arise on the contact surface and the point of maximum shear stress moves towards the surface as the traction coefficient increases. The stress fields arising from the presence of a tangential traction are fully discussed by Johnson (1985), ESDU International (1995) and Bailey and Sayles (1991).

The magnitude of the tangential traction acting on any element of the contact surface has been assumed to be given by Amonton's law of sliding friction, equation 3.6 (Hutchings, 1992).

$$\left|q_{(x)}\right| = \mu p_{(x)} \tag{3.6}$$

The distributions of orthogonal shear stress τ_{xz} and principal shear stress τ_1 arising from the application of combined normal and tangential tractions are shown in Figures 3.15a and 3.15b respectively (after Bailey and Sayles, 1991).

3.5.4. *The effects of surface roughness and asperities*

The review up to the present has considered smooth surfaces only. The effect of surface roughness is to superpose asperity stress fields onto the macro stress fields of the smooth body contact (Bailey and Sayles, 1991). This paper describes a numerical technique for evaluating the complete subsurface stress field resulting from the elastic contact of non conforming rough bodies, based on measurements of their profile. The work indicates how the presence of asperities within the contact region can give rise to high stresses which interact with the smooth body stresses to produce a highly stressed region at or very near to the surface.

The effect of surface roughness alone and the combined effects of sliding friction and surface roughness on the symmetrical distribution of orthogonal shear stress τ_{xz} arising from the normal Hertzian traction are shown in Figures 3.16 and 3.17 respectively (after Bailey and Sayles, 1991). In the case of a ground unrun surface, the results of a purely elastic analysis indicated that the magnitude of many of the subsurface "asperity" stresses were twice the magnitude of the maximum "smooth body" stresses. This analysis gives the worst case of stress, because due to plastic deformation these stresses would be reduced after the first contact stress cycle. The effect of surface roughness and asperities on crack initiation and propagation and back-up roll surface wear is not considered in any of the studies on back-up roll performance except briefly in the paper by Bracht and Bradd (1965). They commented that the results from experimental tests on bearings, indicated that surface finish has an important effect on rolling contact fatigue.

Kapoor et al. (2000) carried out an investigation into the influence of surface roughness in railway rail/wheel contacts operating with a contact pressure below the shakedown limit. Examination of rail cross sections shows severe plastic deformation in a subsurface layer of a few tens of microns thickness and it is hypothesised that asperity contacts are responsible for the observed plastic flow. The results of the experimental simulations and numerical analysis carried out in this work showed that this hypothesis was correct. As the evidence suggested that the roughness of work roll and back-up roll surfaces may have an important influence on crack initiation, early crack propagation and back-up roll surface wear rates and also on the interaction between wear and rolling contact fatigue, these topics were investigated experimentally and the results are discussed in Section 6.4.

3.6. THE RESPONSES OF THE ROLLS

3.6.1. *Introduction*

The responses of back-up rolls to the demands placed upon them are described in literature as surface wear, thermal damage, corrosion damage, work hardening of the

surface layers, surface and subsurface cracking, rolling contact fatigue and spalling. All of these responses, which can be detected both visually or by the use of non destructive testing methods, are considered to make some contribution to the shortening of back-up roll life and in some cases to the catastrophic failure of the rolls (Bracht and Bradd, 1965; Ohkomori et al., 1987; Tait, 1990; Easter, 1996; and Kapadia and Marsden, 1997). The aim of this section of the literature review is to identify the responses of the rolls which should be altered or improved in order to increase resistance to rolling contact fatigue.

3.6.2. *Surface wear*

Back-up roll surface wear is of major concern to mill operators because of its effect on: the cost of roll maintenance, back-up roll life, the work roll/back-up roll interface loading profile (Liddle and Shinozuka, 1996), the control of strip thickness and shape (Easter, 1996) and the possible reduction of rolling contact fatigue life due to the roughening of the roll surface (Bracht and Bradd, 1965).

Ohkomori and Kaku (1997) list the following mechanisms, which should be considered when considering the wear of back-up rolls: adhesive wear, abrasive wear, corrosive wear and fatigue wear.

Typical wear profiles for the back-up rolls used in the finishing train of a hot strip mill are shown in Figure 3.18 (Ohkomori et al, 1987).

It is clear that wear on the back-up roll surface would be expected to influence the propagation rate of rolling contact fatigue cracks. Published evidence for the interaction between wear and rolling contact fatigue is discussed in Section 3.7.6 and and the possibility of such an interaction in this case has been investigated experimentally, with the results presented in Section 6.4.4.

3.6.3. *Crack initiation*

The initiation of cracks on the surface or in the near surface region of back-up rolls can be caused by fatigue at areas which are subjected to high local stresses (Tait,

1990; Kapadia and Marsden, 1997), high reversing shear stresses (Nayak and Paul, 1979), the effects of mill incidents (Ohkomori et al., 1987; Kapadia and Marsden, 1997) and the presence of corrosion pits on the roll surface (Fusada, (1998).

Different types of surface cracking are demonstrated by the following examples. Figure 3.19 shows a slip mark, which occurred near the barrel end of a back-up roll in a hot strip mill (Ohkomori et al., 1987). Figure 3.20 shows several cracks caused by thermal shock at the barrel end of a back-up roll in a hot strip mill (Ohkomori et al., 1987) and Figure 3.21 shows cracks caused by rolling contact fatigue on the surface of a back-up roll in a plate mill (Ohkomori et al., 1987).

An extreme case of surface damage is shown in Figure 3.22. This roll suffered severe frictional damage after operating for one year in a six-stand hot strip mill (Kapadia and Marsden, 1997).

3.6.3.1. Thermal damage

The thermal shock caused by excessive roll slip leads to metallurgical damage and plastic deformation due to high levels of tensile and compressive stresses produced by rapid heating and cooling of the roll surface (Ohkomori et al., 1987; Roberts, 1990). Ohkomori et al. (1987) examined the area near the slip mark shown in Figure 3.19. They found that in this area the hardness (83 HSc) was much higher than the surrounding area (66 HSc). The structure of the material was found to be martensitic, suggesting that it had been heated rapidly above the transformation temperature and quenched immediately by the cooling water. The transition region was found to be softened (50 HSc), probably due to tempering.

3.6.3.2. Corrosion damage

Corrosion fatigue, stress corrosion and the general corrosion damage of back-up roll materials are not considered in any of the available literature apart from one paper on the wear resistance. Corrosion pitting and its effects on the surface roughness and wear of the surface of back-up rolls have been investigated by Fusada (1998). During the study numerous corrosion pits were found on the surface of hot strip mill

back-up rolls, Figure 3.23. It was found that these pits cause roughening of the roll surface and surface wear and that the plastically deformed layer was as deep as the deepest corrosion pits, suggesting that the generation of micro cracks caused by plastic deformation and the formation of corrosion pits are related. It is also suggested that this damage can lead to spalling due to the initiation of cracks beneath the pits.

3.6.3.3. Work hardening

The cyclic rolling contact fatigue stresses experienced by back-up rolls plastically deform the surface layer of the roll barrel causing work hardening of the material. The work hardened surface layer of a forged roll and the micro cracking associated with it are shown in Figure 3.24 (Kapadia and Marsden, 1997). The severity and depth of the work hardening depends on the properties of the roll material and the local work roll/back-up roll interface loads.

Tait (1990), using an eddy current technique, showed that the work hardening varies in bands across the roll surface and the profile correlates with the contours of the rolls with which the back-up roll comes into contact during a campaign. The position of the occurrence of spalling also correlates with the high levels of work hardening, Figure 3.25 (Tait, 1990). Liddle and Shinozuka (1996) show a similar correlation between back-up roll wear profile and work hardening, Figure 3.26.

Tait (1990) states that a laboratory stress analysis has indicated that an overload yield condition may initiate micro fissures at the bottom of the work hardened layer. He goes on to say that, uniform work hardening would not normally cause spalling and that it is the variance between bands of hardening which cause the problem. It was suggested that the residual stresses which are set up combine with the applied stresses to initiate micro fissures causing spall cracking. It is not clear from this work how subsurface micro fissures are produced, but any plastic deformation at the roll surface would be expected to initiate small surface cracks.

3.6.4. *Rolling contact fatigue*

From the proceeding summary, it is clear that there is much field evidence that rolling contact fatigue cracks initiate both at the surface and subsurface, but in the absence of significant subsurface defects there is no clear consensus on the causes of crack initiation or the mechanisms which propagate the cracks. There is also no clear definition of what constitutes rolling contact fatigue in this case.

Also in this case, apart from the collective term of "rolling contact fatigue", there is no detailed explanation by any author of the mechanism or mechanisms by which cracks are propagated from the near surface region into the deeper substrate.

Kapadia and Marsden (1997) obtained values for the shear yield stress for a range of back-up roll materials and compared them with calculated values for the cyclic shear stresses arising from a smooth pure rolling contact. The results of this exercise indicated that the magnitude of the applied stresses was not sufficient to initiate and propagate fatigue cracks in the contact area. As it is known that crack propagation does take place, this implies that the magnitude of the stresses may have been underestimated or that more than one propagation mechanism may be present or both.

The evidence from this review indicated that in this case there is currently no clear understanding of the mechanisms which propagate rolling contact fatigue cracks and that a complete description of the rolling contact fatigue and spalling failure of back-up may be complex and involve several failure mechanisms acting together. It was concluded that in order to carry the project forward, a damage tolerance approach should be adopted and that detailed qualitative and quantitative failure models should be developed.

3.6.5. *Spalling failure*

Spalling failures in back-up rolls occurs in all the stands of the finishing train of hot strip mills. Ohkomori et al. (1987) carried out a study into the frequency of spalling in a hot strip mill over a period of seven years. The results of this study, which are

shown in Figure 3.27, indicated that that the frequency of spalling was greater in the later stands. The nominal Hertzian stresses and the number of roll revolutions per campaign for each stand are shown in Figure 3.28. The higher frequency of spalling in the bottom stands was explained by the existence of high local stress levels near the ends of the roll barrels due to the more concave wear profiles observed in these stands and the higher number of stress cycles experienced by the rolls during a back-up roll campaign. These conclusions were confirmed when it was found that the fatigue damaged layers penetrated deeper into the rolls on these stands.

Other authors also report that spalling near the barrel ends occurs more frequently on rolls with a concave profile and where positive crown work roll bending is applied. A typical spall near the edge of a back-up roll is shown in Figure 3.29 (Tait, 1990).

Kapadia and Marsden (1997) present a schematic model of the five stages of spalling failure Figure 3.30. This model clearly indicates that the surface initiated cracks propagate in the direction in which the contact loads move over the back-up roll surface, but the mechanisms involved in the propagation of the cracks in the "formation of the fatigue band region" are not explained.

The introduction of planned roll maintenance programmes (dicussed in Section 3.2.4), which include the detection, assessment and removal of the material damaged by the above responses, is considered to be one of the main factors in preventing rolling contact fatigue and spalling failure. As these planned roll maintenance programmes only involve the removal of damage on the surface roll barrel, this suggested that the best way to carry the project forward was to concentrate on producing design criteria for resisting the propagation of surface initiated cracks.

3.7. FAILURE MECHANISMS

3.7.1. *Introduction*

It has been concluded earlier in the review that it should be assumed that for the purpose of this work, rolling contact fatigue cracks initiate at the surface of the back-

up roll. On this assumption, the failure mechanisms investigated were all associated with failure at a free surface and the propagation of the resulting critical flaws into the deeper substrate.

Repeated rolling-sliding contact loads subject the roll material at the surface and near subsurface to repeated cycles of complex stress. Under the influence of these stresses, which can be transient or steady state, the responses may be categorised as one of the following: cyclic perfect elasticity, a limited number of cycles of plastic deformation followed by cyclic elasticity (elastic shakedown), cyclic plasticity (plastic shakedown) and incremental collapse (ratchetting) (Johnson, 1989). These responses are shown diagrammatically in Figure 3.31 (Johnson, 1989).

The ideal situation would be to restrict the deformation of the roll material to a perfectly elastic stress-strain cycle, but with current materials the surface layers of the roll barrel experience some degree of plastic deformation and work hardening. Once the material has yielded, the process of shakedown is protective and acts to prevent or reduce any further damage due to the high cyclic stresses. Three different mechanisms can contribute to the shakedown process, which takes place between the first application of load and the steady cyclic state: plastic deformation produces protective residual stresses, strain hardening of the material raises the yield stress and plastic deformation can make the contact more conformal (Johnson, 1989). It has been assumed in this work that the cyclic response of the material determines the mechanisms of crack initiation and early stages of crack propagation.

In a non-aggressive environment fatigue crack growth behaviour can be represented schematically as shown in Figure 3.32 (after Fine, 1979; Suresh and Ritchie, 1984; Dieter, 1988). Crack growth in region II (long crack region) is described by the well known Paris power law and is relatively insensitive to microstructure whereas crack growth in region I (short crack region) is microstructurally sensitive (Yoder et al., 1983).

3.7.2. *Crack initiation*

Much effort has been put into the study of the mechanisms of crack initiation and the time it takes to initiate fatigue cracks. Miller (1984) proposed that fatigue cracks initiate immediately at inherent defects in components and structures and that fatigue limits are associated with non propagating cracks, rather than with the non initiation of cracks. Others such as Baxter (1986) describe the appearance of persistent slip bands which eventually become the site for fatigue cracks, the cracks initiating at extrusions and intrusions on suitably orientated slip bands (Higgins, 1993; Dieter, 1998), see Figure 3.33 (Higgins, 1993). The deepening of the initial crack on planes of high shear stress is referred to as stage I growth, the mode II type propagation taking place along the persistent slip bands (Baxter, 1986; Brown, 1986; Dieter, 1998), Figure 3.34 (Brown, 1986). Slip bands have been observed when the applied stresses have been below the fatigue limit of ferrous metals, so the occurrence of slip bands does not in itself mean that a crack will form. However this damage can have a significant effect on damage accumulation above the fatigue limit (Miller et al., 1986)

Mura (1994) based a theory of crack initiation on the fact that the dislocation structures change to reduce the free energy of the system until the dislocation dipoles are annihilated to form a microvoid (crack). Cheng et al. (1994) used the dislocation pile-up theory to produce a model for the prediction of life under rolling contact fatigue. Near surface crack initiation was investigated by introducing the sliding contact boundary condition. The model indicated that the surface crack initiation life should be shorter than the subsurface crack initiation life under the same stress amplitude conditions. One important experimental result was that the higher the material hardness the longer the crack initiation life.

In the case of rolling-sliding contact, crack initiation and propagation in fatigue may be in competition with the mechanism known as ratchetting (incremental collapse). The ratchetting mechanism is shown diagrammatically in Figure 3.35 (after Tyfour et al., 1996). It has been shown by Tyfour et al. (1996), that ratchetting of the surface layer during the dry phase of a dry/wet rolling-sliding process can cause a significant reduction in the fatigue life of the "driven" disc in a twin disc testing machine.

3.7.3. *Short cracks*

When establishing design criteria, and in particular microstructural criteria, for resistance to rolling contact fatigue, it is essential to consider the growth of small and short cracks.

In non-aggressive environments fatigue cracks can be defined as short if they are microstructurally, mechanically or physically small (Suresh and Ritchie, 1984). Cracks in each category can be described as:

1. Cracks which are comparable in size to the main or effective grain size
2. Cracks which are of a length comparable to the scale of local plasticity
3. Cracks which are simply physically small

Cracks in categories 1 and 2 present continuum mechanics and linear elastic fracture mechanics (LEFM) limitations respectively and physically short cracks which are "long" in terms of both continuum mechanics and LEFM have been shown to propagate more quickly than long cracks under the same nominal driving force (Suresh, 1998). This is important if an attempt is made to predict crack propagation rates for physically short cracks.

Stage I or microstructurally controlled crack growth is typically in a shear mode (mode II) associated with crystallographic planes (Brown, 1986) and the crack faces have a serrated or facetted appearance (Suresh, 1998).

3.7.3.1. Propagation mechanisms

A crack propagated along a slip band will be arrested at the first microstructural barrier unless the cyclic stress range is higher than the fatigue limit, this is shown on the Kitakawa-Takahashi diagram (Brown, 1986). However in the case of rolling-sliding contact the high near surface stresses arising from friction and asperities may propagate a small initiated crack into a critical flaw, even though the stresses only exceed the fatigue limit for a small distance below the surface. If this occurs, the theories of fracture mechanics can be applied to the problem of the continued propagation of short cracks by considering the threshold stress intensity factor range

$\Delta K_{\pi h}$ for mode II crack propagation (Murakami and Hamada, 1997). The adoption of a value for $\Delta K_{\pi h}$ is discussed in the quantitative model for spalling failure presented in Chapter 5.

In rolling contact fatigue the continued propagation of microstucturally short cracks has been found to require the presence of a lubricating fluid. The propagation of cracks in rolling contact test disc specimens was first observed by Way (1935) during his investigation into pitting due to rolling contact. Crack propagation and pitting only occurred when oil was present with a viscosity low enough to allow penetration of the fine cracks. Murakami et al. (1985) and Kaneta et al. (1985) used fracture mechanics methods to study fatigue crack propagation under lubricated rolling-sliding contact. The main points arising from the studies were:

1. Fatigue crack growth is accelerated by the hydraulic effect proposed by Way
2. The direction and magnitude of the friction force are the controlling factors which cause crack mouth opening and penetration of the lubricant
3. Surface cracks under pure rolling are free from the hydraulic pressure effect
4. The cracks in the "driven" surface propagate more easily than those in the "driving" surface
5. The mode II crack (shear) growth extends the crack along the original crack plane. The transition from a crack to a pit is therefore not induced by the shear mode crack growth. Crack growth by mode I (tensile) is necessary for the occurrence of a pit

Bower (1988) investigated three possible effects of the fluid lubricant, each giving different mechanisms for propagating fatigue cracks. The main conclusions are as follows:

1. The fluid may lubricate the crack faces but exert no pressure on them. The cracks then propagate in mode II driven by the reversing shear stresses and helped by the lubrication of the crack faces

2. The fluid may be forced into the crack by the load, prising the crack faces apart (hydraulic mechanism). This will generate substantial mode I and mode II stress intensities at the crack tip

3. The fluid may be trapped inside the crack by the closure of the crack mouth or by the sealing of the mouth by the contact area, the trapped fluid preventing the crack from closing (fluid entrapment mechanism). This will generate mode I stress intensities as the fluid is forced towards the crack tip and increase the mode II stress intensities by keeping the crack faces apart

The propagation of cracks by the hydraulic and fluid entrapment mechanisms are shown schematically in Figures 3.36a(a) and 3.36b (after Bower, 1988). As a result of his work Bower (1988) concluded that the fluid entrapment mechanism would be more likely to produce the crack morphologies observed produced by rolling contact. However in this study, consideration of crack mouth and crack-line loading conditions as the load moves over the crack mouth, Figure 3.36, suggested that the pressurisation of the crack faces may be complex. That is, the hydraulic mechanism may operate in the early part of the cycle and the entrapment mechanism in the later stages, when the crack mouth has been closed by the contact loads. Depending on the shape of the crack mouth, both these mechanisms may be influenced by fluid leakage as the crack grows.

It was expected that the surface initiated, inclined, rolling contact fatigue cracks considered in this study would be physically small, with small crack length/half contact width ratios. This would result in significant positive contributions to the mode I stress intensity factors arising at the crack tips due to the tangential tractions, with their highest values arising in the early part of the passage of the load over the crack mouth. Also it was expected that the negative contribution to the mode I stress intensity factors arising from the effect of the normal traction would be very significant in the middle and later stages of the passage of the load over the crack mouth. It was therefore concluded that for the purpose of the mathematical modelling of crack morphology in this case (Chapter 5), it should be assumed that crack pressurisation would be provided by the hydraulic mechanism.

Bold et al. (1991) found experimentally that a crack propagating in mode II could not be grown more than fractions of a millimetre before branching or crack arrest occurred. In order to produce extended crack growth along the plane of maximum shear, it was found that tensile and shear loads needed to be applied sequentially. Although this sequence was a simplification of the tensile/shear loads predicted by Bower (1988), with a tensile stress range/shear stress range greater than 0.5 this combination did produce coplanar growth in the direction of the maximum shear stress. This experiment demonstrated that coplanar crack growth could be obtained in rail steel, if the loading sequence applied was characteristic of the loads experienced in a rolling contact situation. As the work roll/back-up roll pair is similar to a wheel/rail pair a similar result should be expected.

In two studies on the stress intensity values at the tips of rolling contact fatigue cracks, Bogdanski et al. (1994 and 1996) found that the stress intensity factors were eight times higher when a lubricating fluid was present.

In literature concerning lubricated rolling-sliding contacts there is no simple method presented which will predict when mode I type propagation will commence and whether crack branching will occur. The methods used for the quantification of the critical parameters required for the prediction of rolling contact fatigue crack morphology in this case are described in Chapter 5.

3.7.4. *Long cracks*

3.7.4.1. Propagation mechanisms

Under conditions of lubricated, rolling-sliding contact, the propagation of cracks from the short crack region into the long crack region (stage II, mode I), would be expected to be driven by the mixed mode I/mode II loading conditions arising at the crack tips. At stress intensity factor ranges above the mode I threshold, crack growth is normally characterised by a striated fracture surface, but in steels striations are seen only infrequently (Suresh, 1998).

When considering the mechanisms by which the propagation of long cracks is extended to spalling failure in back-up rolls, Kapadia and Marsden (1997) proposed a model for the propagation of the "fatigue band" (already shown in Figure 3.30). In this model, extended long crack propagation in mode I arises due to the combined effects of residual radial tensile stresses and cyclic subsurface compressive rolling contact fatigue stresses. The variations of these stresses with distance from the contact surface are shown in Figure 3.37 (Kapadia and Marsden, 1997). These stress distributions are presented for demonstration purposes only because the distribution of residual radial tensile stress, although probably realistic, is assumed. The stress model for the propagation of the "fatigue band" is shown in Figure 3.38 (Kapadia and Marsden, 1997). It can be seen from the diagram that, as the inclined crack tip moves deeper into the substrate, the combination of the reducing cyclic, radial, compressive rolling contact stress and increasing radial, tensile, residual stress will eventually produce a cyclic tensile stress sufficient to propagate the crack in a direction parallel to the roll surface.

3.7.4.2. The applicability of linear elastic fracture mechanics

The applicability of using linear elastic fracture mechanics methods for the theoretical prediction of the morphology of rolling contact fatigue cracks in this work is discussed in Section 6.3.2.

3.7.5. *Corrosion effects*

When corrosive attack occurs simultaneously with fatigue loading, a very pronounced reduction of fatigue performance results. The reduction is greater than that produced by prior corrosion of the surface. The existence of a regime in which slow crack growth occurs according to the Paris law is eliminated and small cracks grow quickly into large cracks. A reduction of fifty percent in fatigue life is to be expected (Dieter, 1998)

Stress corrosion is the failure of an alloy from the combined effects of a corrosive environment and a static tensile stress. This stress may result from applied forces or residual stresses (Dieter 1998). The mechanism of stress corrosion is not fully

established but there are several possible mechanisms (Cottrell, 1995). Details of the possible mechanisms are given below:

1. Embrittlement by uptake into the metal of hydrogen released through corrosive attack at the crack tip.
2. Dissolution into the corrosive medium of metal in stacking faults in slip bands
3. Transgranular cracking due to dissolution of plastically deformed metal at the tip of the crack.

There is growing evidence of a link between stress corrosion cracking and hydrogen embrittlement. Corrosion products, which are formed, have a high volume and can generate high stresses due to wedging in a narrow crack (Dieter, 1998). The presence of hydrogen in steel can lead to disastrous brittle fracture. Hydrogen embrittlement is not sensitive to composition but to the strength level of the steel, the problem being most pronounced in high strength alloy steels (Honeycombe and Bhadeshia, 1995). Severe embrittlement can be produced in many metals by very small amounts of hydrogen, body centred cubic and hexagonal close packed metals being most susceptible. Face centred cubic metals are generally not susceptible to this problem. There is not an unequivocal mechanism for hydrogen embrittlement (Dieter, 1998).

The possible embrittlement of high strength steels by the presence of hydrogen is well known by back-up roll manufacturers and care is taken to remove hydrogen during extended heat processes prior to the "Selas" heat treatment process. For this reason, the effect of hydrogen has not been included in the failure models presented in this work.

3.7.6. *Wear mechanisms*

The process of wear is characterised by the steady removal of relatively small particles of material from the surfaces of the bodies in rolling sliding contact. It is not generally a critical mode of failure in rolling contact and wear rates are negligible in pure rolling (Johnson, 1989).

The results obtained from this literature study suggested that a comprehensive study of the wear mechanisms which are involved in the wear of back-up rolls should include adhesive wear, abrasive wear, corrosive wear, ratchetting, fatigue and the effects of oxidation. It is beyond the scope of this study to investigate all these wear mechanisms in detail, but the following factors and mechanisms were considered to be of particular importance in this work.

The wear that takes place in combined rolling-sliding contacts when lubrication is poor has the characteristics of "de-lamination" wear (Suh, 1977). The flakes of metallic debris, 5-50 microns thick, are produced by cracks developing parallel to the surface in the layer of highly deformed material. The initiation of these cracks appears to be common to "de-lamination wear" and rolling contact fatigue. The eventual modes of failure are the competitive (Johnson, 1989).

The last conclusion is supported by an analysis by Fan et al. (1993), who considered the effect of the cyclic loading and the wear rate on the propagation of an initiated crack. The results of the analysis indicated that wear and rolling contact fatigue are competitive and that for a given initial crack length, the crack will behave in four different ways ranging from being worn out to being propagated to spalling failure. The study suggested the crack propagation rate is strongly influenced by material hardness.

Johnson (1995) has reviewed the role of plastic deformation and in particular ratchetting on the processes of metallic wear, but corrosive wear and the effect of oxidation or changes in material properties due to generated temperatures were not considered. Flash temperatures of several hundred degrees can be generated in sliding. Only moderate sliding speeds are needed with most metals before hot spot temperatures become high enough to cause significant oxidation and initiate the wear mechanisms which arise from it (Hutchings, 1992).

Franklin et al. (2001) present a dynamic wear model in which the material is divided into layers, with the material properties varying with depth, as an approximation of real engineering materials at the scale of the microstructure. This model is further extended to a mesh of rectangular elements. Elements with a low yield stress and/or

low ductility would fail relatively early by ratchetting failure and if exposed to the surface, such elements would be removed as wear debris. Importantly failed elements could also be considered to be regions containing a number of micro-cracks or defects or just regions which a crack could propagate.

Beynon and Kapoor (1997), in a study which included a review of several wear mechanisms, describe how a hard ground surface in rolling-sliding contact with a softer smoother surface would subject the latter to pummelling by hard asperities. This would in turn subject a thin layer of the softer surface to severe contact stresses, even at low nominal contact pressures, and cause extrusion of wear slivers. This type of wear mechanism would be expected to play an important role in the wear and rolling contact fatigue performance of back-up rolls and has been investigated experimentally and the results are discussed in Sections 6.4.3 and 6.4.4.

Jin and Clayton (1997) investigated the effect of microstructure on the rolling-sliding wear of low carbon bainitic steels under dry conditions. One of the main conclusions was that the wear resistance of continuously cooled low carbon bainitic steels increased with the amount of carbide-free bainitic structure.

3.8. FATIGUE LIFE

3.8.1. *Introduction*

Models for the prediction of fatigue life in rolling contacts fall into two general categories: engineering models and research models. Engineering models utilise variables for which large amount of field data exist whereas research models, while dealing more rigorously with the mechanisms of failure over small sections of the failure process, are generally supported by only a a limited amount of experimental work. The aim of this review is to examine the main features of an example of each type of model, before considering models specifically dedicated to the prediction of the rolling contact fatigue life of back-up rolls.

3.8.2. *General Engineering model*

Tallian (1992a) reviewed eleven published fatigue life models with the object of identifying consensus parameters and relationships and comparing model strengths and limitations. The results from this work particularly demonstrated the large number of life influencing variables and the complexity of many of the life models.

Following the above review, Tallian (1992b) developed what is claimed to be a new simplified engineering model for spalling life prediction. The author reports that "this model does not claim new insights into the failure process, but does claim to incorporate the most commonly accepted failure mechanisms, functional relationships and variables into an explicitely derived and readily calculated closed form life prediction model". It was considered that although this model makes allowance for many of the factors which influence spalling life, it is essentially an empirical model, with no simple way of determining some of the model parameters. This model requires no detailed insights into the mechanisms of failure or the influence of the material microstructure on spalling fatigue life and is therefore of little use in this case.

3.8.3. *Research model*

Hanson and Keer (1992) developed a three dimensional model for the crack propagation phase of the surface pitting failure process in rolling-sliding contact fatigue. In this analytical life prediction model an initiated pre-pitting crack was simulated as a pressurised, lubricated semicircular inclined planar surface crack in a half space. The crack was assumed to be frictionless on its faces and the cyclic loading conditions were did not vary.

Coupling fracture mechanics analysis with a Paris type power law for crack growth, estimations were obtained for crack propagation life under various conditions of fluid pressure and residual stress. The results indicated that under all conditions, after crack initiation there is a period of stable growth followed by a sudden rapid increase in crack size.

In this model propagation rates in the mixed mode period of crack propagation were determined by replacing the stress intensity factor in the Paris law equation by the energy release rate. The constants in the equation were obtained from short crack propagation data, which were extrapolated where necessary to the smaller crack sizes in the study. Although the results from this work are interesting, the uncertainty of the mill traffic and hence the cyclic loading history experienced by back-up rolls, coupled with the lack of the appropriate short crack growth data would make it difficult to use this type of model for the prediction of the rolling contact fatigue life of back-up rolls.

One important observation from this study was the predicted effect of residual compressive stresses. The results indicated circumferential compressive stresses reduce the crack opening caused by fluid pressure. However for very acute cracks, the component of the residual stress closing force perpendicular to the crack plane is low. For such cracks, this substantially reduces the effect of the residual stresses on crack closure, and hence their effect on mode II and mode I crack growth. This result suggests that, although acknowledging the possible beneficial effects of the compressive residual stresses at the surface of back-up rolls, it would be prudent to ignore their effects when modelling rolling contact fatigue failure in back-up rolls.

3.8.4. *Back-up roll fatigue life models*

Ohkomori et al. (1987) and Easter (1996), in separate studies of back-up roll performance, present curves of rolling contact fatigue life against maximum shear stress τ_{45} and maximum Hertzian contact stress p_0 respectively. These groups of curves, which are in linearized form, are shown for different levels of hardness and are in reasonable agreement. The basis of the curves is not given, but the implication is that they are empirical models. An important feature is that fatigue life increases with material hardness. The results presented in these models, although useful as experimental support for roll maintenance procedures, gives no detailed insights into the mechanisms of failure. The conclusion that fatigue life increases with hardness is important but cannot be used in the detailed

microstructural design of back-up roll materials without information on other mechanical properties such as yield stress and toughness.

3.8.5. *Definition of back-up roll fatigue life*

In much of the literature concerning rolling contact fatigue, the fatigue life of a component is synonymous with the spalling life. However, in this work it was decided that for the purpose of predicting the rolling contact fatigue performance of back-up roll materials subjected to rolling-sliding contact at low levels of slip, it should be assumed that cracks initiate immediately and that fatigue life be defined as the period of shear mode (mode II and mixed mode I/mode II) crack propagation up to the mode I threshold.

3.8.6. *Conclusions*

In view of the absence of detailed loading histories for work roll/back-up roll contacts and accurate short crack propagation data and also the difficulties involved with applying long crack propagation data to physically short cracks, it was concluded that it was not possible to theoretically predict the rolling contact fatigue life of back-up rolls.

It was further concluded that the need for the prediction of rolling fatigue life could be removed if the propagation of surface initiated cracks could be confined to a thin surface layer, which could be periodically removed by grinding. It was therefore decided to investigate whether, using a damage tolerance approach, the required crack morphology could be obtained by the microstructural design of the roll material. The results obtained from this investigation are discussed in Section 6.6.4.

3.9. EXPERIMENTAL SIMULATION

3.9.1. *Introduction*

There are many uncertainties regarding excursions from the normal loading and

operating conditions experienced by back-up rolls during a campaign. These uncertainties and the sheer size of the work roll/back-up pair make difficult to carry out controlled investigations into the mechanisms involved in rolling contact fatigue and spalling failure in the mill. In an attempt to overcome these problems and similar difficulties arising in other situations such as rail/wheel contacts many workers have carried out experimental simulations on twin disc testing machines.

3.9.2. *Twin disc testing machines*

Twin disc testing machines have been used in many laboratory studies of the performance of materials in both lubricated and un-lubricated rolling-sliding conditions. The following examples demonstrate some of the failure mechanisms which can be investigated.

Ohkomori and Kaku (1997) used a twin disc testing machine to investigate the wear performance of two back-up roll materials in lubricated rolling-sliding contact with a relative slip of 9% and Ohkomori et al. (1987) investigated the wear and spalling life under similar experimental conditions. They also investigated the effects of heat shock using a water lubricated stationary work piece and a disc rotating at 1500 rpm.

Bower and Johnson (1989) successfully used a twin disc machine to investigate the near surface plastic flow caused by rolling-sliding contact using markers situated near the surface of each specimen.

In many twin disc machines the rolling contact fatigue tests are run to spalling failure, there being no means of monitoring cracks during the initiation and propagation stages. Garnham and Beynon (1991) remedied this shortcoming by the development of a machine using an eddy current crack detection system. This machine has been since modified and improved by Fletcher and Beynon (2000a) by the addition of a computerised control system and the interfacing of all the instrumentation to a computer based data acquisition system. This machine, which is known as the "SUROS" rolling-sliding testing machine, was used for the experimental simulation in this study. Details of this machine and the methodologies used in the experimental simulations are fully described in Section 4.3.

	C	Si	Mn	Cr	Mo	Ni	V
0.4C3Cr	0.40	0.27	0.61	3.24	0.61	0.22	0.10
0.6C3Cr	0.58	0.25	0.34	3.10	0.47	0.14	0.16
0.8C3Cr	0.81	0.23	0.22	3.07	0.21	0.19	<0.01
0.4C5Cr	0.42	0.31	0.58	4.84	0.61	0.15	0.13
0.8C5Cr	0.80	0.70	0.25	4.83	0.32	0.30	0.01

Table 3.1. Materials for differentially hardened forged back-up roll steels (Honeyman et al., 1996). (Chemical composition by weight %)

Hardness Shore C	C	Si	Mn	Ni	Cr	Mo	Status
45-55	0.5/1.0	0.3/0.8	0.5/1.5	0/1.0	1.5/2.5	0.2/0.5	Est.
55-65	0.3/0.8	0.3/0.8	0.5/1.5	0/1.0	2.5/3.5	0.3/0.6	Est.
60-70	0.3/0.8	0.3/0.8	0.5/1.5	0/1.0	3.0/4.0	0.3/0.6	Est.
60-75	0.3/0.8	0.3/0.8	0.5/1.5	0/1.0	4.5/5.5	0.5/1.5	Dev.

Est. – Established material
Dev. – Material under development

Table 3.2. Materials for differentially hardened cast steel back-up rolls (Cox, 1996). (Chemical composition by weight %)

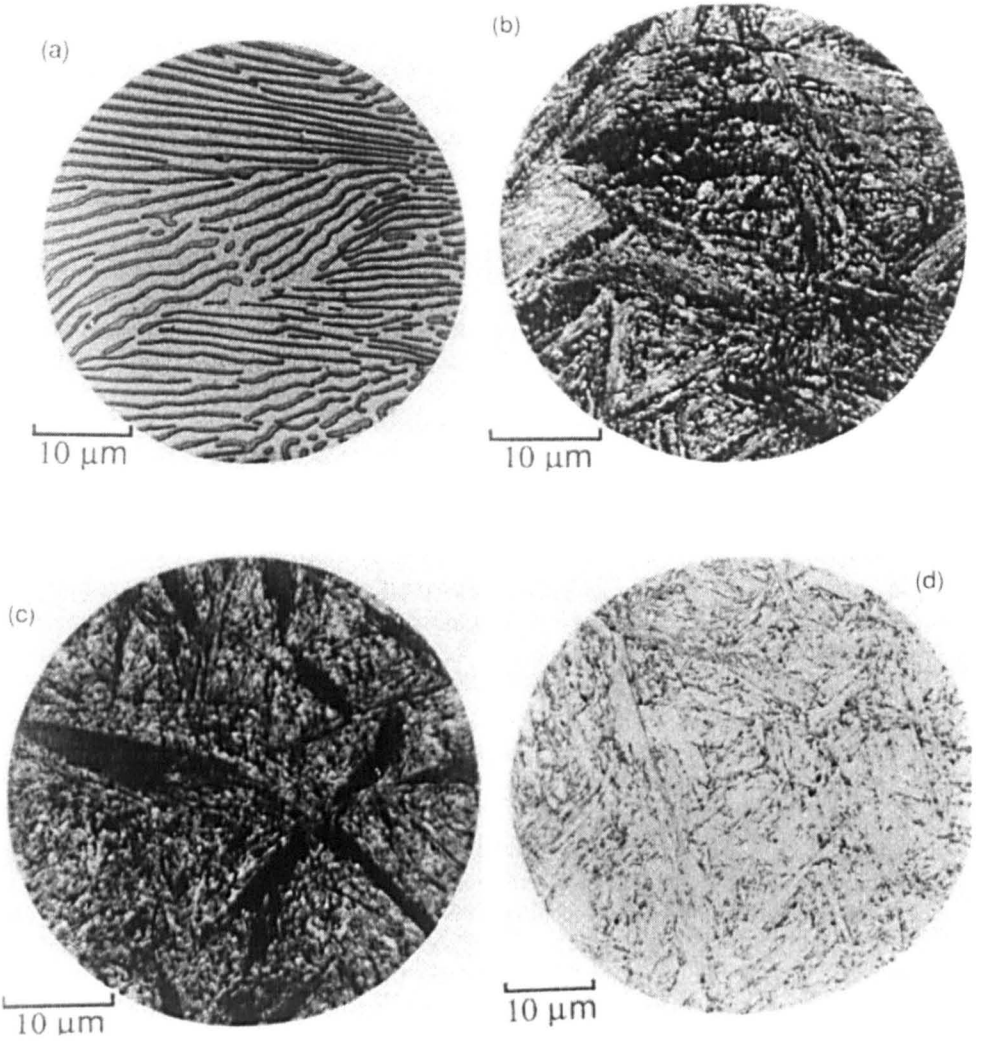

Figure 3.1 Microstructures in a eutectoid steel (a) Pearlite formed at 720°C (b) Bainite obtained by isothermal transformation at 290°C (c) Bainite obtained by isothermal transformation at 180°C (d) Martensite. The micrographs wre taken by Vilella and were published in the book "The Alloying Elements in Steel" (Bain 1939), (Bhadeshia, 1992).

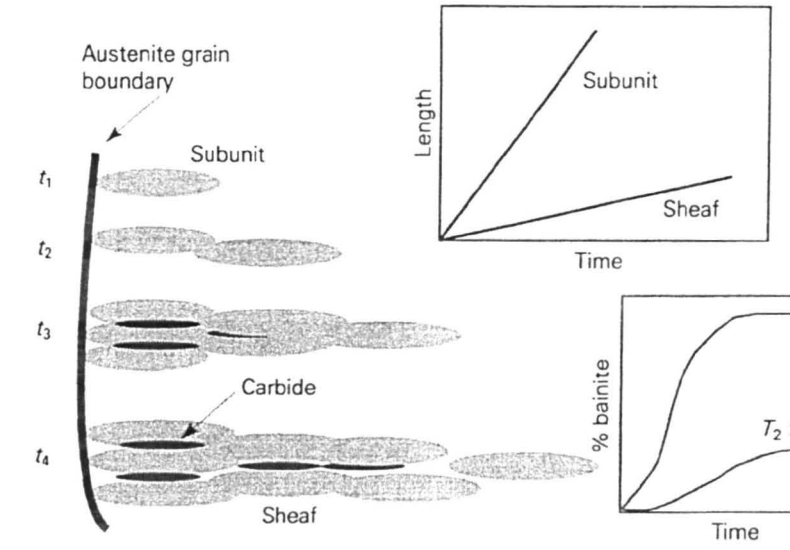

Schematic illustration of the microstructural features relevant in the kinetic description of a bainitic microstructure.

Figure 3.2. The kinetic description of the bainitic microstructure (Bhadeshia and Honeycombe, 1995)

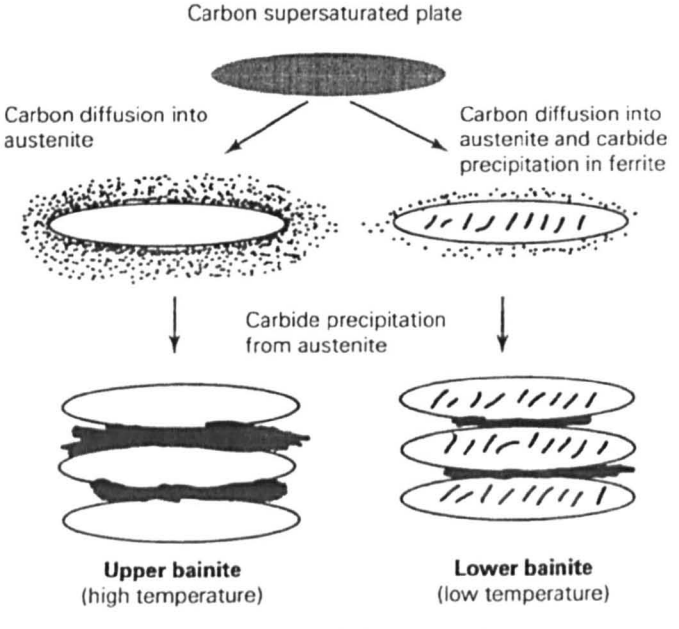

Schematic representation of the transition from upper to lower bainite.

Figure 3.3. The transition from upper to lower bainite (Bhadeshia and Honeycombe, 1995)

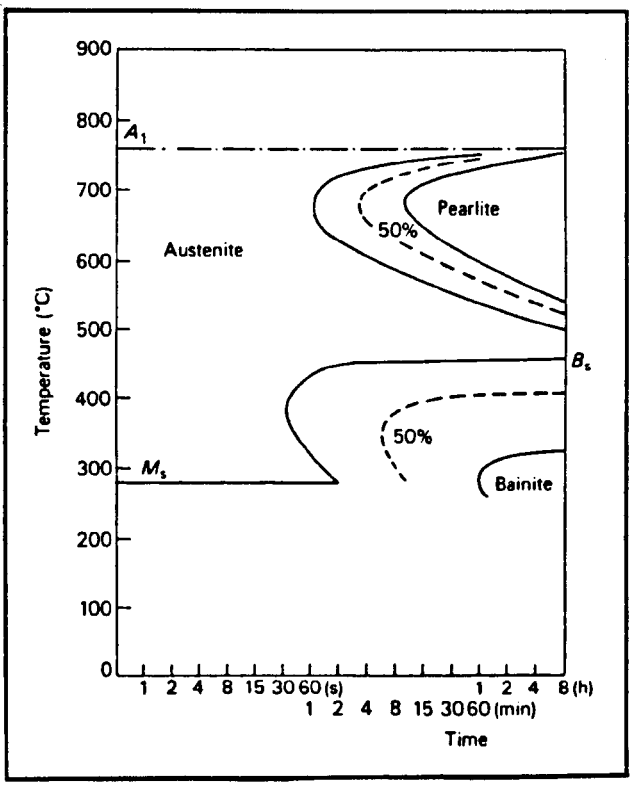

Figure 3.4. TTT curves for Fe-3Cr-0.5C wt% steel (Thelning, 1975)

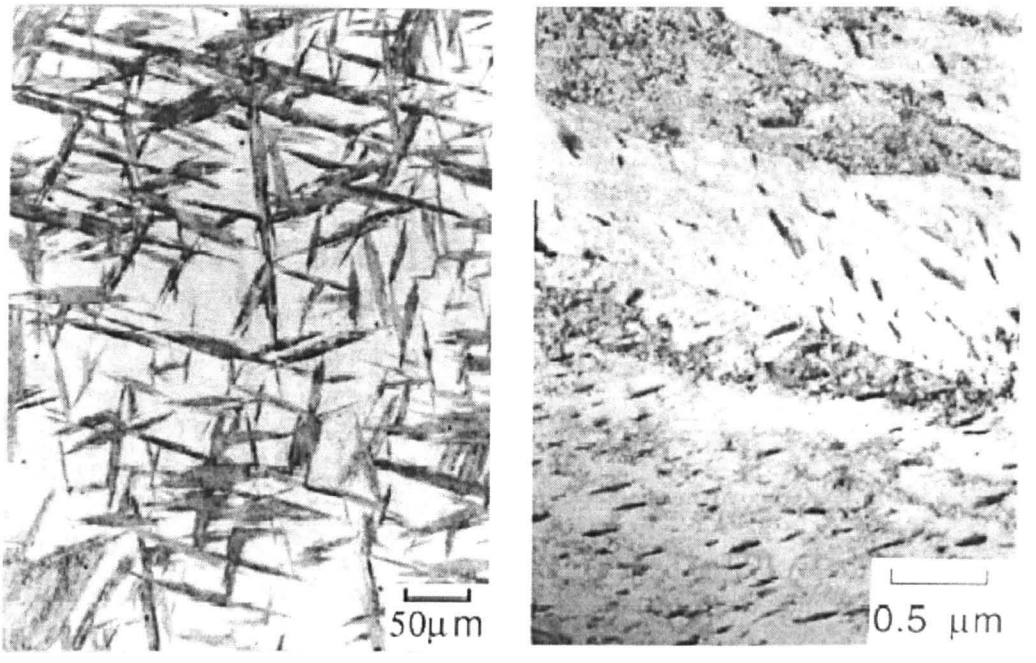

Figure 3.5. (a) Light micrograph illustrating sheaves of lower bainite in a partially transformed (395 °C) sample of Fe – 0.3C – 4Cr wt% alloy. The light etching matrix phase is martensite. (b) Corresponding transmission electron micrograph illustrating a sub-unit of lower bainite (Bhadeshia, 1992).

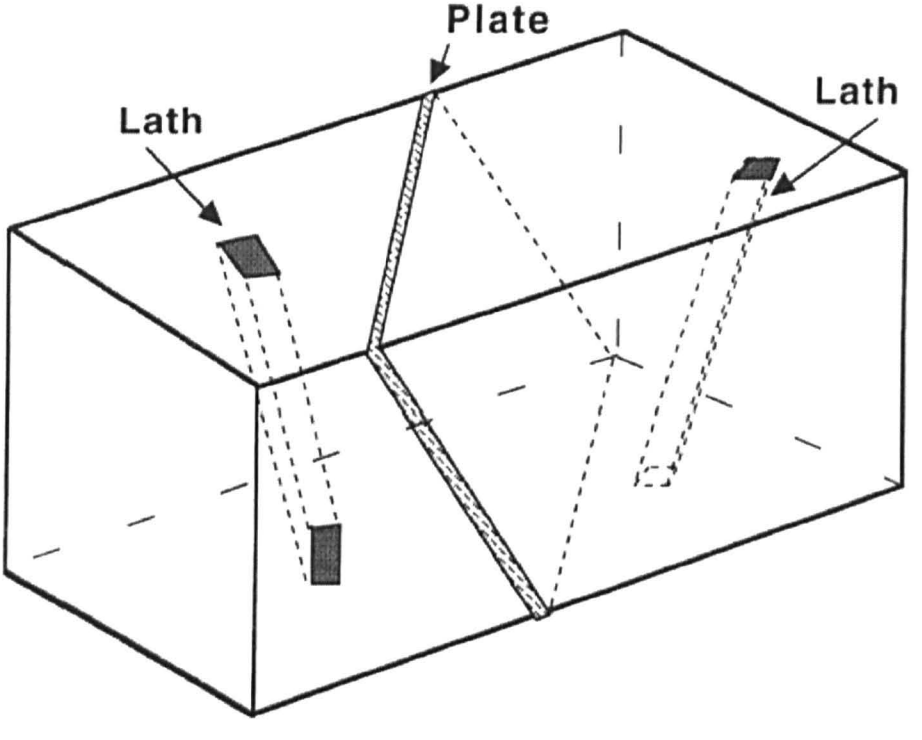

Figure 3.6. Schematic representation of a plate and a lathe of lower bainite (Bhadeshia, 1992).

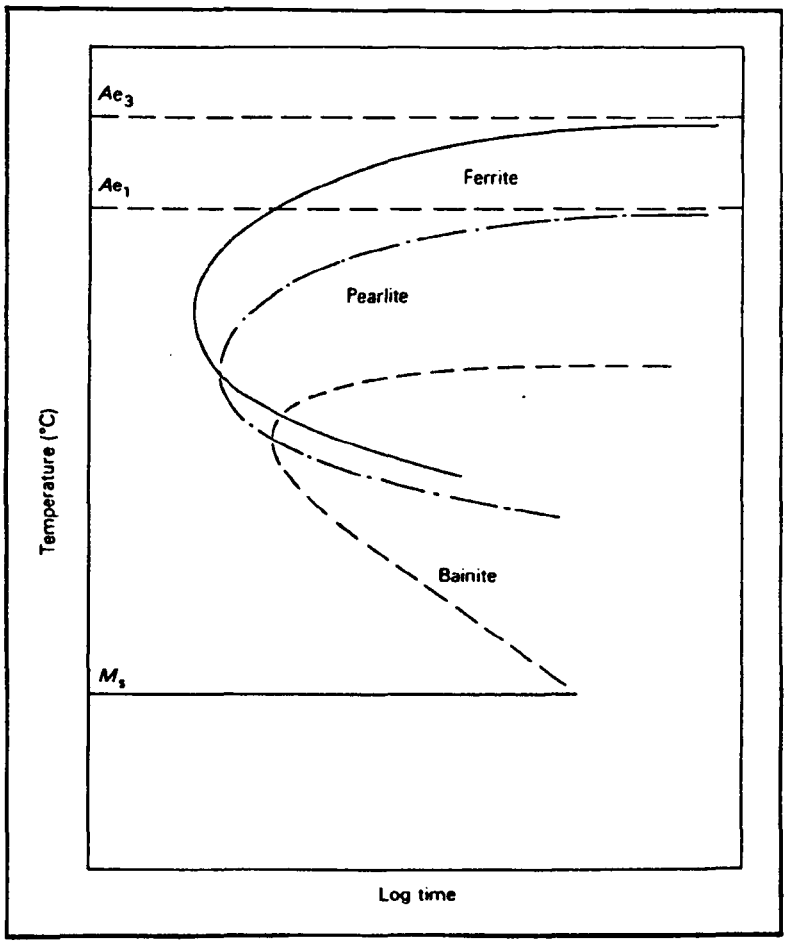

Figure 3.7. Schematic diagram showing the bainite reaction TTT curve for low carbon steel (Irvine and Pickering, 1957)

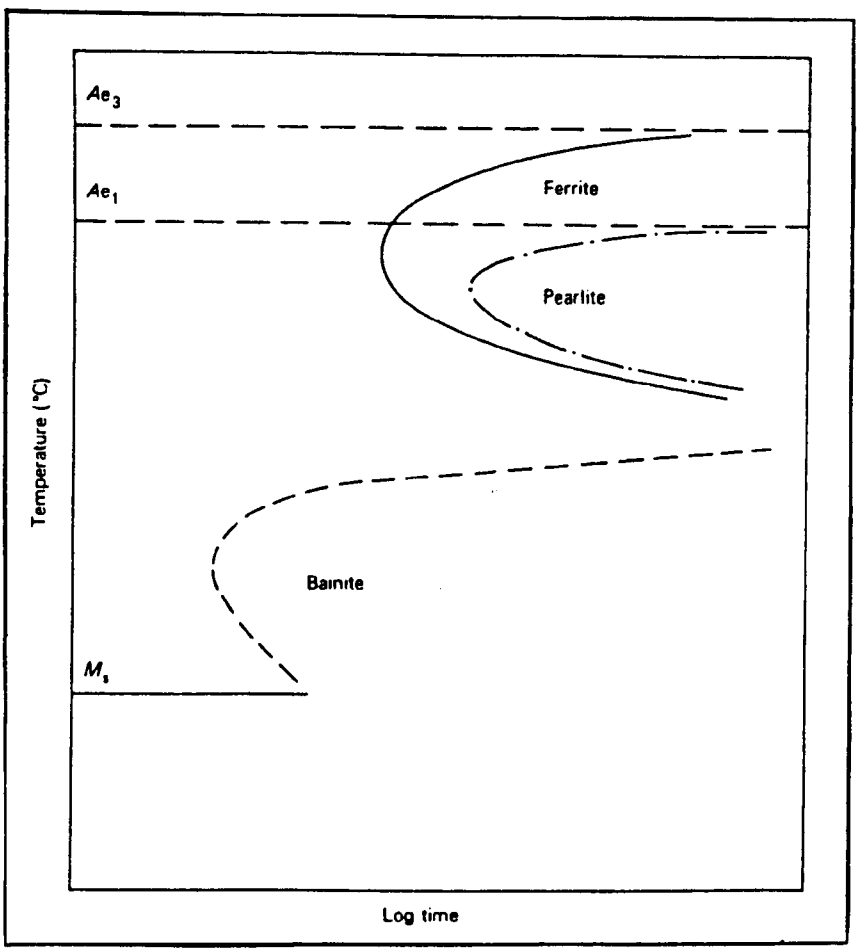

Figure 3.8. Schematic diagram showing the bainite reaction TTT curve for a low alloy steel (Irvine and Pickering, 1957)

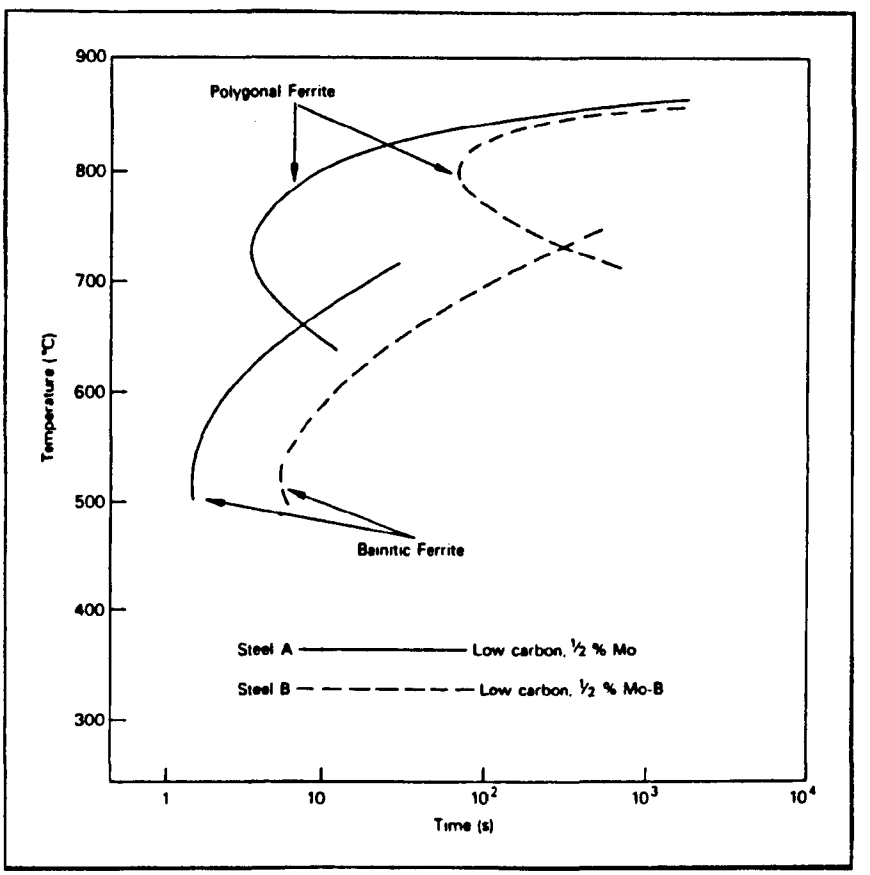

Figure 3.9. Schematic diagram showing the effect of boron on the bainite reaction TTT curve for a low carbon 0.5 Mo steel (Irvine and Pickering, 1957)

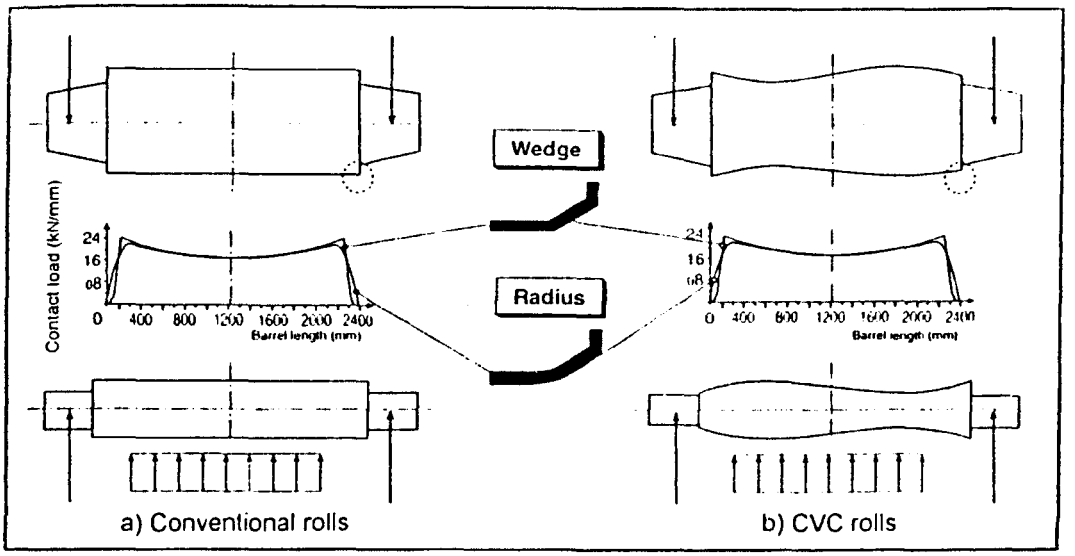

Figure 3.10. The influence of back-up roll edge relief on contact load distribution (Kneppe and Hormes, 1996)

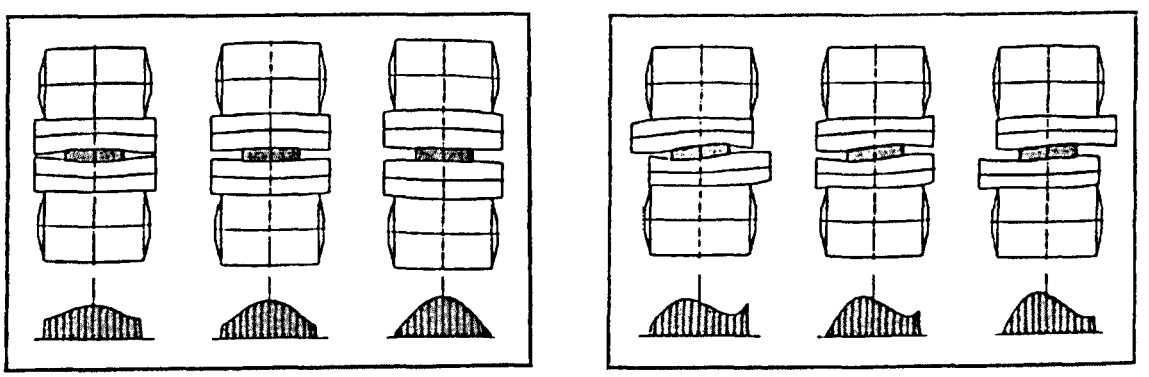

(a) (b)

Figure 3.11. Work roll/back-up roll interface loading profiles (a) Work roll with conventional crown and cylindrical back-roll (b) Work roll with CVC contour and cylindrical back-up roll (Kneppe and Hormes, 1996)

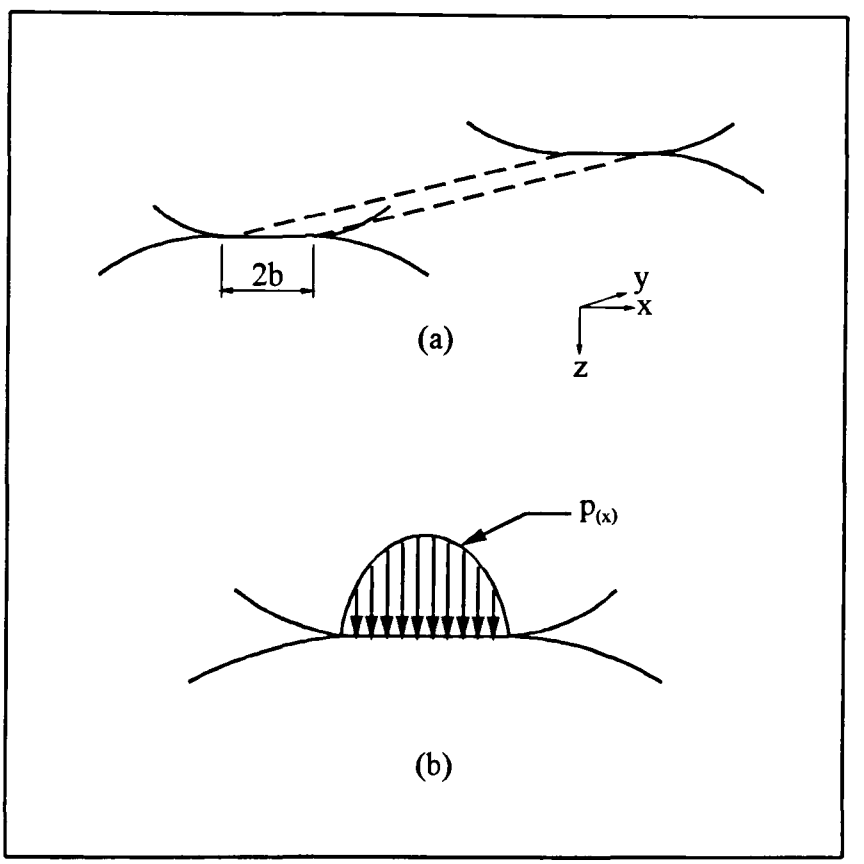

Figure 3.12. (a) Two dimensionally loaded contact of two cylindrical half spaces (b) Normal elliptical pressure distribution given by Hertzian theory

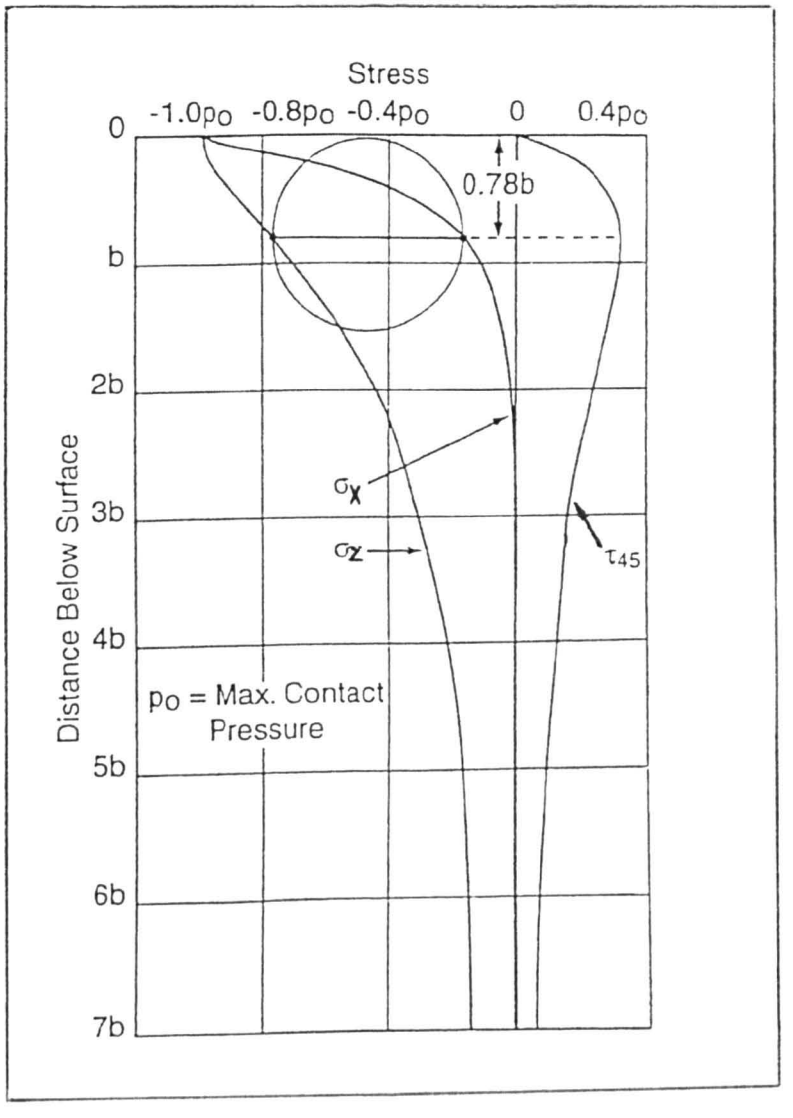

Figure 3.13. Direct stresses and principal shear stress on load axis [$\mu = 0$, τ_{45} is the maximum shear stress on the axis of symmetry] (Kapadia and Marsden (1997)

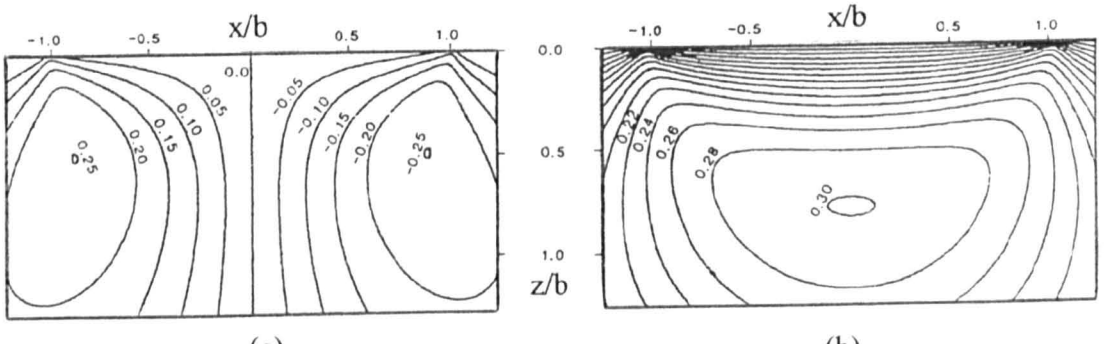

(a) (b)

Figure 3.14. (a) Orthogonal shear stress distribution normalised by p_0 [$\mu = 0$] (b) Principal shear stress distribution normalised by p_0 [$\mu = 0$] (Bailey and Sayles, 1991)

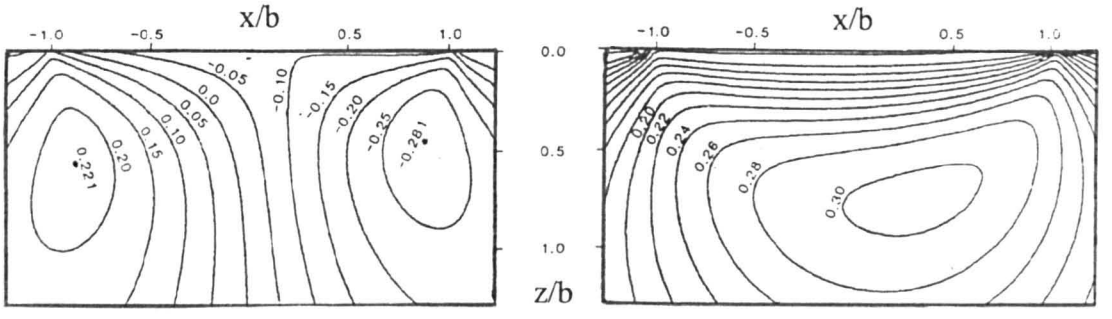

Figure 3.15. (a) Orthogonal shear stress distribution and (b) Principal shear stress distribution arising from the application of combined normal and tangential tractions [$\mu = 0.1$] (Bailey and Sayles, 1991)

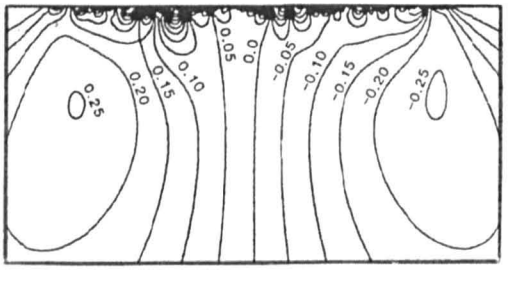

Figure 3.16. The effect of surface roughness on the orthogonal shear stress distribution arising from a normal traction only (Bailey and Sayles, 1991)

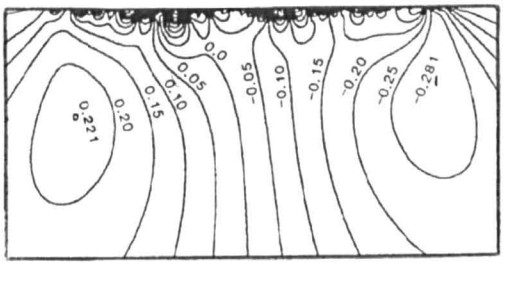

Figure 3.17. The effect of surface roughness on the orthogonal shear stress distribution arising from combined normal and tangential tractions [$\mu = 0.1$] (Bailey and Sayles, 1991)

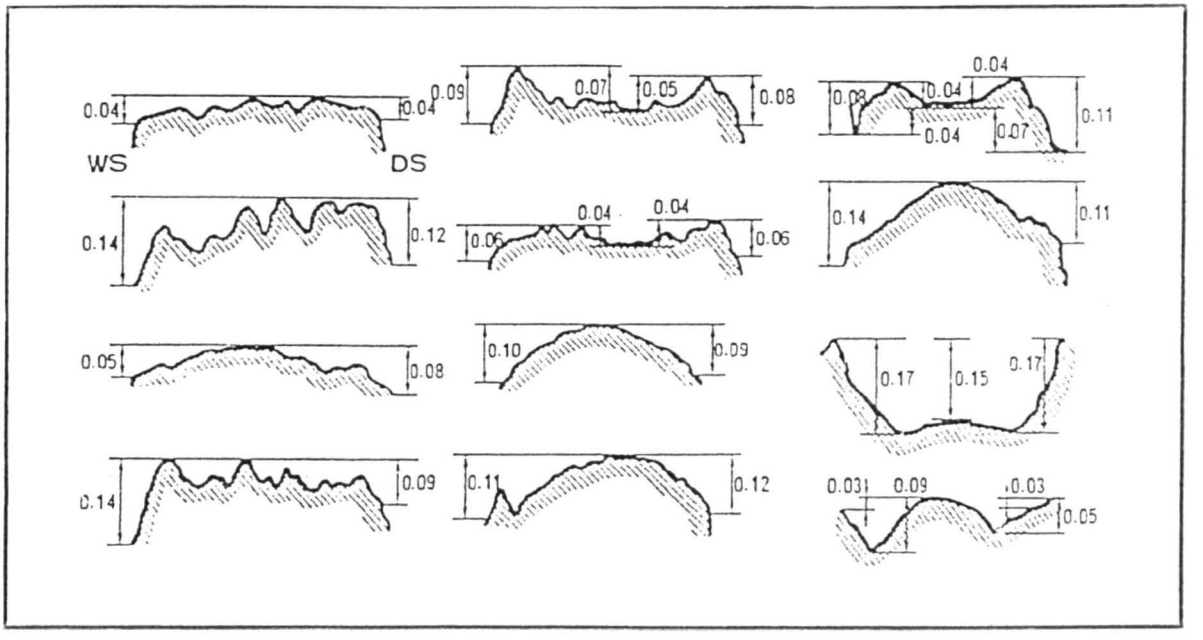

Figure 3.18. Back-up roll wear profiles [units in mm] (Ohkomori et al., 1987)

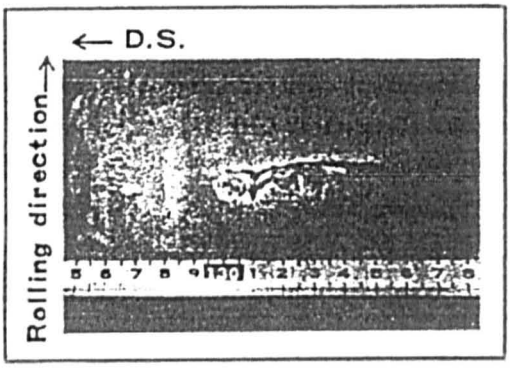

Figure 3.19. Slip mark (Ohkomori et al., 1987)

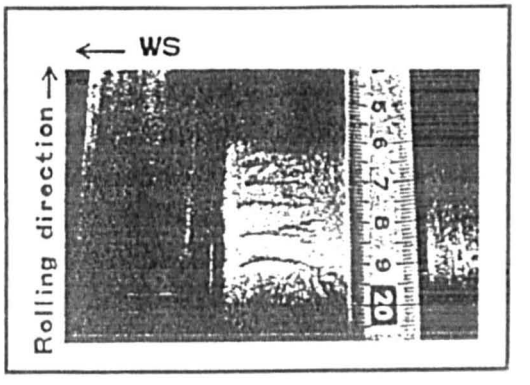

Figure 3.20. Cracks caused by thermal shock (Ohkomori et al., 1987)

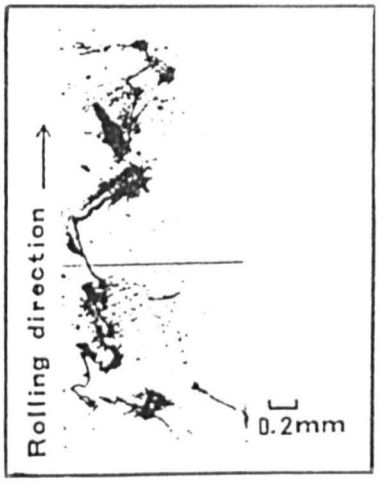

Figure 3.21. Cracks caused by rolling contact fatigue (Ohkomori et al., 1987)

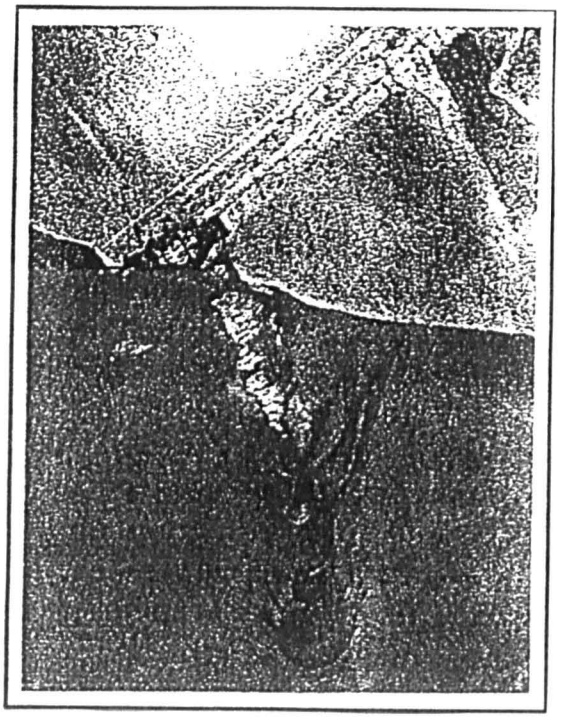

Figure 3.22. Severe frictional damage on the surface of a back-up roll (Kapadia and Marsden, 1997)

Figure 3.23. Numerous corrosion pits found on the surface of a hot mill back-up roll (after rolling 250000 tonnes-stand F2), at a position (a) within strip width, area of corrosion pits = 32% (b) outside strip width, area of corrosion pits = 13% (Fusada, 1998)

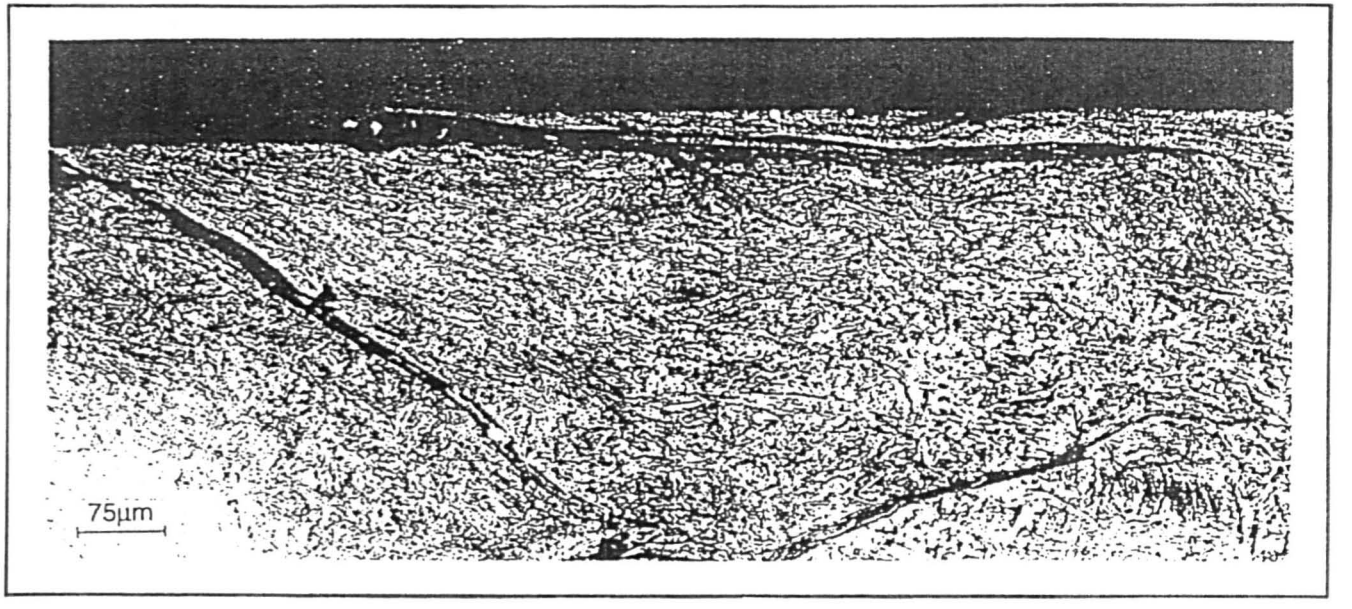

Figure 3.24. Work hardened surface in a forged roll and the fatigue cracking associated with it (Kapadia and Marsden, 1997)

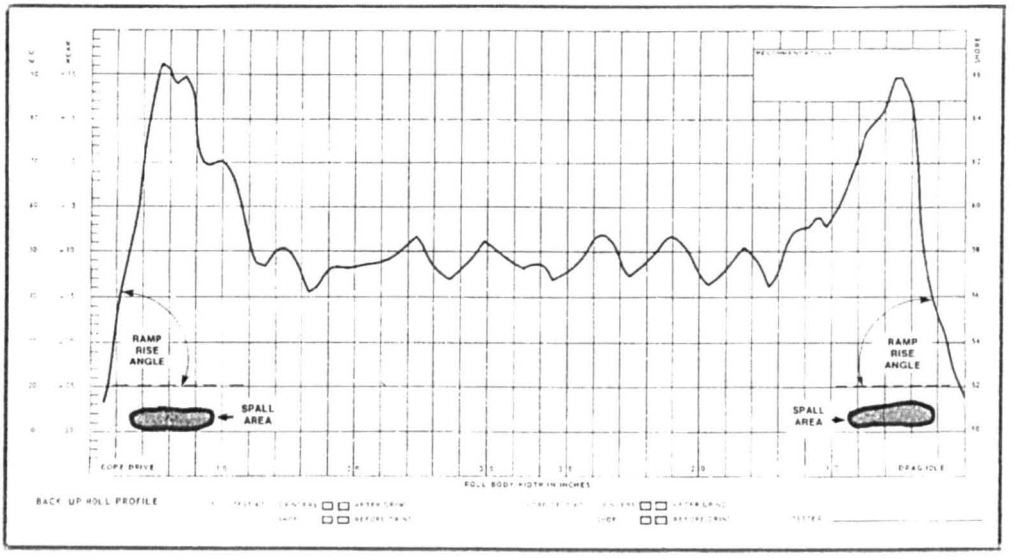

Figure 3.25. Back-up roll hardness profile. Single line eddy current trace showing the ramp rise between circular bands of hardness variation on the surface of a back-up roll (Tait, 1990)

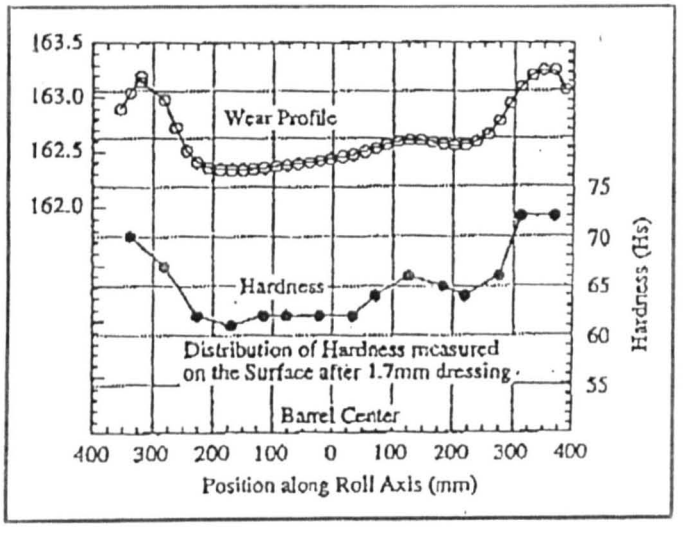

Figure 3.26. Correlation between wear profile and hardness distribution (Liddle and Shinozuka, 1996)

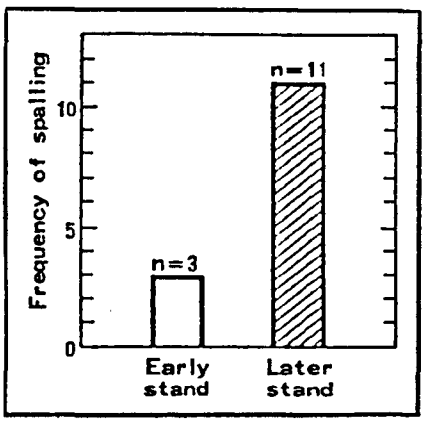

Figure 3.27. Frequency of spalling failure (Ohkomori et al., 1987)

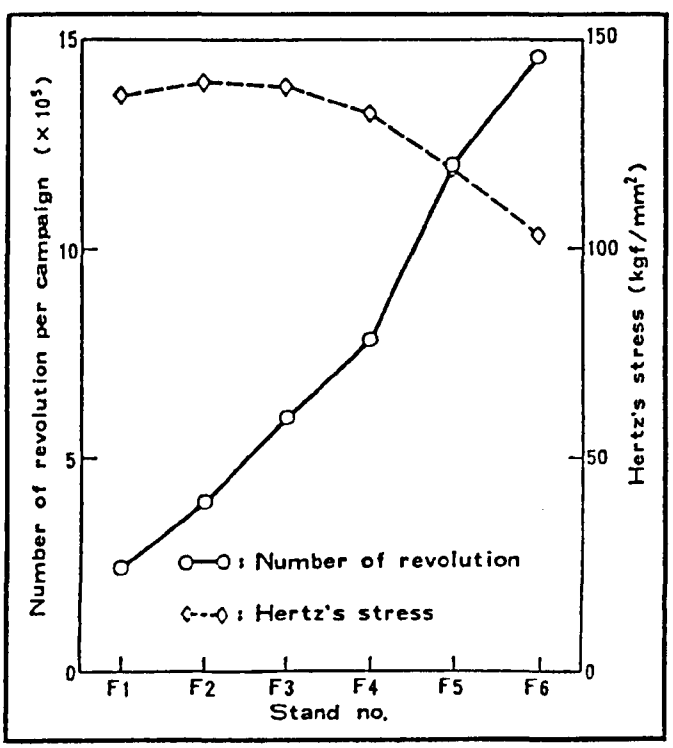

Figure 3.28. Nominal Hertzian stresses and number of revolutions per campaign (Ohkomori et al., 1987)

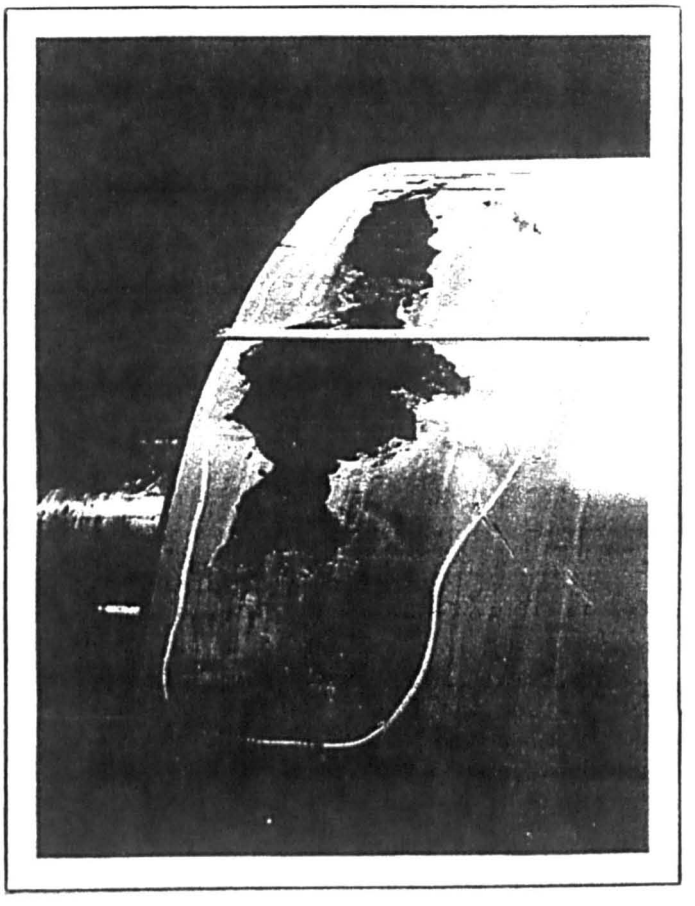

Figure 3.29. Spall near the edge of a back-up roll barrel (Tait, 1990)

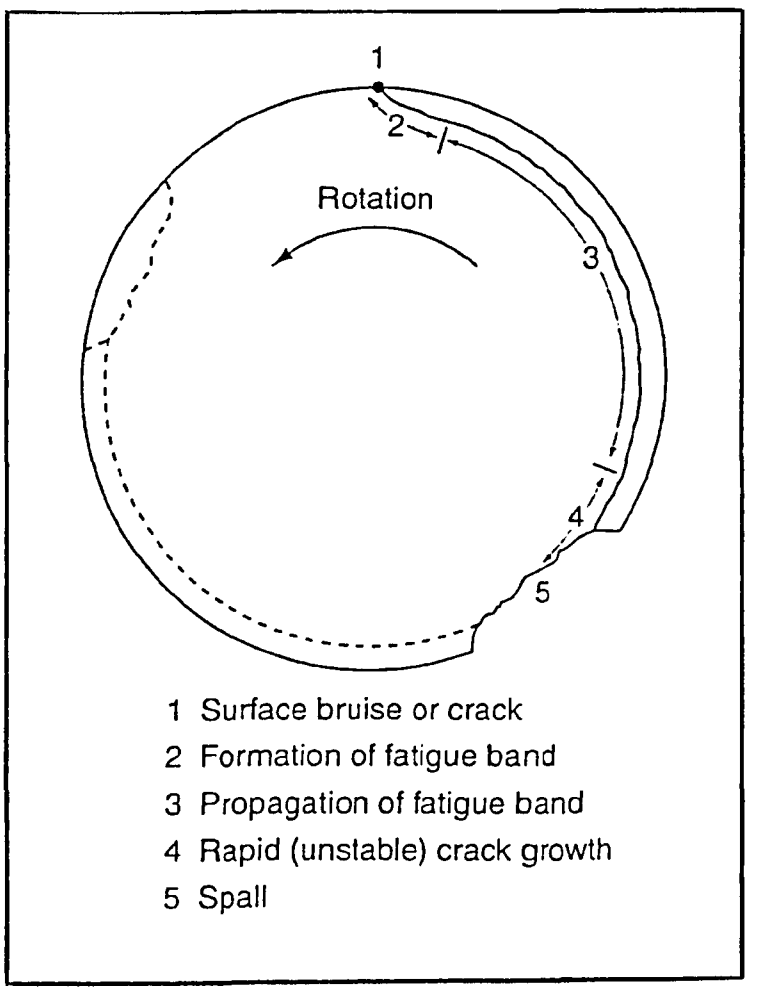

Figure 3.30. Schematic model of the five stages of spalling failure (Kapadia and Marsden, 1997)

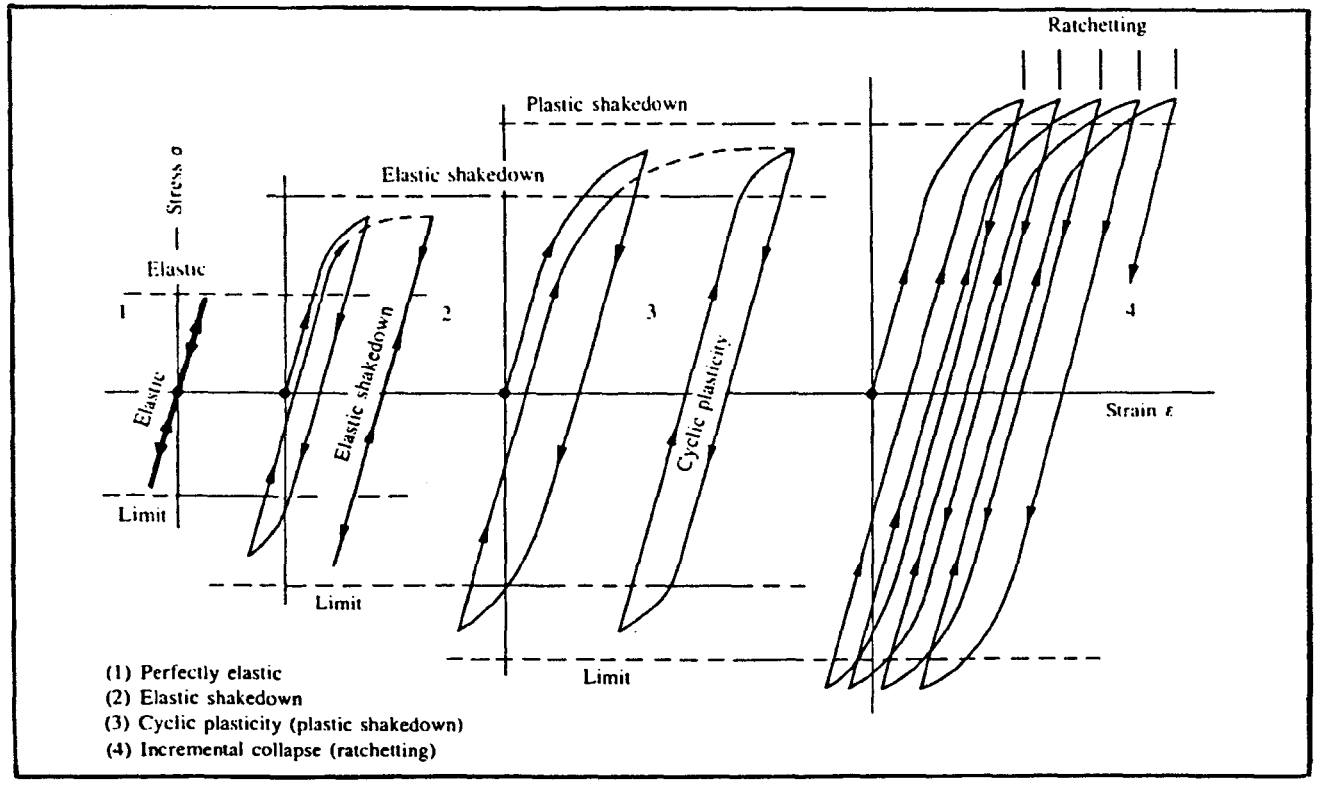

Figure 3.31. Material response to cyclic loading (Johnson, 1989)

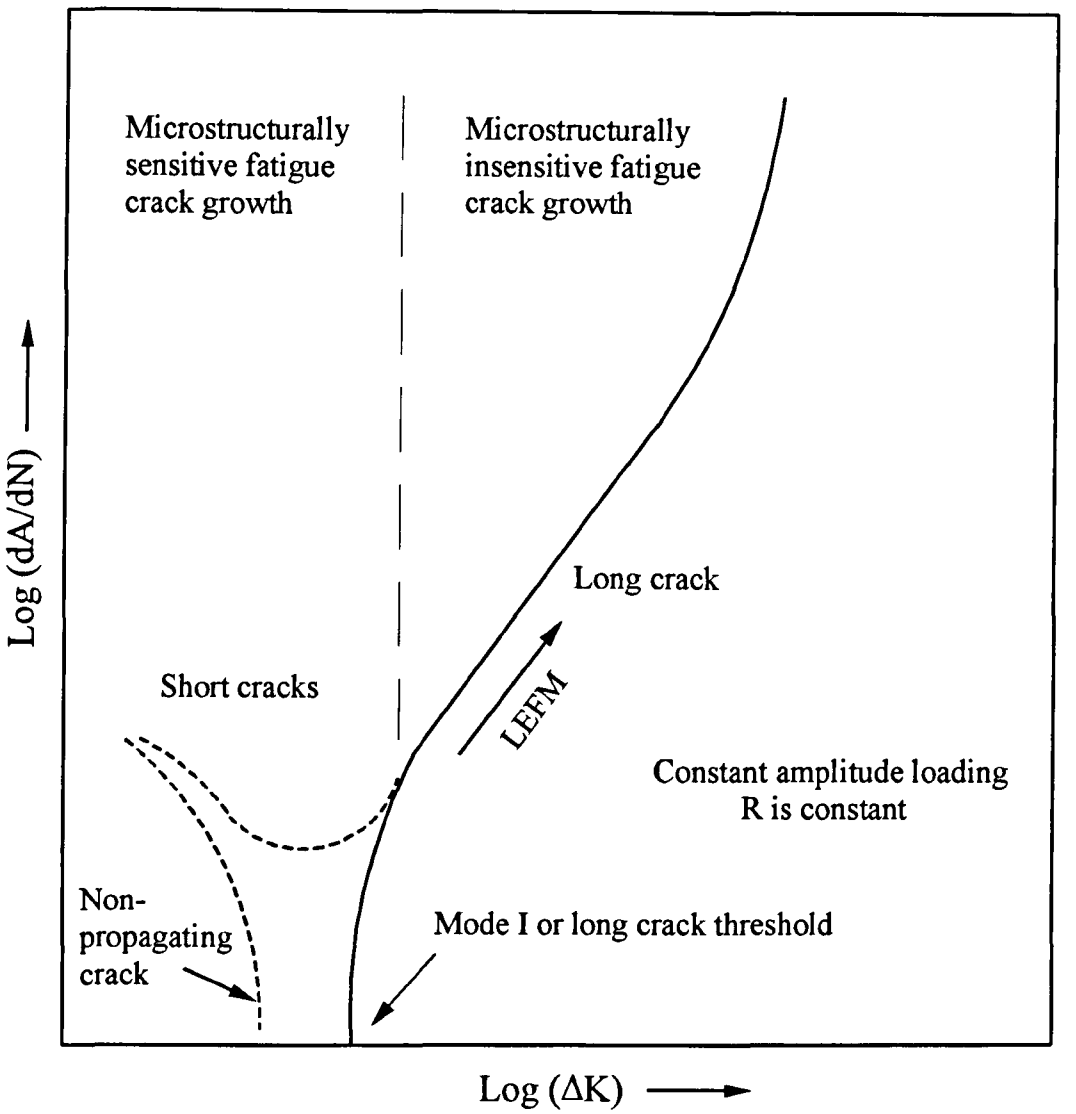

Figure 3.32. Fatigue crack growth behaviour in a non-aggressive environment (after Fine, 1979; Suresh and Ritchie, 1984 and Dieter, 1988)

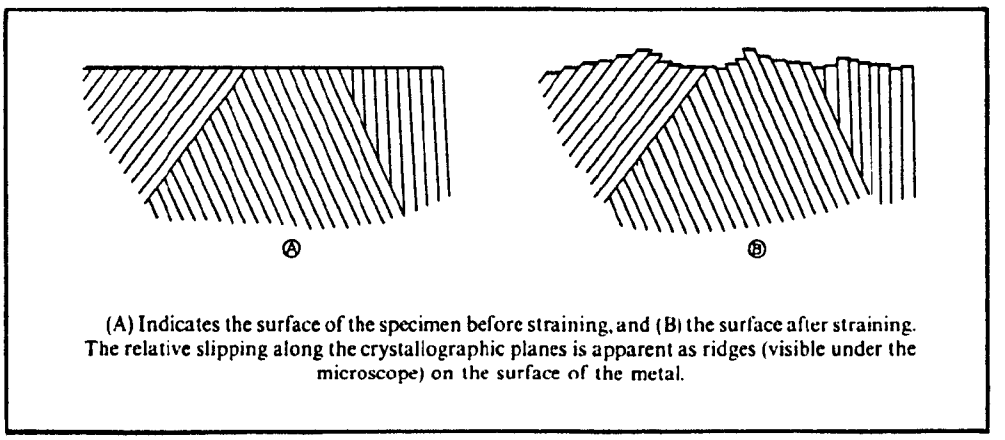

Figure 3.33. The formation of slip bands (Higgins, 1983)

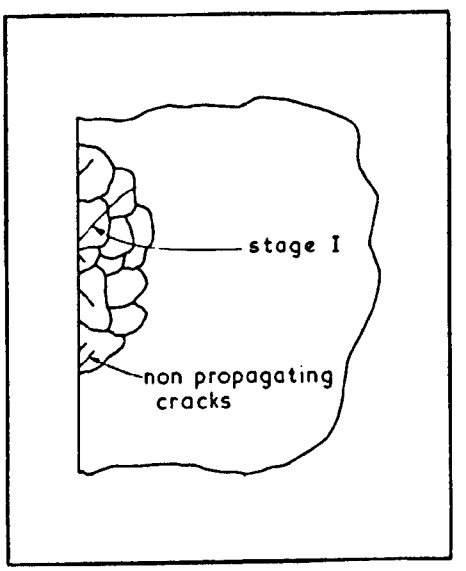

Figure 3.34. Stage I crack growth (after Brown, 1986)

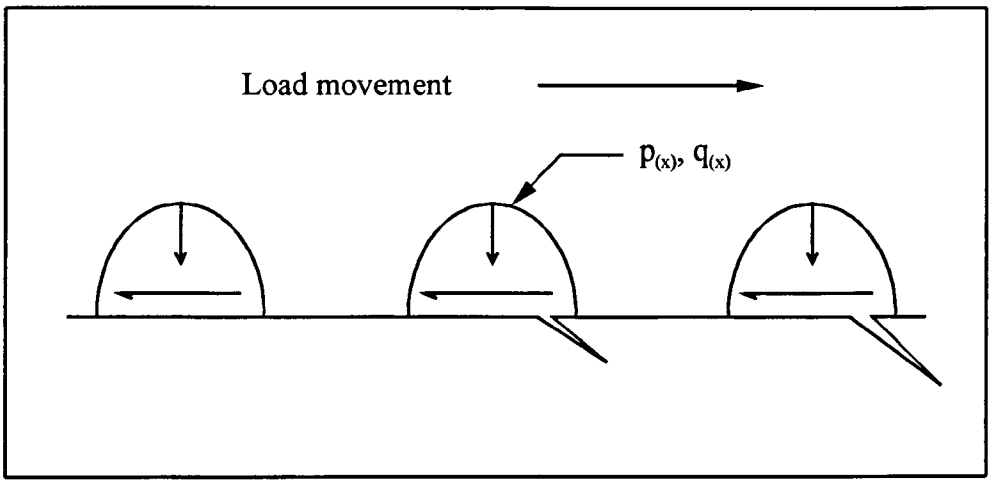

Figure 3.35. Crack initiation and propagation by ratchetting (after Tyfour et al., 1996)

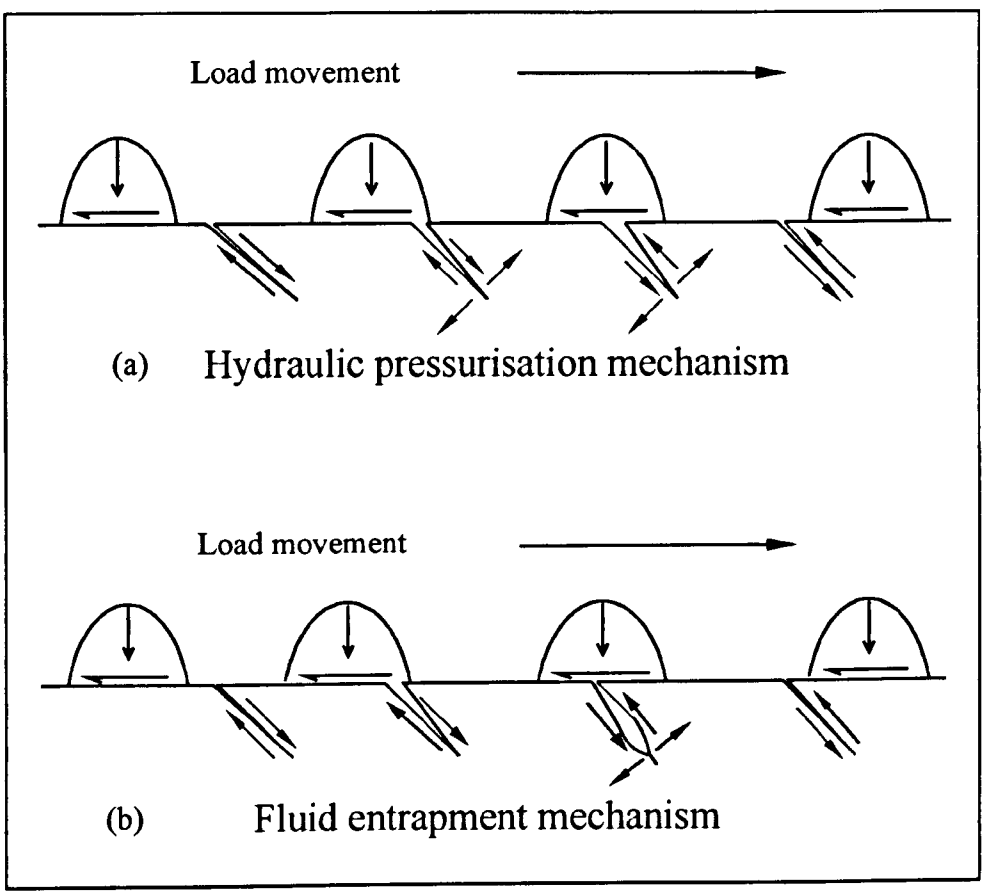

Figure 3.36. Crack propagation by (a) Hydraulic mechanism. (b) Fluid entrapment mechanism. (after Bower, 1988)

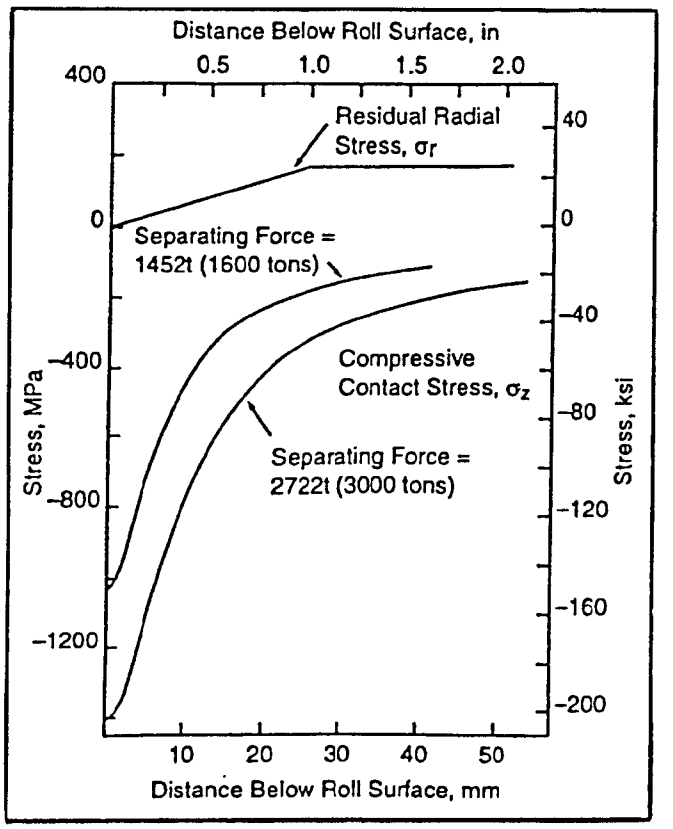

Figure 3.37. Variation of compressive stress σ_z and radial residual stress σ_r with distance below surface (Kapadia and Marsden, 1997)

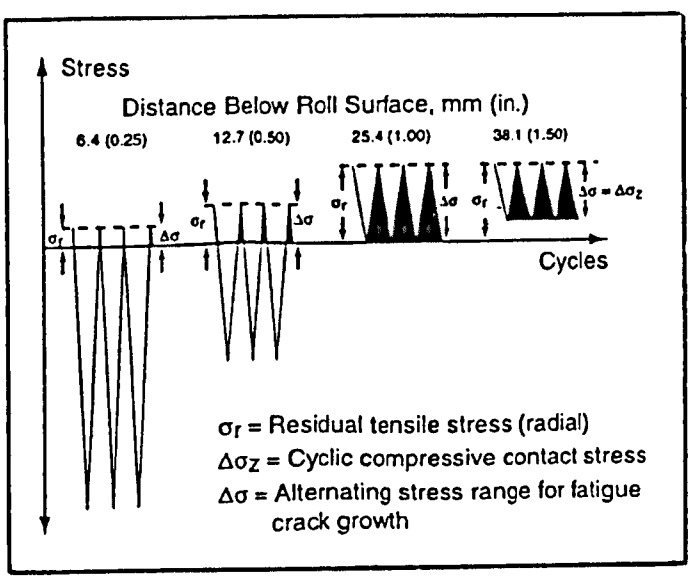

Figure 3.38. Stress model for propagation of fatigue band (Kapadia and Marsden, 1997)

Chapter 4

EXPERIMENTAL WORK

4.1. INTRODUCTION

The rolling contact fatigue and wear performances of a bainitic steel back-up roll material have been investigated by experimental simulation of the loading and operating conditions at the work roll/back-up roll interface using the "SUROS" Rolling-Sliding Testing Machine at the University of Sheffield.

Work roll and back-up roll test disc specimens manufactured from cast HSS and bainitic roll steel respectively were used in the tests. These specimens together with a sample of material spalled from a back-up roll have been subjected to detailed laboratory examination. The test disc specimens and the sample of spalled material were supplied by Sheffield Forgemasters Rolls Limited.

The microstructures of the back-up roll test disc specimens and the sample of roll material have been examined using optical and backscattered electron microscopy, X-ray diffraction (XRD), bulk X-ray texture analysis and electron backscattered diffraction (EBSD).

The morphologies of the rolling contact fatigue cracks produced in both the back-up roll test disc specimens and the sample of spalled material and the influence of microstructure on crack morphology and the resistance to fatigue crack growth have been investigated using optical, scanning electron (SEM) and backscattered electron microscopy.

The metallographical procedures carried out on the laboratory specimens, the description of the "SUROS" Testing Machine, the testing methodology used in the experimental simulations and the recorded experimental results are detailed in this chapter, but the analysis, interpretation and discussion of the results are presented in Chapter 6.

4.2. METALLOGRAPHY

4.2.1. *Introduction*

Laboratory specimens were obtained by sectioning samples taken from the used test discs and the spalled back-up roll material. The sectioning was carried out using silicon carbide cutting off discs or by EDM wire erosion.

4.2.2. *Specimen preparation*

4.2.2.1. Optical microscopy

Specimens for examination by optical microscopy were mounted in Bakelite. After mounting the specimens were polished, the final polish being carried out using a fine diamond paste (1μm). Immediately prior to examination the specimens were etched with a solution of 2% Nital.

4.2.2.2. Scanning electron and backscattered electron microscopy

Specimens for examination using scanning electron and backscattered electron microscopy were mounted and prepared as for optical microscopy. Immediately prior to examination the specimens were etched with a solution of 2% Nital. Etching is not necessary for examination by backscattered electron microscopy but it facilitated switching to scanning electron microscopy if desired.

4.2.2.3. XRD and bulk X-ray texture analysis

Specimens for examination using XRD or bulk X-ray texture analysis were finish machined to give a fine ground finish.

4.2.2.4. EBSD

Specimens for examination using EBSD were finish polished using magnesium oxide. For ease of polishing and mounting in the scanning electron microscope the specimens were mounted in Wood's metal ($T_m \cong 70°C$) inside machined aluminium pots (12mm OD, 12mm overall depth). The specimens were re-polished with magnesium oxide and thoroughly cleaned immediately prior to mounting in the microscope.

4.2.3. *Specimen examination*

4.2.3.1. Optical microscopy

Specimens were examined and photographed on a "Polyvar (MET)" optical microscope fitted with a 35mm camera.

4.2.3.2. Scanning electron and backscattered electron microscopy

Scanning electron imaging (SEI) and backscattered electron imaging (BEI) were carried out on a Jeol 6400 Scanning Electron Microscope fitted with a tungsten filament. The system was operated with an accelerating voltage of 20 kV with a working distance of 15 or 25 mm for SEI and an accelerating voltage of 10 kV with a working distance of 15 mm for BEI.

4.2.3.3. XRD

XRD analysis was performed using a Phillips 1700 X-ray Diffractometer System. The system was operated using a Co Kα source ($\lambda = 0.17889$ nm) at an accelerating voltage of 40 kV and a current of 30 mA. Data was collected over an angle range of 40° to 130°.

4.2.3.4. Bulk X-ray texture analysis

Bulk X-ray texture analysis was performed using a modified Philips (X-ray generator)/Siemens (goniometer) system controlled using a Hilton-Brookes control and data collection system. Data was collected for {103}, {110}, {200} and {211} pole figures using a Co kα source (λ = 0.17789 nm) operating at 40 kV and 30 mA. The data was plotted using the software Textron III.

4.2.3.5. EBSD

EBSD analysis was carried out using a Jeol 6400 Scanning Electron Microscope fitted with a tungsten filament and an EBSD system (HKL Technologies). The system was operated with an accelerating voltage of 20 kV with a working distance of 24 mm and a tilt angle of 70°. The operation of a typical EBSD system is described by Randle and Engler (2001) and is shown schematically in Figure 4.1.

4.2.3.6. Hardness testing

The hardness of specimens was measured on a Vickers Hardness Testing Machine using a 50 kg load and a 2/3 objective.

4.2.3.7. Surface replication

Replicas of contact surfaces were taken using cellulose acetate replication sheets (thickness-35 μm) and acetone as the solvent. The replicas were mounted on glass slides for examination by optical microscopy.

4.3. EXPERIMENTAL SIMULATION

4.3.1. *"SUROS" rolling –sliding testing machine*

Experimental simulation was carried out on the "SUROS" twin disc rolling-sliding testing machine, which is based on a modified Colchester 1600 lathe. The top test disc specimen (back-up roll) is driven by the lathe motor and gearbox and the bottom test disc specimen (work roll) by an AC induction motor. The speed of the latter is controlled using an ABB ACS600 frequency controller.

Loads up to 29 kN can be applied to the test disc interface, producing accurately maintained maximum Hertzian stresses p_o in the range 900 MPa to 1800 MPa. The machine is capable of speeds from 100 rpm to 1600 rpm, at rolling-sliding velocity ratios (slip) from 0% to 20%. The relative slip S is given by equation 4.1.

$$S(\%) = \frac{200\left(r_w N_w - r_b N_b\right)}{r_w N_w + r_b N_b} \qquad (4.1)$$

where r_w and r_b are the radii of the work roll and back-up test discs respectively and N_w and N_b are the revolution counts for the work roll and back-up roll test discs respectively.

The normal load which is necessary to produce the required maximum contact pressure p_0 at the test disc interface was determined using equation 3.2 (section 3.5.2), where for this case $R_1 = r_w$ and $R_2 = r_b$.

Both dry and lubricated tests can be run. Crack detection and the monitoring of crack growth is carried out by a non-contact eddy current crack detection method using an "Elotest B1" crack detection unit. A computerised system is used to control the machine and all the instrumentation is interfaced to a computer based data acquisition system. A schematic diagram of the machine is shown in Figure 4.2 (Fletcher and Beynon, 2000). The layout of the machine and a view of the relative

operational positions of the crack detector probe and back-up roll test disc are shown in Figures 4.3a and 4.3b respectively.

4.3.2. *Test data*

Throughout each test, the data acquisition system digitally recorded the normal force acting at the test disc interface W, the torque on the shaft driving the back-up roll test disc T, the speeds N_b and N_w and number of revolutions (cycles) n_b and n_w experienced by the back-up roll and work roll test discs respectively and the relative slip S.

4.3.3. *Crack detection and assessment*

The method of mounting the test disc specimens in the testing machine is shown schematically in Figure 4.4a. During each test, the track surface of the back-up roll was continuously scanned using the probe of the crack detector system, cracks were identified and their growth visually monitored by observation of the signal displayed on the crack detector screen. The circumferential location of a particular crack was established at the end of the test using the same system.

Prior to each test the crack detector was calibrated using a calibration disc with a thin spark eroded inclined surface crack. The calibration disc had earlier been checked to ensure that it was defect free, before the calibration crack was introduced. Details of the spark eroded defect are given below:

Length	100 μm
Width	3 mm
Angle	45°

Defect located in centre of track

A back-up roll test disc was deemed to have failed when the observed signal on the crack detector was the same size as the signal obtained using the calibration disc.

4.3.4. *Test disc specimens*

4.3.4.1. Specimen design

The test disc specimens for this project were designed to give the largest outside diameter (track diameter) which could be accommodated in the testing machine. This approach ensured the largest possible contact patch size and surface speed during testing. Where possible laboratory samples from used test discs were removed by wire erosion in the form of 2 mm thick rings. Using this technique, an initial track diameter of 55 mm allowed three tests to be carried with each test disc before the minimum diameter of 45 mm was reached.

The nominal outer circumference and track width of both the work roll and back-up roll discs were 173 mm and 10 mm respectively. The detailed design of the specimens is shown in Figure 4.4b

4.3.4.2. Back-up roll test disc specimens

Ten back-up roll test disc specimens were manufactured from material taken from the outer section of the barrel of a cast steel back-up roll. The specimens were then heat treated to give a bainitic microstructure with a surface hardness similar to that of a typical hot strip mill back-up roll. Details of the heat treatments carried on the back-up roll test disc specimens are given in the Appendix. The measured hardness range over all the specimens was 458 HV (61 Shore C) to 497 HV (64 Shore C).

The chemical composition of the material is shown in Table 4.1 and a typical example of the microstructure is shown in Figure 4.5.

Results obtained using XRD analysis indicated that there was no detectable level of retained austenite in the back-up roll test disc specimens.

4.3.4.3. Work roll test disc specimens

Ten work roll test disc specimens were manufactured from a specially cast ingot. The specimens were then heat treated to give a microstructure and hardness similar to a typical hot strip mill work roll. Details of the heat treatments carried out on the work roll test disc specimens are given in the Appendix. The measured hardness range over all the specimens was 797 HV (88 Shore C) to 856 HV (92 Shore C). The chemical composition of the material is shown in Table 4.1 and a typical example of the microstructure is shown in Figure 4.6.

4.3.4.4. Pre-test inspection of test disc specimens

Prior to testing, all the test disc specimens were checked and inspected. The results are shown below:

1. The surface profiles of the tracks of the specimens and their concentricity with the bore were checked on a Taylor Hobson Talyrond 100 machine and were found to be satisfactory. Typical examples of the test records are shown in Figures 4.7 and 4.8
2. The specimens were mounted on the arbor of the "SUROS" Testing Machine and were found to be a satisfactory fit
3. The main dimensions, surface finish and general condition of the specimens were found to be satisfactory
4. Visual inspection revealed no surface damage and inspection using the eddy current crack detection system revealed no significant surface or subsurface defects

4.3.4.5. Surface roughness

The surface roughness of the tracks of selected un-run and run work roll and back-up roll test discs was measured using a Taylor Hobson Surtronic 3+ surface roughness measuring machine.

4.3.4.6. Track surface appearance

The surface appearance of the tracks of both un-run and run work roll and back-up roll test disc specimens was studied by direct optical microscopy or the optical examination of surface replicas.

4.3.5. *Wear testing*

During each simulation the test was stopped periodically and after ultrasonic cleaning in ethanol, the mass of the test disc specimens measured by weighing. Weighing was carried out using a Sartorius Precision Balance BP 210D (± 0.0001g except for Test 1 where the mass of the back-up roll test disc exceeded the capacity of this balance). For Test 1 the precision of the balance used was ± 0.01g. This level of precision was considered acceptable because for this test the lengths of the periods (number of loading cycles) between each weighing were high and the associated mass losses relatively significant. After Test 1, the initial mass of the remaining back-up roll test disc specimens was reduced by removing material from body of the disc by drilling, in order to bring the mass into the range of the high precision balance.

4.4. ROLLING CONTACT FATIGUE TESTS

4.4.1. *Introduction*

The programme of rolling contact fatigue tests was carried out to investigate the wear and rolling contact fatigue performance of the back-up roll material under the representative operating and loading conditions established in Chapter 2. The test parameters and operating conditions used in the experimental simulations are described together with an overview and detailed description of the recorded test results.

4.4.2. *Test parameters and operating conditions*

4.4.2.1. Water lubrication

Distilled water was applied to back-up roll test as shown in Figure 4.3. The water was supplied in sufficient quantity to ensure the existence of a complete meniscus adjacent to the test disc interface.

4.4.2.2. Slip

Tests were carried out at a slip level of either 1% or 5%. The lower slip level ensured that the limiting value of the tangential traction was applied to the back-up roll test disc surface throughout the test. The higher slip level was applied to simulate skidding between the work roll and back-up roll.

4.4.2.3. Test schedules

The test schedules for the parameters and loading conditions for the whole programme of experimental simulations are shown in Table 4.2.

4.4.3. *Overview of test results*

In addition to investigating the wear and rolling contact fatigue performance of the back-up roll material, two other important objectives were to establish the morphologies of typical rolling contact fatigue cracks and to investigate the effect of surface wear on crack propagation.

Early in the testing programme, the roughness of the track surface on the work roll test disc specimens was identified as an important factor affecting the wear performance exhibited by the back-up roll test disc specimens. For the purpose of investigating the influence of track surface roughness on wear and rolling contact fatigue, the outer tracks of the work roll test disc specimens used in tests 9-12 and 14-18 were ground to give an appropriate range of surface roughness. The range

selected was similar to that presented by Caithness et al. (1999) as described in Section 3.2.

An overview of the testing programme with an indication of the type of information obtained from each test is given in Table 4.3.

4.4.4. *Test results*

4.4.4.1. Traction coefficients

The value of the traction coefficient at the test disc interface was determined using equation 4.2,

$$\mu = \frac{T}{Wr_b} \tag{4.2}$$

where T is the measured torque on the shaft driving the back-up roll test disc, W is the measured normal force at the test disc interface and r_b is the radius if the back-up roll test disc.

A typical result showing the magnitude and variation of the value of the traction coefficient during a test run is shown in Figure 4.9.

4.4.4.2. Rolling contact fatigue failure

Crack detector signals, whose presence and location indicated rolling contact fatigue failure, were obtained from either test disc surfaces damaged by high asperity stresses and heavy wear or from large surface initiated cracks which penetrated into the deeper substrate. Typical examples of the latter are shown in Figure 4.10.

4.4.4.3. Detailed test results

Full details of the rolling contact fatigue and wear results obtained during in the experimental simulations are given in Tables 4.4 – 4.19.

Back-up roll test disc								
C	Si	S	P	Mn	Ni	Cr	Mo	V
0.39	0.41	0.022	0.032	0.62	0.18	3.26	0.62	0.10

Work roll test disc										
C	Si	S	P	Mn	Ni	Cr	Mo	Cu	V	W
1.76	0.47	0.025	0.03	0.55	0.63	5.68	3.35	0.11	4.6	2.7

Table 4.1. Chemical composition of test disc materials in weight % (balance Fe)

Test number	B. U. roll test disc	Work roll test disc	B. U. roll test disc diameter (mm)	Work roll test disc diameter (mm)	B. U. roll surface roughness Ra (μm)	Work roll Surface Roughness Ra (μm)	Maximum Contact pressure (MPa)	Slip (%)	Lubrication
1	B1	W1	54.99	54.98			1500	-1	Water
3	B3	W3	54.99	54.99			1500	-5	Water
4	B4	W4	55.01	55.00			1500	-5	Water
5	B5	W5	54.99	54.96			1500	-5	Water
6	B3	W4	51.97	51.98			1500	-5	Water
7	B6	W6	54.95	54.98			1500	-5	Water
8	B7	W7	54.98	54.99			1500	-5	Water
9	B4	W5	52.98	52.99		0.06/0.6	1500	-5	Water
10	B10	W10	55.00	54.96	0.85	0.61	1500	-1	Water
11	B8	W8	55.00	54.99	0.85	0.38	1500	-1	Water
12	B9	W9	55.00	54.98	0.85	0.47	1500	-1	Water
14	B9	W9	49.49	49.35	0.12	0.80	1500	-1	Water
15	B10	W10	49.49	49.37	0.17	0.75	1500	-1	Water
16	B8	W8	49.49	49.48	0.16	0.125	1500	-1	Water
17	B10	W10	49.42	49.37			1500	-1	Water
18	B8	W8	49.48	49.48			1500	-1	Water

Notes
Test 3 was terminated prematurely due to arbor breakage
Test 9 was carried out using two work roll test disc specimens with different surface roughnesses
Tests 17 and 18 were continuations of tests 15 and 16 respectively

Table 4.2. Test parameters and operating conditions used in experimental simulations

Test number	Results obtained
1	Crack morphologies Wear performance Rolling contact fatigue failure
3	Wear performance
4	Wear performance
5	Crack morphologies Wear performance
6	Crack morphologies Wear performance Rolling contact fatigue failure
7	Wear performance
8	Wear performance
9	Wear performance
10	Wear performance
11	Crack morphologies Wear performance
12	Wear performance
14	Crack morphologies Wear performance Rolling contact fatigue failure
15	Wear performance
16	Wear performance
17	Crack morphologies Wear performance Rolling contact fatigue failure
18	Crack morphologies Wear performance Rolling contact fatigue failure

Table 4.3. Overview of testing programme

Number of revolutions (cycles)	Mass of back-up roll test disc (g)	Traction coefficient at end of each run	Comments
0	230.38		
60000	230.12	0.13	
160000	229.66	0.13	
252000	228.69	0.14	RCF failure

Effective range of traction coefficient during test (after 2000 cycles) – 0.12-0.18

Table 4.4. Experimental results – Test 1

Number of revolutions (cycles)	Mass of back-up roll test disc (g)	Traction coefficient at end of each run	Comments
0	206.1212		
100015	205.8950	0.18	
	205.8402		*Specimen re-weighed after modification
200020	205.6337	0.18	
217834	205.5888	0.18	**Large erratic crack detector signals
220025	205.5864	0.17	Test aborted

Effective range of traction coefficient during test (after 2000 cycles) – 0.17-0.20

Table 4.5. Experimental results – Test 3

Number of revolutions (cycles)	Mass of back-up roll test disc (g)	Traction coefficient at end of each run	Comments
0	205.5888		
23542	205.4174	0.18	
45553	205.2708	0.18	
	205.2655		*Specimen re-weighed after modification
101565	205.0036	0.19	
130061	204.9217	0.18	**Large erratic Crack detector signals

Effective range of traction coefficient during test (after 2000 cycles) – 0.17-0.19

Table 4.6. Experimental results – Test 4

Number of revolutions (cycles)	Mass of back-up roll test disc (g)	Traction coefficient at end of each run	Comments
0	204.3249		
45018	203.5803	0.17	
95042	202.9249	0.17	
119061	202.7411	0.17	***Large crack detector signals associated with visual surface damage

Effective range of traction coefficient during test (after 2000 cycles) – 0.16-0.18

Table 4.7. Experimental results – Test 5

Number of revolutions (cycles)	Mass of back-up roll test disc (g)	Traction coefficient at end of each run	Comments
0	186.3756		
50014	186.3148	0.15	
100025	186.2508	0.16	
	185.7084		****Specimen Re-weighed after modification
150067	185.6422	0.16	
200098	185.5741	0.16	RCF failure

Effective range of traction coefficient during test (after 2000 cycles) – 0.14-0.16

Table 4.8. Experimental results – Test 6

Number of revolutions (cycles)	Mass of back-up roll test disc (g)	Traction coefficient at end of each run	Comments
0	206.3203		
10010	206.2904	0.17	
20026	206.2762	0.17	
30040	206.2622	0.17	
40057	206.2473	0.17	
50073	206.2336	0.17	
60101	206.2183	0.17	
70129	206.2043	0.17	

Effective range of traction coefficient during test (after 2000 cycles) – 0.15-0.19

Table 4.9. Experimental results – Test 7

Number of revolutions (cycles)	Mass of back-up roll test disc (g)	Traction coefficient at end of each run	Comments
0	206.1044		
10022	206.0750	0.17	
20033	206.0594	0.17	
30046	206.0449	0.17	
40063	206.0306	0.17	
50098	206.0157	0.17	
60115	206.0017	0.16/0.17	
70152	205.9878	0.16	
80169	205.9724	0.17	
90198	205.9577	0.17	
100227	205.9417	0.17	
110253	205.9269	0.17	
120273	205.9134	0.17	

Effective range of traction coefficient during test (after 2000 cycles) – 0.16-0.19

Table 4.10. Experimental results – Test 8

Number of revolutions (cycles)	Mass of back-up roll test disc (g)	Traction coefficient at end of each run	Comments
0	192.1958		Work roll disc surface roughness Ra 0.06 μm
10026	192.1833	0.16	
20097	192.1706	0.16	
30114	192.1579	0.16	
40134	192.1437	0.15	
50148	192.1292	0.14	
60164	192.1159	0.14	
70189	192.1024	0.13	
80416	192.0366	0.19	Work roll disc surface roughness increased to Ra 0.6 μm
90439	192.0104	0.19	
100499	191.9860	0.20	
110515	191.9631	0.18	
120567	191.9421	0.19	

Effective range of traction coefficient during test (after 2000 cycles) – 0.13-0.20

Table 4.11. Experimental results – Test 9

Number of revolutions (cycles)	Mass of back-up roll test disc (g)	Traction coefficient at end of each run	Comments
0	206.0114		
10024	205.9596	0.15	
20042	205.9081	0.14	
30063	205.7972	0.15	
40087	205.6401	0.16	
50110	205.4700	0.16	

Effective range of traction coefficient during test (after 2000 cycles) – 0.14-0.16

Table 4.12. Experimental results – Test 10

Number of revolutions (cycles)	Mass of back-up roll test disc (g)	Traction coefficient at end of each run	Comments
0	205.9733		
10841	205.9234	0.16	
20936	205.8877	0.16	
30955	205.8468	0.17	
40975	205.7994	0.16	
50990	205.7464	0.16	
76007	205.6195	0.15	
101032	205.5020	0.14	
126047	205.3754	0.14	
151086	205.2426	0.14	

Effective range of traction coefficient during test (after 2000 cycles) – 0.14-0.17

Table 4.13. Experimental results – Test 11

Number of revolutions (cycles)	Mass of back-up roll test disc (g)	Traction coefficient at end of each run	Comments
0	206.3950		
10046	206.3459	0.16	
20063	206.2879	0.15	
30137	206.1882	0.15	
40173	206.0610	0.16	
50192	205.9437	0.16	

Effective range of traction coefficient during test (after 2000 cycles) – 0.14-0.16

Table 4.14. Experimental results – Test 12

Number of revolutions (cycles)	Mass of back-up roll test disc (g)	Traction coefficient at end of each run	Comments
0	171.0692		
10020	171.0292	0.16	
20038	170.9409	0.17	
30082	170.8103	0.17	
40114	170.6715	0.17	***Large erratic crack detector signals

Effective range of traction coefficient during test (after 2000 cycles) – 0.16-0.17

Table 4.15. Experimental results – Test 14

Number of revolutions (cycles)	Mass of back-up roll test disc (g)	Traction coefficient at end of each run	Comments
0	170.6481		
10015	170.6040	0.16	
20262	170.5170	0.16	
30381	170.3827	0.17	
40398	170.2329	0.17	
50411	170.0730	0.18	

Effective range of traction coefficient during test (after 2000 cycles) – 0.16-0.18

Table 4.16. Experimental results – Test 15

Number of revolutions (cycles)	Mass of back-up roll test disc (g)	Traction coefficient at end of each run	Comments
0	170.7371		
10014	170.7204	0.27/0.28	
20025	170.7056	0.22	
30039	170.6903	0.24	
40055	170.6752	0.25	
50069	170.6590	0.20/0.21	

Effective range of traction coefficient during test (after 2000 cycles) – 0.12-0.18

Table 4.17. Experimental results – Test 16

Number of revolutions (cycles)	Mass of back-up roll test disc (g)	Traction coefficient at end of each run	Comments
65469	169.8393	0.17	
80485	169.5941	0.17	
105500	169.1660	0.17	
123518	168.8665	0.17	Large crack detector signals indicating RCF failure

Effective range of traction coefficient (after 2000 cycles) – 0.14-0.17

Table 4.18. Experimental results – Test 17 (Continuation of Test 15)

Number of revolutions (cycles)	Mass of back-up roll test disc (g)	Traction coefficient at end of each run	Comments
65111	170.6349	0.16/0.17	
69789	170.6282	0.14/0.15	RCF failure

Effective range of traction coefficient during test (after 2000 cycles) – 0.12-0.18

Table 4.19. Experimental results – Test 18 (Continuation of Test 16)

Notes

* The chamfers at the ends of the bore diameter were increased to ensure that the head of the clamping screw was in firm contact with the test disc specimen.

** Large erratic crack detector signals, which appeared to indicate rolling contact fatigue failure, were sometimes caused by temporary surface features associated with wear.

*** In this test the influence of wear on the appearance of track surface of the back-up roll test disc specimen could be clearly observed visually during the test.

**** The test was interrupted and the surface of the boss on the test disc specimen was polished to facilitate microscopic examination of the material microstructure.

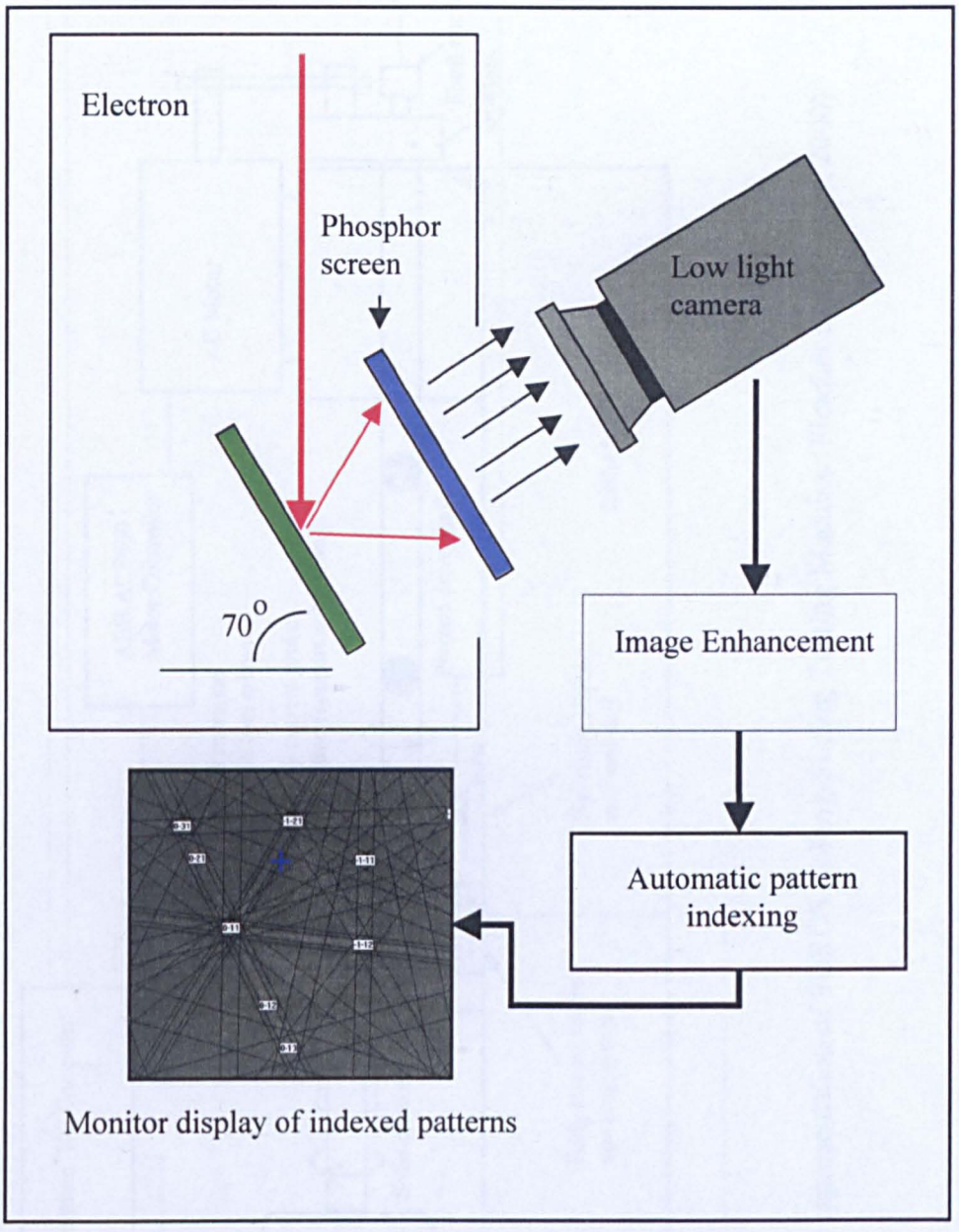

Figure 4.1. Schematic diagram of the arrangement for EBSD examination

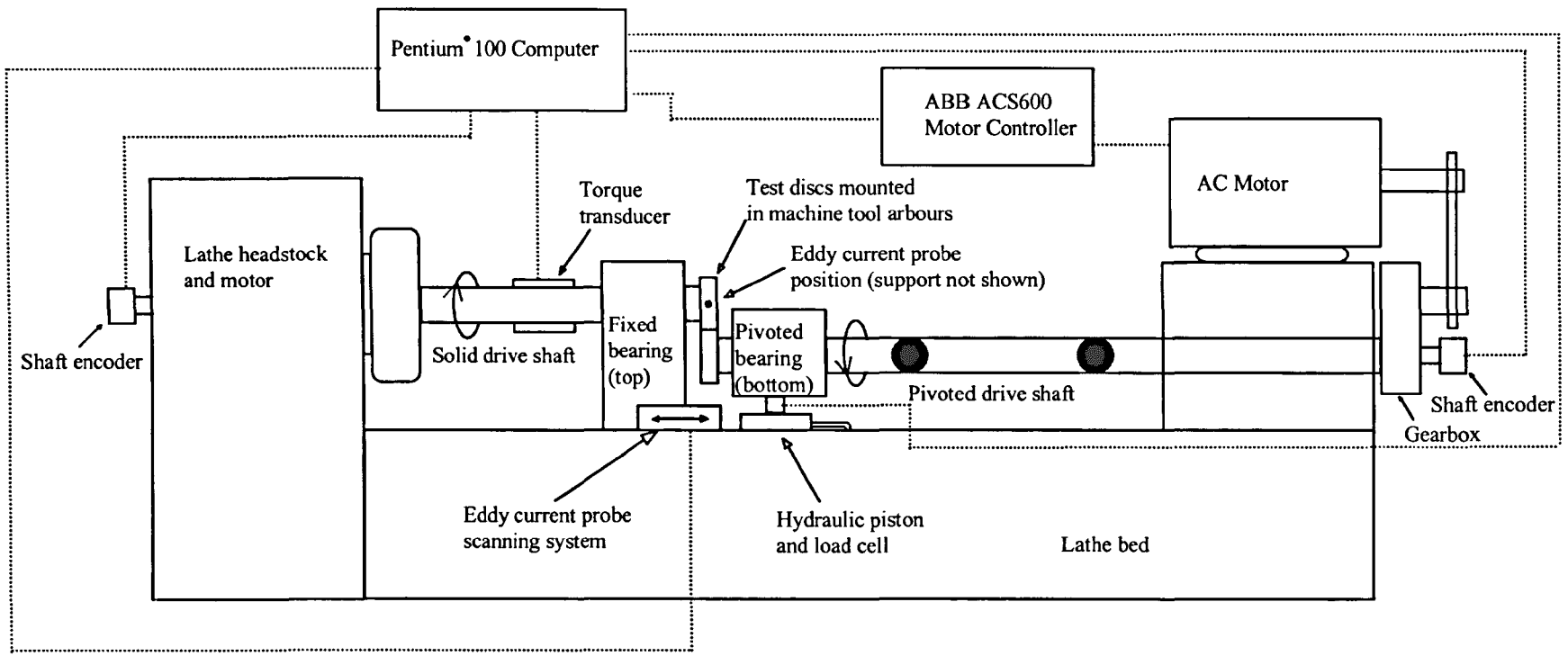

Figure 4.2. Schematic representation of SUROS Rolling-Sliding Testing Machine (Fletcher and Beynon, 2000)

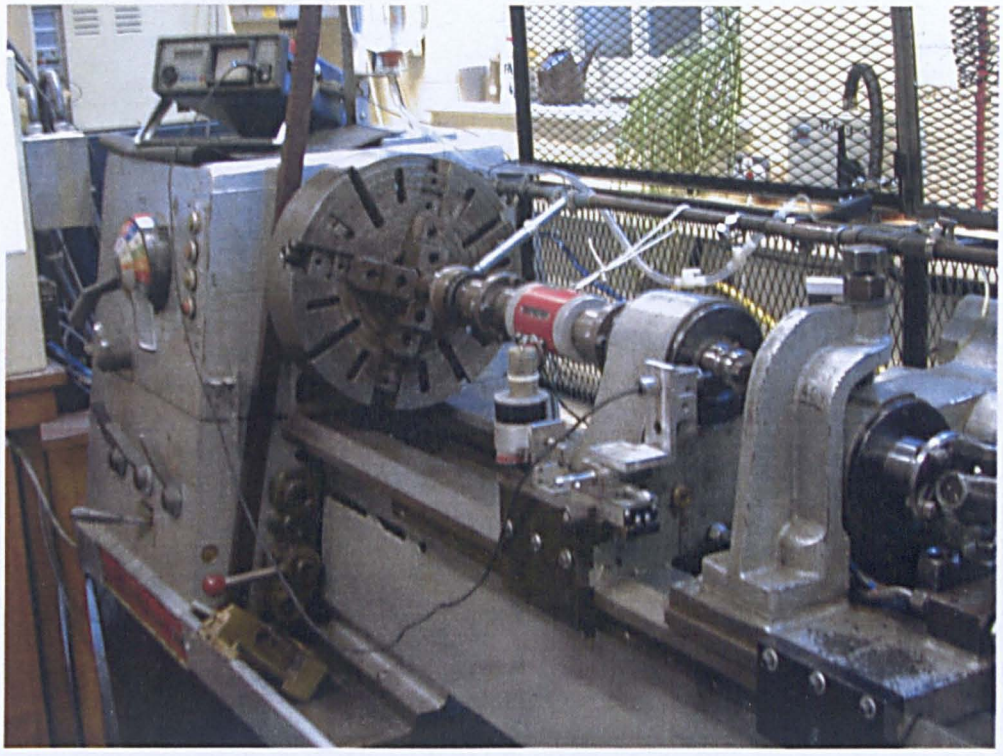

(a)

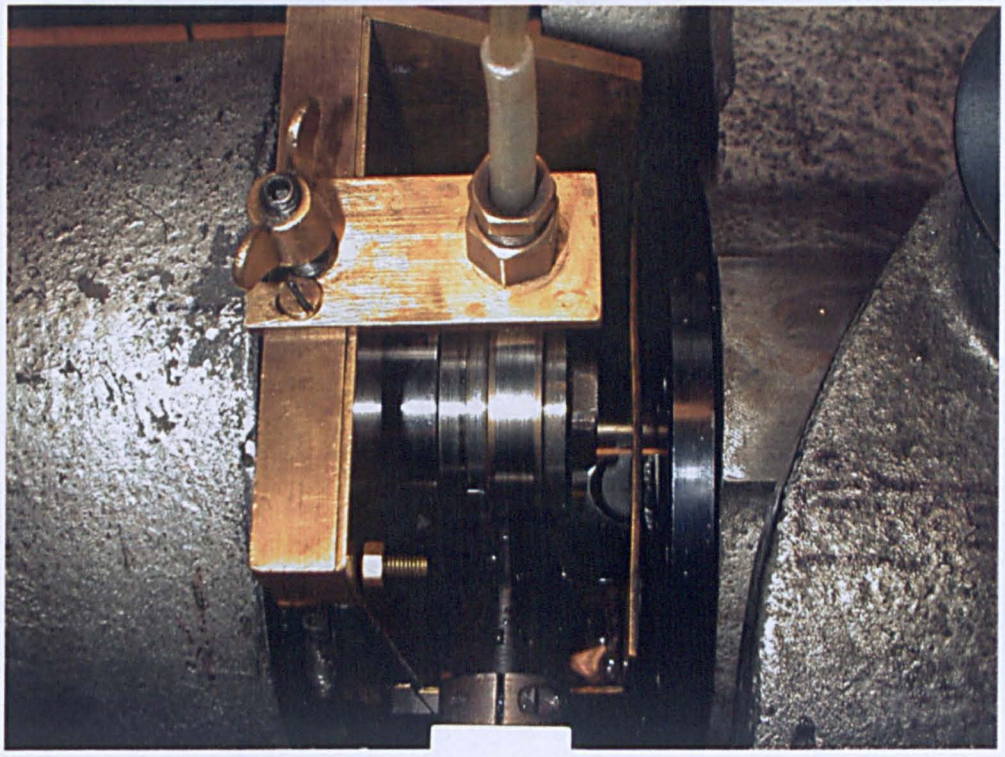

(b)

Figure 4.3. (a) Layout of "SUROS" machine (b) View of crack detector probe

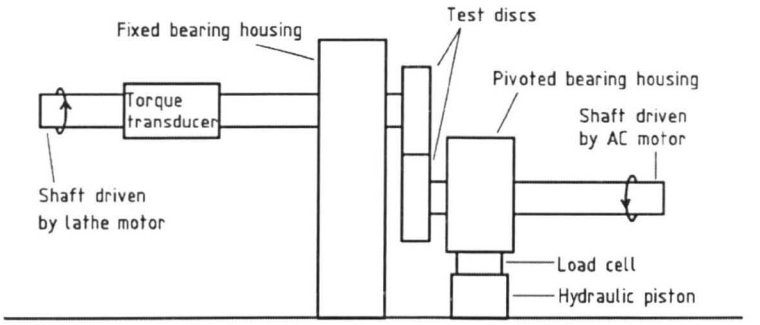

(a)

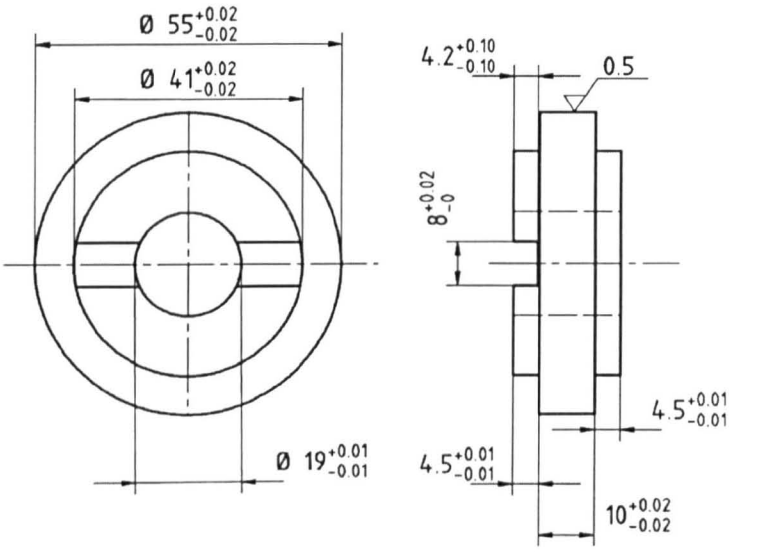

(b)

Figure 4.4. (a) Test method (b) Specimen design

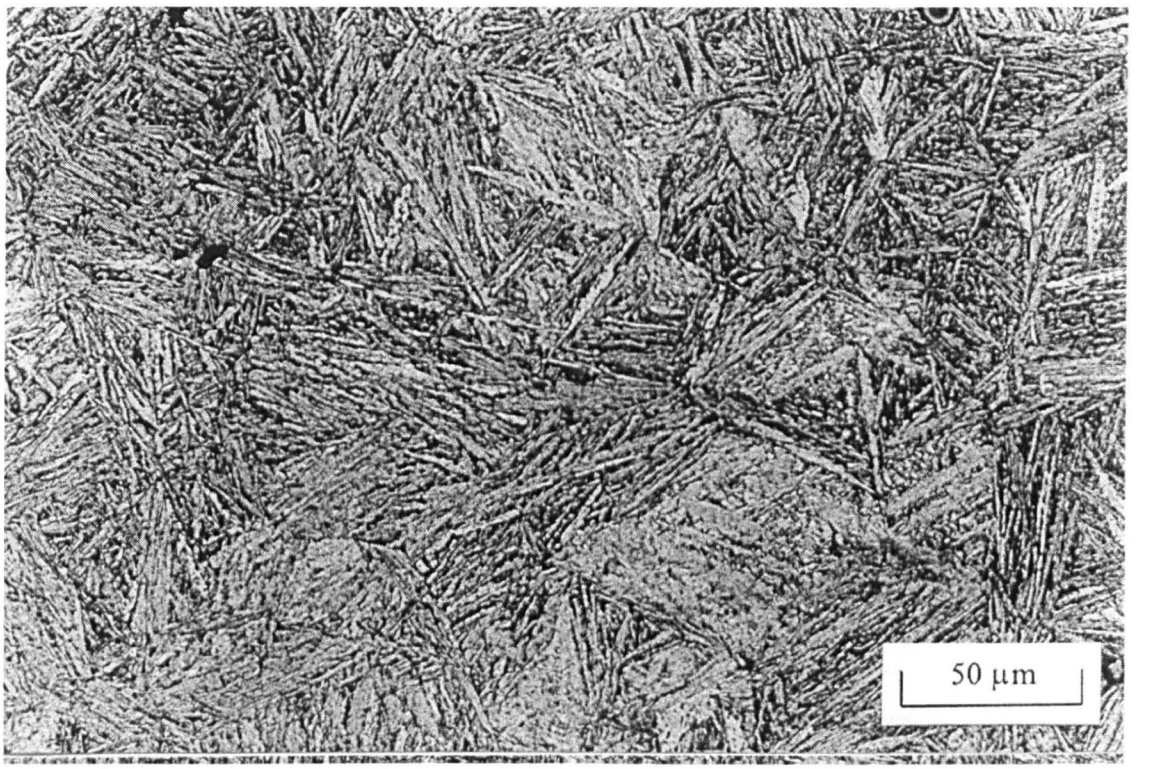

Figure 4.5. Typical example of the microstructure of a bainitic steel back-up roll test disc specimen, polished and heavily etched with 2% Nital

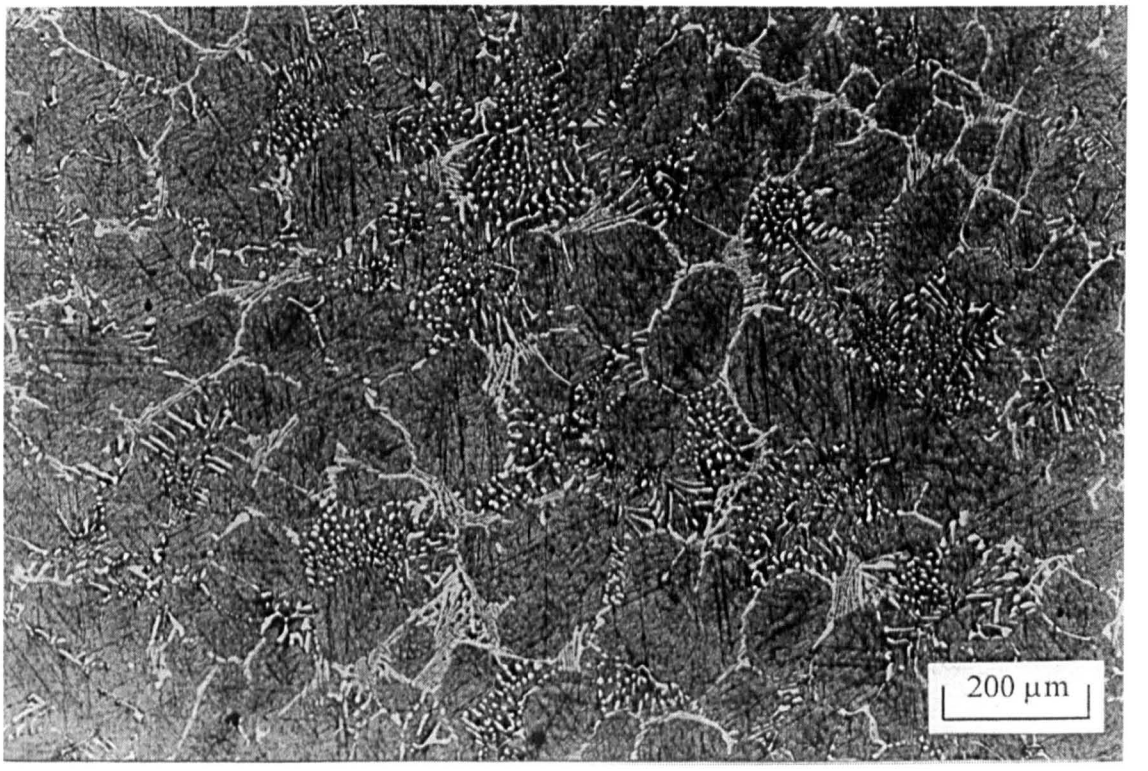

Figure 4.6. Typical example of the microstructure of a HSS work roll test disc specimen, polished and etched with 2% Nital

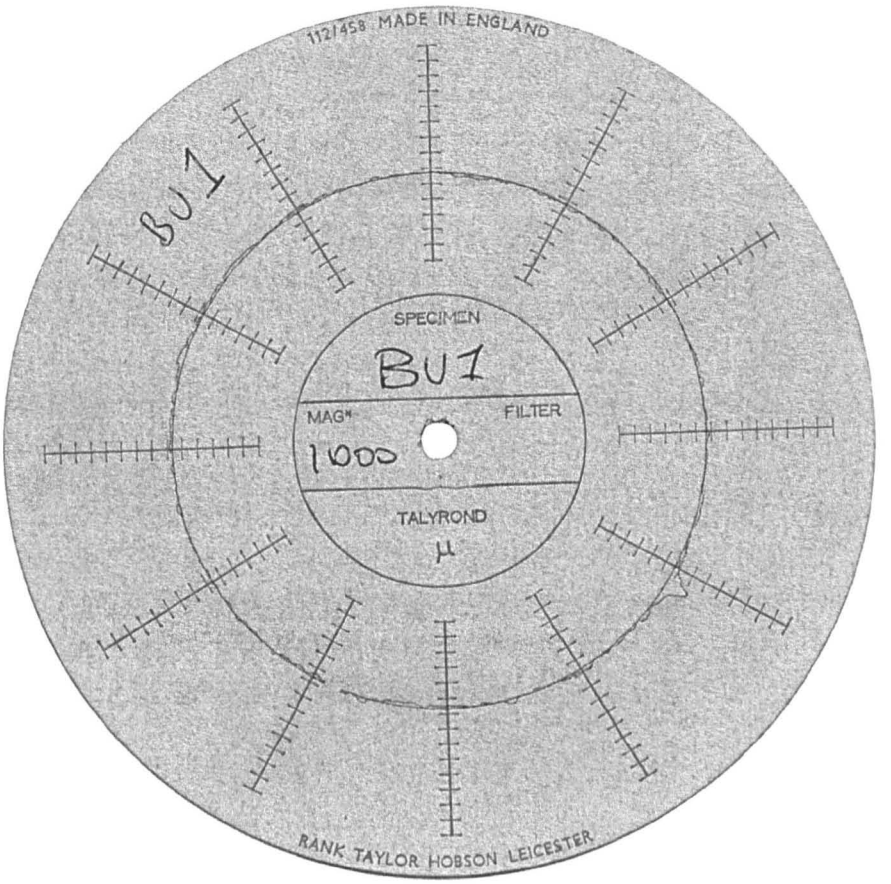

Figure 4.7. Typical record of test disc track profile

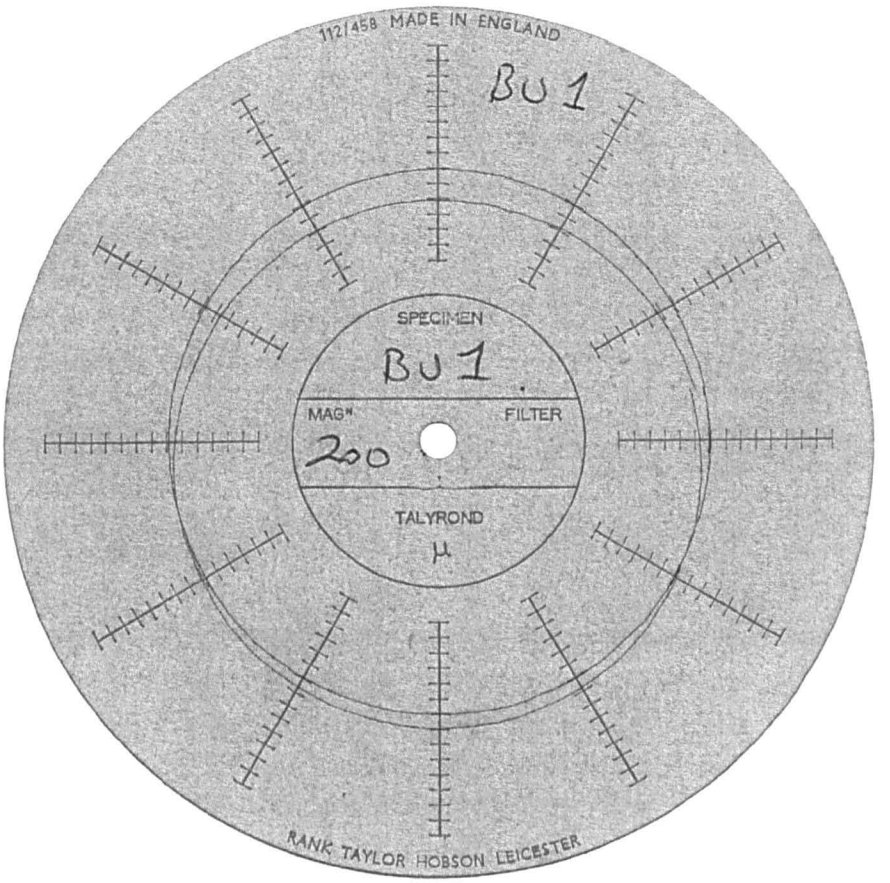

Figure 4.8. Typical record of test disc track/bore concentricity

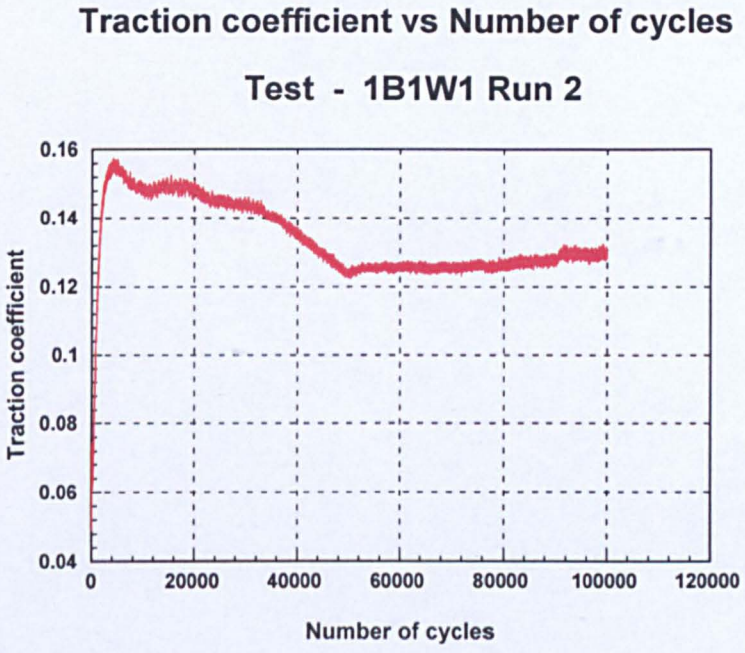

Figure 4.9. Typical record of the traction coefficient during a test run

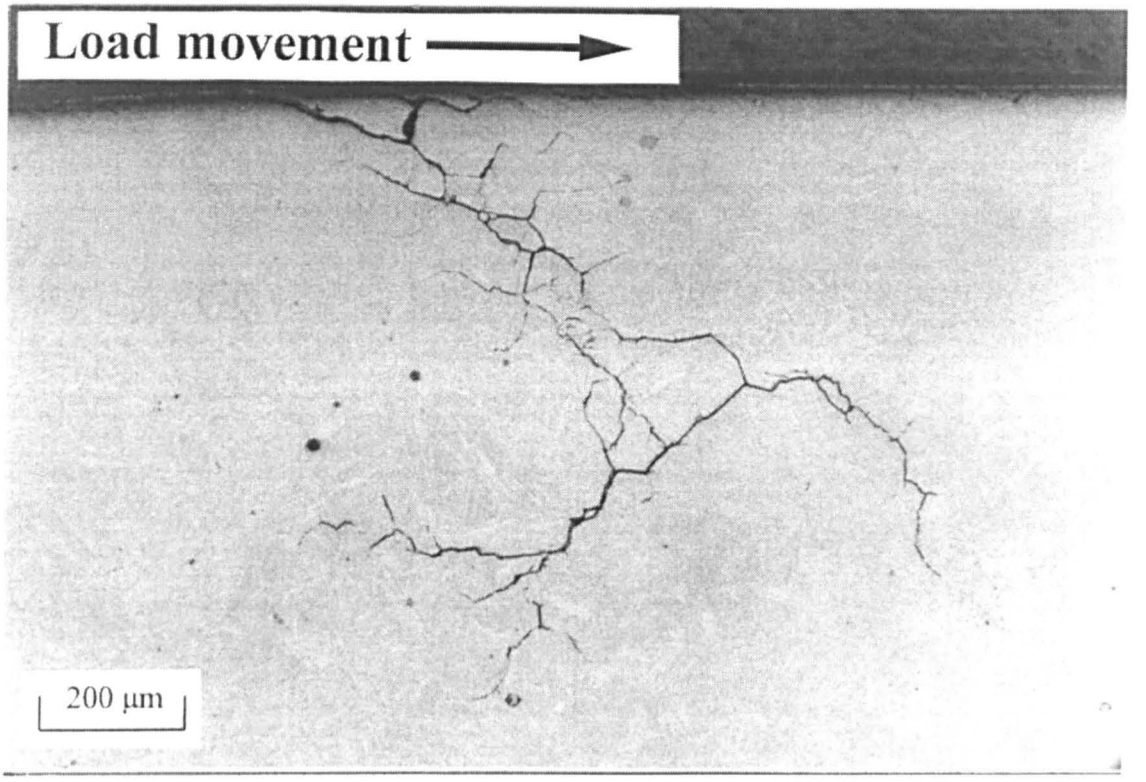

(a) Test 1. (High wear rate – 252000 cycles), specimen B1 polished and lightly etched

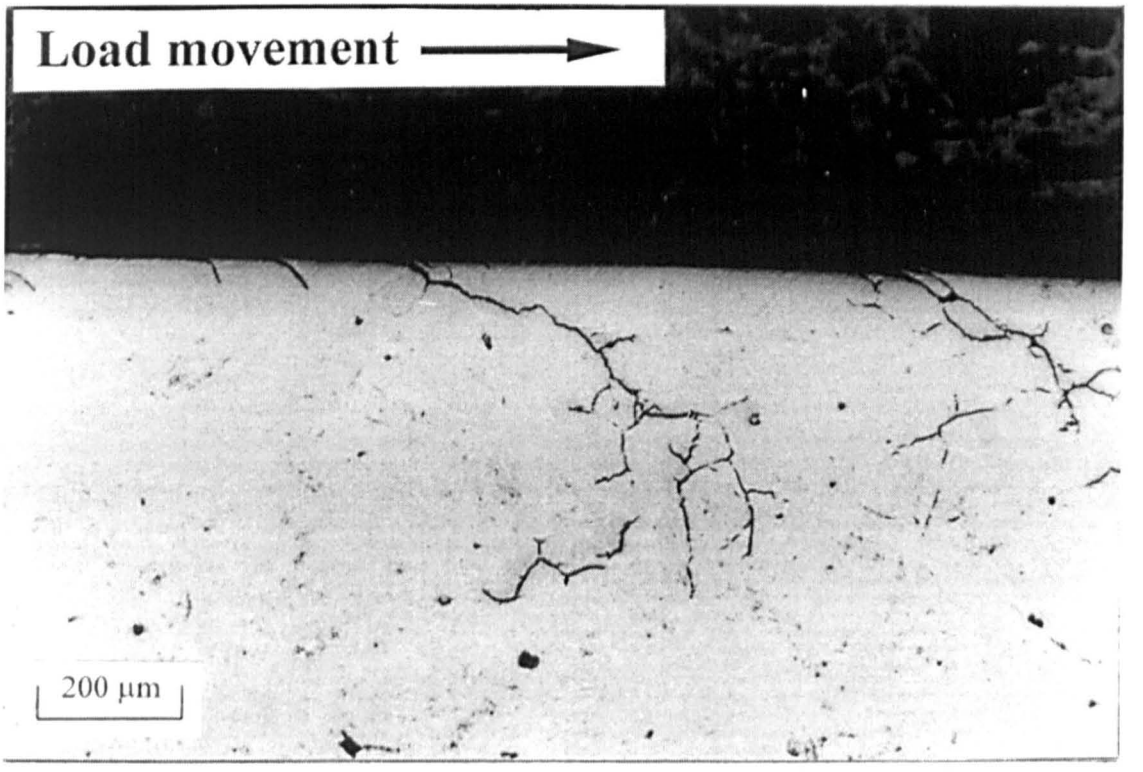

(b) Test 6. (Low wear rate – 200000 cycles), specimen B3 polished and lightly etched

Figure 4.10. Large surface initiated cracks

Chapter 5

MODELLING

5.1. INTRODUCTION

Evidence from the literature review suggested that rolling contact fatigue cracks may be initiated and propagated from critical flaws such as near surface inhomogeneities or alternatively from critical flaws resulting from high roll slip (skidding), mill overloads or the plastic deformation produced by a combination of asperity stresses and the smooth body stresses arising from rolling-sliding contact under what can be considered to be normal operating conditions.

The material and microstructural and mechanical properties required to resist early crack propagation from critical flaws provided by any of these scenarios would be expected to be similar, however controlled experimental simulation and mathematical modelling of the first three loading and operating conditions described above are very difficult. In the light of this, it was considered that the identification of the necessary properties could be accomplished by modelling the initiation and propagation of surface initiated cracks produced by the combination of micro stress fields arising due to surface asperities and the macro stress fields arising from lubricated rolling-sliding contact.

As for the experimental simulations, modelling was carried out assuming normal operating conditions.

The failure models were developed to describe, both qualitatively and quantitatively, failures of the type shown in the schematic model for the five stages of spalling failure presented by Kapadia and Marsden (1997) and shown in Figure 3.30. These models were used as the main bases for the establishment of design criteria for rolling contact fatigue resistance in back-up rolls.

5.2. QUALITATIVE MODELLING

5.2.1. *Assumptions*

5.2.1.1. Loading and operating conditions

It was assumed that the stresses, which initiate and propagate the rolling contact fatigue cracks, arise from the action of the normal and tangential tractions acting at the work roll/back-up roll interface, the presence of surface asperities and the pressurisation and lubrication of the crack faces by the roll coolant. An example of how the presence of surface asperities within the contact region, coupled with the applied loads, could give rise to high asperity stresses which are superposed on the smooth body principal shear stresses (normalised by p_0) is shown in Figure 5.1 (after Bailey and Sayles, 1991, for demonstration purposes only).

5.2.1.2. The response of the material to cyclic loading

For the purposes of the development of this model and the establishment of the structure of the experimental programme, the possible responses of the roll material to the applied stresses were categorised as shown in Figure 5.2 (after Johnson, 1989).

For both the modelling and the required experimental simulations the parameters were chosen to predict and examine the rolling contact fatigue performance under the loading conditions described in categories 1 and 3, Figure 5.2.

5. 2.1.3. General assumptions

The following general assumptions were assumed to apply in this case:

1. The contact between the work roll and back-up roll could be considered as the two dimensionally loaded line contact between two cylindrical elastic half spaces

2. Deformations would take place under conditions of plane strain

3. The friction forces arising at smooth body and asperity contacts would obey Amonton's law of sliding friction

4. Due to the high yield stress of the material, the stress levels assumed for the model would result in crack propagation, which takes place mainly in the elastic region. It was therefore assumed that the laws of linear elastic fracture mechanics would apply

5.2.2. *Qualitative failure model*

5.2.2.1. Model details

In this model, the loads which produce the driving stresses for crack initiation and propagation are the normal and tangential tractions acting on the contact surface and fluid pressure on the crack faces. A schematic diagram showing the separate phases of the proposed qualitative contact and fracture mechanics model and the previously established system parameters is shown in upper part of Figure 5.3. The value used for the surface traction coefficient is negative because the tangential traction operates in the direction opposite to the load movement.

5.2.2.2. Crack initiation and small crack propagation

Cracks are rapidly initiated and propagated through a thin plastically deformed surface layer (Phase 1-2, Figure 5.3) by a combination of surface shear and asperity stresses or the combination of high stresses and thermal damage which occurs during mill incidents. The inclined cracks are propagated in the direction of the load movement, and in the direction opposite to the tangential traction (since the work roll drives the back-up roll).

5.2.2.3. Short and long crack propagation

In phases 2-3 and 3-4, Figure 5.3, crack propagation is in mode II or mixed mode I/mode II, propagation being assisted by water lubrication of the crack faces and fluid pressurisation of the crack by the hydraulic mechanism (See section 3.7.3.)

In phases 3-7 and 4-5 crack propagation is in mode I, controlled by the effects of crack pressurisation and lubrication of the inclined crack faces, as proposed by Way (1935) and supported by Bower (1988) and others.

In phase 5-6 cracks are propagated by a combination of residual radial tensile stresses and cyclic radial compressive contact stresses, as proposed by Kapadia and Marsden (1997).

5.2.2.4. System parameters

The system parameters required for the quantitative modelling were the values of the maximum normal traction (contact pressure) p_0 and the traction coefficient μ at the work roll/back-up roll interface. The value used for the maximum contact pressure (1500 MPa) was the same as that used in the experimental simulations. The value of 0.14 used for the traction coefficient was reasonably representative of the value measured in the middle and later stages of Test 1.

5.2.3. *Model validation*

The general qualitative model was developed to predict the possible crack morphologies for a range of system geometries from the test disc pair to the large-scale contact pair of work roll and back-up roll.

For the case of the test disc pair, the qualitative model was validated by the examination of the morphologies of cracks produced in test disc B1, during Test 1. Examples of the observed rolling contact fatigue cracks are shown in the lower part of Figure 5.3. The observed morphologies indicated that the inclined surface initiated cracks propagated in the direction of the load movement and that for crack lengths greater than 100 μm the first branching tended to be upturning. It was considered that these results provided sufficient validation to justify moving to the quantification of the model.

5.3. QUANTITATIVE MODELLING

5.3.1. *Methodology*

The qualitative model was quantified using the results of a contact and fracture mechanics analysis and material properties presented in published literature. Crack morphology was investigated by determining the mode I and mode II stress intensity factors at the crack tips and then using these results to theoretically predict the most probable directions of crack propagation. The analysis was carried out from crack initiation to just beyond the point at which mode I threshold was reached, this being the range of crack propagation most influenced by the material microstructure.

5.3.2. *Microstructural barriers to fatigue crack growth*

For the purpose of establishing the main barriers to fatigue crack growth and defining the effective grain size of the material, the surface initiated cracks were assumed to be semi-circular cracks propagating through a three-dimensional microstructure.

Gladman and Pickering (1983), when describing the main features of the bainitic microstructure, identify the ferrite packet and prior austenite grain boundaries as the high angle boundaries within the microstructure. High angle boundaries, in this case, are defined as areas in the microstructure where a propagating crack must change direction significantly in order to continue propagation along similar crystallographic planes.

Observations of cracks produced in test discs in early experimental simulations indicated that cracks initiated and commenced propagation along suitably orientated prior austenite grain boundaries and between ferrite packets or groups of packets. In the case of ferrite packets or groups of packets it was assumed that small cracks would propagate along the ferrite packet/carbide boundaries until the semi-circular cracks reached the packet edges.

It follows from this discussion that the main barriers to fatigue crack growth should occur at high angle prior austenite grain boundaries and the more numerous ferrite packet boundaries. It was therefore assumed, for the purpose of this application, that the smallest dimension of the ferrite packets could be considered to be the effective grain size.

5.3.3. *Model parameters*

5.3.3.1. Loading and operating conditions

The system parameters and operating conditions were assumed to be those presented in the schematic diagram for the qualitative model (Figure 5.3). Where crack face friction was assumed to influence the value of the mode II stress intensity factors, the value of the coefficient of crack face friction μ_{cf} was assumed to be 0.14, which was the mean value measured in the middle and later stages of Test 1.

5.3.3.2. Contact half widths

The calculations for the contact half widths for both the test disc pair and the work roll back-up roll pair are presented in the Appendix. Typically the former have contact half widths of approximately 0.3 mm and the latter 6 mm.

5.3.4. *Fatigue crack growth rates*

Kapadia and Marsden (1997) present the results of a series of fatigue crack growth tests on several back-up roll steels with varying mechanical and microstructural properties. A schematic summary of these results for mode I crack propagation is shown in Figure 5.4 (after Kapadia and Marsden, 1997). The range of possible mode I thresholds derived from this summary has been used for the prediction of crack morphology in this work.

5.3.5. *Mode I crack propagation threshold*

In order to predict the commencement of mode I (tensile mechanism) crack propagation and the subsequent crack morphology it was necessary to establish a representative value for the threshold mode I stress intensity factor range ΔK_{Ith}. Inspection of the data shown in Figure 5.4 indicated that, for the back-up roll materials tested, the value lies between 5.5 and 10 MPa$\sqrt{m}$ for a load ratio of 0.05.

5.3.6. *Mode II crack propagation threshold*

In order to determine the crack length at which crack propagation in the mode II (shear mechanism) would commence, it was necessary to determine a value for the threshold stress intensity factor range in mode II. No mode II values are available for very small cracks in bainitic steels, but as a result of a study concerning fatigue crack growth under mixed mode conditions, Otsuka et al. (1975) determined a value of 1.5 MPa$\sqrt{m}$ for mode II threshold in low carbon steels. This value has been applied by Kaneta et al. (1985) in a study of fatigue crack growth in rolling-sliding contact.

The propagation of small and short cracks would be expected to take place preferentially along the ferrite/carbide boundaries in low carbon steels and the ferrite packet/carbide boundaries in bainitic steels ie. though similar microstructural features. It was therefore considered that the value of 1.5 MPa$\sqrt{m}$ would be a reasonable value for early crack propagation in bainitic roll steels.

5.3.7. *Assumptions*

The qualitative model assumes that, once an initiated crack has been propagated through the plastically deformed surface layer, the crack becomes a flaw of critical size and that for preferentially orientated cracks, propagation then continues without arrest. In order to justify this assumption and to demonstrate that the use of a quantitative damage tolerance model is valid, it was necessary to establish that the following criteria were satisfied:

1. Cracks were rapidly propagated through a thin plastically deformed layer (phase 1-2, Figure 5.3).
2. The mode II stress intensity factor range ΔK_{II} determined at point (2) in the qualitative model, Figure 5.3, was greater than the assumed threshold value for mode II crack propagation ΔK_{IIth}.
3. Some inclined cracks were propagated to the crack lengths at which the predicted maximum mode I stress intensity factor range was equivalent to a value within the mode I threshold range presented by Kapadia and Marsden (1997).

The first criterion was tested by examination of the near surface plastic deformation and associated small cracks produced in the test discs used in experimental simulations and in a sample of spalled back-up roll material and other field evidence. Plastic deformation was revealed by sectioning and etching the specimens. The second and third criteria were tested by the determination of the mode I and II stress intensity factors at the crack tips for the crack lengths observed in the samples described above. The method of determining of the mode I and mode II stress intensity factors at the tips of surface initiated, inclined rolling contact fatigue cracks is described in the next section.

5.3.8. *Stress intensity factors*

5.3.8.1. The applicability of linear elastic fracture mechanics

Linear elastic fracture mechanics was deemed to be valid if:

1. The crack length, at which the threshold for mode I crack propagation was reached, was such that the main microstructural barriers to fatigue crack growth had been breached and the crack could be assumed to be propagating in a continuum.
2. The plastic zone ahead the tip of the fatigue crack was small when compared with the distance of the crack tip to any boundary of the member. Dowling (1993) suggests that the criterion for this assumption to be valid is that the ratio of the distance of the crack tip from the boundary of the member to $2r_{cyclic}$ should

be greater than 4. In this case $2r_{cyclic}$ represents the cyclic plastic zone size (diameter) arising under conditions of plane strain.

The validity of these assumptions was tested once the stress intensity factors had been determined for a range of inclined crack lengths and angles.

5.3.8.2. Cyclic plastic zone size

Dowling (1993) presents equations for determining approximate values for the plastic zone size $2r_{cyclic}$ ahead of the tips of fatigue cracks propagating in perfectly elastic-plastic materials. A general form of these equations, modified to express the applied mode I stress intensity factor range in terms of the maximum mode I stress intensity factor K_{max} and the load ratio R, and also to include cyclically hardening and softening materials, is shown in equation (5.1).

$$2r_{cyclic} = C\left[\frac{K_{\max}(1-R)}{2\sigma'_y}\right]^2 \tag{5.1}$$

where σ'_y is the cyclic yield stress and the value of C is $1/\pi$ for plane stress and $1/3\pi$ for plane strain.

By specifying the state of stress and the appropriate loading conditions, the cyclic plastic zone sizes determined using this equation can be used to confirm the applicability of the use of linear elastic fracture mechanics and also to test the validity of using the crack propagation data presented by Kapadia and Marsden (1997) for cracks produced under conditions of rolling contact fatigue.

For the cases of work roll/back-up roll and test disc contacts, the deformations were considered to take place under conditions of plane strain. It was also assumed that premature crack closure would not occur and that the effective load ratio R under rolling contact fatigue conditions would be -1 (plastic superposition being valid only up to the point of complete load reversal (Suresh, 1998)).

Yoder et al. (1983) suggest that for a given material the mode I threshold is reached when the cyclic plastic zone size is the same as the mean effective grain size. A comparison of the calculated cyclic plastic zone sizes arising at the crack tips (equation 5.1) indicates that for a given value of the maximum mode I stress intensity factor, the cyclic plastic zone size may be greater under the conditions assumed for rolling contact (plane strain, R = -1) than for the deformation and loading conditions (plane strain, R = 0.05) used by Kapadia and Marsden (1997). This result suggests that under rolling contact conditions the roll materials may exhibit mode I thresholds that are lower than those presented by Kapadia and Marsden. It was nevertheless considered reasonable to use the threshold data presented by Kapadia and Marsden to predict the trends in crack morphology.

5.3.8.3. Determination of the stress intensity factors

There are many methods available for the determination of the stress intensity factors. Some of the most popular methods are listed below and discussed by Hills and Nowell (1994):

1. Finite element analysis
2. Boundary element analysis
3. Green's Function methods
4. Dislocation density and other related strain nucleii techniques

The choice of method depends on the application, but the most important factors in this case are: the rapidly changing contact stress fields and the associated high stress gradients, the presence of a lubricating fluid and the effects of crack closure in the predominantly compressive stress fields.

For the crack propagation mechanisms assumed to be operating in the quantitative model, convenient methods for calculating the stress intensity factors are presented by Fletcher and Beynon (1999a and 1999b). These methods are simple to use and the results compare well with those from more complex models. The computations were carried out for two distinct crack line loading conditions as described below:

1. Water lubricated, inclined surface breaking cracks with crack face friction under conditions of normal and tangential contact loading (Fletcher and Beynon, 1999a).
2. Pressurised, fluid filled, inclined surface breaking cracks under conditions of normal and tangential contact loading (Fletcher and Beynon, 1999b). For the loading conditions considered in this study, the properties of the lubricating fluid and the geometry and dynamics of the system may cause some attenuation of the fluid pressure along the crack length. The applied pressure was therefore assumed to decrease linearly from the normal Hertzian contact pressure at the crack mouth to zero at the crack tip. This crack line loading condition has been assumed by several authors of crack pressurisation models, for example Kaneta et al. (1985).

These models, which make use of the appropriate Green's functions presented by Rooke et al. (1992) for cracks at angles of 0, 15, 30, 45, 55 and 60° to the surface normal, were used to predict the crack lengths at which the mode II and Mode I threshold values were reached.

Preliminary calculations of the values of the stress intensity factors for which Green's functions are available indicated that, for the prevailing combinations of contact load, contact half width, coefficient of traction and crack face friction coefficient (the crack face friction coefficient could not be measured, but was assumed to be equal to the surface traction coefficient, see Section 5.3.3.1), the highest stress intensity factors arose at the tips of cracks propagating at an angle of 60° to the surface normal (see Figure 6.8). The analysis was therefore concentrated on cracks propagating at this angle. The use in the computations of Green's functions for inclined cracks propagating at 60° to the surface normal was justified by examination of the morphology of the cracks produced in the test discs. The main observations were:

1. The largest cracks propagated at approximately 60° to the surface normal
2. Cracks, which propagated at angles significantly greater than 60° to the surface normal, tended to remain in the surface layer or were removed by surface wear.

5.3.8.4. Mode of crack propagation

Separate computations were carried out to determine the crack lengths at which mode II (shear mechanism) and mode I (tensile mechanism) crack growth would commence in the back-up roll test discs and back-up rolls.

5.3.8.5. Mode II stress intensity factors

In order to establish the crack length at which mode II (shear mechanism) propagation would commence, the values of the mode II stress intensity factor ranges were determined using the crack face friction model (Fletcher and Beynon, 1999a). A schematic diagram of the stress intensity factors arising at the crack tips as assumed in this model is shown in Figure 5.5a.

The mode II stress intensity factor range was determined by calculating change in the value mode II stress intensity factor as the load moved from position 1A to position 1D, Figure 5.5a. The system parameters used in the calculations were: maximum contact pressure p_o = 1500 MPa, inclined crack angle θ = 60°, surface traction coefficient μ = -0.14 and crack face coefficient of friction μ_{cf} = 0.14.

The results for the test disc, for a crack length of 20 μm, are shown in Figure 5.6a. The maximum values for the mode II stress intensity factors were obtained by simply the adding the mode II stress intensity factor contributions arising from the normal and tangential tractions. The model therefore includes the assumption that crack propagation would be in the direction of the original crack line. Otsuka et al. (1975) found that small cracks emanating from pre-crack tips and propagating in mode II (shear mechanism) propagated in the original crack growth direction, so this assumption is reasonable.

5.3.8.6. The determination of the maximum mode I stress intensity factors

In order to establish the crack length at which mode I (tensile mechanism) propagation would commence, the values of the mode I stress intensity factors K_I and

the mode II stress intensity factors K_{II} arising at the crack tip as the load moves across the mouth of the crack (shown schematically in Figure 5.5b) were calculated using the crack pressurisation model (Fletcher and Beynon, 1999b). The maximum value of the mode I stress intensity factor K_σ and the predicted direction of mode I crack propagation ϕ (direction of maximum mode I stress intensity factor K_σ) were then determined by substituting the values of K_I and K_{II} in equation (5.2) given by Erdogan and Sih (1963) using assumptions proposed by Kaneta et al. (1985),

$$K_\sigma = \cos\frac{\phi}{2}\left[K_I \cos^2\frac{\phi}{2} - \frac{3}{2}K_{II}\sin\phi\right] \qquad (5.2)$$

where, $Ki = K_{iN} + K_{iT} + K_{iP}$ and $i = I,II$

Suffixes N,T and P represent contributions from the normal traction, tangential traction and crack pressurisation respectively.

5.3.8.7. Mode I threshold – test discs

The crack lengths at which the determined maximum mode I stress intensity factor K_σ reached values within the threshold range presented by Kapadia and Marsden (1997) (loading condition 2B Figure 5.5b) were determined using the crack pressurisation model with the following system parameters: maximum contact pressure p_o = 1500 MPa, inclined crack angle $\theta = 60^o$ to surface normal and surface traction coefficient μ = -0.14.

The results for an inclined crack with a length of 130 μm are shown in Figure 5.6b. This plot shows the value of K_σ as the contact loads move adjacent to and across the crack mouth over a range of six times the contact half width. To ensure that the crack growth directions predicted by equation (5.2) were realistic, in each case the results for values of K_σ and ϕ were only used where the value of K_I was positive (point "P"- Figure 5.6b). This approach also allows the superposition of the contributions to the stress intensity factors, without the possibility of the invalidation of the values obtained for the stress intensity factors due to full or partial crack face

contact. Crack face contact at this point is unlikely because the majority of the crack is not covered by the load, see Figure 5.5b, load position 2B.

The values of the contributions to the mode I and mode II stress intensity factors, at the point of maximum, positive resultant mode I stress intensity factor K_{σ}, for cracks with lengths of 70, 100, 130 and 190 μm, are shown in Table 5.1.

5.3.8.8. Mode I and mode II thresholds – back-up rolls

Similar computations were carried out to determine the inclined crack lengths at which the mode II and mode I thresholds would be reached in back-up rolls. The results showed that the mode II threshold would be reached at a crack length similar to that obtained for the test discs.

The results obtained for the maximum mode I stress intensity factors K_{σ}, indicated that for back-up roll materials with mode I thresholds which lie within the range shown in Figure 5.4 (after Kapadia and Marsden, 1997), threshold would be reached at crack lengths between 350 and 750 μm. The full set of results is shown in Table 5.2.

5.3.9. *Predictions for crack morphology*

Otsuka et al. (1975) found that crack growth would always occur in mode I (tensile mechanism) in preference to mode II (shear mechanism) if both were possible. That is, if $\Delta K_{II} > \Delta K_{IIth}$ and $\Delta K_{\sigma} > K_{Ith}$. In this quantitative model, this criterion has been used in conjunction with the appropriate crack line loading conditions to predict the crack morphology.

The results for the prediction of the crack growth in mode II (shear mechanism) and mode I (tensile mechanism), for both the back-up roll test discs and the actual back-up rolls, are shown in Figure 5.7. The results shown are for values for the maximum mode I stress intensity factor K_{σ} of approximately 4, 5.5, 7 and 10 MPa$\sqrt{m}$.

5.3.10. *Model validation*

5.3.10.1. Plastically deformed surface layers

Microscopic inspection of the plastically deformed surface layers in back-up roll test discs and the spalled back-up roll material revealed that the depth of plastic deformation in both reached approximately 15 μm below the surface. For an inclined crack propagating at an angle of 60° to the surface normal, the plastically deformed surface layers can therefore contain a crack length of about 30 μm. These observations confirmed that the inclined surface cracks in both test discs and back-up rolls would be propagated to the length required (20 μm) for the assumed mode II threshold (1.5 MPa$\sqrt{m}$) to be reached.

5.3.10.2. Test disc pair

In order to validate the model a range of the largest cracks produced in two back-up roll test discs used in the experimental simulations were examined using optical, scanning electron and back-scattered electron microscopy.

The results from Test 1 (test duration 252000 cycles, maximum contact pressure 1500 MPa, -1% slip and water lubrication) and from Test 6 (test duration 200000 cycles, maximum contact pressure 1500 MPa, -5% slip and water lubrication) were examined in detail. Examples of observed inclined surface initiated cracks are shown in Figures 5.8a (Test 1) and 5.8b (Test 6). These cracks propagated at approximately 60° to the surface normal and in both cases showed evidence of upward branching at lengths between 70 and 180 μm. Branching at lengths in this range is in good agreement with the predictions of the quantitative model (Figure 5.7). Some cracks observed in both tests showed evidence of surface initiated inclined cracks extending to or interacting with large subsurface cracks. Examples of these cracks are shown in Figures 4.10a (Test 1) and 4.10b (Test 6). The total radial wear on the surface of back-up roll test discs shown in these last two examples was 124 μm and 21μm respectively. An inspection of the near surface morphology of these cracks reveals that the morphologies are similar and the in the latter case the

large upturning branch is 50 μm deeper below the surface. It is not possible to make a more accurate comparison than this because it is not possible to ascertain when a particular crack initiates during a test.

5.3.10.3. Work roll/back-up roll pair

Samples of spalled material from a back-up roll were examined using optical and back-scattered electron microscopy. Many small surface initiated cracks were observed in the plastically deformed surface layer of the spalled material. A typical example of these cracks, which propagated at approximately 60° to the surface normal, is shown in Figure 5.9a. A section showing the crack mouth (though not the point of crack initiation) and crack line of the spall is shown in Figure 5.9b. The crack line shows evidence of an inclined surface crack, which has propagated at a shallow angle to a length of approximately 2 mm, before turning down sharply to penetrate into the deeper substrate of the roll barrel. No evidence was seen of an up-turning crack.

Back-up roll test disc

Test disc diameters = 55 mm Contact half width = 359 μm

Crack Length μm	Crack Angle θ	K_{IP} Fluid Pressure MPa√m	K_{IIP} Fluid Pressure MPa√m	K_{IN} Normal Traction MPa√m	K_{IIN} Normal Traction MPa√m	K_{IT} Tangential Traction MPa√m	K_{IIT} Tangential Traction MPa√m	Max. K_I (K_σ) MPa√m	Prop. Angle ϕ
70	60°	4.30	-2.42	-1.71	0.57	0.76	0.78	3.80	+31°
100	60°	6.00	-3.39	-2.21	0.79	0.74	0.81	5.41	+35°
130	60°	7.78	-4.39	-2.77	1.09	0.72	0.82	7.00	+37°
190	60°	11.12	-6.27	-3.68	1.63	0.65	0.83	10.16	+39°

Table 5.1. Stress intensity factors

Back-up roll

Work roll dia. = 0.75 m, Back-up roll dia. = 1.4 m, Contact half width = 6156 μm

Crack Length μm	Crack Angle θ	K_{IP} Fluid Pressure MPa√m	K_{IIP} Fluid Pressure MPa√m	K_{IN} Normal Traction MPa√m	K_{IIN} Normal Traction MPa√m	K_{IT} Tangential Traction MPa√m	K_{IIT} Tangential Traction MPa√m	Max. K_I (K_σ) MPa√m	Prop. Angle φ
200	60°	6.65	-3.75	-8.86	4.86	2.18	2.54	4.21	-70.5°
350	60°	5.59	-3.15	-2.99	0.86	2.84	2.65	5.47	-7.4°
500	60°	7.83	-4.41	-3.76	1.14	2.96	2.84	7.08	+7°
750	60°	11.17	-6.30	-4.76	1.39	3.10	3.03	10.03	+21°

Table 5.2. Stress intensity factors

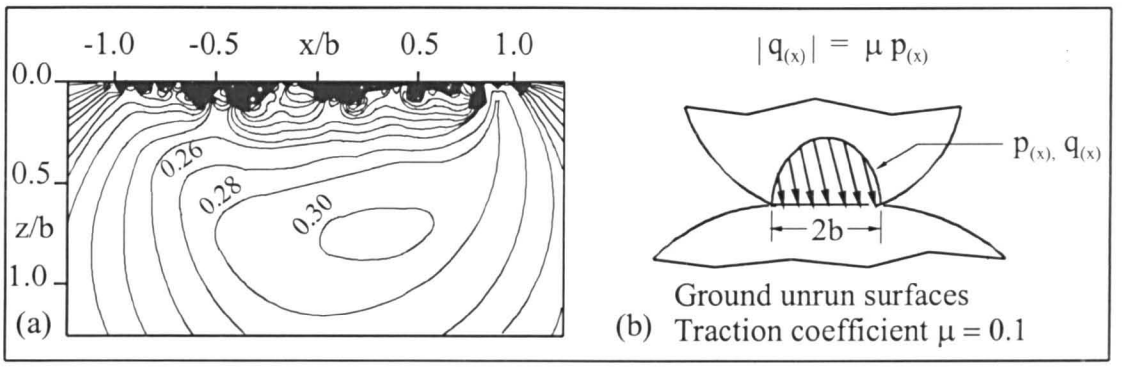

Figure 5.1. Principal shear stresses with surface roughness and sliding friction (after Bailey and Sayles, 1991)

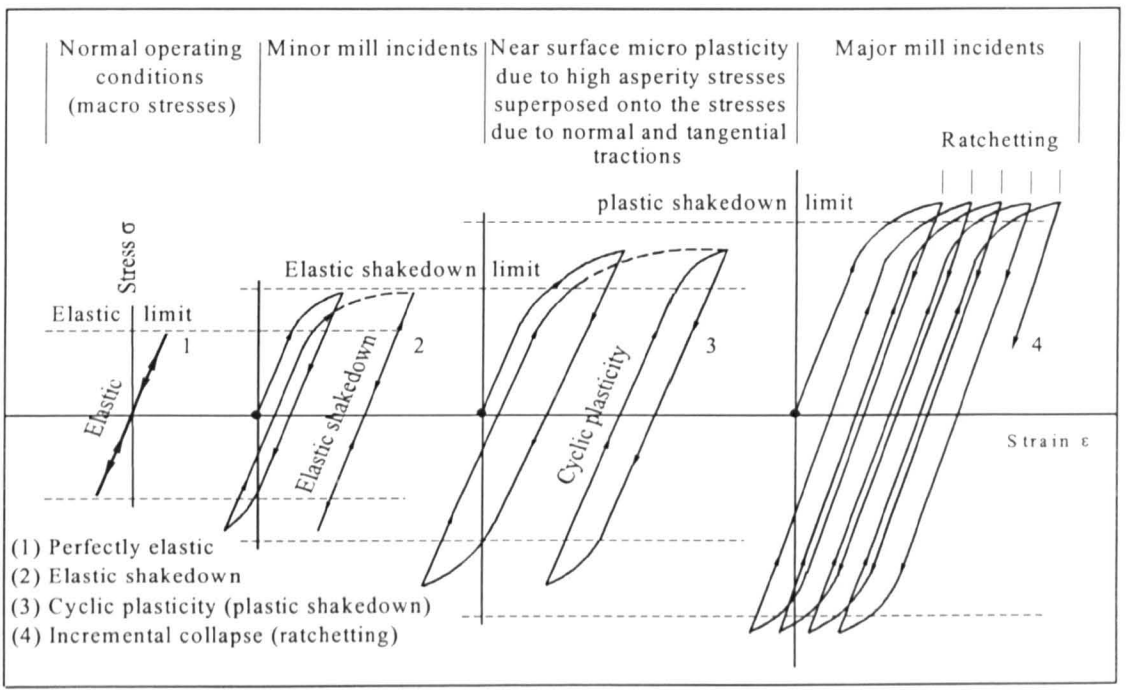

Figure 5.2. Material response to cyclic loading (after Johnson, 1989)

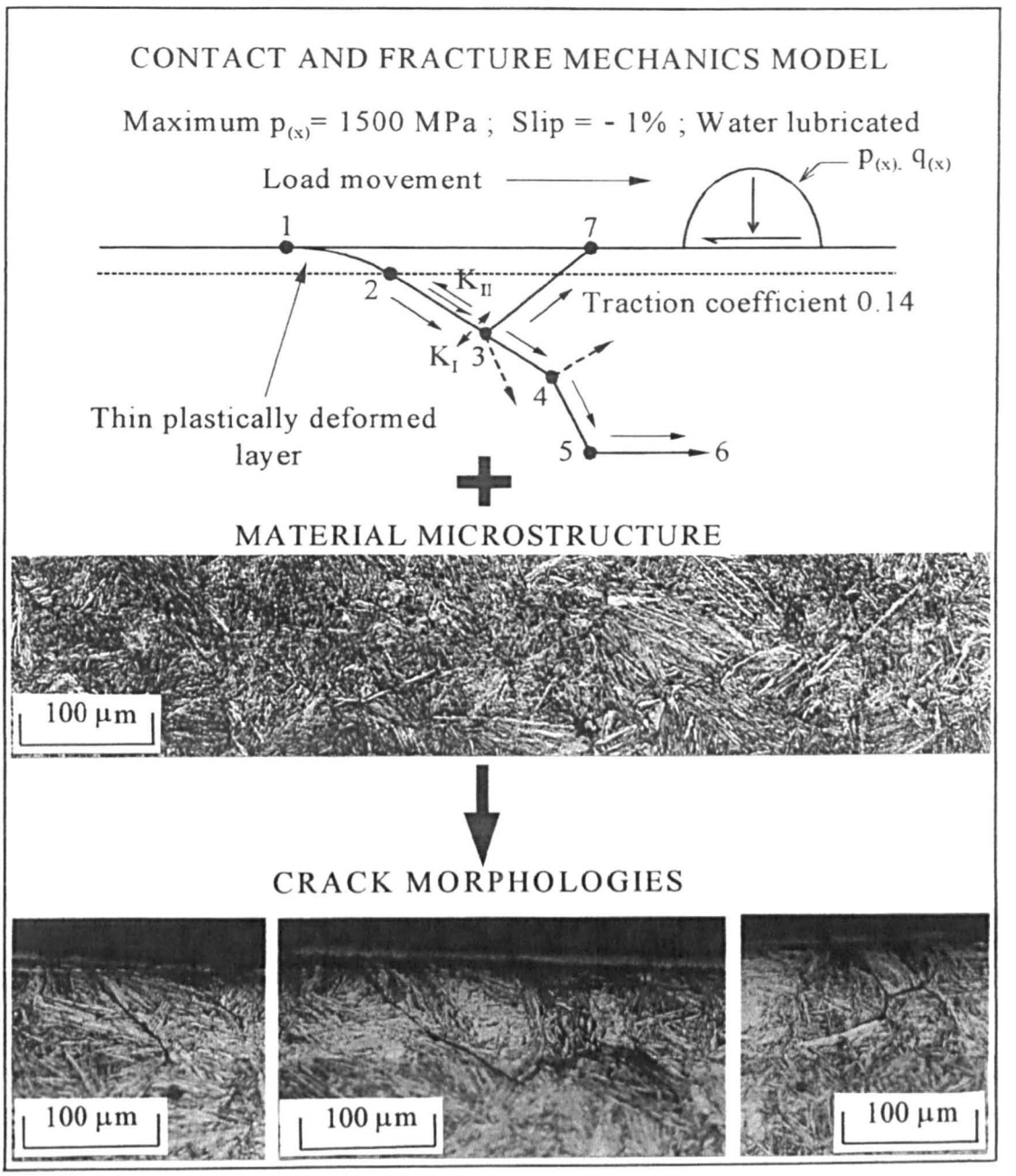

Figure 5.3. Qualitative failure model

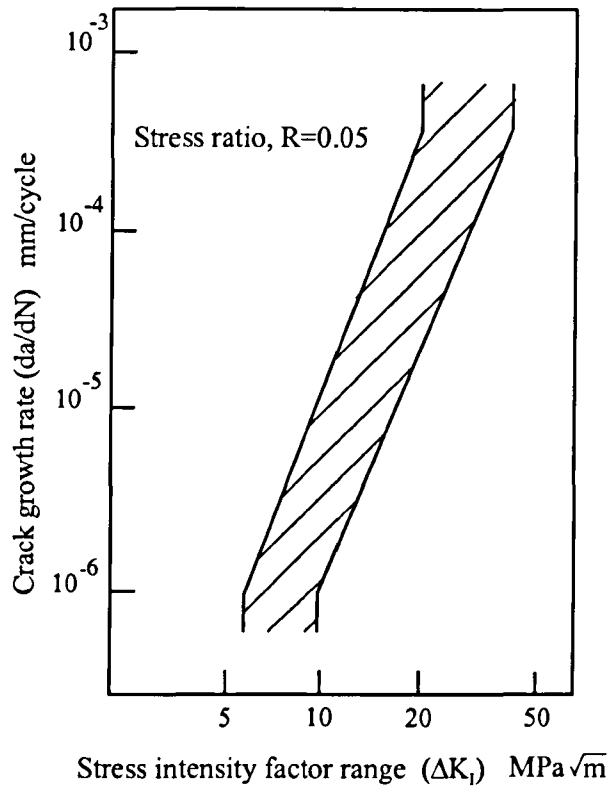

Figure 5.4. Mode I fatigue crack growth rates for back-up roll steels (after Kapadia and Marsden, 1997)

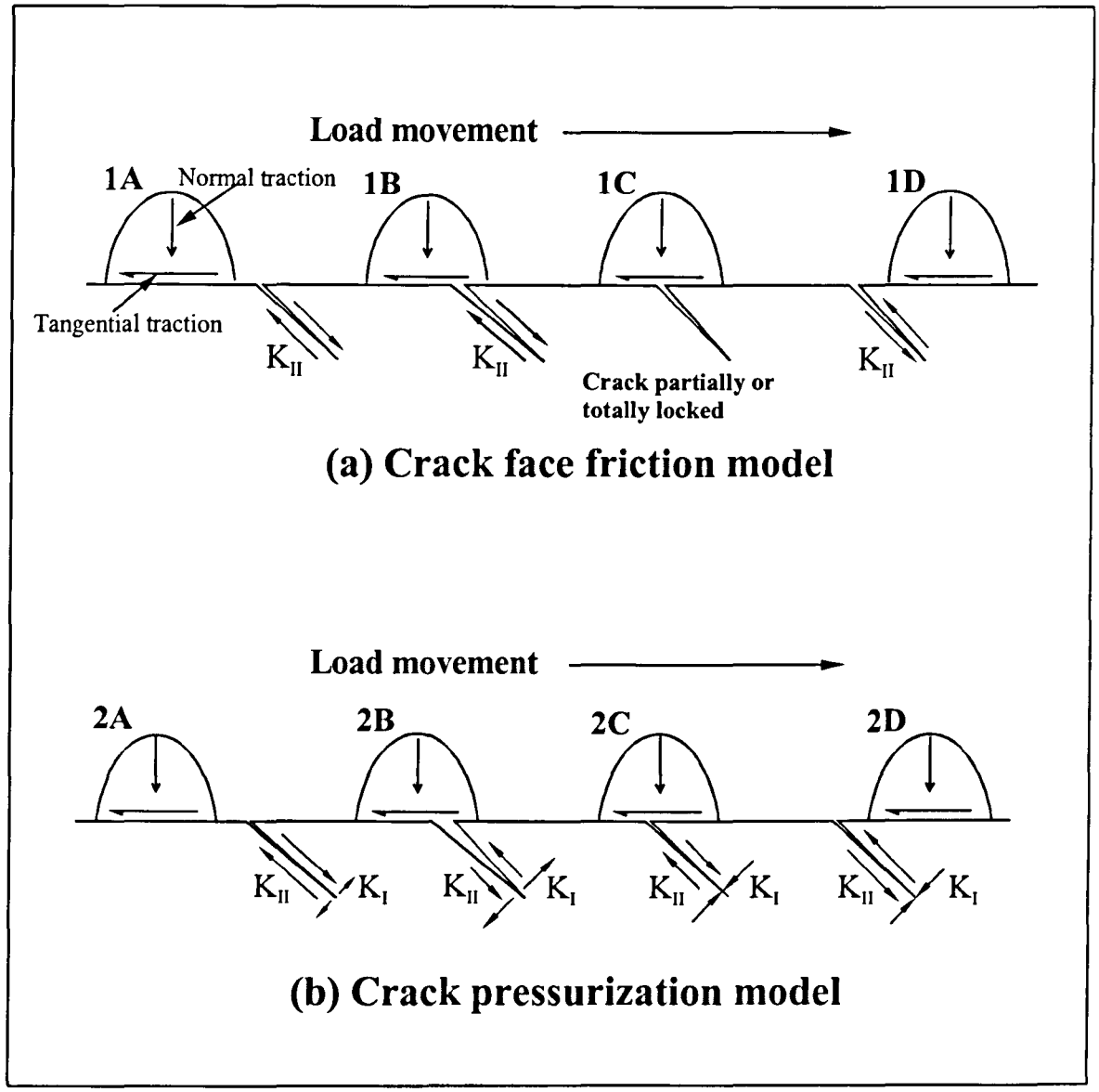

Figure 5.5. Schematic of stress intensity factors arising at the crack tips

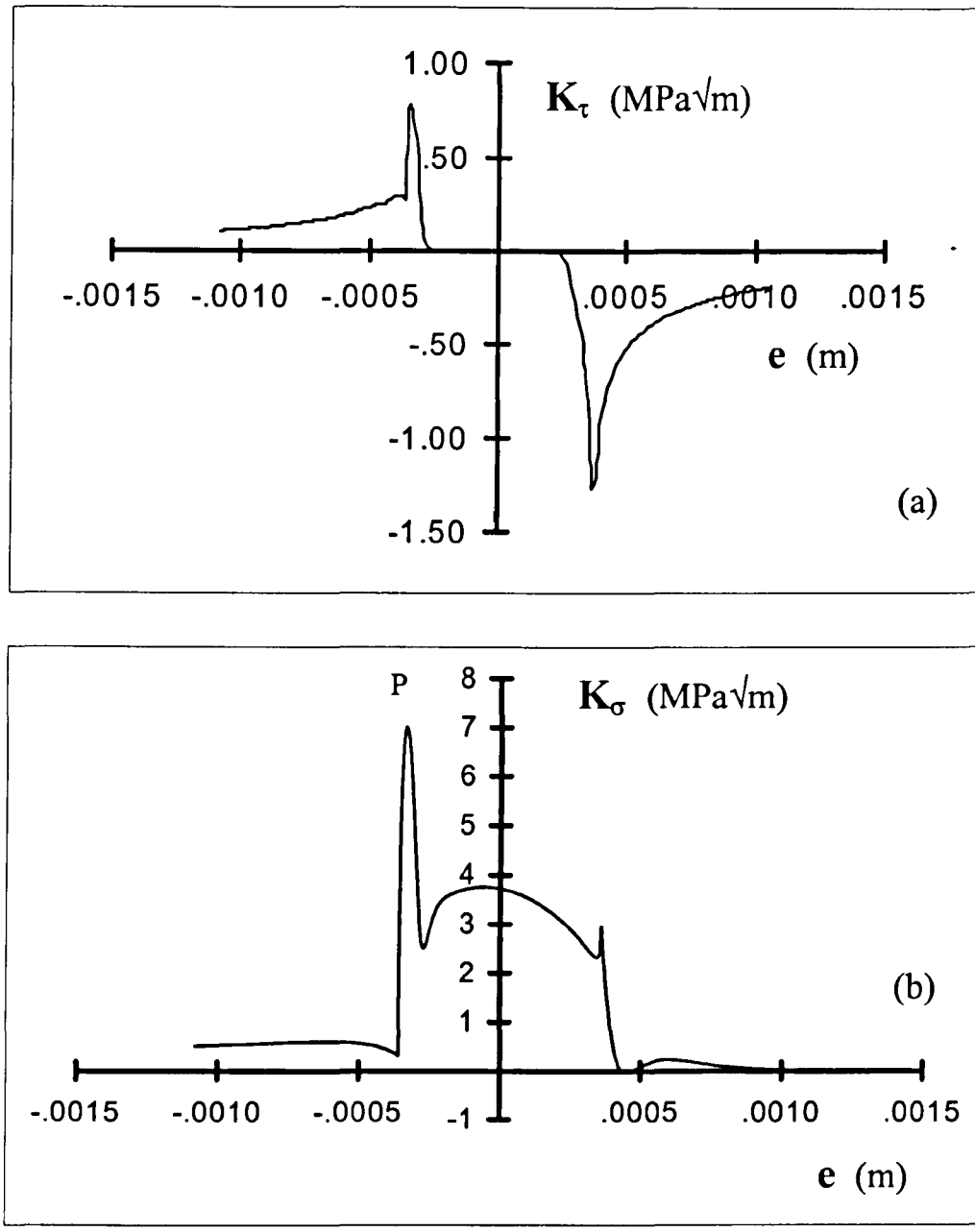

Figure 5.6. (a) Mode II stress intensity factor K_τ - test disc (crack length 20 μm, crack angle 60° to surface normal, maximum contact pressure 1500 MPa, coefficient of traction – 0.14, coefficient of friction (crack face) 0.14). (b) Mode I stress intensity factor K_σ - test disc (crack length 130 μm, crack angle 60°, maximum contact pressure 1500 MPa, coefficient of traction –0.14). **e** is the distance between the centre of the contact patch and the crack mouth as the load moves over the crack mouth.

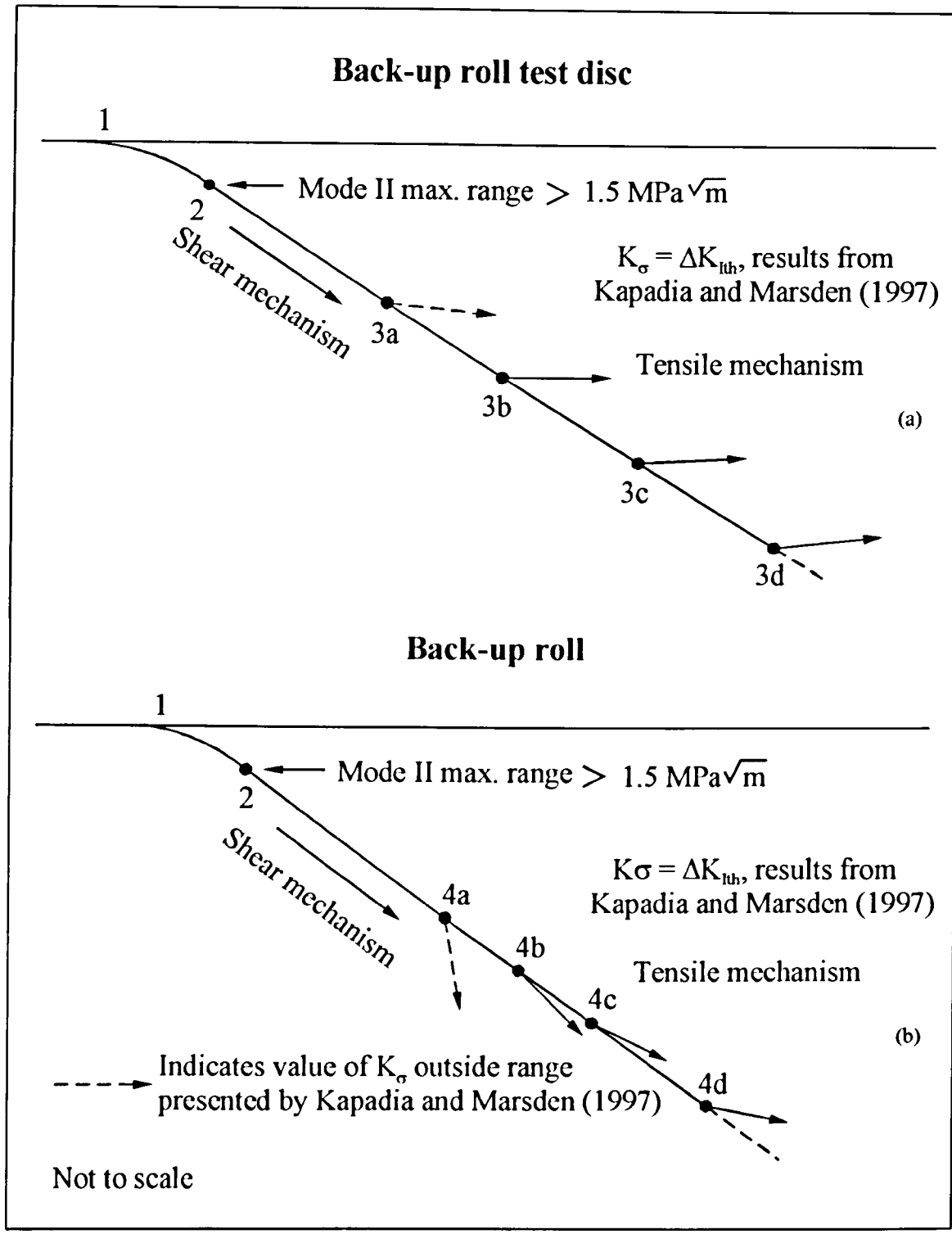

Figure 5.7. Schematic diagram of predicted crack morphology (a) Back-up roll test disc – crack length at point 2 (20 μm), tensile mode results for different inclined crack lengths 3a (70 μm, $K_\sigma \approx$ 4 MPa√m), 3b (100 μm, $K_\sigma \approx$ 5 MPa√m), 3c (130 μm, $K_\sigma \approx$ 7 MPa√m) and 3d (190 μm, $K_\sigma \approx$ 10 MPa√m), see Table 5.1a. (b) Back-up roll – crack length at point 2 (20 μm), tensile mode results for different inclined crack lengths 4a (200 μm, $K_\sigma \approx$ 4 MPa√m), 4b (350 μm, $K_\sigma \approx$ 5 MPa√m), 4c (500 μm, $K_\sigma \approx$ 7 MPa√m) and 4d (750 μm, $K_\sigma \approx$ 10 MPa√m), see Table 5.1b.

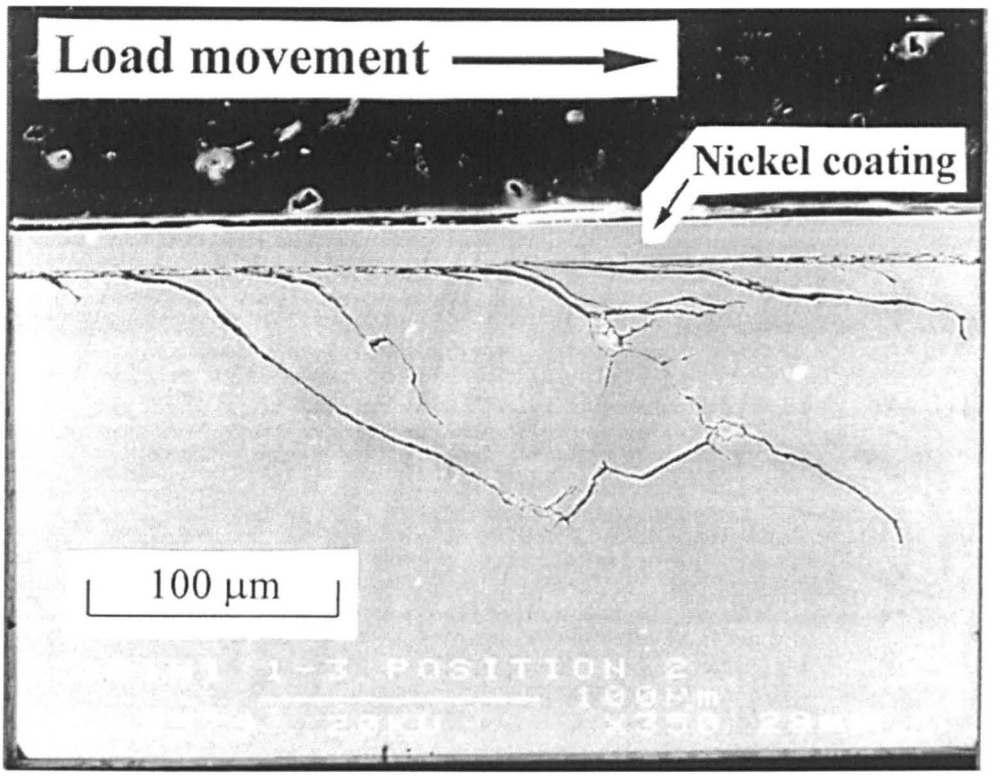

(a) Test 1 (high wear rate – 252000 cycles), specimen B1 polished and lightly etched

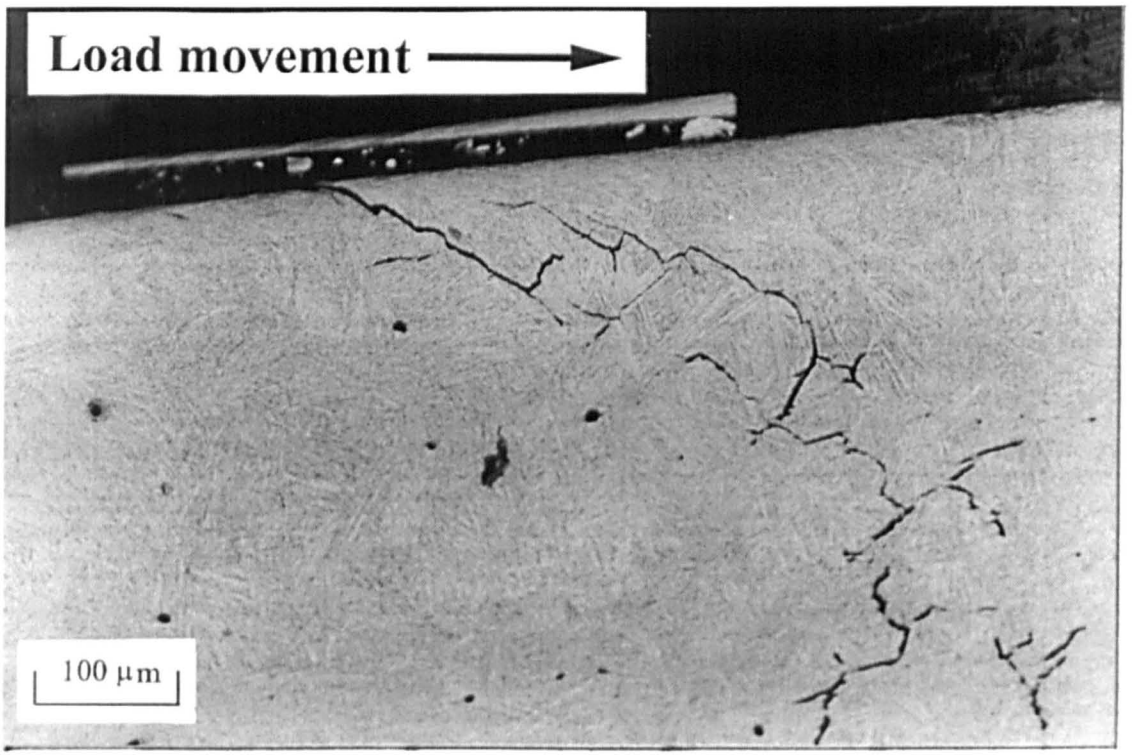

(a) Test 6 (low wear rate – 200000 cycles), Specimen B3 polished and etched

Figure 5.8. Intermediate length cracks

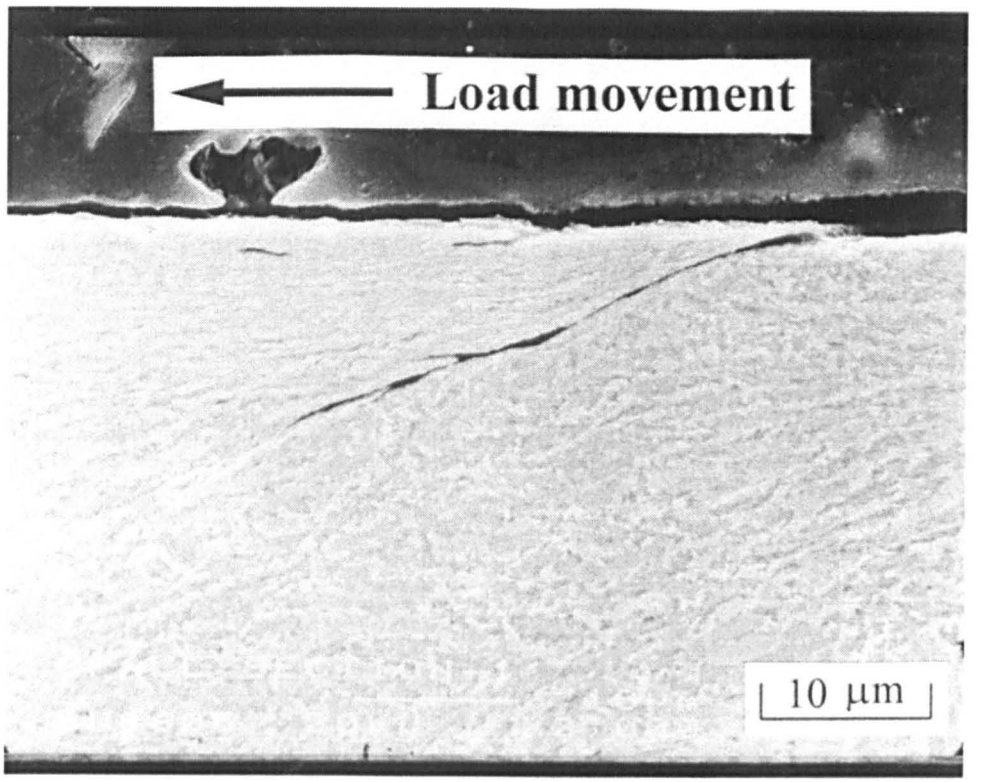

(a) Small crack in plastically deformed layer, polished and etched

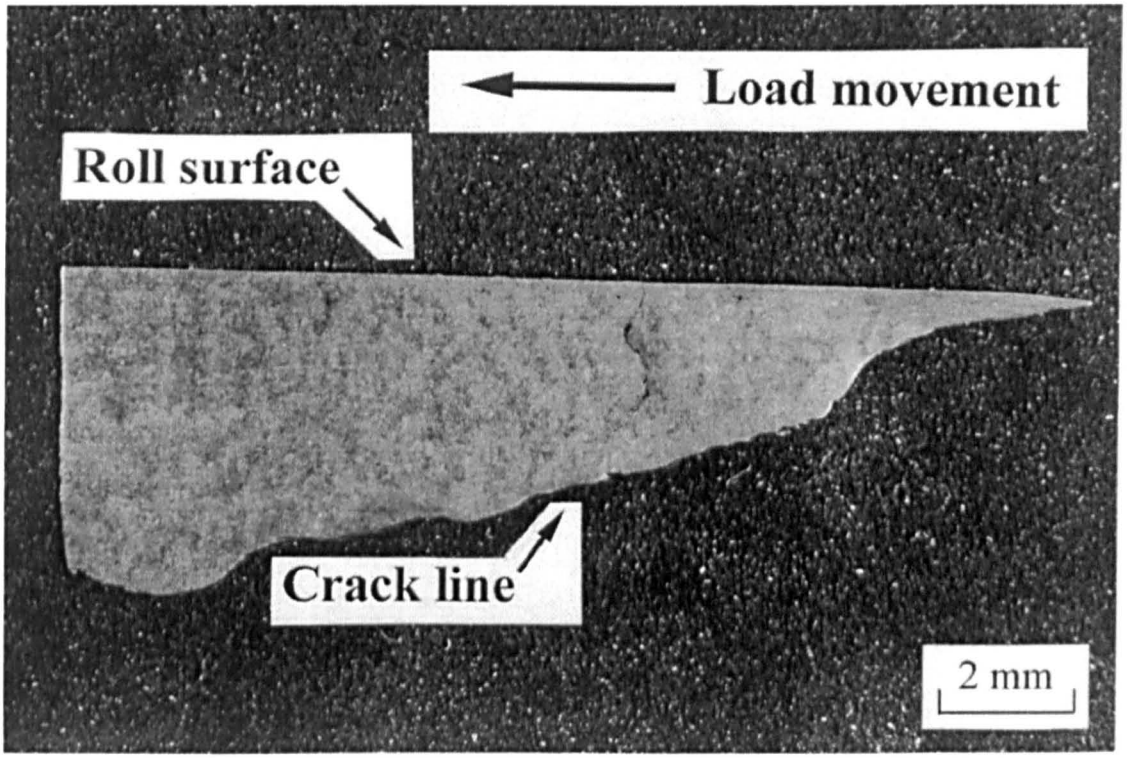

(b) Section of spall crack line, polished and etched

Figure 5.9. Sample taken from spalled material from a back-up roll

Chapter 6

DISCUSSION

6.1. INTRODUCTION

The first aim of this discussion is to consider the results obtained from the experimental programme in terms of the implications for the predictions of crack morphology and the assumptions made during the development of the qualitative and quantitative models. Further aims are to investigate the interaction between wear and rolling contact fatigue in this case and to identify links between mechanics and microstructure which can be used to improve the microstructural design of bainitic back-up roll materials.

6.2. QUALITATIVE MODEL

6.2.1. *Subsurface crack morphology*

It is clear that the qualitative failure model predicts the morphologies of cracks produced in test specimens under simulated operating conditions and also cracks observed in a sample of spalled back-up roll material. Inspection of the details of the cracks also indicates that the observed morphologies are stress driven, but are modified by the material microstructure and operating conditions.

The crack morphologies observed in both test discs and the spalled material from a back-up roll indicate that the initial direction of surface crack propagation is determined by the direction of the tangential traction (back-up roll driven by the work roll) and is therefore in the direction of the load movement over the roll surface. This observation is in agreement with Bower (1988) as discussed in Section 3.7.3.1. The possible influence of microstructure on the early propagation of rolling contact fatigue cracks and in the other phases of the qualitative and quantitative failure models is discussed further in Section 6.5.

6.2.2. *Surface crack morphology*

Optical micrographs of the surface morphologies of cracks produced in back-up roll test disc specimens B1 (Test 1) are shown in Figures 6.1 and 6.2 and for test disc specimens B3 (Test 6) and B5 (Test 5) in Figures 6.3 and 6.4 respectively. For comparison, the surface morphology of a sample of spalled material from a back-up roll is shown in Figure 6.5. Inspection of these results shows that both the appearance and dimensions of the features on the surfaces of the test discs and back-up roll are very similar. One of the possible reasons for these similarities is that the scale of the effective microstructural features of the spalled material and the back-up roll test disc materials are similar, as shown in Figures 6.6 and 6.7. The results of tests designed to investigate the possible influence of the surface roughness of the work roll test disc specimens on the surface morphology of cracks produced in the back-up roll test disc specimens are discussed in Section 6.4.

6.2.3. *Operative mechanisms*

The loading mechanisms which make positive contributions to the mode I stress intensity factor K_I acting at the inclined tips are the tangential traction and the pressurisation of the crack faces by the roll coolant. At the longer crack lengths, the latter makes the more significant contribution and is also mainly responsible for the mode II stress intensity factor K_{II}, which causes up-turning cracks.

For crack pressurisation to occur it has been assumed that, at the point when the effective crack tip loading occurs, the crack mouth should be completely contained within the contact patch. Inspection of surface morphology of the cracks shown in Figures 6.1-6.5 indicates that, for the small cracks considered in this study, it is possible that this condition would be satisfied for a significant number of the observed crack mouths. This issue is discussed further in Section 6.3.3.3.

If fluid leakage occurs and there is no crack pressurisation, the effective crack tip loading will be restricted to the contributions from the normal and tangential tractions up to points 5 and 7 in the qualitative failure model, Figure 5.3. Crack propagation would then be in lubricated mode II or mixed mode I/ mode II, the only contribution

of a positive mode I stress intensity factor being made by the tangential traction as the load approaches the crack mouth. In phase 5-6 of the model, crack propagation is unaffected by fluid leakage as the process is driven by the combination of the compressive stresses arising from the action of the normal traction and the residual stresses remaining after the roll manufacturing processes.

In the absence of crack pressurisation, the rate of crack propagation in the period up to the point of mode I threshold should be slower than for the pressurised case. Therefore, for the purposes of establishing design criteria, it should be assumed that crack pressurisation does occur.

6.3. QUANTITATIVE MODEL

6.3.1. *Damage tolerance approach*

The results show that, with the extent of the plastically deformed layers that arise during normal operating conditions and the surface damage which is known to occur in mill incidents, it is extremely likely that a flaw of critical size will develop at the roll surface. The predictions of the quantitative model indicate that, if in phase 1-2 of the failure model a crack is propagated to a minimum length of 20 μm, then the mode II stress intensity range would exceed the mode II threshold and propagation would then continue under normal operating conditions. The propagation of these flaws could continue first in mode II (shear mechanism), followed by mixed mode I/mode II and then mode I (tensile mechanism). This confirms that it is appropriate to use a damage tolerance approach when establishing design criteria for rolling contact fatigue resistance in back-up rolls.

6.3.2. *The applicability of linear elastic fracture mechanics*

Examination of the microstructures of the test discs and spalled back-up roll material revealed that in both cases, even if originally propagated along the ferrite packet/ carbide boundaries in preferentially orientated grains, cracks with lengths in excess of 100 μm would be expected to have propagated through several grains (ferrite

packets). The cracks were therefore assumed to have breached the microstructural barriers to fatigue crack growth and effectively to be propagating in a continuum.

Some of the cracks observed had propagated to lengths greater than 100 μm where the determined maximum mode I stress intensity factor ranges at the crack tips were greater than the minimum mode I threshold for the type of back-up roll materials considered. Using the nominal monotonic yield stress for the material of 1100 MPa (assuming no cyclic hardening or softening) and the stress intensity factors given in Tables 5.1 and 5.2, the plastic zone sizes $2r_{cyclic}$ were determined using equation (5.1) and compared with the relevant crack tip to boundary dimensions. The results are shown in Table 6.1. For inclined cracks propagating at 60° to the surface normal, the ratio $a/2r_{cyclic}$, (where a is the crack length) must be greater than 8 (Dowling, 1993) for linear elastic fracture mechanics to be applicable. All values of the ratio $a/2r_{cyclic}$ were well in excess 8, confirming that the use of linear elastic fracture mechanics was valid.

With both the above criteria apparently satisfied it was considered that in principle the morphology of the cracks could be predicted using linear elastic fracture mechanics. However, since the cracks predicted in this study are physically small, falling into the definitions of small cracks given by Suresh (1998) and are produced under loading conditions different from those used to determine fatigue crack propagation data, care must be taken when applying the results presented by Kapadia and Marsden (1997). The main considerations are discussed below:

1. Suresh (1998) presents evidence that, for the materials and crack sizes considered in this study, the values of the threshold mode I stress intensity ranges should be crack size independent. It was therefore considered that it was acceptable to use the threshold data without any adjustment for crack size.
2. Small cracks are known to propagate faster than long cracks when subjected to the same value of mode I stress intensity factor range. It was therefore considered that the data could not be reliably used to predict the propagation rates of the cracks.
3. Theoretical predictions for the cyclic plastic zone sizes at the crack tips suggest that, under rolling contact conditions and in the absence of crack closure effects,

the roll materials may exhibit mode I thresholds which may be 50% lower than those presented by Kapadia and Marsden (1997). In this case mode I threshold would be reached at shorter inclined crack lengths and smaller crack length/contact half width ratios, with the consequent differences in the predicted directions for the initial mode I crack propagation. For the test discs the direction of crack propagation indicated by the direction of the maximum stress intensity factor K_σ is relatively insensitive to the value at threshold, but for the back-up roll case mode I thresholds where the value of the maximum mode I stress intensity factor is below 5 MPa$\sqrt{m}$ could result in sharply down-turning cracks, see Figure 5.7.

6.3.3. *Validation of adopted modelling parameters*

6.3.3.1. Inclined crack angle

The decision to model inclined rolling contact fatigue cracks which initially propagated at 60° to the surface normal was validated by experimental observations and the results obtained from the computations for the stress intensity factors arising at the crack tips. In addition a comparison of the computed results obtained for cracks propagating at 45° and 60° to the surface normal is shown in Figure 6.8. Examination of these results for both the test disc pair and the work roll/back-up roll pair indicates that the predicted stress intensity factors are greater for cracks propagating at 60° than for cracks propagating at 45°. This result confirms that for practical purposes that the adoption of an inclined crack angle of 60° was reasonable in this case.

6.3.3.2. Coefficient of crack face friction

Since it was not possible to obtain an unambiguous value for the coefficient of crack face friction, in the modelling programme (Section 5.3) the same value was used for both the coefficient of crack face friction and the traction coefficient (0.14). The computed values for the mode II stress intensity factor ranges for an inclined crack length of 30 μm for both the test disc pair and the work roll/back-up roll pair were 2.54 MPa$\sqrt{m}$ and 2.42 MPa$\sqrt{m}$ respectively. These mode II stress intensity factor ranges are well in excess of mode II threshold (1.5 MPa$\sqrt{m}$) determined by Otsuka et

al. (1975). In order to investigate the effect of changing the value of the coefficient of crack face friction, the mode II stress intensity factor ranges were computed for the test disc pair for values of 0.1, 0.14, 0.18 and 0.2. The model predicted that changing the value of crack face friction from 0.14 to 0.2 would only reduce the mode II stress intensity factor range by 7%. This result indicates that, even if the coefficient of crack face friction was higher due to factors such as crack face roughness, for the modelling parameters used there is a strong possibility that a flaw of critical size would develop at both the test disc and back-up roll surface. In addition and most importantly, the assumptions made and the results obtained from the modelling are supported by the experimental observations.

6.3.3.3. Fluid leakage

The results obtained from the quantitative modelling indicated that the effective loading of the crack by fluid pressurisation occurs when the crack mouth is contained within the leading edge section of contact patch with a width of the order of 50 μm for the test disc pair and 500 μm for the work roll/back-up roll pair, see Figure 6.9. These results in conjunction with the surface morphologies shown in Figures 6.1-6.5, confirm that a significant number of the observed crack mouths could be effectively covered by the contact surfaces. The shape of the crack mouth could therefore be a controlling factor in the continued growth of many surface initiated cracks.

The results also suggest that crack pressurisation has a dramatic effect on the stress intensity factors arising at the crack tips, even though the key stage of crack pressurisation takes place when the contact pressures (and hence the fluid pressures) at the crack mouth are relatively low. This leads to the possibility that the dynamics of the system coupled with the fluid pressure at the crack mouth may contribute significant crack tip loading even if some fluid leakage occurs.

6.3.4. *Stress intensity factors*

An understanding of the influence of the various system parameters on the resulting stress intensity factors is somewhat intuitive. However, to gain an insight into the relative contributions of the normal edge traction, tangential edge traction and

pressurisation of the crack faces and the general trends, it was necessary to obtain results for a large number and variety of system conditions.

The following observations were of particular interest:

1. The maximum value of the mode I stress intensity factor K_σ occurs very shortly after the contact covers the crack mouth (point "P"- Figure 5.6b). This suggests that the value of K_σ should be relatively insensitive to the maximum contact pressure at the larger crack length/contact half width ratios where crack pressurisation is the dominant factor. The results presented in Figure 6.10 show that at the longer crack lengths, for both the test disc pair and the work roll/back-up roll pair, a 66% increase in contact pressure results in only a 30% increase in the value of the maximum mode I stress intensity factor K_σ at the crack tips. Support for this observation can be found in the work by Fletcher and Beynon (2000b), who found that in tests carried out on rail steel specimens under similar conditions on the "SUROS" testing machine, crack growth rate showed some insensitivity to the maximum contact pressure.
2. For any given set of loading parameters, the direction of the maximum mode I stress intensity factor arising at any point on the inclined crack line is dependent on the crack length/contact half width ratio A at that point. The effect of increasing the value of the mode I threshold, and hence the value of A at which the mode I threshold is reached, on the predicted crack morphology is shown in Figure 6.11.
3. At sufficiently small crack length/contact half width ratios, the contributions to the stress intensity factors arising from the normal and tangential tractions become very significant and result in "down-turning" maximum mode I stress intensity factors. Due to the partial dependence on the tangential tractions, this effect will be greater as the value of the coefficient of traction increases.

6.3.5. *Crack morphologies*

6.3.5.1. Back-up roll test discs

Examination of the cracks produced in the back-up roll test discs confirmed the predictions of the theoretical analysis, that in the mode I threshold region branch

cracks tended to be up-turning. Down-turning branches were observed in small cracks, but these were mostly associated with triple points at grain boundaries and other microstructural features. At crack lengths in excess of 200 μm, combinations of up-turning and down-turning cracks were observed, but these were associated with large areas of subsurface failure. Under the loading conditions used in the experimental simulations, subsurface fatigue failure may be due to the magnitude of the reversed orthogonal shear stresses, but predictions of the total crack morphology arising from the interaction of surface initiated cracks with subsurface cracks is outside the scope of this analysis.

6.3.5.2. Back-up rolls

The results of the theoretical analysis presented in this study may be used to predict some of the types of failure observed in back-up rolls, particularly ribbon fatigue and strip spalling (Kapadia and Marsden, 1997) , which are produced by surface initiated rolling contact fatigue cracks. Further analysis is needed to gain insight into the failure mechanisms, which propagate the cracks into the deeper substrate and lead to "crumble" fatigue and the exfoliation of large fragments of material out of the roll surface. It is not clear at this stage whether the last two phenomena are the result of the propagation of surface initiated cracks into the deeper substrate or whether they are the result of the interaction of surface initiated cracks with areas of subsurface failure.

6.4. WEAR AND ROLLING CONTACT FATIGUE

6.4.1. *Introduction*

The results obtained from the experimental simulations suggest that wear on the contact faces has a major effect on the initiation and propagation of rolling contact fatigue cracks. Unlike most fatigue situations, under rolling contact fatigue conditions, wear on the contact surface continuously produces new sites for crack initiation. This is particularly important when cracks tend to initiate only at sites with preferentially orientated microstructural features. The discussion in this section is

directed at the experimental evidence for identifying the most important operative wear mechanisms and particularly at the influence of the roughness of the contact faces on wear and rolling contact fatigue.

6.4.2. *Wear modelling*

An important feature of the presented qualitative failure model is the influence of surface asperities and the associated local stress fields on both the initiation and early propagation of rolling contact fatigue cracks. The presence of surface asperities was also expected to have an important influence on the operative wear mechanisms acting at the test disc and work roll/back-up roll interfaces.

The presence of surface asperities in this case coupled with the results of a study of the possible wear mechanisms suggested that the dominant wear mechanisms operating at the surface of both the back-up roll test discs and actual back-up rolls would be:

1. Abrasive wear due to the presence of metallic carbides and the hard matrix of the high speed steel counter-face.
2. Machining or ploughing of the bainitic steel surface by the hard asperities on the high speed steel counter-face.
3. Ratchetting and fatigue wear resulting from the severe local contact stresses.

The above deductions, coupled with an analysis of the contact stress fields arising due to the actions of the normal and tangential tractions and the assumed near surface effects of the asperity stresses, indicated that there should be a high level of similitude between the wear mechanisms operating at the interfaces of the test disc pair and the work roll/back-up roll pair. This suggests that the wear results obtained during the experimental simulations can be reasonably used to predict the wear performance of the work roll/back-up roll pair under the same loading and operating conditions.

6.4.3. *The influence of contact face surface roughness*

6.4.3.1. Work roll test disc surface roughness

The surface morphologies of the tracks of the work roll test disc specimens can be considered to fall into four main categories: "smooth" ground (un-run), "rough" ground (un-run), run with partial removal of the ground surface and run with full removal of the ground surface. Surface replicas of typical examples of disc track surfaces falling into these four categories are shown in Figures 6.12a, 6.13a, 6.14 and 6.15 respectively. The effect of each of these types of surface finish was examined in detail during Tests 1 and 9-18 of the experimental programme.

6.4.3.2. Wear performance at –1% slip

In order to investigate the influence of work roll test disc surface roughness on the wear performance of the baintic steel back-up roll test discs under what have been assumed to be normal operating conditions, a series of tests under conditions of –1% slip was carried out using work roll test discs which had been prepared with track surface roughnesses in the range Ra 0.1 μm to Ra 0.75 μm (Table 4.2). This range is similar to that given by Caithness et al. (1999) for HSS work rolls entering service in the former BSSP hot strip mill at Llanwern. Examples of the transverse surface profiles of typical "smooth" and "rough" ground test disc surfaces are shown in Figures 6.12b and 6.13b respectively.

The wear results obtained from five of these simulations (tests 10-12, 15 and 16), translated into surface removal rates, are presented in Figure 6.16. In each test the back-up roll test disc was subjected to 50000 loading cycles. This test duration encompasses the range of loading cycles which would be experienced by the back-up rolls in a seven stand hot strip mill during a typical round (see Section 2.2.2).

Examination of the results and the associated roughness measurements for both the work roll and back-up roll test discs shows that over the first 10000 cycles the wear rate was dependent on the surface roughness of both the work roll and test disc tracks.

After the initial 10000 cycles, the wear rate for the remainder of each test appeared to depend only on the initial roughness of the work roll test disc. This was true even in the later stages of the tests where an increasing amount of the initial ground finish on the work roll test disc had been removed by wear, see Figure 6.14. In Test 11 where the initial roughness of the track of back-up roll test discs was relatively high, there was a significant reduction in wear rate after the first 10000 cycles. In all tests where the initial roughness of the track of the work roll test disc was above Ra 0.38 μm, there was a significant increase in wear rate after the first 20000 cycles.

In general the results suggest that:

1. A significant contribution to the wear rate in the first 10000 cycles was due the removal of the initial ground finish on the back-up roll test disc.
2. A smooth ground finish on the work roll test disc track resulted in a wear rate similar to that produced by a worn track where the initial ground finish had been completely removed by wear.
3. After the first 10000 cycles, the wear performance was dominated by the initial roughness of the ground finish on the track of the work roll test disc.
4. The initial roughness of the ground finish on the track of the work roll disc determined the contribution to the wear rate arising from machining and ploughing of the back-up roll test disc track and also appeared to be the main factor affecting the initiation of and contributions made by ratchetting and fatigue wear. The results also indicated that, where the initial roughness of the track of the work roll test disc was above Ra 0.38 μm, ratchetting and fatigue wear became dominant in the later stages of the tests.

Inspection of the surfaces of the tracks on the back-up roll test discs at the end of Tests 10, 11 and 12 indicated that although similar in shape, the scale of the surface features appeared to be related to the surface wear rate (and by implication the initial surface roughness of the work roll test disc). The track surfaces of test discs B10 and B8 are shown in Figures 6.17 and 6.18 respectively.

It follows from the above observations that in this case, even with the complex interaction of the various dominant wear mechanisms, with a carefully constructed

programme of wear tests it may be possible to use the results obtained to develop a comprehensive quantitative wear model.

6.4.3.3. Wear performance at –5% slip

It is known from field evidence that the contact areas between back-up and work roll surfaces are sometimes subjected to periods of high level slip or "skidding". In order to investigate the wear performance of bainitic back-up roll steels at higher levels of slip, a series of tests was carried out under conditions of –5% slip. Tests 3-8 were carried out to establish the general trends in wear and rolling contact fatigue performance at high levels of slip and Test 9 was specifically carried out to examine the effect of substantially increasing the roughness of the track of the work roll test disc in mid test. The test was commenced with a work roll test disc surface roughness of Ra 0.06 μm and was run for an initial duration of 70000 cycles. At the end of this period the work roll test disc surface roughness was increased to Ra 0.6 μm and the test run for a further 50000 cycles. Surface replicas of the run and un-run track surfaces of the work roll test discs used in this test are shown in Figures 6.19 and 6.20.

Inspection of the surface features of the tracks of the back-up roll test discs at the end of Tests 5 and 6 (Figures 6.4 and 6.3) showed that, under conditions of –5% slip, the surface appearance depends very much on the surface wear rate. At high wear rates the track appearance was similar to those observed in tests carried out at –1% slip, but at low wear rates the surface had a burnished appearance.

The wear results obtained from Test 9, translated into surface removal rates, are presented in Figure 6.21. An examination of these results shows that increasing the surface roughness of the work roll test disc in mid test led to an immediate and large increase in the surface wear rate on the back-up roll test disc surface over the next 10000 cycles. However, this effect was only temporary and the wear rate fell rapidly over the subsequent 10000 cycles.

In the first phase of Test 9 there was no crack detector indication of any significant fatigue crack growth. This confirmed the observations in the similar short duration, low wear rate Tests 7 and 8. However after the second phase of Test 9, a significant

crack was found to have propagated from the back-up roll test disc surface. Micrographs of this crack and the morphology of the surface of test disc B4 at the end of the test are shown in Figures 6.22 and 6.23 respectively.

The results from Tests 3-8 demonstrated that in all the continuous high slip tests, whatever the initial wear rate and test duration, there was no increase in wear rate throughout the duration of the test. This suggests that the large increase in wear rate observed in Test 9 arose from the ploughing of the back-up roll surface by the asperities on the "rough" ground track surface of the work roll test disc. This was confirmed by the subsequent reduction in wear rate, which occurred due to the rapid removal of the ground surface on the work roll test disc under the high slip conditions. The rapid removal of the "rough" ground surface on the work roll test disc appears to have suppressed the initiation of the mechanism of fatigue wear of the back-up roll test disc surface which was observed in the tests carried out at –1% slip.

The results obtained from the programme of wear tests has:

1. Highlighted the influence of the roughness on the hard counter-face on the wear performance of the bainitic back-up roll steel.
2. Provided important insights into the possible interactions between wear and rolling contact fatigue in this case and provided the basis for further tests to investigate the phenomenon.

6.4.4. *The interaction between wear and rolling contact fatigue*

The work presented by Fan et al. (1993) suggests that under conditions of rolling contact fatigue and surface wear, there may be a wear rate that gives an optimum balance between the rate of surface wear and the propagation of surface initiated rolling contact fatigue cracks. It follows therefore that for this case it may be possible to determine an optimum work roll surface roughness which gives an acceptable balance between rolling contact fatigue and wear.

The results of an analysis carried out by Kapoor et al. (2002), concerning the truncation by wear of surface initiated rolling contact fatigue cracks initiated at

railway rail/wheel contacts, indicated that the life of railway rails is controlled by fatigue crack growth and/or wear depending on the wear rate.

In order to test this hypotheses Tests 17 and 18 were carried out as extensions to Tests 15 and 16 respectively and the results are presented, together with the results previously obtained from Tests 1 and 11, in Figure 6.24. Tests 1, 17 and 18 were run to rolling contact fatigue failure as indicated by the crack detection system and the results from Test 11 were used as a pointer to the initial roughness of the track of work roll disc W1 which was used in Test 1. The roughness of test disc W1 was not measured directly before the start of Test 1, but the roughness can be inferred by matching the wear rates of the back-up roll test discs B1 and B8.

Examination of the results presented in Figure 6.24 clearly indicates that under conditions of experimental simulation there may indeed be an work roll test disc surface roughness which gives an acceptable balance between surface wear and rolling contact fatigue. Micrographs showing examples of the morphology of the cracks produced in back-up roll test disc B1 (Test1) have already been presented in Figures 4.10a and 5.8b and the morphologies of the cracks produced in test discs B10 (Test 17) and B8 (Test 18) are shown in Figures 6.25 and 6.26 respectively.

Conditions of high work roll test disc surface roughness and high surface wear rate (Test 17) produced numerous large near surface cracks (Figure 6.25) and conditions of low work roll surface roughness and low surface wear rate (Test 18) produced a long penetrating shear crack with no branching (Figure 6.26). Under the latter operating conditions, the number of initiated cracks would be expected to be low, but once initiated cracks would be expected to propagate rapidly due to the low rate of surface wear.

In the tests carried through to rolling contact fatigue failure, which was associated with long penetrating cracks (Tests 1, 6 and 16/18), low surface wear rates on the back-up roll test disc were accompanied by the shorter fatigue lives. This apparent relationship, between low wear rate and low fatigue life, is intuitively reasonable and is supported by the work by Fan et al. (1993).

It would appear from the results of this work that the roughness of the hard counter-face is the dominant factor in the ploughing wear mechanism, can be an important factor in the fatigue wear mechanism and also has an important influence on the propagation of rolling contact fatigue cracks. Importantly, the tests carried out at both levels of slip indicate that it may be very desirable to carefully control the variation in the surface roughness of work rolls presented to the mill and also to aim to keep the value of the surface roughness to the optimum determined by the testing programme.

6.5. LINKS BETWEEN MECHANICS AND MICROSTRUCTURE

6.5.1. *Introduction*

In order to establish criteria for the microstructural design of a back-up roll material, it was necessary to link mechanics to microstructure by relating crack propagation paths and morphologies to specific microstructural features of the materials of both the test discs and the spalled material from a back-up roll. Once crack propagation in mode I has been established, the rate of crack propagation, though unpredictable, would be expected to increase rapidly and can be considered to be insensitive to microstructure. For these reasons, the material can be assumed to have failed if mode I crack propagation is established. Therefore, for the purposes of this exercise, crack propagation was divided into three parts; crack initiation and propagation through the plastically deformed surface layer up to mode II threshold, inclined crack propagation in mode II and mixed mode I/mode II, and crack propagation at and shortly after mode I threshold.

6.5.2. *Crack initiation and propagation up to mode II threshold*

6.5.2.1. Test disc specimens

In the qualitative and quantitative models, the hypothesis put forward for the initiation and early propagation of the surface initiated cracks was that the cracks would initiate and propagate along the preferentially orientated boundaries between the ferrite packets and carbides and would be driven by the high stresses in the plastically

deformed layer. Examples of cracks propagating in this way are shown in Figure 6.27. The growth of such cracks may be arrested by the subsequent presence of sudden barriers to crack growth or progressive changes in the orientation of the ferrite packet/ carbide boundaries. Typical examples of these types of barriers to crack growth in the test disc specimens are shown in Figure 6.27.

6.5.2.2. Material spalled from a back-up roll

Examination of the near surface region of material spalled from a back-up roll revealed ferrite packet/carbide boundaries similar to those observed in the test disc specimens and micro cracks propagating in the plastically deformed surface layer, see Figure 6.28.

6.5.3. *Inclined crack propagation*

6.5.3.1. Barriers to fatigue crack growth

The thickness of the plastically deformed surface layers and the cracks observed in both the test disc specimens and the spalled material confirmed that the cracks could be propagated to crack lengths where the calculated mode II stress intensity factors would breach the assumed mode II threshold. In order to establish the effective barriers to the mode II and mixed mode I/mode II growth of the inclined surface cracks, the morphologies of cracks produced in several test disc specimens were examined. The main barriers to fatigue crack growth appeared to be the boundaries of the ferrite packets. An example of the growth of a crack being arrested at the boundary of a ferrite packet is shown in Figure 6.29.

With the boundaries of the ferrite packets apparently identified as the main barriers to crack growth, it was necessary to establish that:

1. The packet boundaries were high angle or high misorientation boundaries.
2. The bulk crystallographic textures of the materials were sufficiently random to make these boundaries effective.

6.5.3.2. Micro texture

The results obtained from ESBD analysis of the microstructures of the test disc and spalled materials are shown in Figures 6.30-6.33. The EBSD micrographs presented in Figures 6.30 (their evidence of a small amount of specimen drift in the top left hand section of the micrograph) and 6.31 show the boundaries of the ferrite packets and indicate that the packet dimensions of the two materials are of the same order. However, the ferrite packets in the test disc material appear to be more acicular in shape and the effective grain size smaller than those observed in the spalled material, where the packets appear to be more granular in shape.

The results showing the misorientation angle distributions and misorientation axes for the test disc material and spalled material are shown in Figure 6.32. The results indicate that the majority of the boundaries between the ferrite packets are high misorientation boundaries (> 50°). These results are supported the work of Gourgues et al. (2000), who found similar distributions in an EBSD study which included bainitic steels.

The misorientation axes for a large number of misorientations were found to be lie close to the <110> and <111> directions. Slip in BCC metals is found to occur on the {110}, {112} and {123} planes, but always in the <111> (close packed) direction (Dieter, 1988). Rotation of the stereographic projections for the <110> and <111> directions through angles of 55° and 57° respectively results in the misorientation of some of the above planes and a large number of substantial misalignments of the <111> directions. This result confirms that observed misorientations should create effective barriers to fatigue crack growth at the ferrite packet boundaries.

6.5.3.3. Bulk texture

The results of the bulk texture analyses, shown in Figures 6.33 and 6.34, indicate that the bulk textures of the test disc material (0.3-2.0 x random) and the spalled material (0.2-1.7 x random) are both sufficiently random to ensure that the prior austenite grain boundaries will provide barriers to fatigue crack growth. These barriers will

therefore underpin the effectiveness of the observed high misorientation packet boundaries within the prior autenite grains as barriers to fatigue crack propagation.

6.5.4. *Mode I threshold*

Yoder et al. (1983), after an analysis of the grain size and yield strength dependence of near-threshold fatigue crack growth in a range of steels, concluded the mode I stress intensity factor range ΔK_T at transition from microstructurally sensitive to microstructurally insensitive crack growth is the point at which the cyclic plastic zone size attains the mean effective grain size. For a martensitic steel, Yoder et al. (1983) deduced that that the effective grain size of the material was the size of the packet of martensitic laths. This hypothesis supports the assumption made in this work, that the effective grain size of the baintic steel back-up roll material should be the smallest dimension of the ferrite packets. In the case of the materials tested by Yoder et al (1983), ΔK_T also approximated to the mode I threshold ΔK_{th}.

It follows from this result that, if at mode I threshold the mean effective grain size can be equated to the cyclic plastic zone size given by equation (5.1), then the mean effective grain size $\bar{d}$ can be expressed as:

$$\bar{d} = C\left[\frac{K_{\max th}(1-R)}{2\sigma'_y}\right]^2 \qquad (6.1)$$

where, $C = 1/3\pi$, $R = -1$ and K_{maxth} is the maximum mode I stress intensity factor at the crack tip at threshold.

Inspection of the micrographs of inclined cracks with upward branching, presented in Figures 4.10, 5.8 and 6.35, indicated that, with an allowance made for the level of surface wear observed in low wear rate tests, a reasonable figure for the length of the inclined cracks at mode I threshold was 180 μm. The computed value of the maximum mode I stress intensity factor at this crack length was 9.4 MPa√m. Using this value and assuming that the cyclic yield stress is equal to the monotonic yield stress (1500 MPa√m), equation (6.1) predicts a value of 7.7 μm for the mean

effective grain size of the material. This result was validated by inspection of the EBSD grain map of the test disc material shown in Figure 6.30. The results show that mean value of smallest dimension of the observed ferrite packets lies in the range 5-10 μm, which is in good agreement with the predicted value.

Rearrangement of equation (6.1) gives an expression for the mode I threshold (expressed as the maximum mode I stress intensity factor at threshold) for materials under conditions of rolling contact, in terms of the yield stress and mean effective grain size, see equation (6.2).

$$K_{\max th} = 3.07\sigma_y\sqrt{\bar{d}} \qquad (6.2)$$

6.6. DESIGN CRITERIA

6.6.1. *Overview*

The results obtained in this project have been used to specify the demands placed on back-up rolls and have also been used to establish design criteria for resistance to rolling contact fatigue. The latter has been achieved by the formulation of practical qualitative and quantitative recommendations for the mechanical and microstuctural design of bainitic steel back-up roll materials, back-up roll re-dressing procedures and the surface roughness of both work roll and back-up rolls presented to the mill.

6.6.2. *Loading and operating conditions*

The most important factors affecting the demands placed on back-up rolls have been established as: the maximum contact pressure, the effect of a tangential traction, the presence of a lubricating fluid in the form of the roll coolant and the influence of asperity stresses.

The determination of a value for the maximum contact pressure at the work roll/back-up roll interface and the identification of the important operating conditions

were essential in arriving at the basis for experimental and modelling programmes. However, of equal importance was the recognition of the important part played by the roughness of the HSS counter-face in the rolling contact fatigue and wear performance of bainitic roll steels. The control of asperity stresses in the early part of each round depends on the ground finish applied to the roll surfaces during re-dressing, attention to this problem should therefore be included in the roll maintenance procedures.

6.6.3. *Microstructural design of a bainitic steel back-up roll material*

The results of the work on the design of bainitic back-up roll materials indicated that the resistance of the material to crack propagation and crack morphologies, which may result in catastrophic failure of the rolls, depends on the control of carbide distribution, the limitation of the length of the carbide/ferrite packet boundaries by control of prior austenite grain size (early crack propagation) and the maximisation of the value of the parameter $\sigma_y\sqrt{\bar{d}}$, equation (6.2) (and hence the mode I threshold). Limiting prior austenite grain size also promotes the nucleation of bainitic ferrite at prior austenite grain boundaries at the expense of acicular ferrite, which may nucleate intragranulary at inclusions within large prior austenite grains (Bhadeshia,1992).

The trends identified as a result of the work on the prediction of crack morphology indicated that the higher the value of the mode I threshold the more likely the initial inclined shear crack will be longer and the subsequent propagation will produce upturning cracks. Conversely the lower the mode I threshold the more likely that cracks will propagate into the deeper substrate, leading to catastrophic failure.

XRD analysis of the material used for the manufacture of the back-up roll test disc specimens did not indicate the presence of any retained austenite. This result meant that it was not possible to investigate the influence of retained austenite on the rolling contact fatigue performance of the test material. Bhadeshia (1992) suggests that a small amount of fairly stable austenite should lead to an improvement in the fatigue properties of bainitic steels, due to the higher ductility of the austenite. However, such an improvement can only be expected if the austenite is stable and does not

transform to martensite under the action of the applied stresses. On balance, due to the uncertainties concerning the stability of any retained austenite, it should be conservatively assumed that its presence is detrimental to the damage tolerance properties of back-up roll materials.

6.6.4. *Roll maintenance*

The most important specifications required for the roll maintenance programme as identified by this work are the amount of material which should be removed during the re-dressing of back-up rolls and the roughness of the final ground finish on both the work rolls and the back-up rolls.

The theoretical predictions for crack morphology indicated that, for a crack length/half contact width ratio of approximately 0.2, the direction of the maximum mode I stress intensity factor would be parallel to the contact surface. Extending this normalised result to the back-up roll case, the equivalent crack length would be 1200 μm with a predicted maximum stress intensity factor in excess of 15 MPa$\sqrt{m}$. If a mode I threshold with a maximum stress intensity factor of this magnitude could be achieved, the results suggest that for cracks propagating at 60° to the surface normal, the maximum depth to which the crack would propagate would be limited to less than 0.7 mm. It is however unlikely that, under rolling contact fatigue conditions, the necessary level of mode I threshold could be achieved using the materials considered in this project.

For materials exhibiting mode I thresholds with maximum stress intensity factors at the top end of the range presented by Kapadia and Marsden (1997), mode I crack propagation was predicted to commence in a direction close to the direction of the inclined shear crack. With the methods used in this project it was not possible to theoretically predict trends in crack morphology after mode I threshold. However with the predicted directions of the initial mode I propagation being close to the direction of the existing shear crack, there should be a tendency for the mode I crack propagation to become slowly upturning in line with the predictions of the quantitative model. Therefore, although under conditions of mode I crack growth, crack propagation would be faster, the maximum depth to which the crack would

propagate should again be less than 0.7 mm. If it is assumed that the crack pressurisation mechanism is operating, this argument provides a reasonable guide for specifying the amount of material, which should be removed during redressing of back-up rolls manufactured from bainitic materials with higher but realistic mode I thresholds.

Evidence for the possibility of a work roll surface roughness which gives an acceptable balance between wear and rolling contact fatigue has been discussed previously in Section 6.4.4, but from the point of view of the roll maintenance procedures it is useful to present the selected wear data obtained from the experimental simulations as shown in Figure 6.36.

The results from tests carried out at -1% slip, show how the mean surface removal rate of material from the tracks of the back-up roll test discs (from 10000 – 40000 cycles) varied with work roll test disc surface roughness. These results highlight the sudden increase in wear rate when the roughness of the track of the work roll test disc was increased to Ra 0.47 μm and seem to suggest that a work roll surface roughness in the range Ra 0.3 μm to Ra 0.4 μm may result in optimum back-up roll performance. The practicality of adopting this standard is supported by data presented by Caithness et al. (1999), which suggests that producing this desirable level of surface roughness is a reasonable proposition in a modern roll shop.

Inspection of the wear results presented in Figure 6.16 shows that, in the first 10000 cycles of the experimental simulations carried out at –1% slip, the roughness of the track of the back-up test discs significantly influenced the wear rate. For this reason and the possible influence of back-up roll surface roughness on the initial level of asperity stresses it would seem reasonable, if practical, to maintain initial back-up roll surface roughness at around the same level as work roll surface roughness.

Test disc			
Crack length (a) μm	K_σ MPa√m	$2r_{cyclic}$ μm	Crack length/$2r_{cyclic}$
70	3.80	1.26	55
100	5.41	2.55	39
130	7.00	4.30	30
190	10.16	9.01	21
Back-up roll			
Crack length (a) μm	K_σ MPa√m	$2r_{cyclic}$ μm	Crack length/$2r_{cyclic}$
200	4.21	1.35	129
350	5.47	2.62	135
500	7.08	4.40	114
750	10.03	8.82	85

Table 6.1. Ratios of crack length/plastic zone size (diameter)

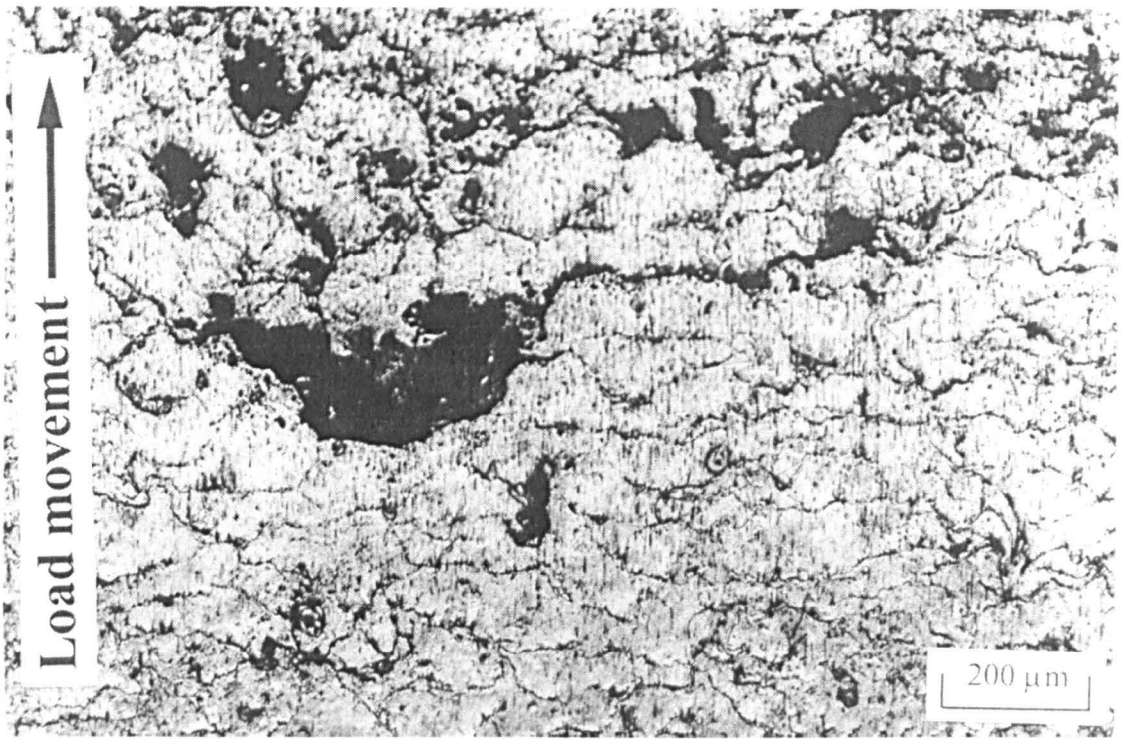

Figure 6.1. Optical micrograph showing the surface morphology of specimen B1 in the region of the dominant crack, at the end of Test 1 (252000 cycles, -1% slip)

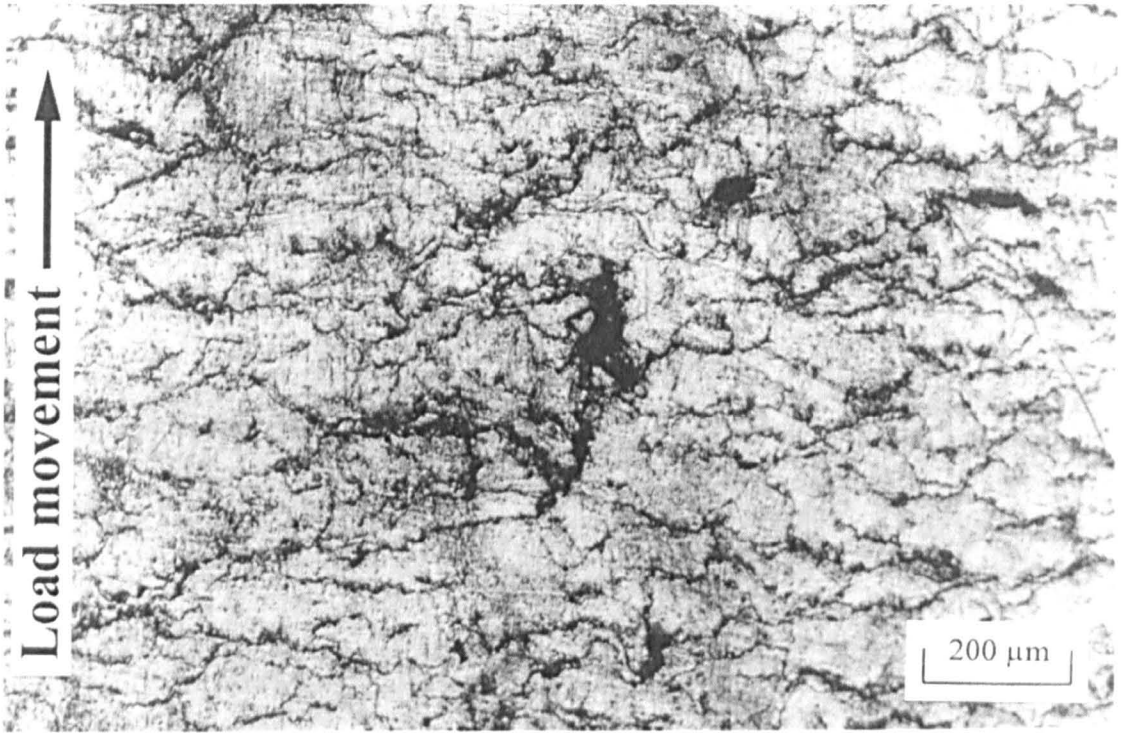

Figure 6.2. Optical micrograph showing the surface morphology of specimen B1 at the end of Test 1 (252000 cycles, -1% slip)

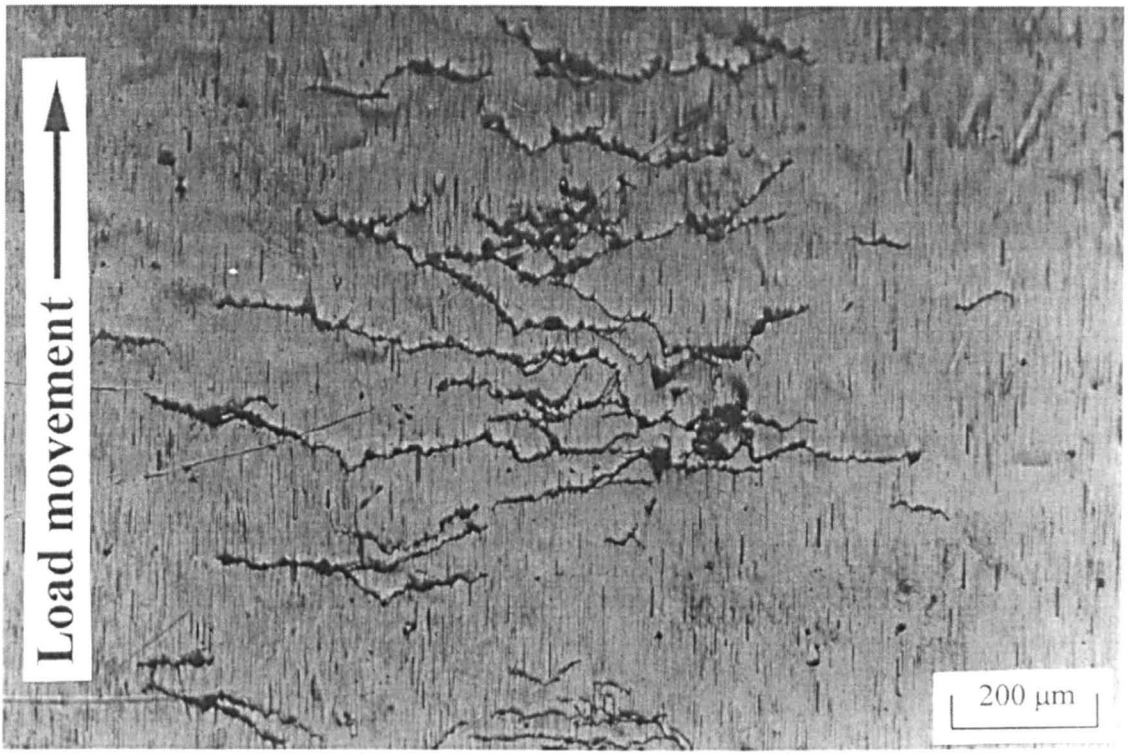

Figure 6.3. Optical micrograph showing the surface morphology of specimen B3 at the end of Test 6 (200098 cycles, -5% slip)

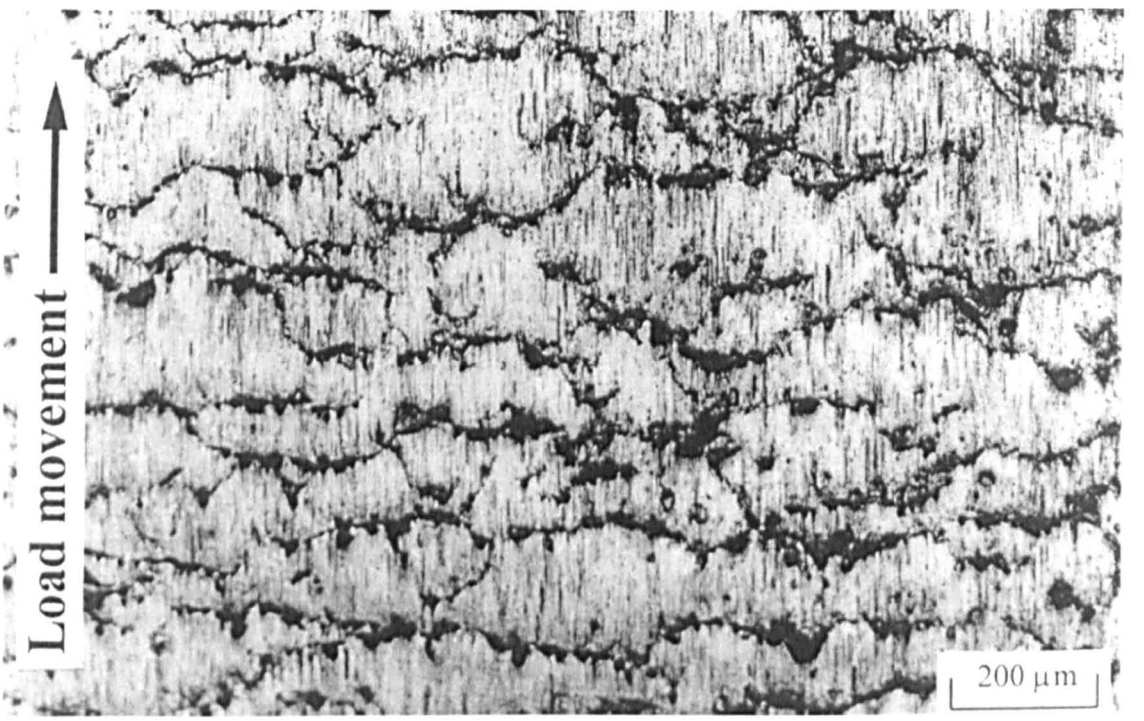

Figure 6.4. Optical micrograph showing the surface morphology of specimen B5 at the end of Test 5 (119061 cycles, -5% slip)

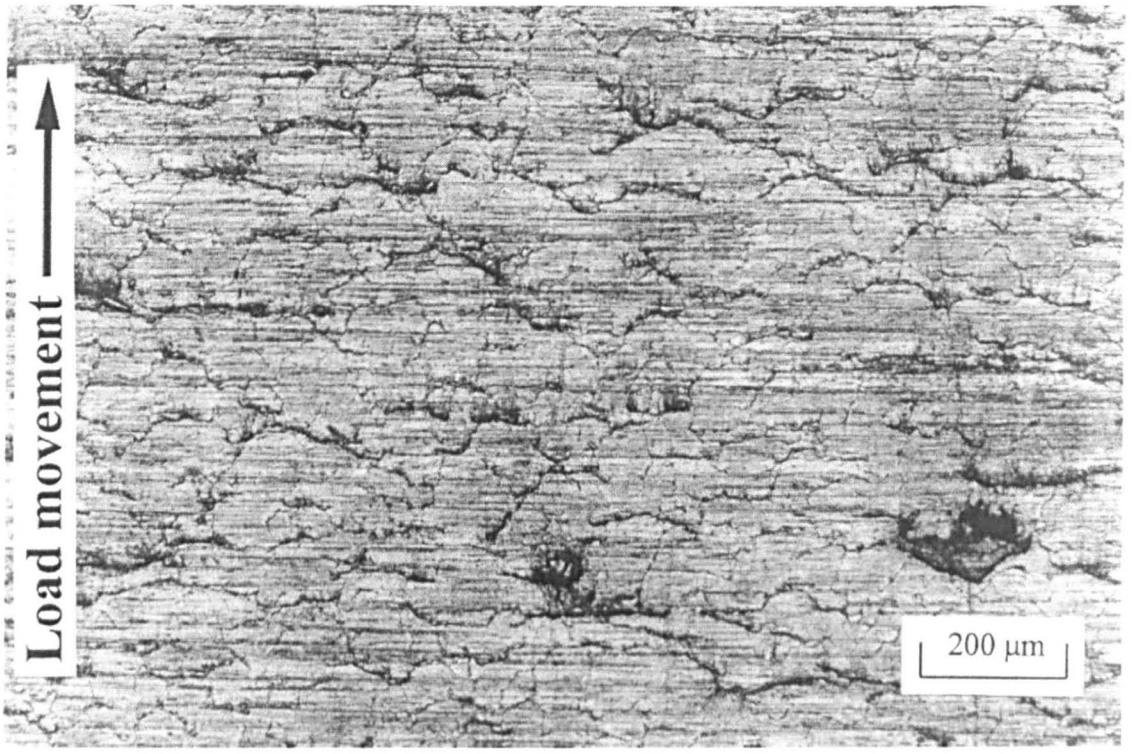

Figure 6.5. Optical micrograph showing the surface morphology of the sample taken from the fragment of spalled back-up roll material

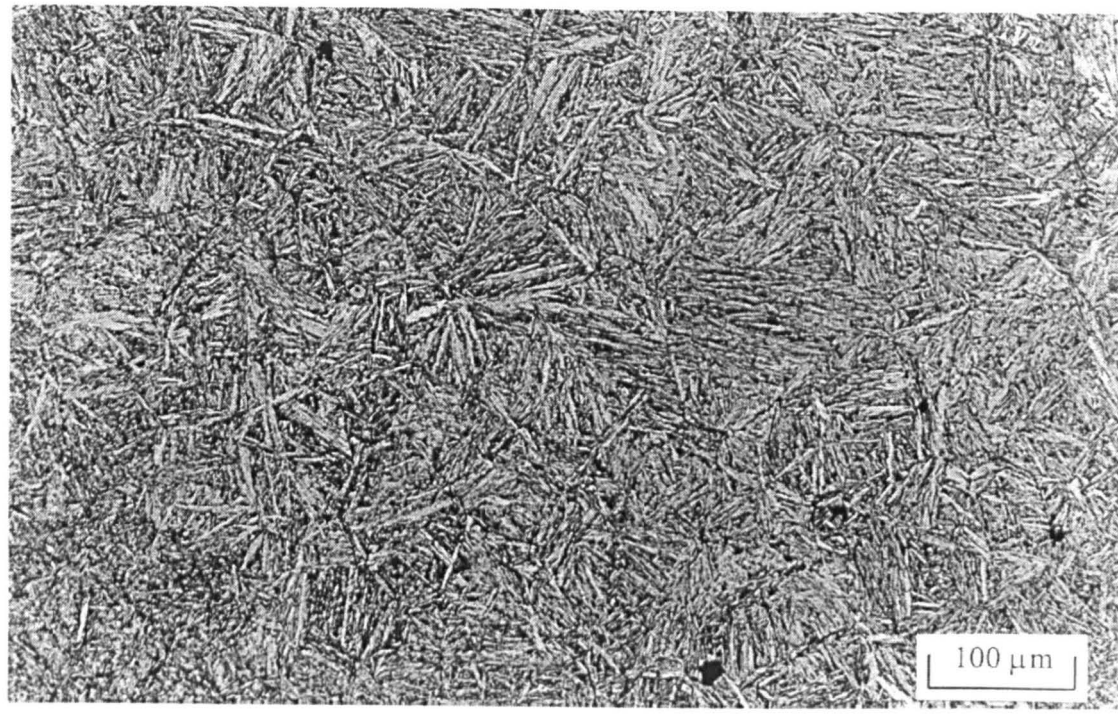

(a)

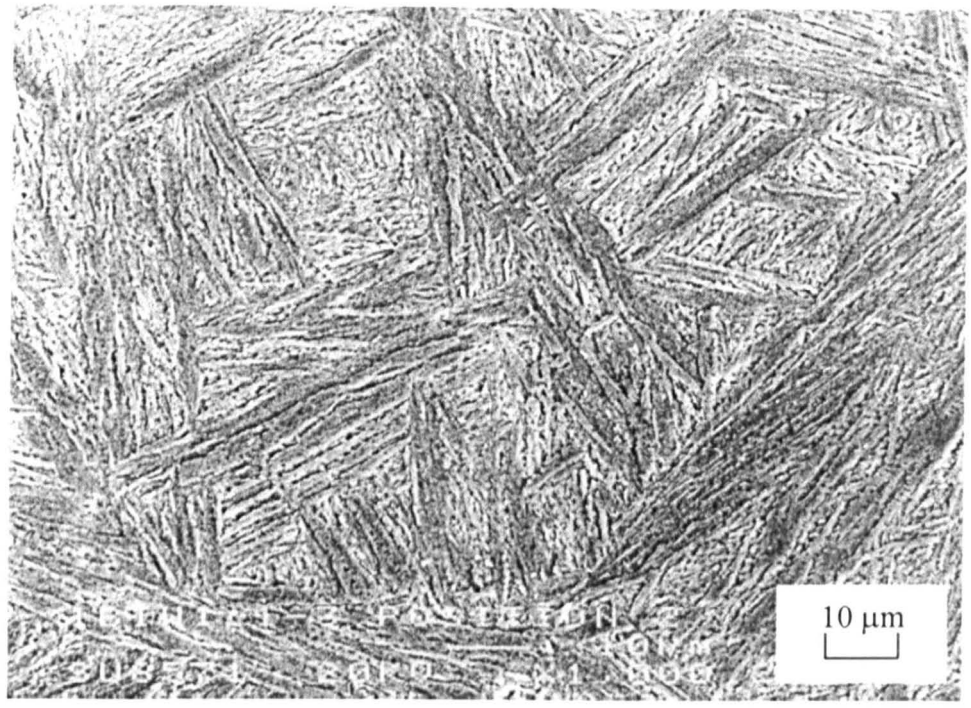

(b)

Figure 6.6. (a) Optical micrograph of the microstructure of a typical back-up roll test disc specimen, polished and etched with 2% Nital (b) BEI micrograph of the material of a typical back-up roll test disc specimen

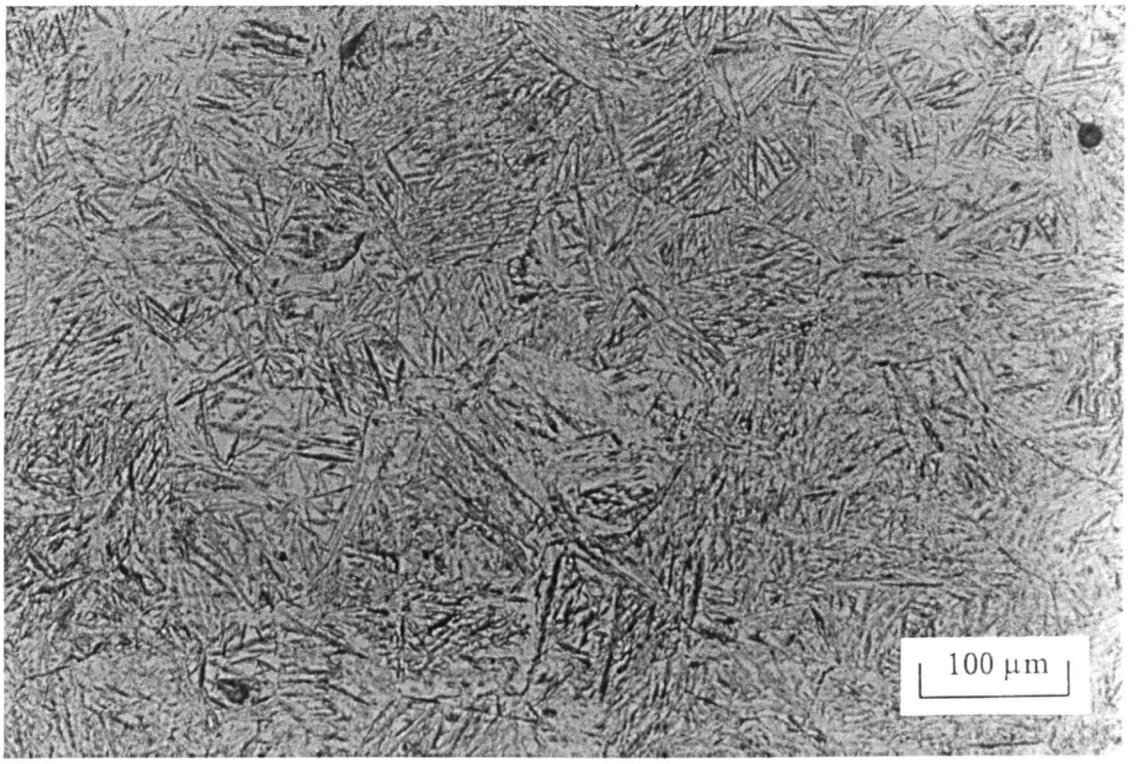

(a)

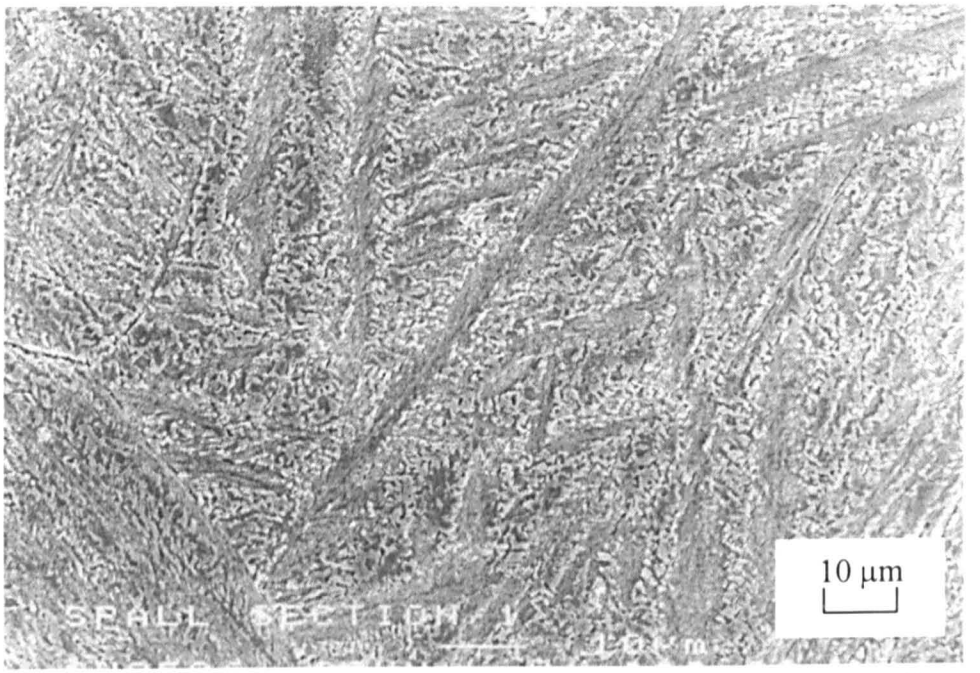

(b)

Figure 6.7. (a) Optical micrograph of the microstructure of material spalled from a back-up roll, polished and etched with 2% Nital (b) BEI micrograph of material spalled from a back-up roll, polished and etched with 2% Nital

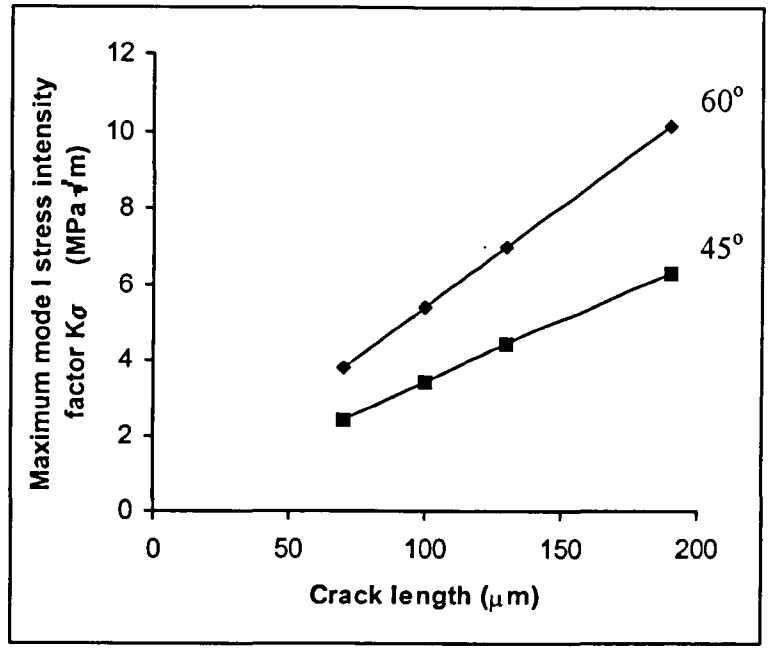

(a)

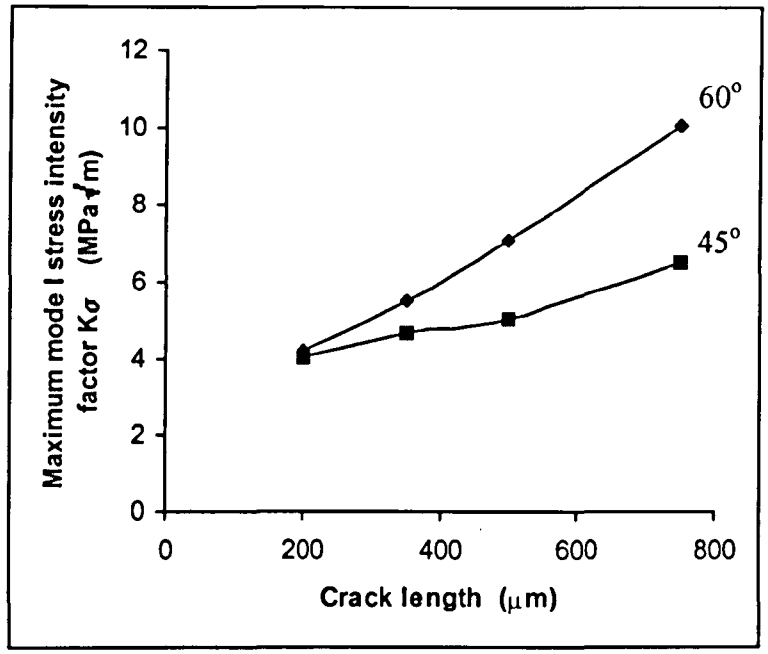

(b)

Figure 6.8. Predicted maximum mode I stress intensity factors arising at the inclined crack tips for cracks propagating at 45° and 60° to the surface normal, for pressurised cracks with a maximum contact pressure of 1500 MPa and traction coefficient of 0.14 for (a) Test disc pair (b) Work roll/back-up roll pair

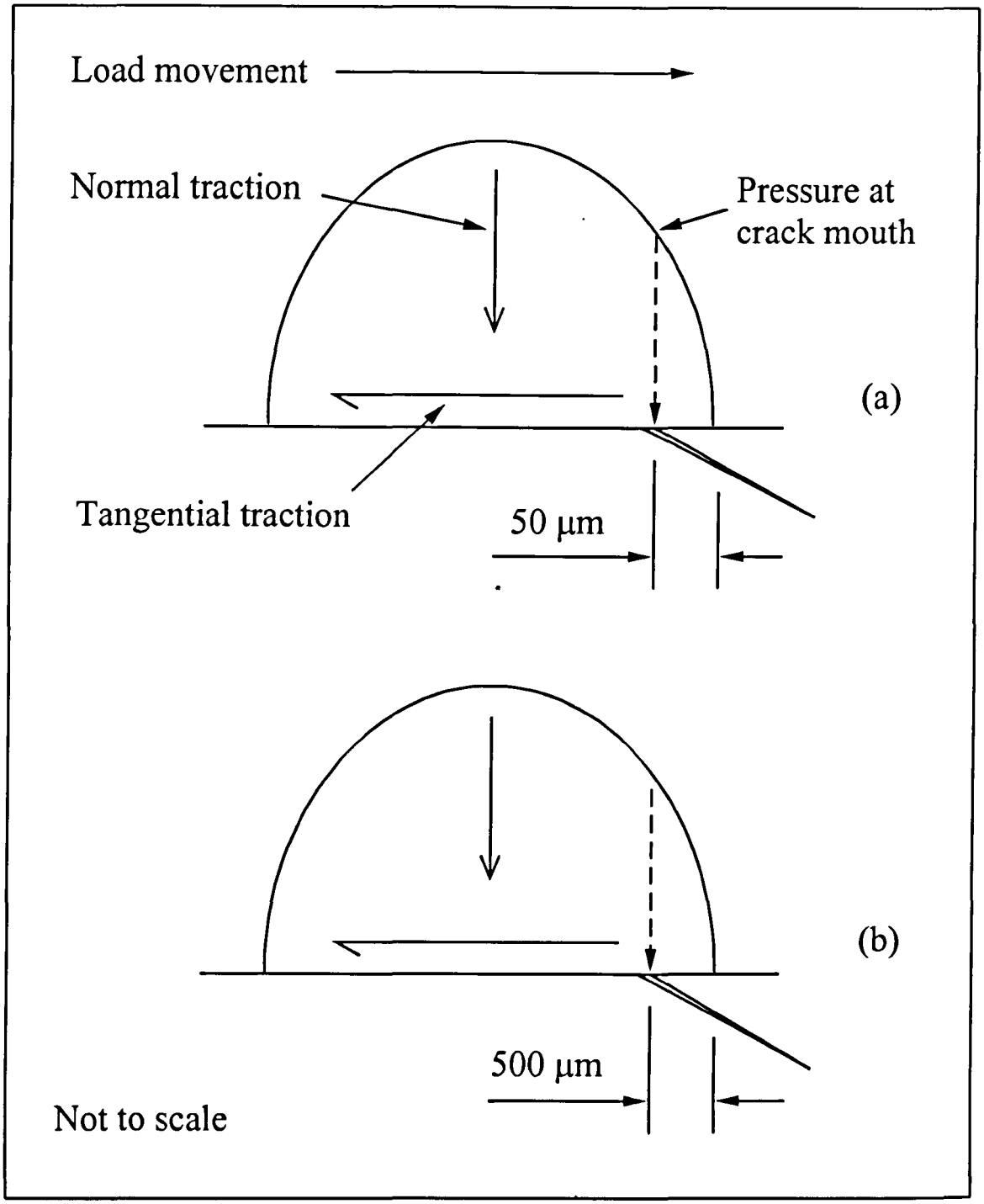

Figure 6.9. Schematic diagram showing the approximate width of contact patch, which is available to cover the crack mouths at the point when the effective crack pressurisation takes place for (a) The test disc pair (b) The work roll/back-up roll pair

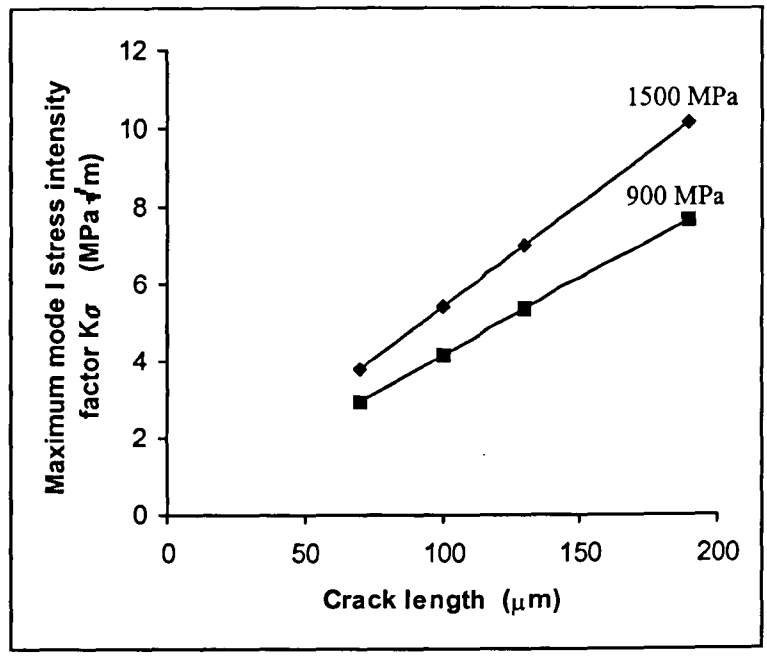

(a)

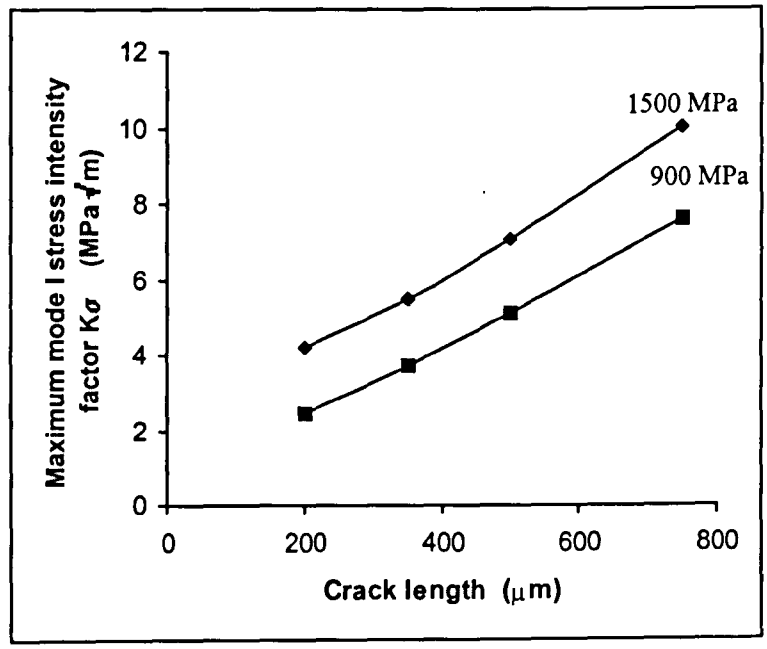

(b)

Figure 6.10. Predicted maximum mode I stress intensity factors arising at the inclined crack tips for maximum contact pressures of 900 MPa and 1500 MPa, for pressurised cracks propagating at 60° to the surface normal and with a traction coefficient of 0.14 for (a) Test disc pair (b) Work roll/back-up roll pair

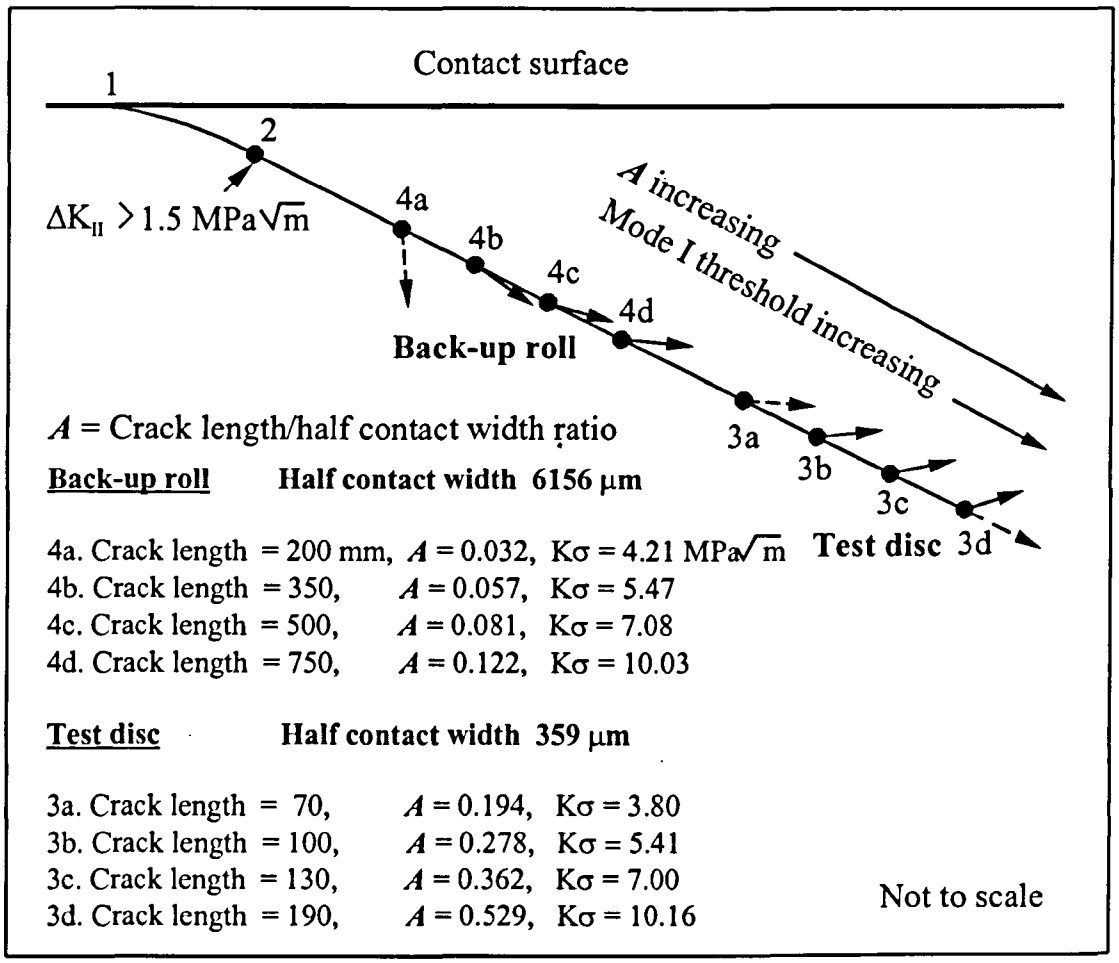

Figure 6.11. The effect of increasing the mode I threshold and hence the value of A at which the mode I threshold is reached

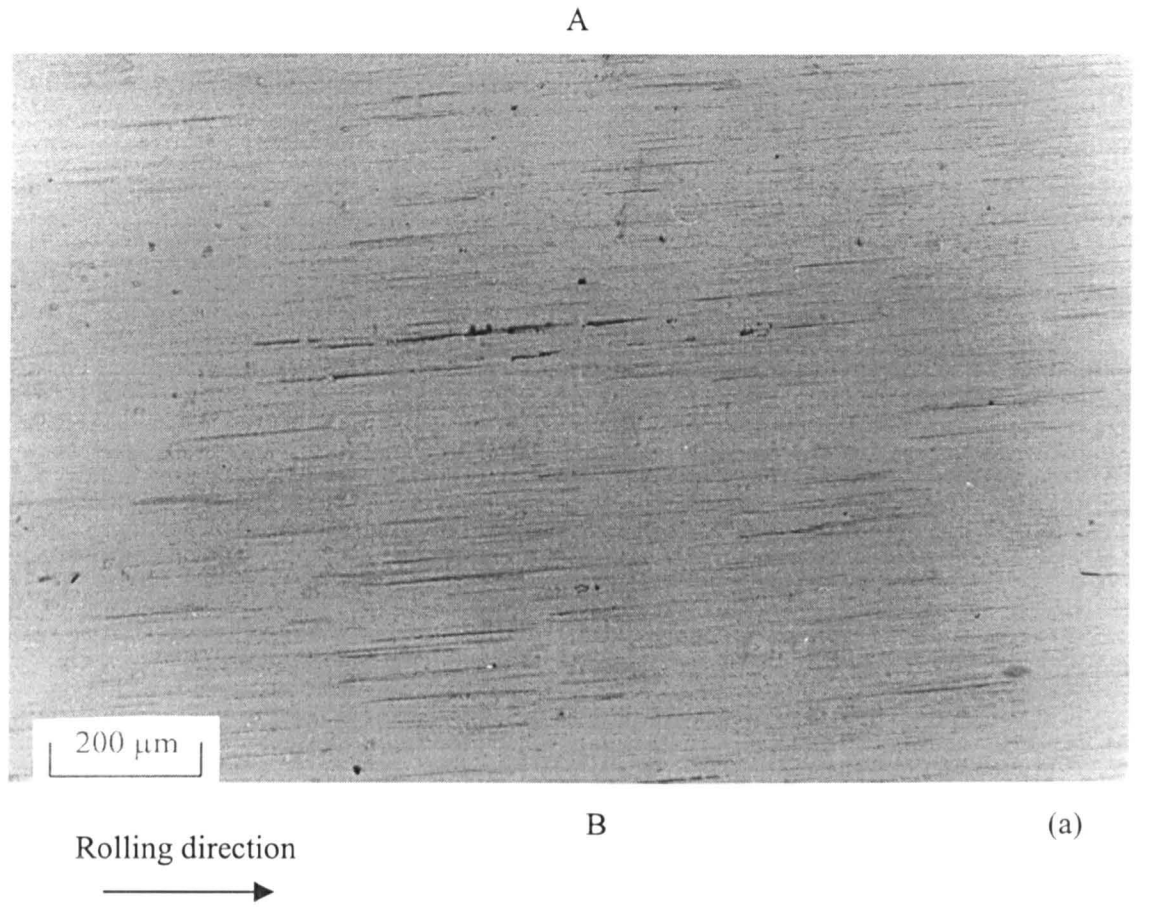

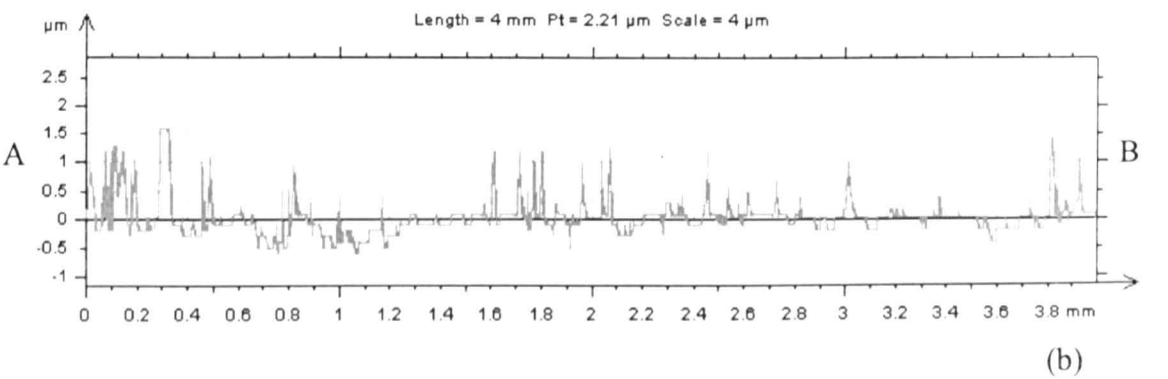

Figure 6.12. (a) Replica of the surface of test disc W8 at the start of Test 16 (b) Transverse surface contour of test disc W8 at the start of Test 16 (direction A – B)

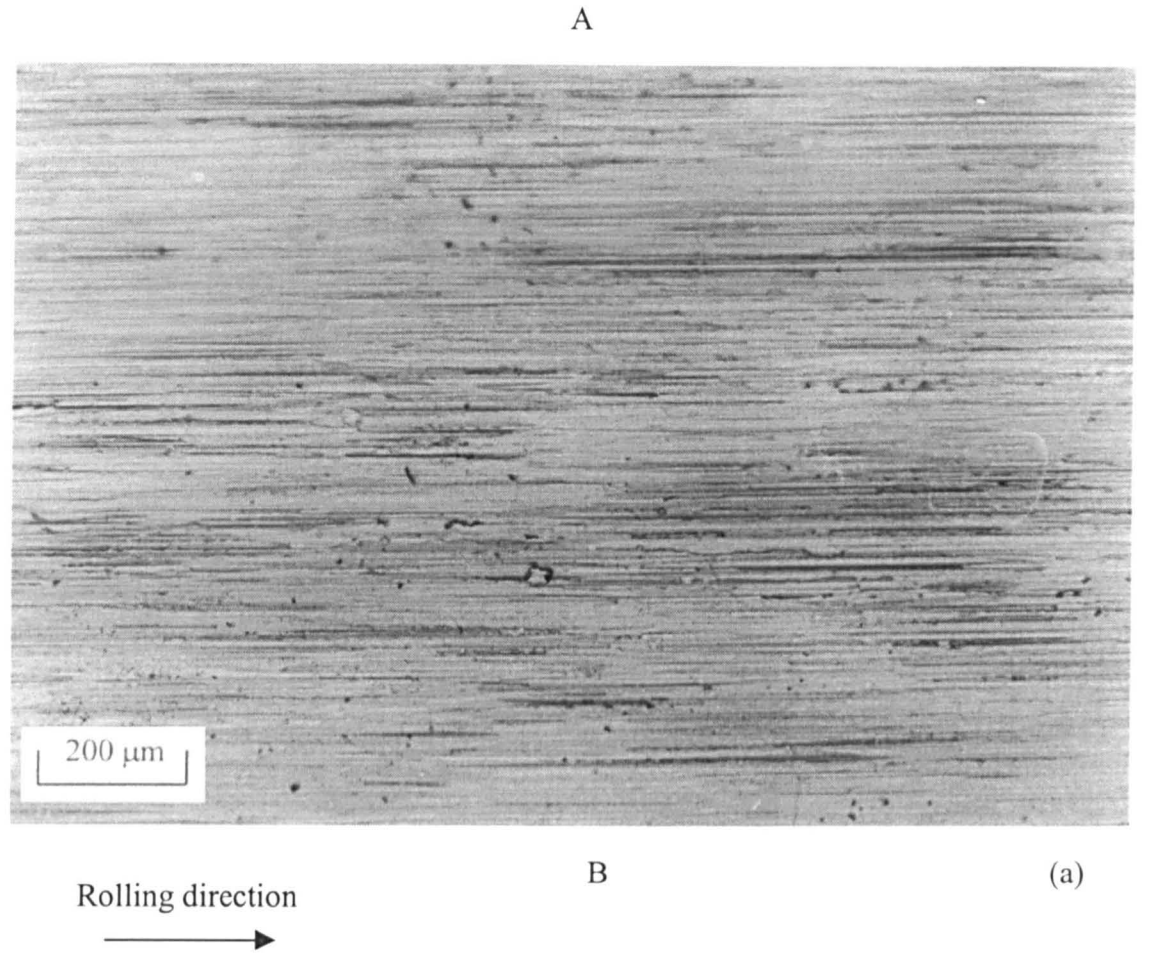

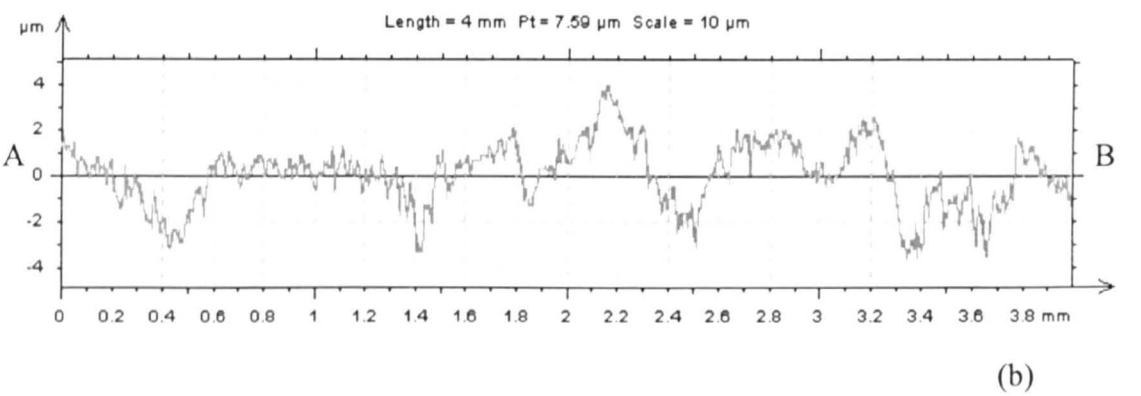

Figure 6.13. (a) Replica of the surface of test disc W10 at the start of Test 15 (b) Transverse surface contour of test disc W10 at the start of Test 15

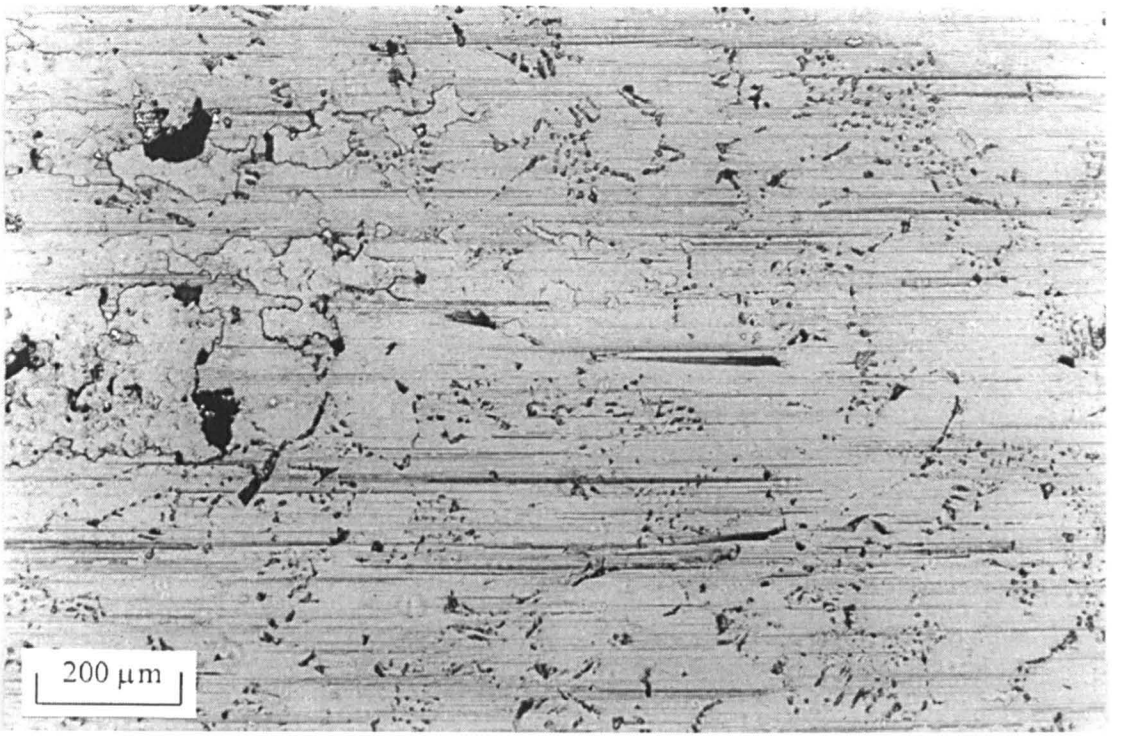

Figure 6.14. Replica of the surface of test disc W1 at the end of Test 1 (-1% slip, 252000 cycles

Figure 6.15. Replica of the surface of test disc W3 at the end of Test 6 (-5% slip, 200098 cycles)

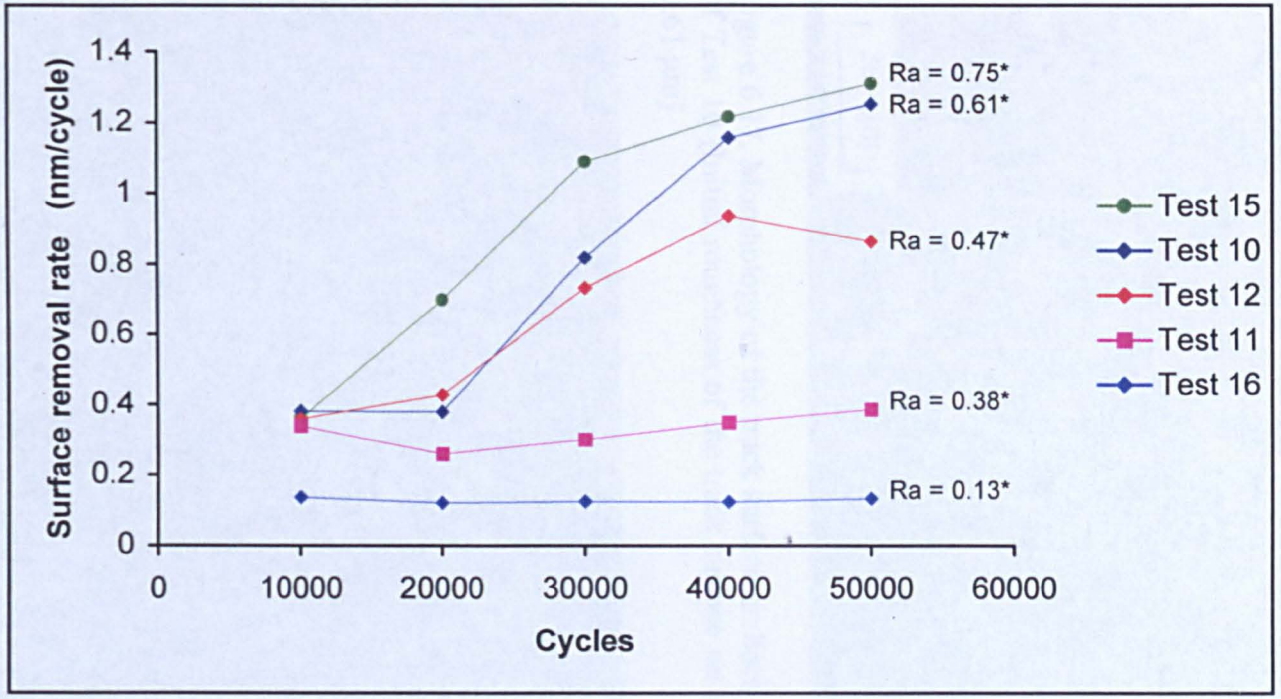

*Surface roughness of the track on the work roll test disc measured μm

Roughness of the track on the back-up test discs	Tests 10,11 and 12	– Ra = 0.85 μm
	Test 15	– Ra = 0.17 μm
	Test 16	– Ra = 0.16 μm

Figure 6.16. Results obtained from the experimental simulations at –1% slip showing the influence of the roughness of the track surfaces on the work roll and back-up roll test discs on the wear performance of the bainitic steel back-up roll material

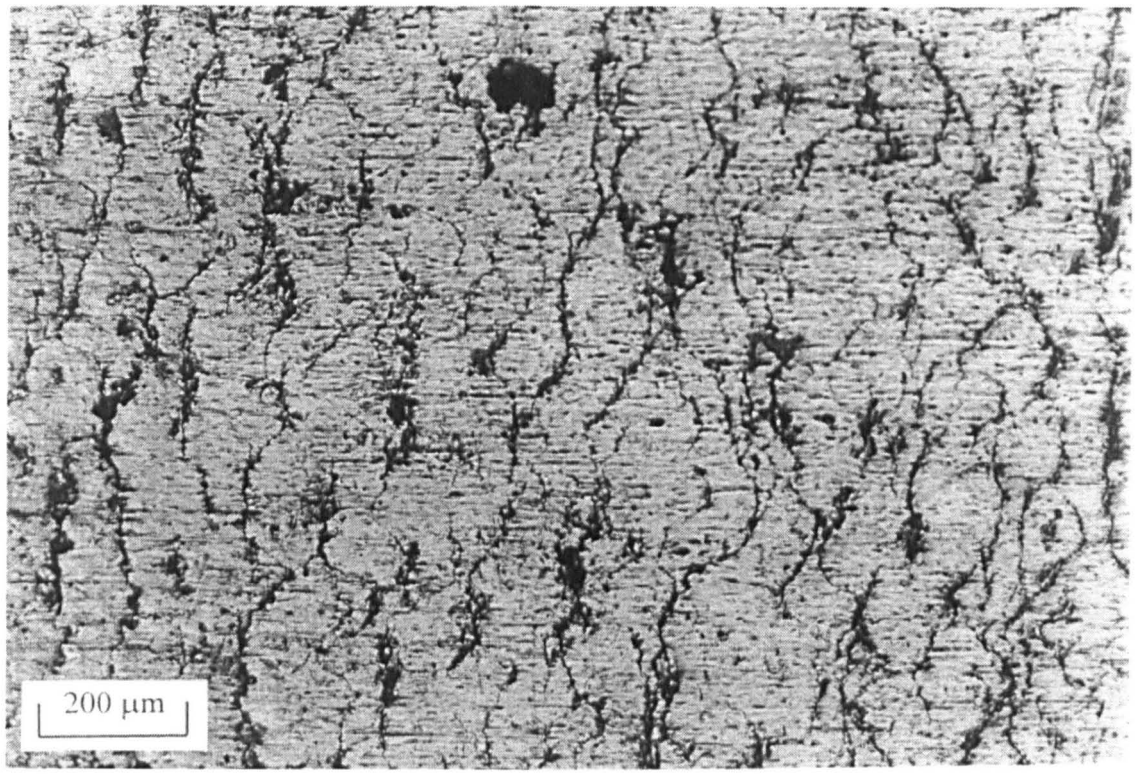

Figure 6.17. Morphology of the track surface on back-up roll test disc B10 at the end of Test 10 (Initial roughness of the track surface on work roll test disc W10 – Ra = 0.61 μm)

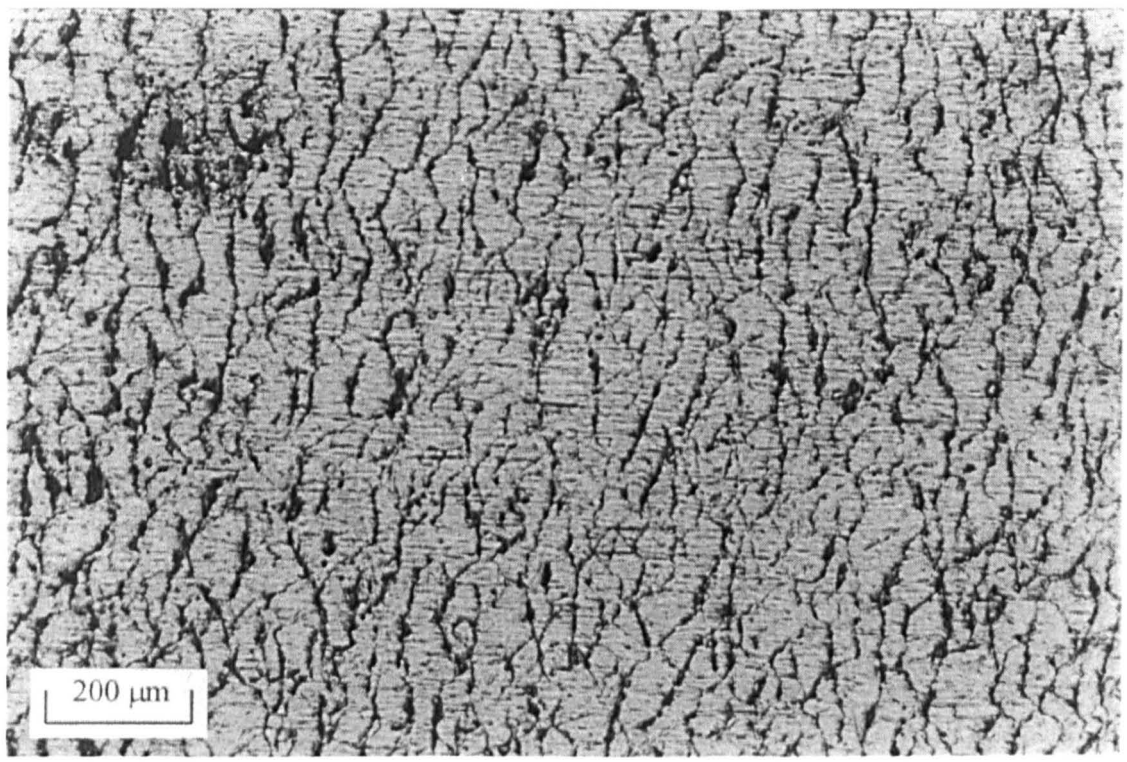

Figure 6.18. Morphology of the track surface on back-up roll test disc B8 at the end of Test 8 (Initial roughness of the track surface on work roll test disc W8 – Ra = 0.38 μm)

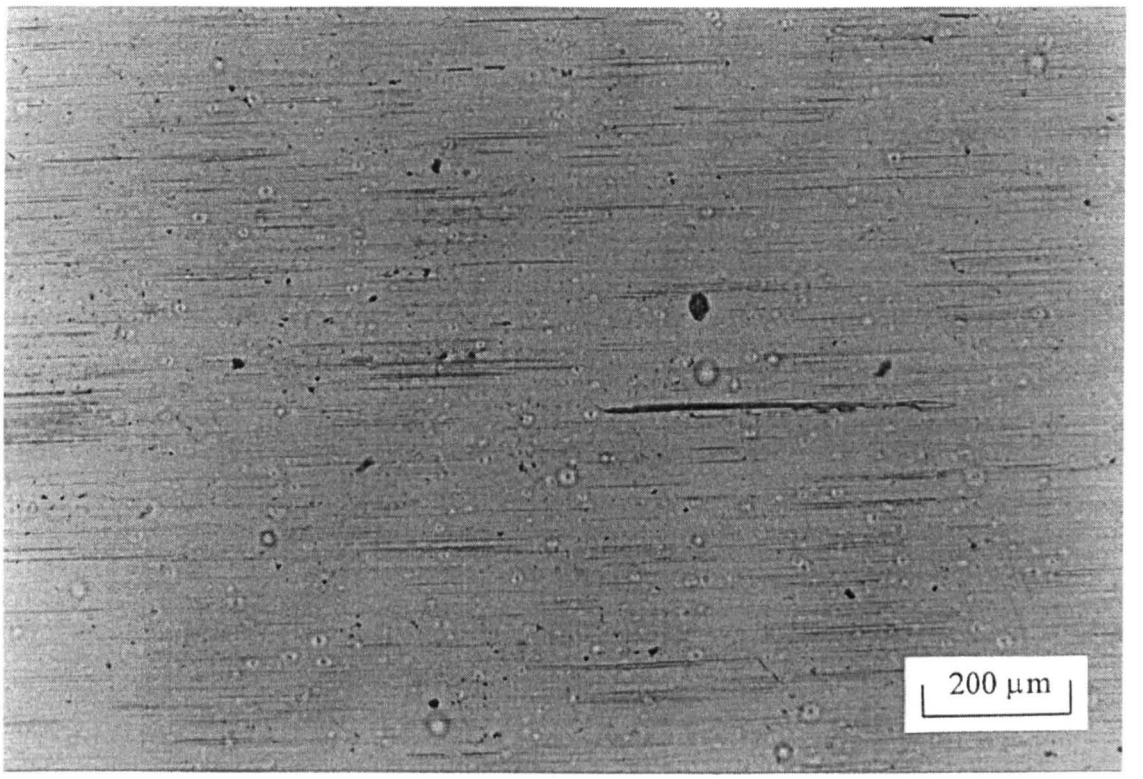

(a)

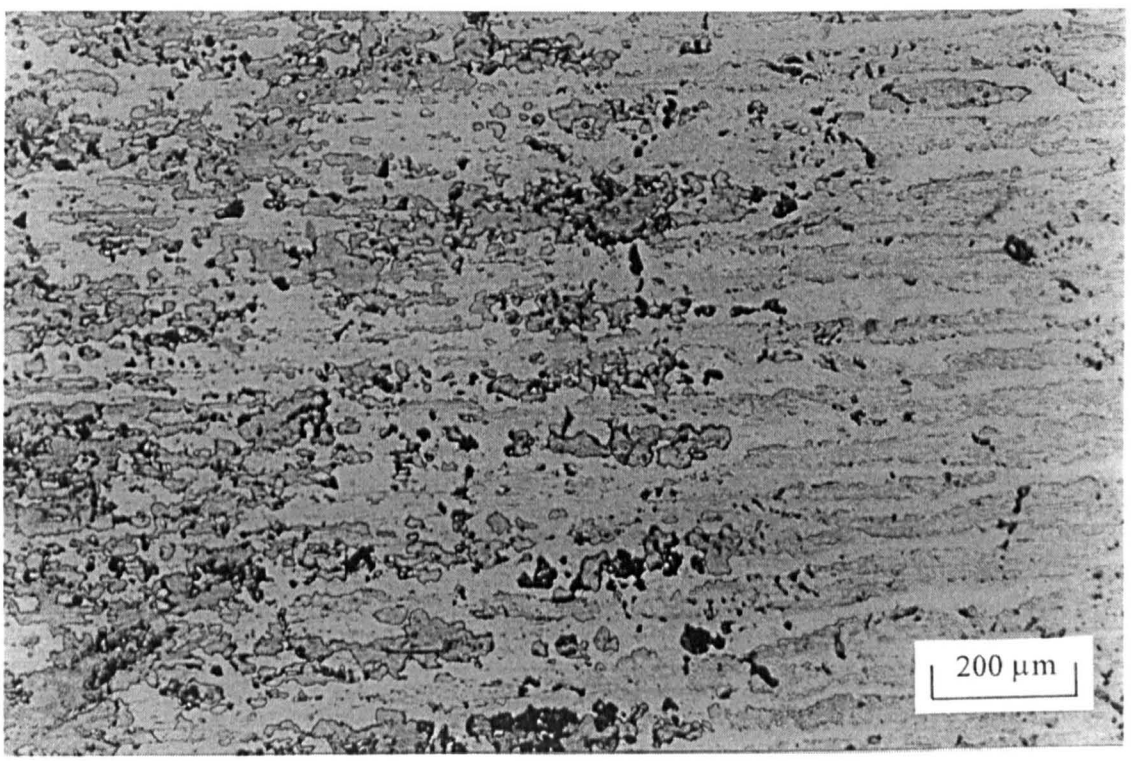

(b)

Figure 6.19. (a) Replica of ground surface (Ra 0.06 μm) of test disc W5 at the start of the first phase of Test 9 (b) Replica of the worn surface of test disc W5 after 70000 cycles (end of the first phase of Test 9)

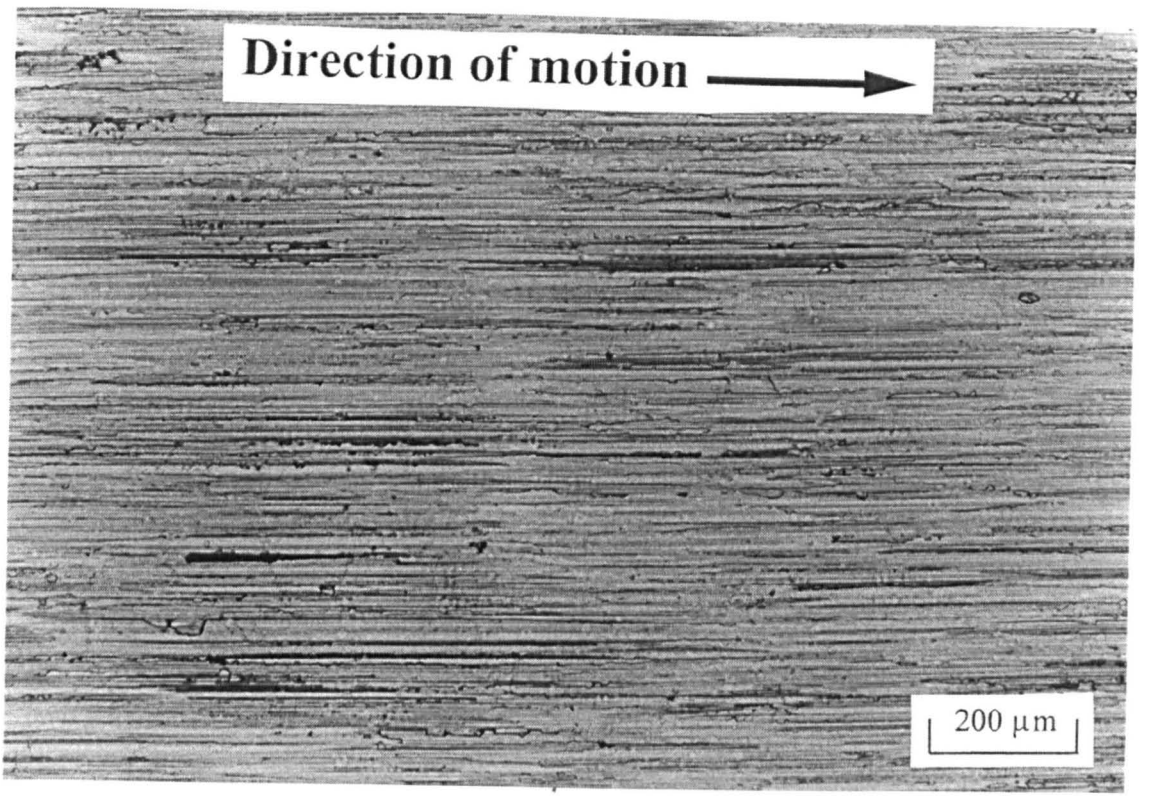

(a)

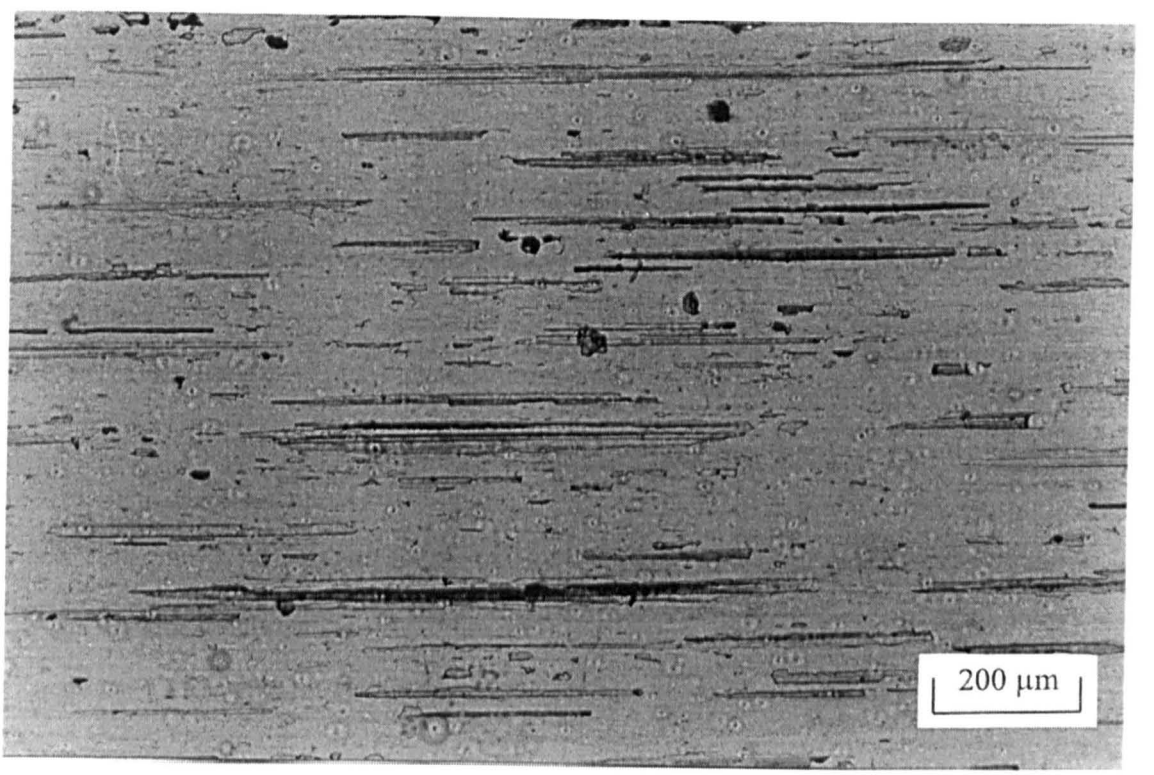

(b)

Figure 6.20. (a) Replica of ground surface (Ra 0.6 μm) of test disc W5 at the start of the second phase of Test 9 (b) Replica of the worn surface of test disc W5 after 50000 cycles (end of the second phase of Test 9)

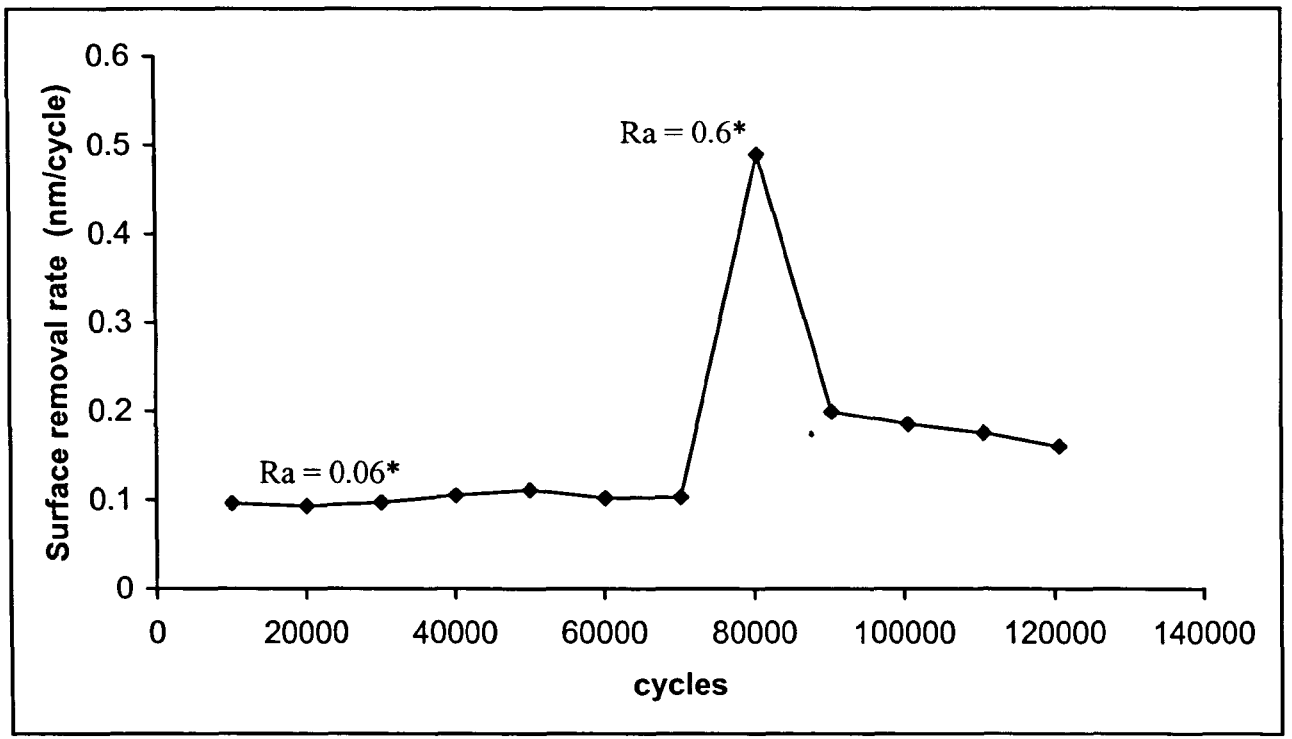

*Surface roughness on the track of the work roll test disc measured in μm

Figure 6.21. Results obtained from the experimental simulation at –5% slip (Test 9) showing the effect of increasing the roughness of the track surface on the work roll test disc in mid-test on the wear performance of the bainitic back-up roll material

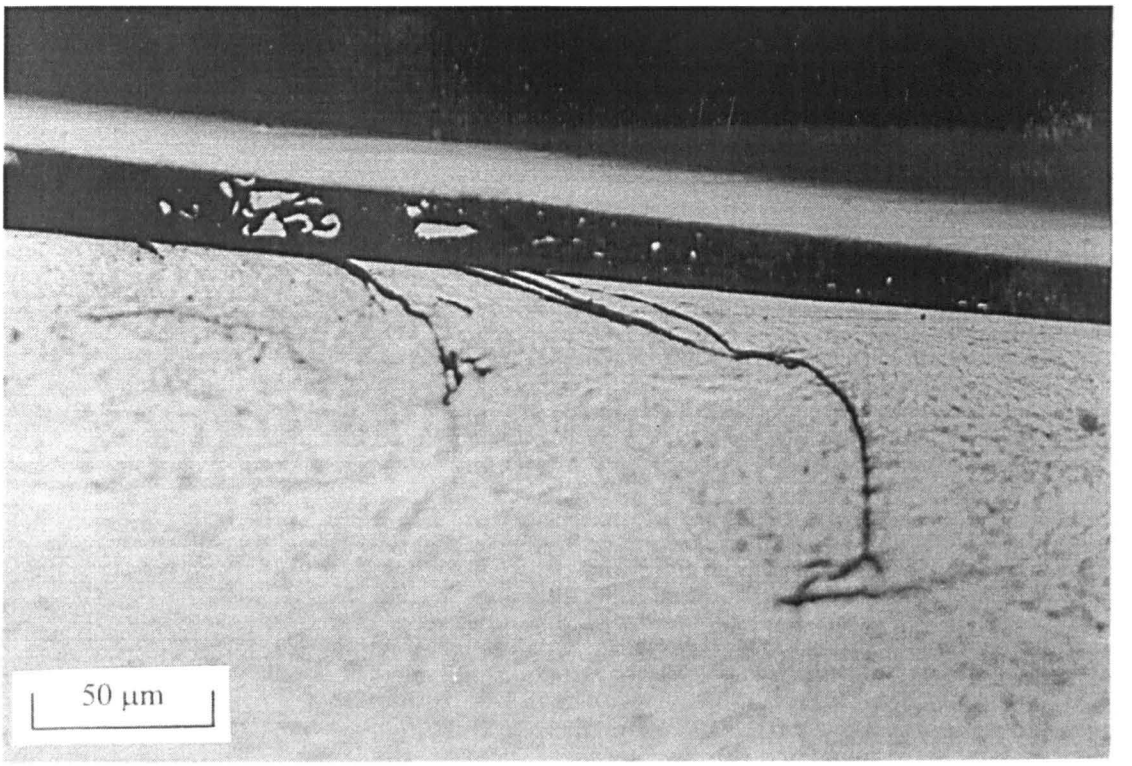

Figure 6.22. Crack propagated from the surface of back-up roll test disc B4 at the end of Test 9 (test carried out with a "smooth" work roll disc [Ra 0.06 μm] for 70000 cycles and a "rough" work roll disc [Ra 0.6 μm] for 50000 cycles

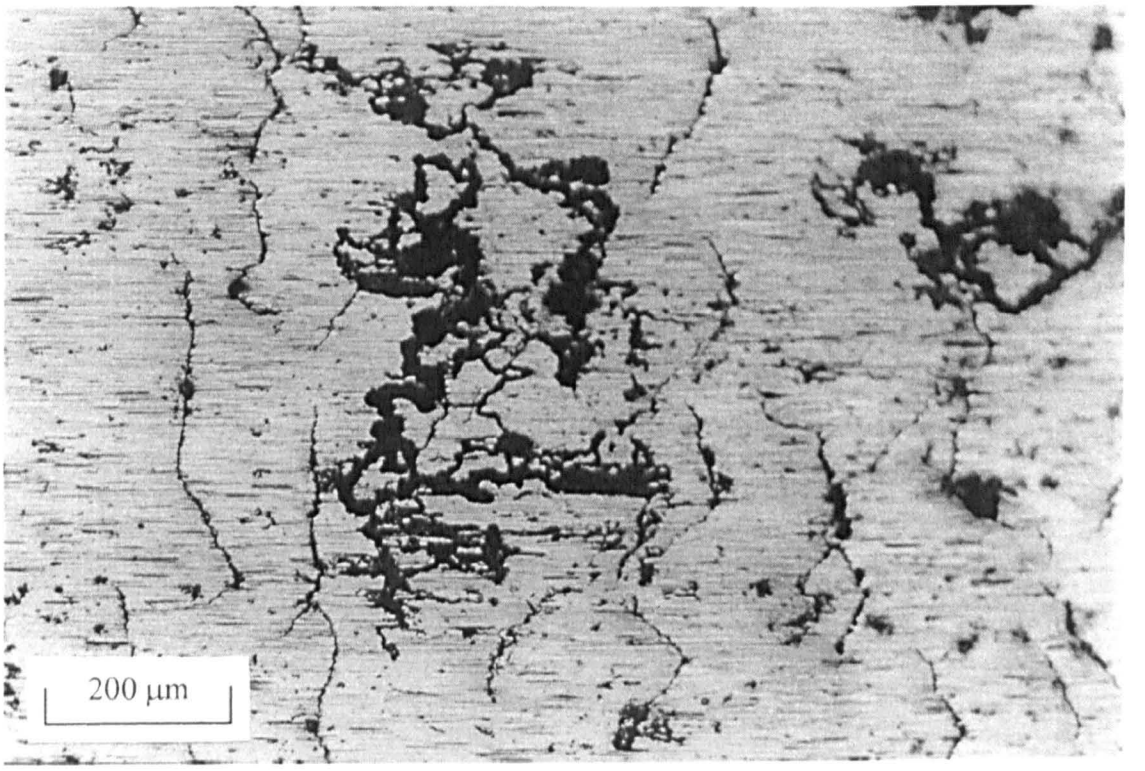

Figure 6.23. Morphology of the track surface of back-up roll test disc B4 at the end of Test 9

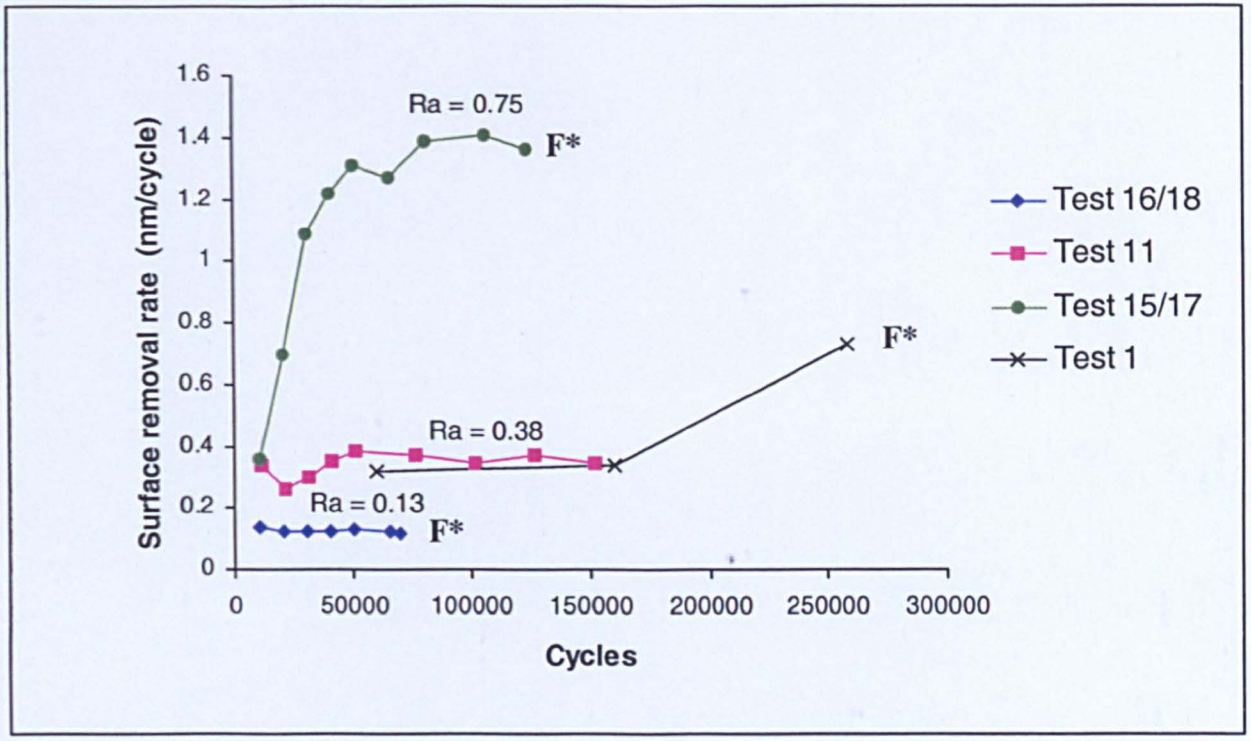

* Failure as indicated by the eddy current crack detector system
Surface roughness of the track on the work roll test disc measured in μm

Figure 6.24. Results obtained from experimental simulations carried out to rolling contact fatigue failure as indicated by the crack detection system (tests carried out at -1% slip)

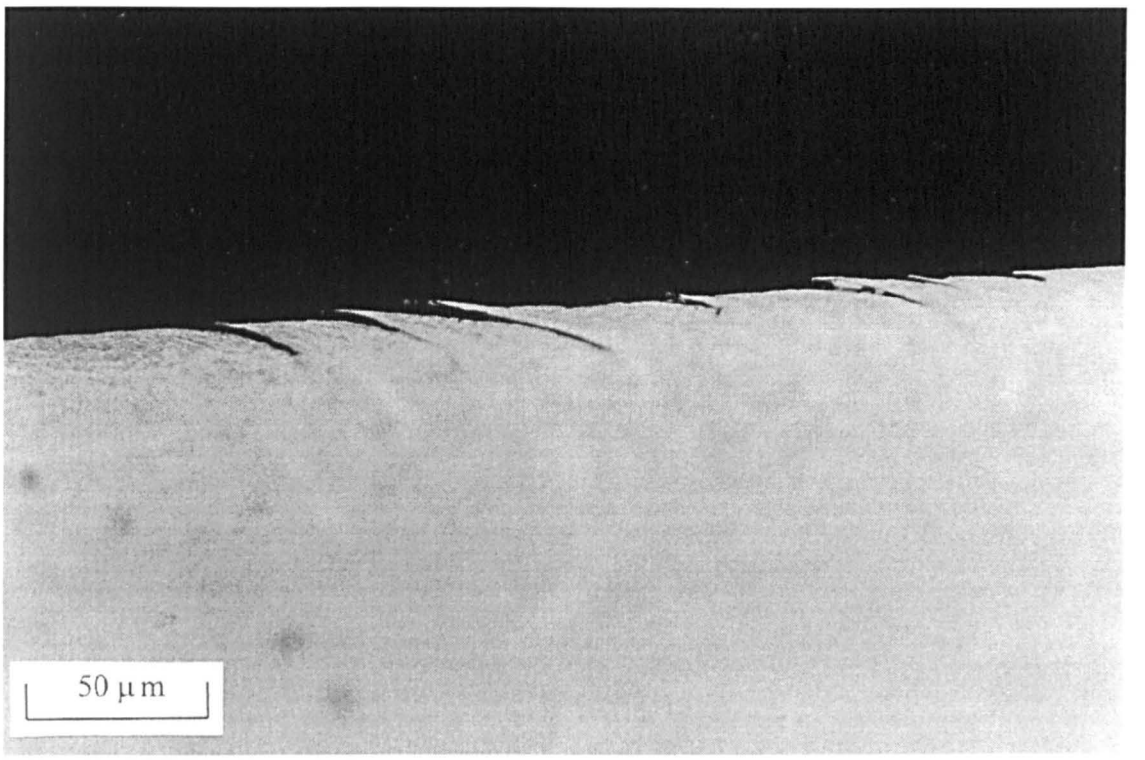

Figure 6.25. Crack propagated from the surface of back-up roll test disc B10 at the end of Test 15/17 (initial roughness of the track on the work roll test disc – Ra = 0.75)

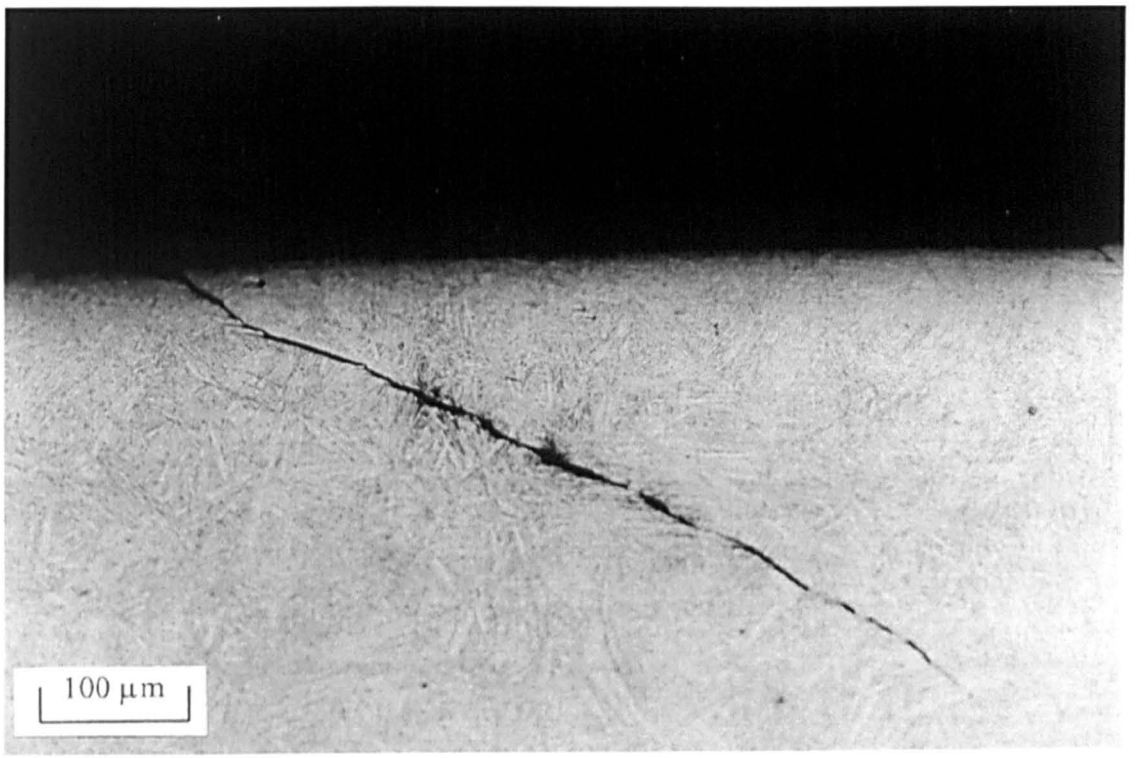

Figure 6.26. Crack propagated from the surface of back-up roll test disc B8 at the end of Test 16/18 (initial surface roughness of the track on work roll test disc – Ra = 0.13)

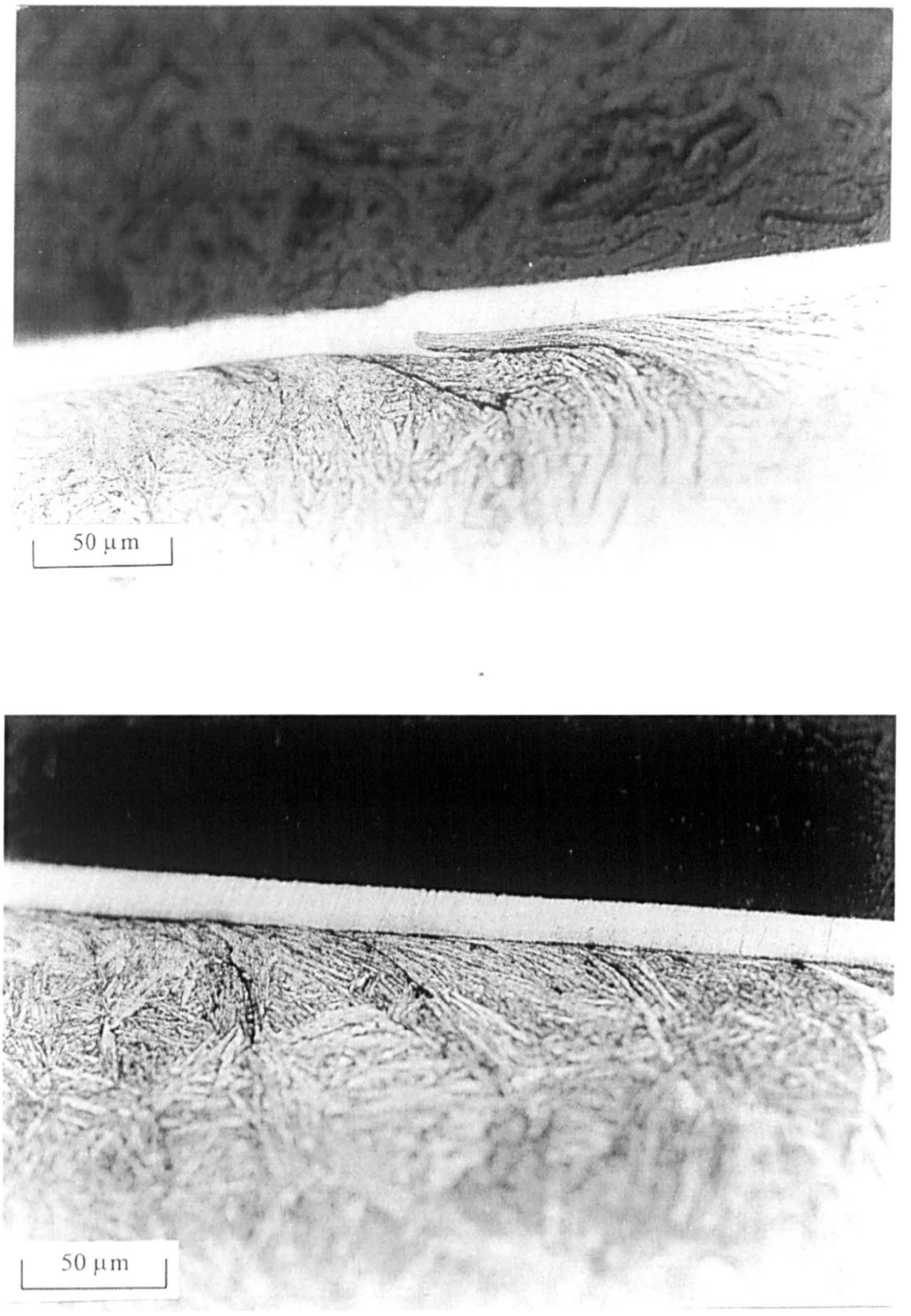

Figure 6.27. Micrographs showing small cracks propagating in the plastically deformed surface layer of test disc B5 at the end of Test 5

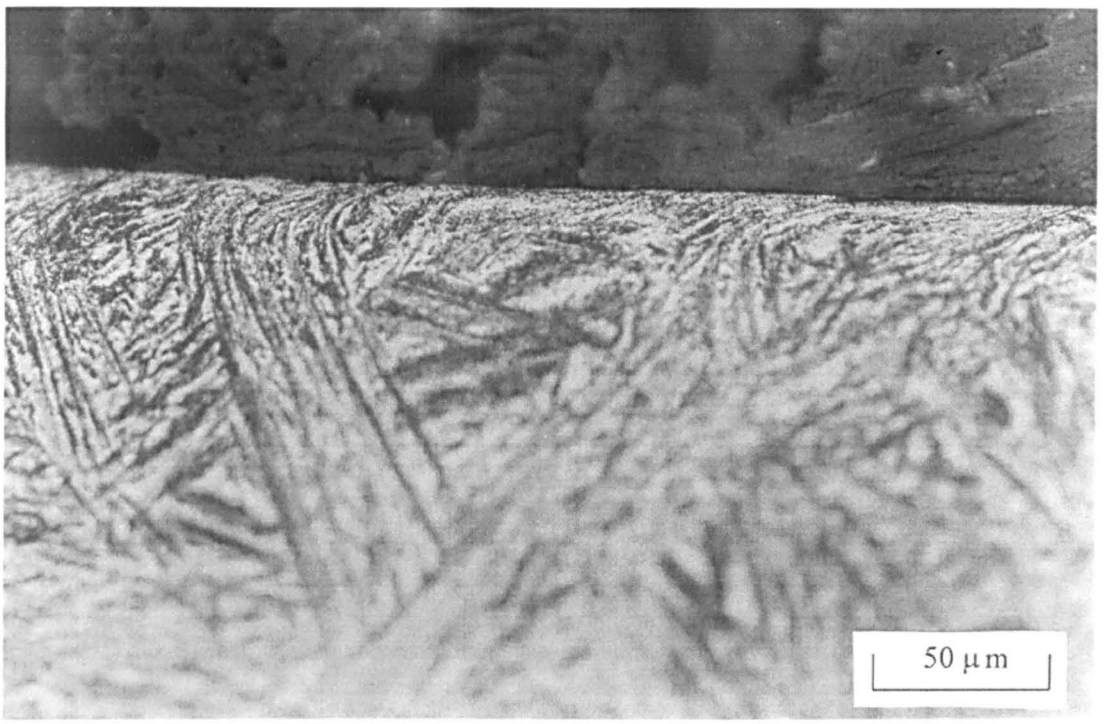

(a)

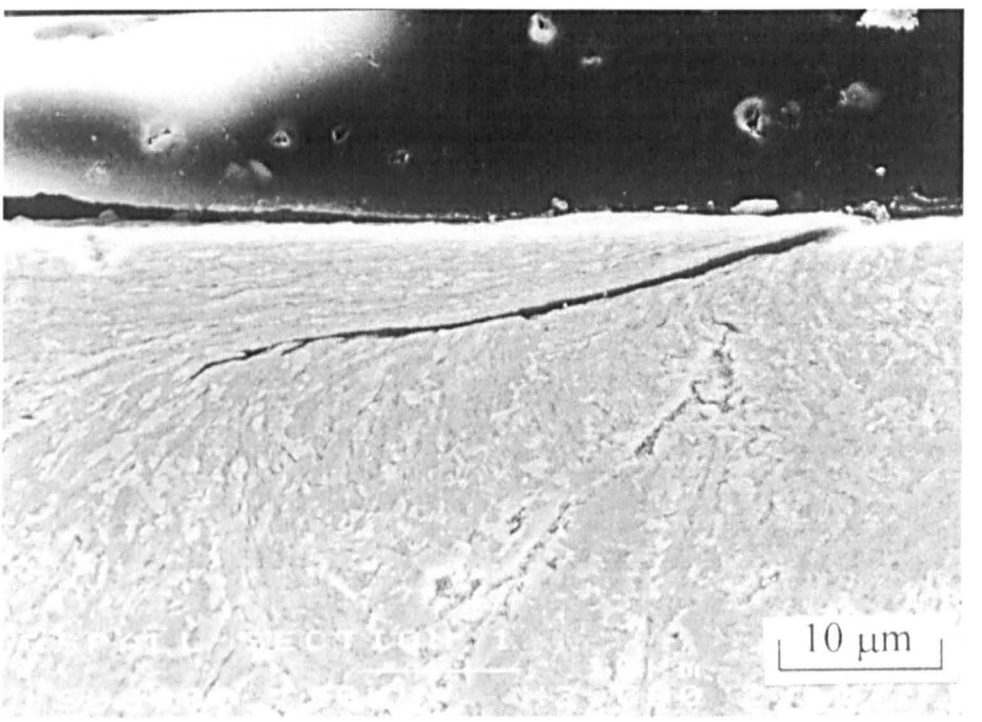

(b)

Figure 6.28. (a) Micrograph showing surface initiated micro cracks propagating in the plastically deformed surface layer and along preferentially orientated ferrite packet/carbide boundaries in a sample taken from spalled material from a back-up roll (b) BEI micrograph showing a typical micro crack

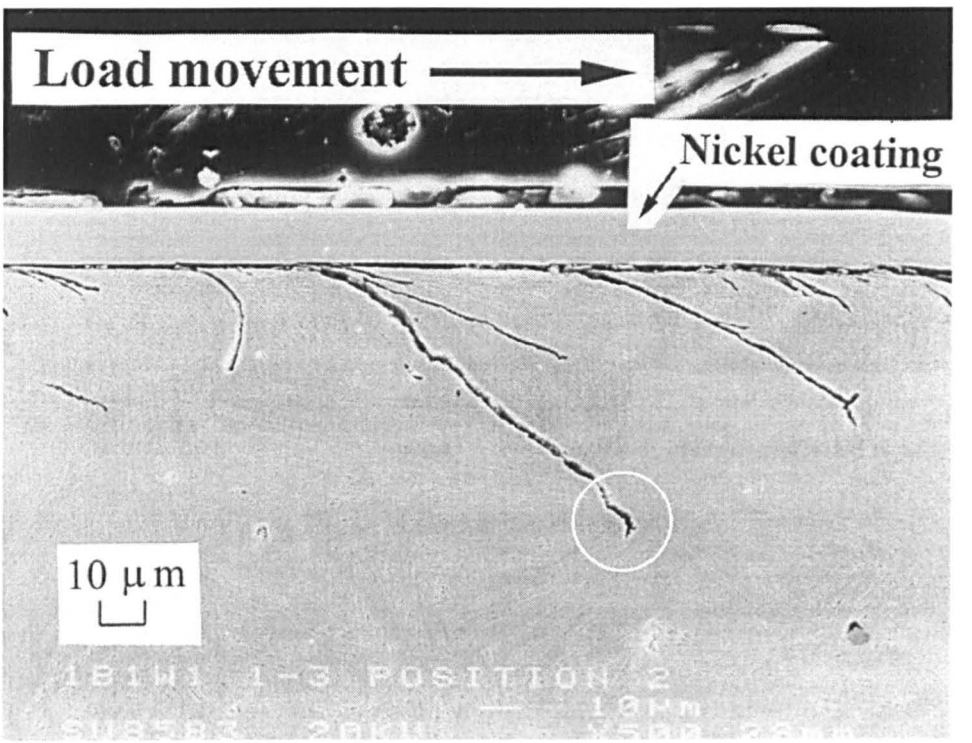

(a)

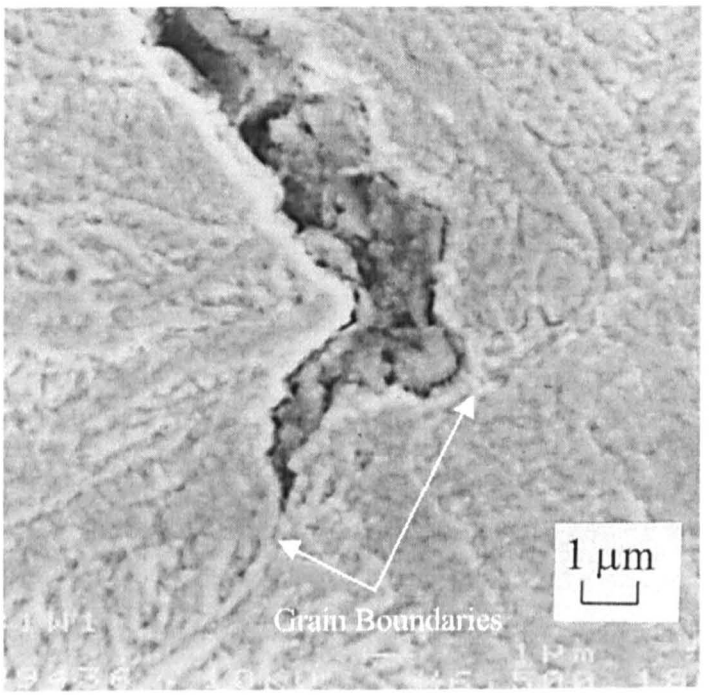

(b)

Figure 6.29. (a) BEI micrograph showing inclined crack propagating from the surface of test disc B1 at the end of Test 1 (b) BEI micrograph of the crack tip, showing of the growth of the inclined crack arrested by the presence of ferrite packet

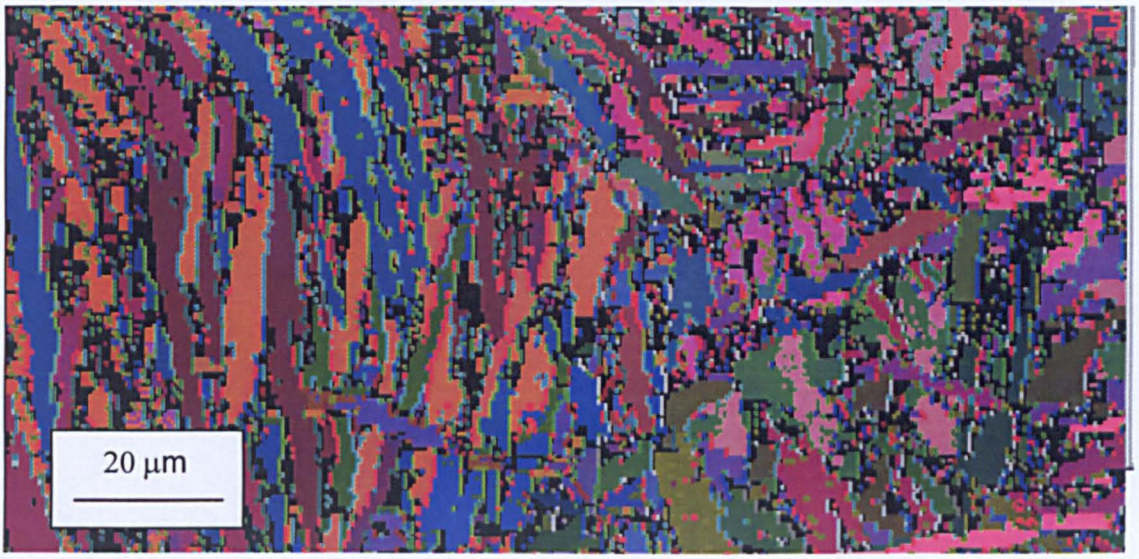

Figure 6.30. EBSD micrograph – Test disc material

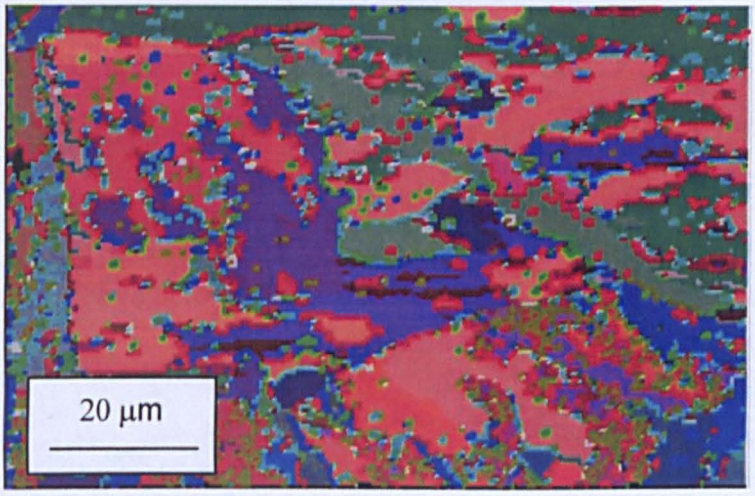

Figure 6.31. EBSD micrograph – Material spalled from a back-up roll

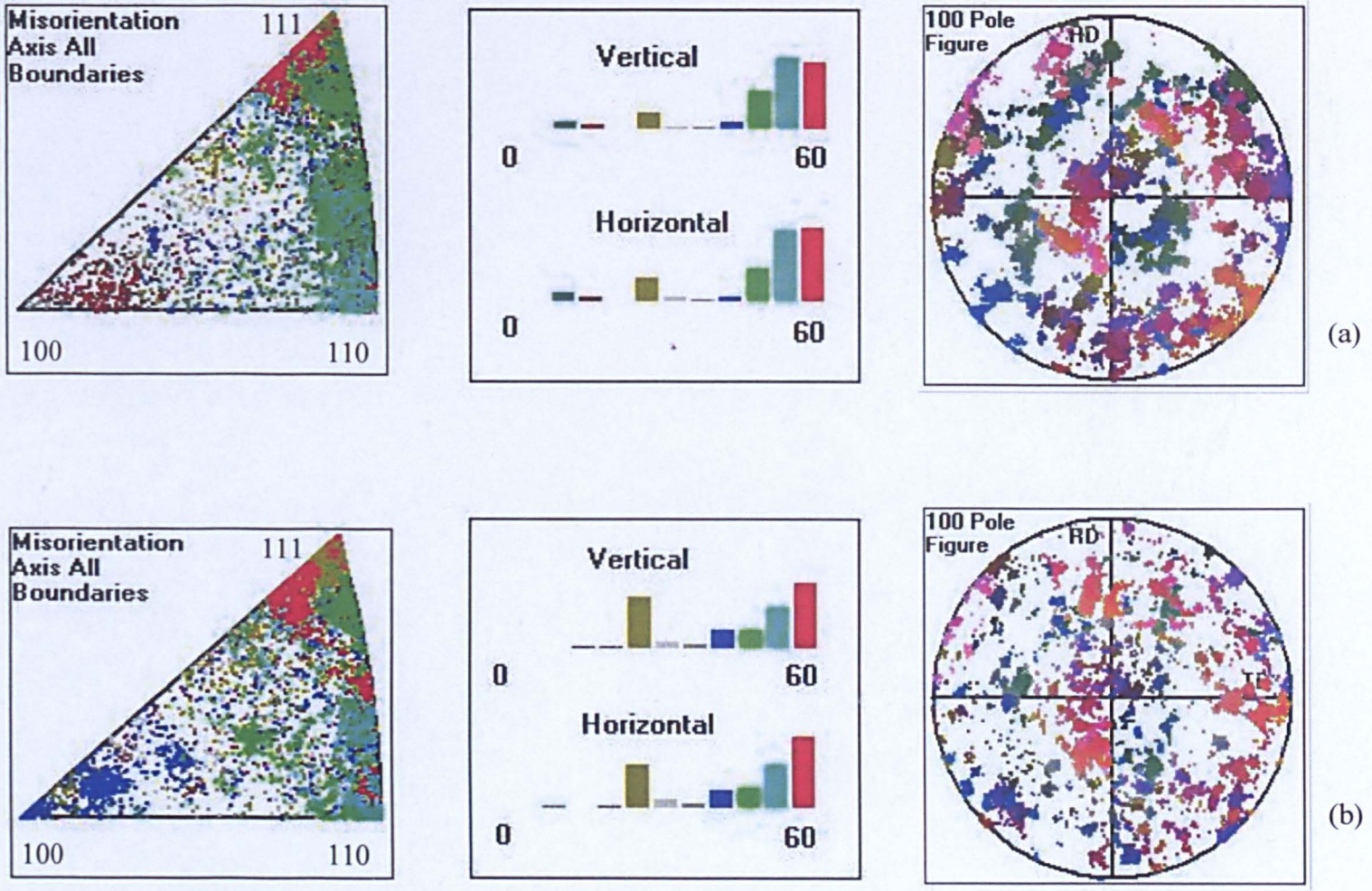

Figure 6.32. Misorientation axes and angle distributions at the edges of the grain boundaries for (a) The test disc material (b) The sample of material spalled from a back-up roll

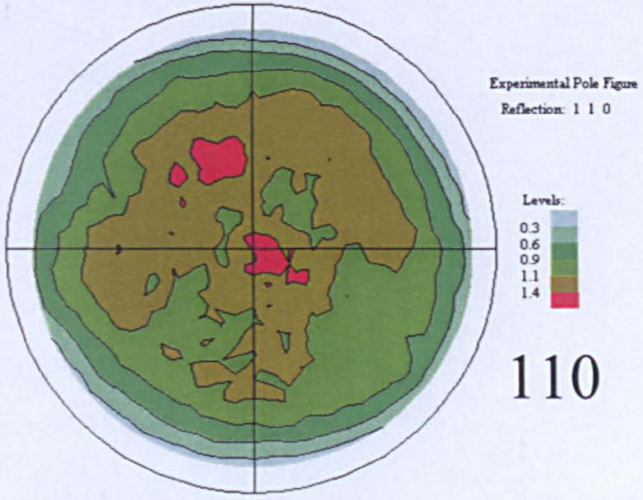

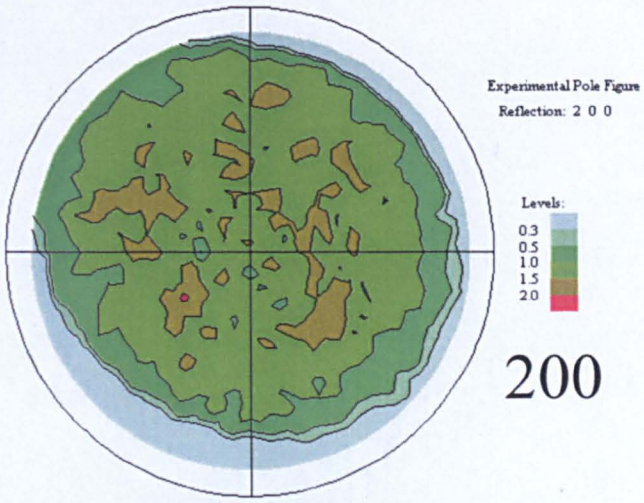

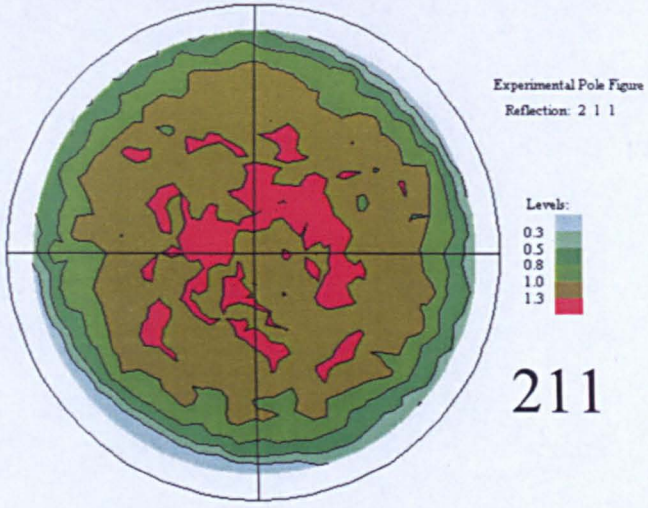

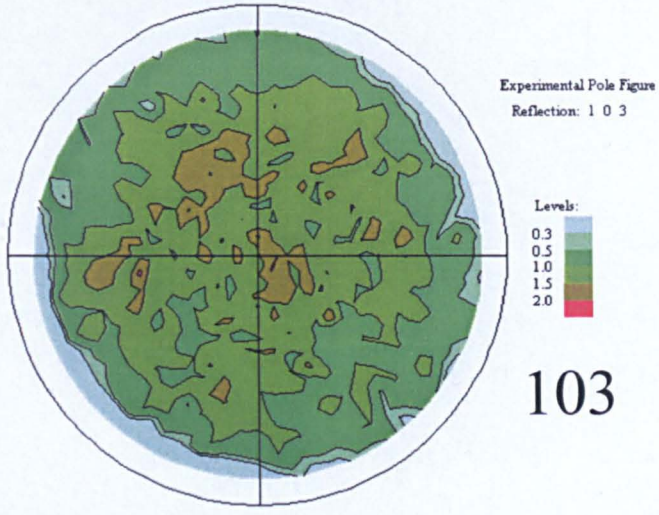

6.33. Bulk X-ray texture analysis – Test disc material

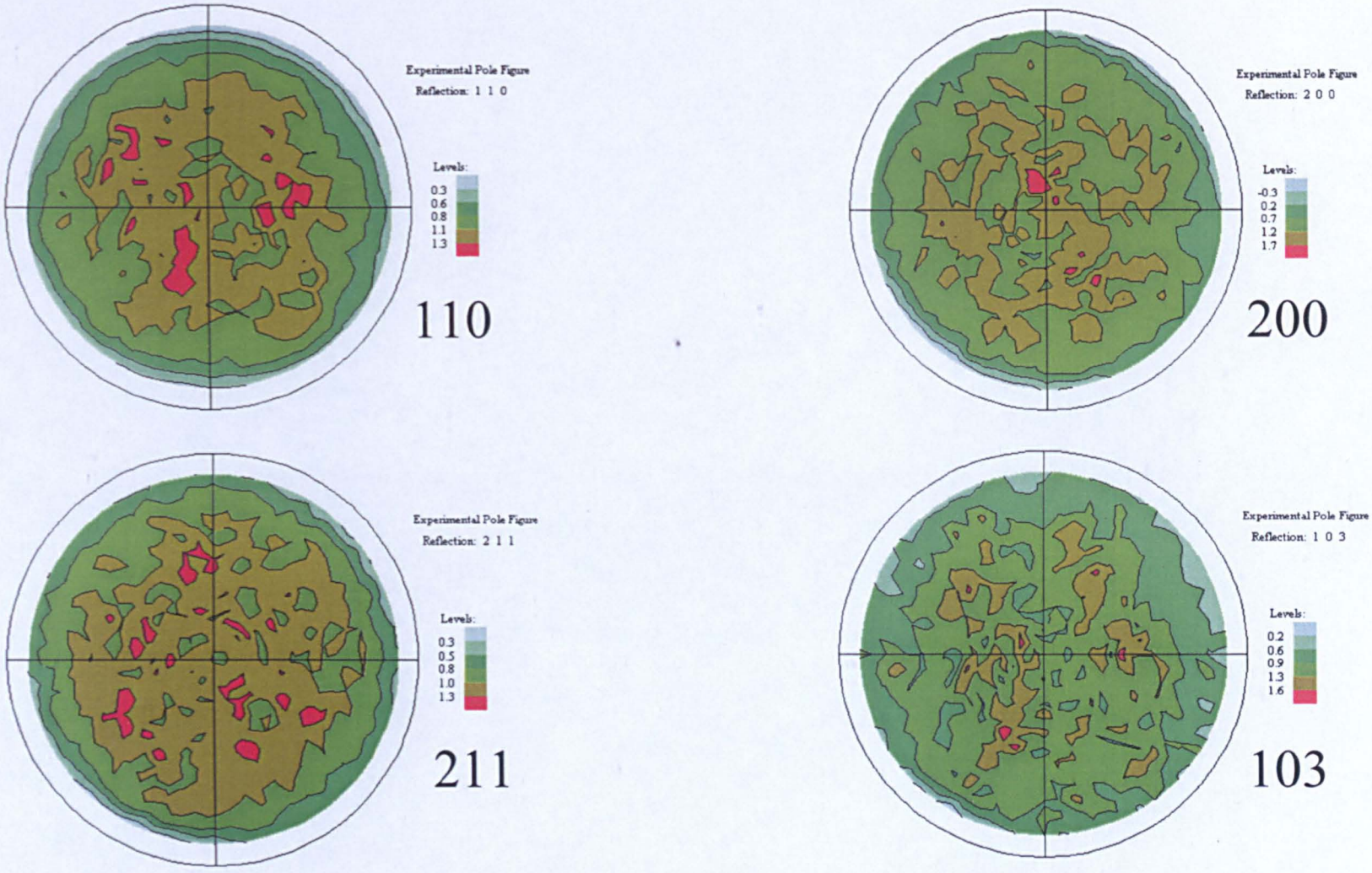

Figure 6.34. Bulk X-ray texture analysis – Material spalled from a back-up roll

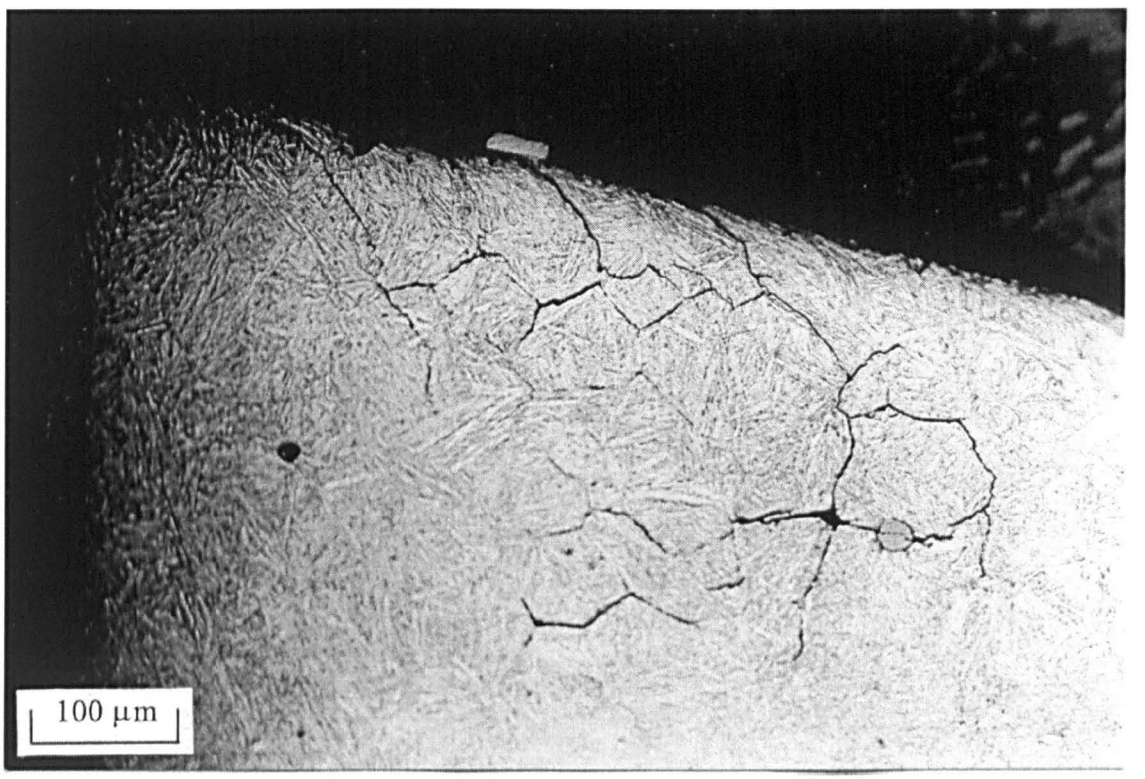

Figure 6.35. Micrograph showing multiple surface cracks with upturning branches at similar inclined crack lengths (test disc B3, Test 6, low wear rate test – total surface wear = 21 μm)

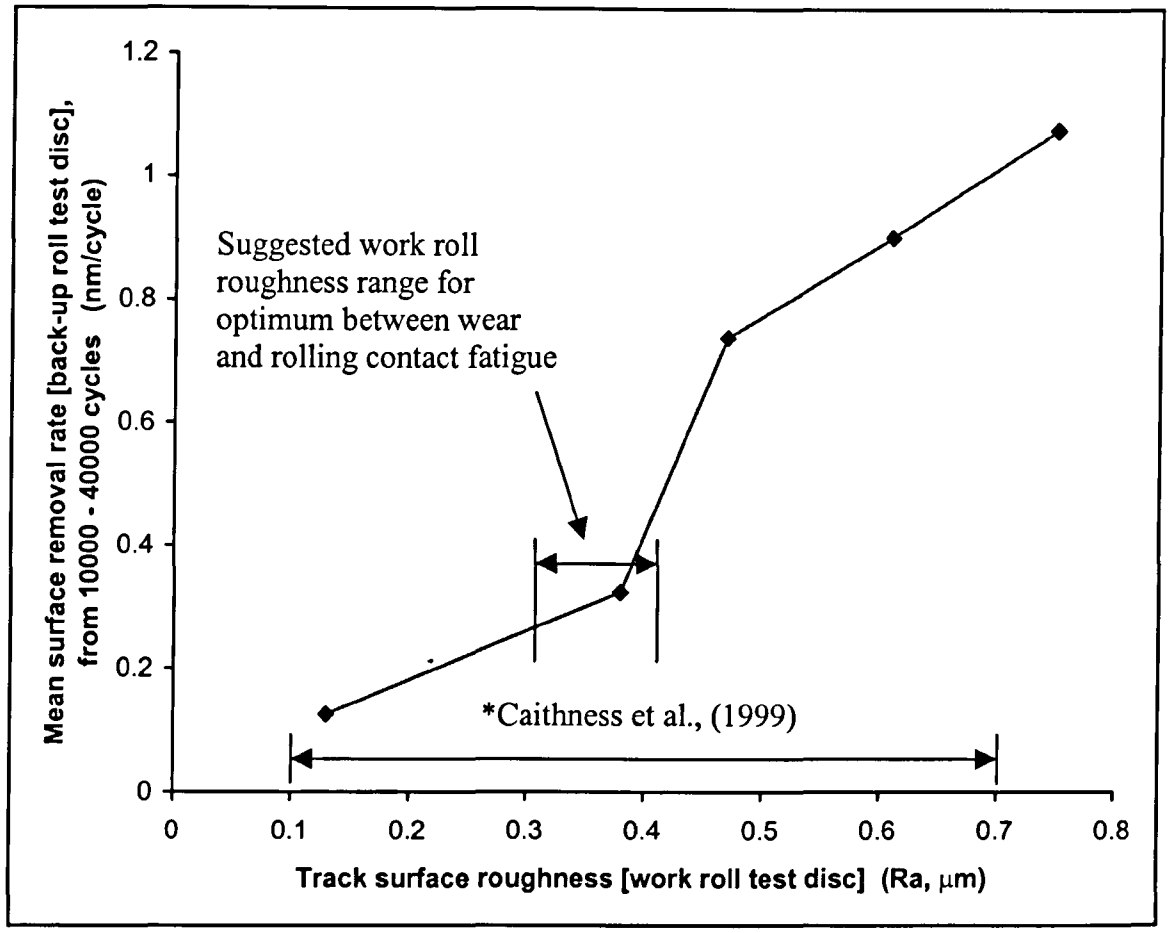

* Range of ground finishes on the surface of HSS work rolls entering service at the former BSSP Llanwern Hot Strip Finishing Mill

Figure. 6.36. Wear results (-1% slip) showing suggested work roll surface roughness range, which should give optimum between wear and rolling contact fatigue performance

Chapter 7

CONCLUSIONS

The results of this work have provided important insights into the possible mechanisms involved in the initiation and propagation of surface initiated rolling contact fatigue cracks in back-up rolls and have also produced practical quantitative recommendations for the design of bainitic steel back-up roll materials, roll maintenance and performance testing of back-up roll materials. Details of the main conclusions are given below.

7.1. MODELLING AND TESTING OF BACK-UP ROLL MATERIALS

1. The modelling of rolling contact failure in back-up rolls and the testing of the rolling contact fatigue performance of back-up roll materials on the "SUROS" Rolling-Sliding Testing Machine should be carried out assuming a maximum contact pressure of 1500 MPa, operating conditions of –1% slip and water lubrication, and with the roughness of the ground finish on work roll disc counter-face lying in the range Ra 0.3 μm to Ra 0.4 μm.

2. An important result of this work has been the demonstration of the necessity of combining the results of both experimental simulation and modelling when predicting the morphology of cracks likely to be produced in back-up rolls based on the experimental results obtained for the much smaller test disc specimens.

7.2. MODE I STRESS INTENSITY FACTORS

1. Under conditions of crack pressurisation, the values of the mode I stress intensity factors at the inclined crack tips rise to a maximum shortly after the load moves over the crack mouth.

2. At longer inclined crack length/half contact width ratios, where crack pressurisation is the more dominant loading factor, the predicted maximum mode

I stress intensity factors at the crack tips are relatively insensitive to the maximum contact pressure.

7.3. MATERIAL DESIGN

1. A damage tolerance approach should be adopted when designing back-up materials for resistance to rolling contact fatigue.

2. The processing route for the back-up roll material should aim to produce a tempered lower bainitic steel microstructure. The length of the carbide/ferrite packet boundaries should be limited by controlling the prior austenite grain size and the highest possible mode I threshold should obtained by maximising the mechanical and microstructural parameter $\sigma_y\sqrt{\bar{d}}$, where σ_y is the yield stress of the material and $\bar{d}$ is the main effective grain size of the ferrite packets (the smallest dimension of the ferrite packets).

3. In the outer shell of the back-up roll barrel the volume fraction of second phases of pearlite, retained austenite and martensite should be kept to a minimum.

7.4. ROLL MAINTENANCE

1. Changes to the specifications for back-up roll maintenance programmes should not be made without weighing the increased risk of rolling contact fatigue failure and the associated costs against the possible cost savings predicted by the economic model.

2. The results obtained from the experimental simulations using test disc specimens indicated that, for an optimum balance between wear and rolling contact fatigue, the ground finish on surface of re-dressed work rolls should lie in the range Ra 0.3 μm to Ra 0.4 μm.

3. For back-up roll materials with mode I thresholds at the top of the range presented by Kapadia and Marsden (1997) and under conditions of crack

pressurisation, the diametral amount of material removed during re-dressing should be 2 mm.

4. Where practical, the roughness of the ground surface on redressed back-up rolls should be similar to that on the surface of the work rolls.

Chapter 8

SUGGESTIONS FOR FUTURE WORK

8.1. INTRODUCTION

The work presented in this thesis has focussed on the study of surface initiated rolling contact fatigue cracks with the aim of producing criteria for both the design of bainitic steel back-up roll materials and the maintenance of rolls, which will improve resistance to the propagation of such cracks. Observations made during the course of the work have highlighted several areas of study, where the results obtained would, when coupled with the results of this work, provide a valuable aid to increasing the overall performance of back-up rolls. Areas recommended for study are described below.

8.2. SUBSURFACE FAILURES

There is much field evidence that a significant number of catastrophic back-up roll failures occur which are associated with subsurface defects at depths significantly below the contact surface. Assuming that the cracks associated with these failures initiate at the subsurface defects, it is clear that the stresses driving the propagation of the cracks may not be the stresses arising from rolling contact.

If crack propagation in this case is not driven by rolling contact stresses, the driving stresses may result from the combination of residual stresses and the cyclic direct and shear stresses arising from the rotation of the roll. The results obtained from this investigation into the feasibility of this combination of stresses as the mechanism for driving these cracks could provide an explanation of the type of failure described above.

The work would involve a full stress analysis of the loaded roll coupled with finite element modelling of both the temperature distributions in back-up rolls during heat treatment and the residual stresses remaining in bainitic steel back-up rolls at the end of the manufacturing process.

8.3. THREE BODY CONTACTS

In hot flat rolling there is clearly the opportunity for three body contacts where debris may pass through the contact between the work roll and back-up roll. The deformation mechanisms and stresses arising from such contacts have been previously studied for such contacts as rolling element bearings. A similar study for the work roll/ back-up roll contact would provide useful information concerning the influence of bruising and denting on the initiation and early propagation of rolling contact fatigue cracks and also may provide some insight into the possibility of initiating subsurface cracks in areas subjected to the high rolling contact stresses arising from the effects of three body contacts.

8.4. BACK-UP ROLL COMPOSITION AND MANUFACTURE

The conclusions presented in this thesis include recommendations for optimising the microstructural design of bainitic back-up roll materials. Based on these recommendations, it is suggested that a project be carried out to improve the rolling contact fatigue performance of back-up rolls by specifying the necessary composition and processing route for bainitic back-up roll steels. The first part of this project would involve determining the optimum processing parameters in the "Selas" and other heat treatments in the processing routes for various material compositions. This would be followed by a programme of testing on the "SUROS" Rolling-sliding Testing Machine, to compare the rolling contact fatigue performance of potential back-up roll materials produced during the development programme.

8.5. BACK-UP ROLL WEAR PERFORMANCE

The results obtained from experimental simulations carried out to investigate the possible influence of the surface roughness of high speed steel work rolls on the surface wear rate of back-up rolls and also the interaction between wear and rolling contact fatigue have indicated that there may be an optimum surface roughness, which provides an acceptable balance between wear on the back-up roll surface and the initiation and rate of propagation of rolling contact fatigue cracks.

It is suggested that a project should be carried out with the aim of confirming these findings and establishing qualitative models and quantitative models for the surface wear of back-up rolls in this case. The aim would be achieved by using the results of a theoretical study of possible wear mechanisms in conjunction with the results obtained from a programme of experimental simulations carried out on the "SUROS" Rolling-Sliding Testing Machine to identify the contributions from the dominant operative wear mechanisms.

REFERENCES

Bailey D. M. and Sayles R. S. (1991) Effect of surface roughness and sliding friction on contact stresses. *Trans. ASME Jour. Trib.*, **113**, 729-738.

Barbadillo J. J. and Trozzi C. J. (1981) Mechanism of banding in hot strip mill work rolls. *Iron and Steel Engineer, Jan.*, 63-72.

Baxter W. T. (1986) The growth of persistant slip bands during fatigue. *The Behaviour of Short Fatigue Cracks, EGF Pub.1, Mech. Eng. Pub., London,*193-202.

Betts W. H. and Baxter H. L. (1990) Rolls in todays rolling mills. *Rolls for the Metalworking Industries, ISS,* 23-30.

Beverley I., Jenkins A. J. and Watkins D. J. (1999) Computerised roll shop management system in the hot strip mill at British Steel Port Talbot Works. *Conf. ROLLS 2000+ "Advances in Mill Roll Technology", Inst. of Materials.*, 205-214.

Beverley I., Robertson T. and Woodland M. (1999) Developing the use of high speed work rolls in the hot strip mills of British Steel. *Conf. ROLLS 2000+ "Advances in Mill Roll Technology", Inst. of Mat.*, 81-90.

Beynon J. H. and Kapoor A. (1997) The interaction of wear and rolling contact fatigue. *R. A. Smith (ed.), Reliability Assessment of Cyclically Loaded Engineering Structures*, Kluwer Academic Publishers, Netherlands, 1-26.

Bhadeshia H. K. D. H. (1992) *Bainite in Steels.* Institute of Materials, London.

Bodnar R. L., Ohhashi T. and Jaffee R. I. (1989) Effects of Mn, Si and purity on the design of 3.5NiCrMoV, 1CrMoV and 2.25Cr-1Mo bainitic alloy steels. *Metall. Trans. A*, Vol. **20A**, 1445-1459.

Bogdanski S., Olzak M. and Stupnicki J. (1996) Numerical stress analysis of rail rolling contact fatigue cracks. *Wear*, **191**, 14-24.

Bogdanski S., Olzak M. and Stupnicki J. (1994) Simulaton of crack growth in rails due to transient load. *Proc. 4th Int. Conf. On Contact Mechanics and Wear of Railway Rail/Wheel Systems.*

Bold P. E., Brown M. W. and Allen R.J. (1991) Shear mode crack growth and rolling contact fatigue. *Wear*, **144**, 307-317.

Bower F. (1988) The influence of crack friction and trapped fluid on surface initiated rolling contact fatigue cracks. *Trans. ASME J. Trib.*, 110, 704-711.

Bower F. and Johnson K. L. (1989) The influence of strain hardening on the cumulative plastic deformation in rolling and sliding contact. *J. Mech. Phys. Solids,* **37**, 4, 471-493.

Boyd J. W. and Maddalena A. (1990) Roll Shop-Automated roll grinding. *Rolls for the Metalworking Industries, ISS,* 157-163.

Bracht N. A. and Bradd A. A. (1965) Factors affecting back-up roll life. *Iron and Steel Year Book.*

Brooksbank D. and Andrews K. W. (1970) Stress fields around inclusions and their relation to mechanical properties. *Conf.-Production and Application of Clean Steels, Balalonfured, Hungary, Pub. 1972, ISI London,* 186-198.

Brown M. W. (1986) Interfaces between long, short and non-propagating cracks. *The Behaviour of short Fatigue Cracks, EGF Pub. 1, Mech. Eng. Pub., London,* 423-429.

Caithness L., Cox S. and Emery S. (1999) Surface behaviour of HSS in hot strip mills. *Conf. ROLLS 2000+ "Advances in Mill Roll Technology", Inst. of Mat.*, 111-120.

Cheng W., Cheng H. S., Mura T. and Keer L. M. (1994) Micromechanics model of crack initiation under contact fatigue. *Trans. ASME Jour. of Trib.*, Vol. **116**, 2-7.

Collins D. B. (1996) HSS rolls through 2000. *Conf.-Rolls 2000, Inst. of Mat.*, 90-100.

Corallo V. (1999) Roll surface and quality inspection in unmanned roll shops. *Conf. ROLLS 2000+ " Advances in Mill Roll Technology", Inst. of Mat.*, 215-224.

Cottrell Sir Alan (1995) *An Introduction to Metallurgy. 2nd Edition, Institute of Materials.* The University Press, Cambridge.

Cox S. (1996) Cast steel back-up rolls. *Conf.-Rolls 2000, Inst. of Mat.*, 126-132.

Dieter G.E. (1998) *Mechanical Metallurgy.* McGraw Hill, London.

Dowling N. E. (1993*) Mechanical Behaviour of Materials.* Prentice-Hall Inc., New Jersey.

Easter H. C. (1996) Inlands application of forged steel back-up rolls for hot and cold mills. *I and S. M., 27-34.*

Eibe W. W. (1990) History of the development of rolling mills and rolls. *Rolls for the Metalworking Industries, ISS*, 15-22.

Erdogan F. and Sih G.C. (1963) On the crack extension in plates under plane loading and transverse shear. *J. Basic Engng. Trans. ASME.*, Series D, **85**, 519-527.

ESDU International-London, *Contact Phenomena I, II, III, Items-78035 (1995), 84017 (1994), 85007 (1994).*

Fan H., Keer L. M., Cheng W. and Cheng H. S. (1993) Competition between Fatigue crack propagation and wear. *ASME Jour. Trib.*, **115**, 141-147.

Fine M. E. (1980) Fatigue resistance in metals. *Metallurgical transactions A*, **11A**, 365-379.

Fletcher D. I. and Beynon J. H. (1999a) A simple method of stress intensity factor calculation for inclined surface-breaking cracks with crack face friction under contact loading. *Proc. Instn. Mech. Engrs.* **213 Part J**, 481-486.

Fletcher D. I. and Beynon J. H. (1999b) A simple method of stress intensity factor calculation for inclined fluid filled surface-breaking cracks under contact loading. *Proc. Instn. Mech. Engrs.* **213 Part J**, 299-304.

Fletcher D. I. and Beynon J. H. (2000a) Development of a machine for closely controlled rolling contact fatigue and wear testing. *ASTM*, 267-275.

Fletcher D. I. and Beynon J. H. (2000b) The effect of contact load reduction on the fatigue life of pearlitic rail steel in lubricated rolling-sliding contact. *Fatigue Fract. Engng. Mater. Struct.*, **23**, 639-650.

Franklin F. J., Widijarta I. and Kapoor A. (2001) Computer simulation of wear and rolling contact fatigue. *Wear*, **251**, 949-955.

Fusada T. (1998) Recent developments in wear-resistant back-up rolls. *I. and S. M., Pub. of Iron and Steel Soc., Feb.*, 33-38.

Garnham J. E. and Beynon J. H. (1991) The early detection of rolling-sliding contact fatigue cracks. *Wear*, **114**, 103-116.

Ginzburg V. B., Fereidoon A. B. and ISSA R. J. (1997) Application of coolflex model for analysis of work roll thermal conditions in hot strip mills. *Iron and Steel Engineer, Nov.*, 38-45.

Gladman T. and Pickering (1983) The effect of grain size on the mechanical properties of ferrous metals. *Yield Flow and Fracture of Polycrystals* (edited by Baker T. N.), 141-198. Applied Science Publishers, London and New York.

Gourgues A. F., Flower H.M. and Lindley T. C. (2000) Electron back scattering diffraction study of acicular ferrite, bainite and martensitic steel microstuctures. *Mats. Sci. and Tech.*, **16**, 26-40.

Hanson M. T. and Keer L. M. (1992) An analytical life prediction model for crack propagation occurring in contact fatigue failure. *STLE Trib. Trans.*, **35**, 3, 451-461.

Higgins R. A. (1993) *Engineering Metallurgy 1-Applied Physical Metallurgy, 6th Edition.* Edward Arnold, London.

Hills D. A. and Nowell D. (1994) *Mechanics of Fretting Fatigue.* Kluwer Academic Publishers, Dordrecht.

Honeycombe R. W. K. and Bhadeshia H. K. D. H. (1995) *Steels-Microstructure and Properties, 2nd Edition.* Edward Arnold, London.

Honeyman G. A., Kearney M. G. and Crabbe M. W. (1996) The effect of chemical composition on the mechanical and tribological properties of high integrity back-up rolls. *Conf.-Rolls 2000, Inst. of Mat.*, 133-144.

Hutchings I. M. (1992) *Tribology-Friction and Wear of Engineering Materials.* Edward Arnold, London.

Irvine K. J. and Pickering F. B. (1957) Low carbon bainitic steels. *J. Iron and Steel Inst.*, **187**, 292.

Jin N. and Clayton P. (1997) Effect of microstructure on rolling/sliding wear of low carbon bainitic steels. *Wear*, **202**, 202-207.

Johnson K. L. (1985) *Contact Mechanics.* Cambridge University Press, Cambridge.

Johnson K. L. (1989) The strength of surfaces in rolling contact. *Proc. of Inst. Mech. Engs.*, **203**, 151-163.

Johnson K. L. (1995) Contact mechanics and the wear of metals. *Wear*, **190,** 162-170.

Kaneta M., Yatsuzuka H. and Murakami Y. (1985) Mechanism of crack growth in lubricated rolling/sliding contact. *ASLE Trans.*, vol. **28**, 407-414.

Kapadia B. M. and Marsden K. W. (1997) Spalling behaviour of back-up roll materials. *39th MSWP. Conf.*, 1-38.

Kapoor A., Franklin F. J., Wong S. J. and Ishida M. (2002) Surface roughness and plastic flow in rail wheel contact. *Wear*, **9152**, 1-8.

Kapoor A., Schmid F. and Fletcher D. (2002) Managing the critical wheel/rail interface. *Railway Gazette International*, 25-28.

Kerr E. J., Hishon A., Hill W. J. and Webber R. J. (1999) High speed steel work rolls at Dofasco's hot mill. *Conf. ROLLS 2000+ "Advances in Mill Roll Technology", Inst. of Mat.*, 61-69.

Kneppe G. and Hormes P. (1996) Operation of CVC rolls in hot and cold rolling mills. *37th MSWP Conf. Proc., ISS*, **XXXIII,** 303-316.

Kudo T. (1999) HSS Rolls: Carbide morphology and properties. Conf. *ROLLS 2000+ " Advances in Mill Roll Technology", Inst. of Mat.*,71-80.

Li F. (1997) Thermo-elastic-plastic modelling of heat treatment processes – with particular reference to large steel rolls. *PhD thesis, Queen Mary and Westfield College, University of London.*

Liddle A. J. and Shinozuka K. (1996) Hot strip mill back-up roll performance improvement program by joint work between B.H.P. and J.C.F.C. *Paper Presented to SEAISI Taiwan Seminar Nov. 1996 Kauhsiung Taiwan.*

Marston L. W., Price S., Mees J. and Kearney M. G. (1999) Improved in-service performance of large forged back-up rolls through the development of steel chemistry and process improvements. *Conf. ROLLS 2000+ "Advances in Mill Roll Technology", Inst. of Mat.*, 281-291.

M^{c}Corry I. (1999) The development of a cast 5% chromium back-up roll. *Conf. ROLLS 2000+ "Advances in Mill Roll Technology", Inst. of Materials*, 293-300.

Miller K. J. (1984) Initiation and growth of short fatigue cracks. *Fundamentals of Deformation and Fracture, Eshelby Memorial Symposium, Cambridge University Press, Pub. 1985.*

Miller K. J., Mohamed H.J. and de los Rios E. R. (1986) Fatigue damage accumulation above and below the fatigue limit. *The Behaviour of Short Fatigue Cracks, EGF Pub.1, Mech. Eng. Pub.*, 495-511.

Mura T. (1994) A theory of fatigue crack initiation. *Mat. Sci. and Eng., A176,* 61-70.

Murakami Y, Kaneta M., and Yatsuzuka H. (1985) Analysis of surface crack propagation in lubricated rolling contact. *ASLE Trans.*, **28**, 1, 60-68.

Murakami Y. and Hamada S. (1997) A new method for the measurement of of mode II fatigue threshold stress intensity range $\Delta K_{\tau th}$. *Fatigue Fract. Engng. Mater. Struct.*, **20**, 863-870.

Navarro A. and de Los Rios E. R. (1992) Fatigue crack growth modelling by successive blocking dislocations. *Proc. R. Soc. Lond.*, A, **437**, 375-390.

Nayak L. and Paul K. (1979) Contact fatigue failure of rolls of hot strip mill. *Indian J. Tech.*, **17**, 293-298.

Ochmori Y. and Maki T. (1991) Bainitic transformation in view of the displacive mechanism. *Mats. Trans., JIM*, **32**, 8, 631-641.

Ohkomori Y. and Kaku K. (1997) High wear resistance and toughness back-up roll for hot strip mill. *SEA ISI Quar., April.*

Ohkomori Y., Kitagawa I., Shinozuka K., Miyamoto R., Yazaki S. and Inoue M. (1987) Cause and prevention of spalling of back-up rolls for hot strip mill. *Pub. In Tetsu-to- Hagane 73, Presented to symposium of the 110th meeting. Oct. 1985.*

Otsuka A., Mori K. and Miyata T. (1975) The condition of fatigue crack growth in mixed mode condition. *Engng. Fract. Mech.* **7**, 429-439.

Ott G. A. (1990) Manufacture of forged steel rolls. *Rolls for the Metalworking Industries, ISS,* 113-120.

Ott G. A. (1996) The influence of roll metallurgy on the wear characteristics of forged hardened rolls. *Conf.-Rolls 2000, Inst. of Materials*, 147-162.

Randle V. and Engler O. (2000) *Introduction to Texture Analysis: Macrotexture, Microtexture & Orientation Mapping.* Taylor and Francis, London

Reynolds W. T., Aaronson H. I. and Spanos G. (1991) A summary of the present diffusionist views on bainite. *Mats. Trans., JIM*, **32**, 8, 737-746.

Roberts W. L. (1990) The rolling process mechanical engineering explanation. *Rolls for the Metalworking Industries, ISS*, 31-54.

Rooke D. P., Rayaprolu D. B. and Alibaldi M. H. (1992) Crack-line and edge Green's functions for stress intensity factors of edge cracks. *Fatigue and Fract. Engng. Mater., Struct.*, **15**, 441-461.

Ryu J-H. and Park J. (1999) Thermal fatigue and wear properties of high speed steel roll for hot strip mill. *Conf. ROLLS 2000+ "Advances in Mill Roll Technology", Inst. of Mat.*, 91-99.

Scoular T. and McPate W. A. (1990) Manufacture of cast steel rolls. *Rolls for the Metalworking Industries, ISS,* 95-111.

Shelestowsky G. (1990) Roll shop-Part II – Application of N. D. T. in the roll shop. *Rolls for the Metalworking Industries, ISS,* 151-156.

Suh N. P. (1977) An overview of the delamination theory of wear. *Wear,* **44,** 1-16.

Suresh S. (1998) *Fatigue of Materials,* 2nd *Edition.* Cambridge University Press, Cambridge.

Suresh S. and Ritchie R. O. (1984) Propagation of short fatigue cracks. *International Metals Reviews,* **29,** No.6, 445-476.

Tait W. H. (1990) Roll shop, Part I-The nature and causes of in-service defects. *Rolls for the Metalworking Industries, The Iron and Steel Society,* 135-149.

Tallian T. E. (1992) Simplified contact fatigue life prediction model-Part1: Review of published models. *ASME Jour. of Trib.,* **114,** 207-213.

Tallian T. E. (1992) Simplified contact fatigue life prediction model-Part II: New model. *ASME Jour. of Trib.,* **114,** 214-222.

Thelning (1975) *Steel and its Heat Treatment.* Bofors Handbook, Butterworth.

Timoshenko S. P. and Goodier D. N. (1970) *Theory of Elasticity.* McGraw hill-London.

Tyfour W. R., Beynon J. H. and Kapoor A. (1996) Deterioration of rolling contact fatigue life of pearlitic rail steel due to dry-wet rolling-sliding contact. *Wear,* **197,** 255-265.

Way S. (1935) Pitting due to rolling contact. *ASME J. Applied Mechanics,* **2,** A49-A55.

Werquin J. C., Caillard J. C. and Kotlar Tice D. (1990) The rolling process-metallurgical demands and responses of the rolls. *Rolls for the Metalworking Industries, Iron and Steel Society,* 55-71.

Williams J. A. (1994) *Engineering Tribology* Oxford University Press, New York.

Williams J. A., Dyson I. N. and Kapoor A. (1999) Repeated loading, residual stresses, shakedown and tribology. *J. Mater. Res.*, **14**, 1548-1459.

Yammamoto S., Yokoyama H., Jamada K. and Niikura M. (1995) Effects of the austenite grain size and deformation in the unrecrystallized region on bainite transformation. *ISIJ International*, Vol. **35**, 8, 1020-1026.

Yanaka T. (1990) Manufacture of Roll sleeves. *Rolls for the Metalworking Industries, ISS,* 121-134.

Yoder G .R., Cooley L. A. and Crooker T. W. (1983) A critical analysis of grain size and yield strength dependence on near-threshold fatigue crack growth in steels. *Fracture Mechanics.* Special Technical Publication 791, **I**, 348-365. Philadelphia: American Society for Testing and Materials.

APPENDIX

A1. TYPICAL STRIP MILL DATA

HOT STRIP MILL

Detail	Number of rolls (m)	Roll Length (m)	Work roll dia. (m)	Work roll Face speed (m/min)	Back-up Roll dia. (m)
Vertical Scale breaker	2	0.23	1.07	61.3	-
Horizontal Scale breaker	2	1.96	0.91	65	-
Reversing Rougher	4	2.03	1.2	302	1.58
No. 1 Finisher	4	2.03	0.68	64/144	1.4
No. 2 Finisher	4	2.03	0.714	106/251	1.4
No. 3 Finisher	4	2.03	0.708	175/416	1.4
No. 4 Finisher	4	2.53	0.690	218/607	1.4
No. 5 Finisher	4	2.53	0.686	272/749	1.4
No. 6 Finisher	4	2.53	0.706	305/805	1.4
No. 7 Finisher	4	2.53	0.714	357/893	1.4

Work roll bending F1 – F3
Work roll shifting and bending F4 – F7
Mill capability: Width range: 675mm – 1880mm
Gauge range: 1.2mm – 17.5mm
Both roughing and finishing mills have automatic roll change

Number of coilers: 2
Maximum coil weight: 34 tonnes
Maximum coil diameter: Internal: 762mm
External: 2015mm
Maximum gauge coiled: 17.5mm

COLD STRIP MILLS

2030mm Five Stand Tandem mill

Maximum coil weight:	34000Kg
Maximum diameter of coil:	2135mm
Maximum strip width:	1854mm
Maximum entry gauge:	4.78mm
Minimum entry gauge:	1.9mm
Maximum exit gauge:	2.0mm
Minimum exit gauge:	0.3mm
Maximum finished speed:	720 m/min

ROLL DETAILS

Work roll diameter (maximum):	559mm
Back-up roll diameter (maximum):	1346mm

1420mm Five stand Tandem Mill

Maximum coil weight:	22680Kg
Maximum diameter of coil:	1830mm
Maximum strip width:	1270mm
Maximum entry gauge:	3.56mm
Minimum entry gauge:	1.83mm
Maximum exit gauge:	2.0mm
Minimum exit gauge:	0.25mm
Maximum finished speed:	1500 m/min

ROLL DETAILS

Work roll diameter (maximum):	584mm
Back-up roll diameter (maximum):	1346mm

DO NOT SCALE.

IF IN DOUBT – ASK !

THIRD ANGLE PROJECTION.

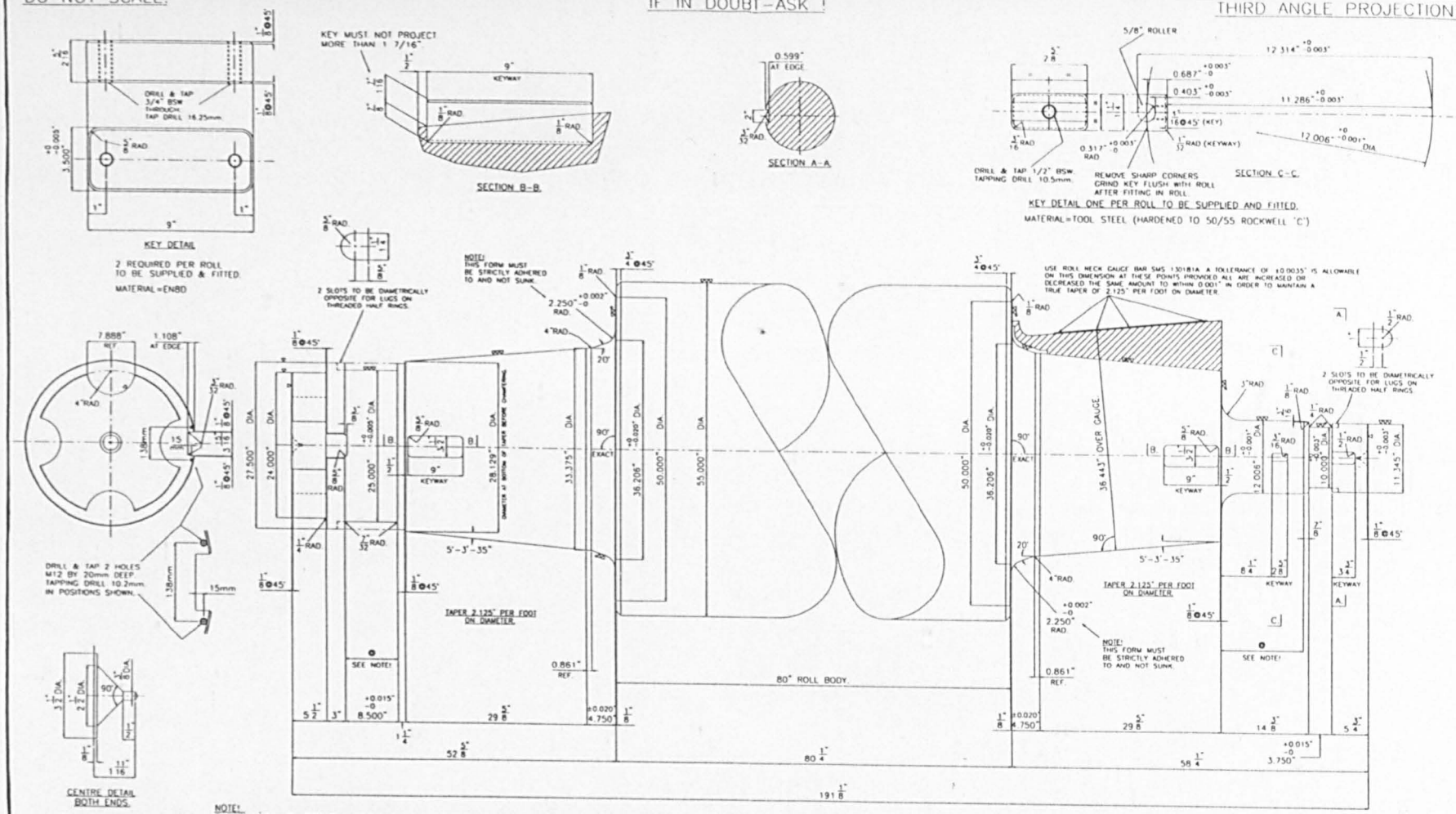

British Rollmakers Corporation

A MEMBER OF THE SHEFFIELD FORGEMASTERS GROUP OF COMPANIES.

WESTON ROAD, CREWE, CHESHIRE, ENGLAND. CW1 1DB

TELEPHONE 44 (0) 270 250567 / 213412
FACSIMILE 44 (0) 270 250552 / 212351
TELEX 36149

REVISION A.	REVISION B.	REVISION C.
REVISION E.	UNCONTROLLED DOCUMENT	

REVISION D.	CUSTOMERS ORD. No. 4330-41-12-12-001 C COATBRIDGE DRG. A1 1378.	ESTIMATED FINISHED WEIGHT. TONNES. 32 KG. 695
	PURPOSE IN MILL. BACK UP ROLL.	

▽▽▽▽ GRIND & POLISH 4-16	BARREL DIAMETER.	BARREL LENGTH.	OVERALL LENGTH.
▽▽▽ SMOOTH GRIND 16-32	55"	80 1/4"	191 1/8"
▽▽ MACHINE & POLISH 32-64			
▽▽ MACHINE TO LIMITS 32-64			
▽ MACHINE 64-125			

REFERENCES. O/N 1906 F7569	ALL MACHINED DIMENSIONS WITHOUT LIMITS. BRITISH ± 0.010" METRIC ± 0.25mm	DRAWN BY & DATE. A.J.ADAMS 25-4-97	STROKE NO. 1	DRAWING NO. / 4832	REV.
SCALE. 1:1 CAD.		CHECKED BY & DATE. J.HAMBROOK 27-6-97			

DO NOT SCALE. IF IN DOUBT–ASK ! THIRD ANGLE PROJECTION.

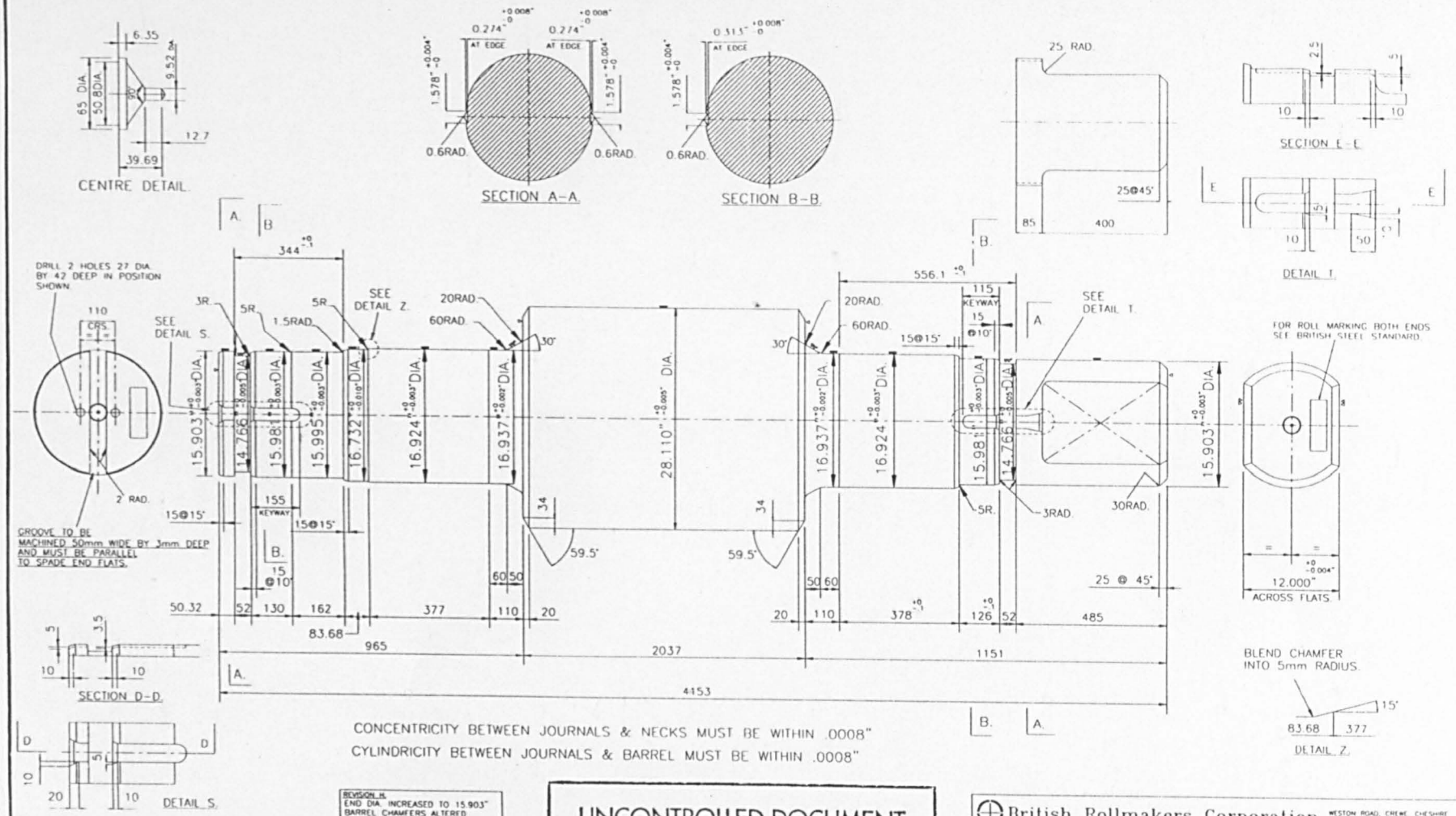

UNCONTROLLED DOCUMENT

British Rollmakers Corporation
A MEMBER OF THE SHEFFIELD FORGEMASTERS GROUP OF COMPANIES
WESTON ROAD, CREWE, CHESHIRE, ENGLAND. CW1 1DB
TELEPHONE +44 (0) 270 250587 / 213412
FACSIMILE +44 (0) 270 250552 / 212194
TELEX 36169

REVISION A. DRAWING BOUGHT IN LINE WITH CUSTOMERS LATEST CUSTOMERS REVISION. DWG. No. 4330.35.12.12.125 REV.D
A.J.ADAMS 26-9-91

REVISION B. GROOVE ADDED TO TOP END OF ROLL TO ENABLE THE CUSTOMER TO SLOT THE SPADE END INTO COUPLING AS OF CUSTOMERS LETTER.
A.J.A. 9-10-91

REVISION C. CENTRE RECESS DIA. AND GROOVE BOUGHT IN LINE WITH CUSTOMERS LATEST DWG. 4330.35.12.12.125 REV E
A.J.A. 9-12-91

REVISION D. DETAIL OF FILLER KEY AND HOLES DRILLED INTO KEYWAYS TO HOLD THEM ADDED AS OF NEW CUSTOMERS DRAWING 4330.35.12.12.125 REV F
A.J.A. 5-3-97

REVISION E. KEYWAY HOLES DIMENSIONED FROM RECESS FACE AT M/C SHOP REQUEST.
A.J.A. 24-4-92

REVISION F. ROLL LENGTH INCREASED BY 10mm, END DIA WAS 404 NOW 403, KEYWAYS ONE SIDE ONLY DRILLED & TAPPED HOLES REMOVED FROM KEYWAYS, 2 HOLES ADDED IN END FACE. REV J. A.J.A. 2-11-94

REVISION G. LEAD KEYWAY ONLY ADDED TO OTHER SIDE OF THE ROLL AS OF NEW CUSTOMERS DRAWING 4330.35.12.12.125 REV K
A.J.ADAMS 20-12-94

REVISION H. END DIA. INCREASED TO 15.903" BARREL CHAMFERS ALTERED. 30 RAD ADDED TO SPADE CHAMFER KEYWAY LEADS ALTERED.
A.J.A. 12-1-96

CUSTOMERS DWG. No.	4330.35.12.12.125 REV M.
PURPOSE IN MILL	HSM FIN ROLLS
ESTIMATED FINISHED WEIGHT	TONNES 8 – KG 500

000 GRIND & POLISH	4–16	
000 SMOOTH GRIND	16–32	
00 MACHINE & POLISH		
00 MACHINE TO LIMITS	32–64	
0 MACHINE	64–125	

BARREL DIAMETER	BARREL LENGTH	OVERALL LENGTH
714	2037	4153

REFERENCES O/N 7377
SCALE 1:1 CAD.
ALL MACHINED DIMENSIONS WITHOUT LIMITS. BRITISH ± 0.010" METRIC ± 0.25mm
DRAWN BY & DATE JCH/AJA 12-1-96
CHECKED BY & DATE

STROKE NO.	DRAWING NO.	REV.
1	4262	H

A3. HEAT TREATMENTS CARRIED OUT ON TEST DISC SPECIMENS

Back-up roll test disc specimens (cast bainitic steel)

Anneal - Ramp to 980 °C and hold for 2 hours
- Furnace cool to 550 °C and hold for 2 hours
- Ramp to 830 °C and hold for 4 hours
- Cool at maximum rate of 10°C/hour to 650 °C
- Furnace cool

Harden - Preheat at 650 °C
- Ramp to 1000 °C and austenitise for 1.5 hours
- Air cool to 320 °C
- Ramp to 560 °C and temper for 2 hours
- Furnace cool

Work roll test disc specimens (high speed steel)

Harden - Ramp to 960 °C and hold for 1hour
- Ramp tp 1050 °C and austenitise for 2 hours
- Air cool to 400 °C and hold for 1 hour
- Air cool

Temper - Ramp to 550 °C and hold for 2 hours
- Furnace cool to below 150 °C
- Ramp to 550 °C and hold for 2 hours
- Furnace cool to below to below 150 °C
- Air cool

A4. CALCULATIONS OF CONTACT HALF WIDTHS

Combining equations 3.2 and 3.4 gives an equation for the contact half width b as shown below:

$$b = \frac{2p_0R}{E^*} \qquad \text{(A1)}$$

where, the values of R and E^* are given by equations 3.4 and 3.5 respectively.

Test disc pair

P_0 = 1500 MPa
R = 0.01375 m
E^* = 115 x 10^3 MPa

Therefore the half contact width b = 359 μm

Work roll/back-up roll pair

P_0 = 1500 MPa
R = 0.236 m
E^* = 115 x 10^3 MPa

Therefore the half contact width b = 6156 μm